Durham University

Durham E-Theses

Elastic wave propagation in embankment dams

M. D. Linton

How to cite:

Linton, M. D. (1982) Elastic wave propagation in embankment dams. Doctoral thesis, Durham University.

Use policy

The full-text may be used and/or reproduced, and given to third parties in any format or medium, without prior permission or charge, for personal research or study, educational, or not-for-profit purposes provided that:

- a full bibliographic reference is made to the original source
- a https://etheses.durham.ac.uk/id/eprint/10389/ is made to the metadata record in Durham E-Theses
- the full-text is not changed in any way

The full-text must not be sold in any format or medium without the formal permission of the copyright holders.

Please consult the full Durham E-Theses policy for further details.

Academic Support Office, The Palatine Centre, Durham University, Stockton Road, Durham, DH1 3LE
e-mail: e-theses.admin@durham.ac.uk Tel: +44 0191 334 6107
https://etheses.durham.ac.uk

ELASTIC WAVE PROPAGATION IN EMBANKMENT DAMS

by

M.D. LINTON

A thesis submitted to the
University of Durham
for the degree of
Doctor of Philosophy

Graduate Society

May 1982

DURHAM UNIVERSITY
- 5 AUG 1982
SCIENCE LIBRARY

The copyright of this thesis rests with the author. No quotation from it should be published without his prior written consent and information derived from it should be acknowledged.

ELASTIC WAVE PROPAGATION IN EMBANKMENT DAMS

M.D. LINTON

Abstract

This study investigates the stresses produced in an embankment dam as a result of excitation due to elastic plane waves. A two dimensional finite element model is used to represent an embankment and its substructure.

The model uses a quadrilateral element, formed from triangles with a condensed internal node, which gives a better prediction of stress direction than a constant strain triangle. The equations of motion are assembled with lumped mass and damping matrices, and solved by direct integration using a fourth order Runge-Kutta algorithm. For time-steps in the range of stability this algorithm is shown to be accurate and easy to use. It is shown that the range of stability is considerably reduced with the inclusion of damping, and so damping was not included in the models studied.

Tests show that for a finite element grid to model elastic wave propagation it is essential for there to be at least eight elements per wavelength. If this requirement is violated the predicted stresses are seriously affected, and the results of previously published studies must be judged against this condition. The model grid is designed to meet this requirement for the propagation velocity typical of dam materials and the frequencies typical of seismic events.

Two models, (a) homogeneous and (b) layered, are excited by P and S waves at several angles. The consequent distortions of static stress distributions are varied, but exhibit conditions that could lead to failure by slumping or by tensional cracking close to the crest. The severity of the stresses was greater in the cases of (a) S-waves, (b) angled waves, (c) layered models.

The physical processes producing the stress distributions are examined. It is concluded that the stress distributions are dependent on the angle of incidence and are not capable of explanation in terms of natural modes of vibration only.

Acknowledgements

I wish to thank Dr. R.E. Long for the help and advice that he has given me as my supervisor for this thesis. Also my thanks go to other colleagues at Durham University for the many useful conversations I have had with them.

This research has been supported by a studentship awarded by the National Environmental Research Council to whom I am most grateful. Also I must thank the University of Technology, Lae, Papua New Guinea for a period of six months study leave which enabled me to commence my studies in Geophysics.

Finally, my thanks go to Elaine Hodgkinson for her invaluable help in producing the type script.

Contents

Chapter 1. Embankment dams and seismic waves : methods of study

1.1. Introduction

The prediction of the behaviour of a large dam when subjected to an earthquake is clearly of concern to the civil engineer. The serious consequences of the failure of a dam especially if situated close to a populated region, can hardly be exaggerated. For example it was felt necessary to evacuate temporarily some 80,000 people as a result of damage to the Lower San Fernando Dam after the earthquake there in 1971. However, considering the many thousands of dams that exist throughout the world, the number of reported failures of dams due to earthquake is very small (Haws and Reilly (1981)). It would appear that the designs used for large dams are inherently sound; but the engineer would be more confident in his decisions if the behaviour of large dams subject to earthquake could be analysed with some precision.

It is the aim of this study to provide some insight into the dynamic processes of seismic wave propagation on interaction with a structure typical of an embankment dam. This, it is hoped, will contribute to the engineers understanding of the forms of failure that might occur in a dam subject to a severe earthquake; but, as will be made clear in this study, in view of the many limitations that surround the method of analysis, the conclusions can only be regarded as suggestive of the nature of the processes involved and not as a definite analysis.

DURHAM UNIVERSITY
- 5 AUG 1982
SCIENCE LIBRARY

1.2. A possible subject division

There are two broad aspects to the problem of seismic interaction with large dams; one area concerns matters that are primarily seismological whilst the other deals with the dynamic response of a structure to excitation. If the problem is considered to be divided in this way, the aim of the seismologist's deliberations is to arrive at a record of a seismic event, which is to be used as the input for the structural engineer's analysis. This record might be of the form of an actual strong motion record, or a synthetically produced seismogram. For the engineer each of these contains its advantages. The strong motion record has the merit of being that of a true earthquake, containing all the fine detail that is characteristic of a seismic event. However it has the obvious disadvantage of being the record of the wrong event. To suppose that the record from another site (or even at the proposed site of a dam) will be a close approximation to a future event is not justified; though in the absence of other information this may be the best that the engineer can use for his design decisions. There is therefore good reason for attempting to predict the form of strong motion records directly from earthquake source models. Some of this work is reviewed in section 1.3.

This study falls into the second of the two divisions just proposed, in that it is an analysis of the dynamic response of a structure to a given disturbance. The methods that have been used for this kind of problem are reviewed in section 1.4.

1.3. Determination of strong ground motions

Attempts at finding an analytic solution for the ground motion from a given earthquake source began with the pioneering study of Lamb (1904). The problem is of considerable analytic difficulty, and such solutions that have been obtained apply only to simplified situations such as the displacement due to a moving point source in an infinite homogeneous space. The modelling of a simple fault was carried out by Aki (1968) for an infinite medium, and a comparison of several dislocation models and their resulting motions in an infinite medium, using the method of Aki, is the subject of the paper by Anderson and Richards (1975). An advance was made by Israel and Kovack (1977) by deriving a solution for an elastic half space; and more detailed numerical solutions were obtained by Bouchon (1980 a,b,) for both strike slip and dip slip faults.

These papers (and the many others that contribute to the same area of of study) reveal clearly that the difficulty of analysis and the complexity of the solutions. This complexity of grounds motions is shown on the papers of Bouchon (1980 a,b,), with graphical illustrations of components of displacement in three direction at the surface. In the case of a strike slip fault there are large amplitudes in both horizontal directions, whereas the dip slip fault has large amplitudes in the vertical component and that which is horizontally along the strike line of the fault.

A further point is well brought out in these papers, and in Murphy et.al. (1971) is the amplification of the ground motion if there is a surface layer of low velocity sediments. Also the effect of topography on surface motion has been studied by Bouchon (1973), Boore (1973) and Rodgers et.al. (1974), leading to the conclusion that ground amplification could also be caused by surface features such as mounds.

These results point to the need to consider the dynamic response of a structure in relation to its immediate surroundings, and indeed the papers cited above were motivated by the strong motion record of the San Fernando earthquake of 1971 which was made at the site of the Pacoima Dam. Besides providing one of the very few strong motion records taken at a dam site, it was especially notable for the high values of acceleration that were observed. One of the horizontal components recorded a value of 1.25g (Bouchon (1973)). Bouchon etc., concluded that this high value was in part due to the position of the seismometer which was at the top of a ridge alongside the dam.

Prior to the Pacoima record the most commonly used strong motion record for a standard was the El Centro earthquake of 1940. It was from a study of this record that Newmark (1965) took 0.6g as the maximum acceleration that needed to be accounted for in any design. This is now regarded as inadequate.

1.4. Response of dams to earthquakes

The simplest form of analysis of the response of a structure to a seismic event is a static one, in which the acceleration of the disturbance is replaced with an equivalent force. This method is given by Newmark (1965), and is used by him to explain various observed effects of earthquake, in particular the sliding of blocks along possible lines of failure.

A dynamic analysis of dams was given by Clough and Chopra (1966), using the finite element method. Of available numerical approaches this method has many attractions, especially its ability to model arbitary geometries and variations in materials. This study, too, uses the finite element method for those reasons, but certain workers have used finite difference methods for the solution of elastic wave propagation problems e.g. Ilan et al.(1979). However the finite element method has proved the most popular approach to wave propagation problems, whether they be seismic waves or some other form of wave.

An important feature of the method of Clough and Chopra is that the seismic disturbance is applied at all the nodes along the base of the embankment in the form of horizontal and vertical accelerations. The base is therefore a rigid surface, and so in this model there is no interaction between the embankment and the underlying soil or rock. Vibration problems which consist of an elastic body attached to a rigid surface with a prescribed motion are particularly suited to solution by the method of "mode superposition". This method was used by Clough and Chopra, but since it is not used in this study a description of the method is given in the next section.

1.5. The method of mode superposition

As will be shown in chapter 2 any finite element analysis of a dynamics problem leads, as a result of the discretisation that is uses, to a finite set of ordinary second order differential equations. These are written, using matrices, as

$$[M]\,[\ddot{q}] + [C]\,[\dot{q}] + [K]\,[q] = [Q(t)] \qquad 1.5.1.$$

In this equation the matrices $[M]$, $[C]$ and $[K]$ are determined respectively by the inertial, damping and elastic properties of the continuum being modelled. The vector $[q]$ has as its components the displacements of certain selected nodes in the continuum, and $[Q(t)]$ is a vector of specified loads (or displacements) acting at some or all of the nodes. The derivation of this equation is given in section 2.4.

Once equation 1.5.1 has been assembled the problem is to determine $[q]$, the unknown displacements, as a function of time. In this study this is done using a direct integration algorithm. The method of mode superposition is an alternative to this.

The key to the method is that there exists a matrix $[X]$, called the modal matrix, which can be used to decouple the equation set 1.5.1.

This matrix is found by solving the eigenvalue problem

$$[K][q] = \omega^2 [M][q] \qquad 1.5.2.$$

For n degrees of freedom this will give n eigenvalues ω_i^2, with corresponding eigenvectors $[q_i]$. The modal matrix is defined as the matrix of these eigenvectors, and so satisfies

$$[K][X] = [M][X][\Lambda]$$

where $[X] = [[q_1] \quad [q_2] \quad \cdots \quad [q_n]]$

and $$[\Lambda] = \begin{bmatrix} \omega_1^2 & & & \\ & \omega_2^2 & & \\ & & \ddots & \\ & & & \omega_n^2 \end{bmatrix}$$

It is then possible to show that (Desai and Abel (1972), pp 358-361, Zienkiewicz (1977) pp 545-546)

$$[X]^T [M][X] = [D] \qquad 1.5.3.$$

and $$[X]^T [K][X] = [D][\Lambda]$$

where $[D]$ is also a diagonal matrix. (Since the eigenvectors $[q_i]$ are not uniqueley determined, it is possible to normalise them in such a way that $[D]$ is the identity matrix).

In order to effect the uncoupling it is necessary to assume that the modal matrix diagonalises the damping matrix also. We therefore assume that

$$[X]^T [C] [X] = 2 [\Gamma] [W] [D] \qquad 1.5.4.$$

where $[W]^2 = [\Lambda]$ and

$$[\Gamma] = \begin{bmatrix} c_1 & & & \\ & c_2 & & \\ & & \ddots & \\ & & & c_n \end{bmatrix}$$

The elements of Γ are termed modal damping ratios, and most experimental data gives information on these, rather than the elements of $[C]$ (Desai and Abel (1972) p.359).

A change is now made to modal co-ordinates using

$$[q] = [X] [y] \qquad 1.5.5.$$

which, together with 1.5.3 and 1.5.4., transforms 1.5.1 to

$$[D][\ddot{y}] + 2[\Gamma][W][D][\dot{y}] + [D][\Lambda][y] = [X]^T [Q(t)] \qquad 1.5.6.$$

The coefficients of each of the terms on the left hand side are all diagonal matrices, and so the set of equations 1.5.6., is decoupled

into a set of n equations each of the form

$$\ddot{y}_i + 2 c_i \omega_i \dot{y}_i + \omega_i^2 y_i = \frac{p_i(t)}{d_i} \quad i=1,2,\ldots n \qquad 1.5.7.$$

where the d_i are the elements of $[D]$ and $p_i(t)$ is the ith element of the column vector $[X]^T [Q(t)]$. Each equation of 1.5.7. can be solved by standard methods.

The eigenvalues, ω_i, are the natural frequencies of vibration for the system described by equation 1.5.1. with zero right handside, and the corresponding eigenvectors $[q_i]$ are termed normal modes. Each equation of 1.5.7. therefore gives the response of the system to each normal mode. The exact solution to 1.5.1. is given by the solutions to 1.5.7. which are "superposed" using 1.5.5.

The primary disadvantage of this method from a numerical point of view lies in the solving of the eigenvalue problem 1.5.2., which can become quite prohibitive for a large number of degrees of freedom. This is partially circumvented by calculating only the normal modes corresponding to the lowest frequencies, and so solving only a few of the equations of 1.5.7. For instance in the analysis of Clough and Chopra (1966) the response of a system with 110 degrees of freedom is modelled with only 15 modes.

The shortcomings of truncating the number of modes is discussed

by Hansteen and Bell (1979). They report that if only the first few modes are used, then, even though it may be possible to obtain reasonable values for displacemnets, the stresses calculated from these displacements may be seriously in error. One of the causes of error is that only the first few components of the modal load vector, $[X]^T$ $[Q(t)]$, enter into the calculations. Hansteen and Bell discuss a method by which the static displacement due to the ignored components are included. They show, however, that this correction is only valid if all mode frequencies up to and including those frequencies of the forcing loads are used in the calculation. If this condition is not met then it is better not to use the correction at all.

1.6. The inclusion of substructure

The principle of failing of the method of mode superposition as originally applied was that it isolated the embankment dam from the underlying substructure. This means that such effects as the amplification of seismic waves by a layered geology, as discussed in section 1.3., are not included in the model. Another question that should be asked is to what problem are we really finding the solution? Since the base of the dam, which is the source of the motion, is kept rigid it must act as a reflecting surface for any waves that are generated inside the embankment, and after a short time a set of standing waves will be formed in the dam. When all the modes are superposed what is given is primarily a steady state

solution. This is not a fault of the mode superposition method as such - which, after all, is just a means of solving the equations 1.5.1. - but, since it is effectively a solution in the frequency domain rather than directly in the time domain, it does not draw attention to the way in which the wave initially propagates in the structure.

It is thus clear that a strict division between the seismological and engineering aspects, as given in section 2.2., is undesirable, and that for a better understanding of the response of a structure to a seismic event the substructure should be included as well. Substructure methods which analyse the motions of the structure and the underlying soil separately, together with certain conditions governing compatibility along the interface, have been proposed by Gutierrez and Chopra (1978), and Fedock and Schreyer (1981). Certain advantages of the mode superposition method are retained for the study of the structure, but these methods are best used for the study of structures which are rigid comparative to the underlying soil, as, for example, a nuclear power station.

The approach adopted in this study is to treat the structure and as much as possible of the underlying soil as a unified whole. The reflecting base to the embankment that was implicit in Clough and Chopra's original method is therefore transferred to a surface at some distance beneath the embankment. To do this the number of nodes has to be increased considerably, as is shown in detail in chapter 6,

but the finite element formulation still leads to a set of equations of the form of 1.5.1. It would be possible to solve this set by mode superposition, but there are two main reasons for not doing so. First, the eigenvalues obtained would give the natural frequencies of vibration for the whole region modelled, both embankment and substructure. It is to be expected that the frequencies of vibration that are pertinent to the motion of the embankment would be high compared to those of the substructure, and so for mode superposition to be realistic a large number of modes would be required. This inefficiency of mode superposition is recognised by Gutierrez and Chopra (1978). Second, since we are interested in the transient process of the effect of a propagating wave entering and then leaving an embankment, a method which is more directly in the time domain may make it easier to appreciate the physical changes that are taking place while the wave interacts with the structure. For these reasons the equations of motion are solved by a direct integration algorithm which allows us to study the displacements and stresses for as many time-steps as we wish. The algorithm is described in chapter 3.

1.7. Integrated studies

A fully integrated approach has been urged by Long (1981), in which the division of the problem suggested in 1.2. is not made. This would involve modelling, not only the embankment, but the earthquake source as well, and the interaction between the dam

and the substructure would automatically be included. Such a model would require, as well as knowledge of the materials of the dam and its surroundings, parameters concerning the rupture along a proposed fault line.

In so far as this study includes as much of the substructure as was possible it is a step towards an integrated model. The model used in this study has the facility to model the propagation of plane waves of either P or S type, which may enter the structure at various angles of incidence. In this way a range of possible inputs, each corresponding to different seismic events, can be explored. This enables conclusions to be drawn on how seismic waves in general are likely to affect embankments, rather than how an embankment responds to a particular earthquake of the past.

However this study does not go to the point where the source of elastic waves is included in the model. Furthermore, the need for a sufficiently fine mesh of elements to satisfactorily model any wave propagation, which is discussed in chapter 5, suggests that a finite element model which includes both the fault and its ruputre together with the embankment would be impracticable. In order to tie the two halves of the problem together it may be that an integration could be made of the analytic solutions to fault rupture, such as those discussed in 1.3., with a finite element model of the embankment and its immediate surroundings.

Chapter 2 The Finite element Method

2.1 Introduction

The contents of this chapter follow in the main the lines of Desai and Abel (1972).

An essential of the finite element method is the division of the region under consideration into a finite number of descrete elements, each of which is bounded by sides and nodes. The nodes are situated at the joins of sides, but may also be placed at some intermediate point of a side or somewhere inside the element. The displacement of any point inside the element is then determined from the displacements at the nodes of the element using what have been termed the shape functions for the elements and which depend only on its geometry. Thus in turn the strain energy and kinetic energy of each element may be determined from the displacements of the nodes. In this way we can write down an energy equation, or, as in the present case use Hamilton's principle since we have a dynamics problem, and use this to determine the nodal displacement-time history.

In order to show how this is put into practice we describe the necessary properties of shape functions in general and of the particular shape function that is required for the simple triangular element that forms the basis of this study.

If an element has nodal displacements $q_1, q_2, \ldots q_n$ then the shape functions $N_1, N_2, \ldots N_n$, are chosen so that the displacement $\underline{u}$ at a general point is given by

$$\underline{u} = N_1 \underline{q}_1 + N_2 \underline{q}_2 + \ldots + N_n \underline{q}_n$$

The functions N_1, N_2, etc. will be functions of position, so

$$N_i = N_i (x,y,z)$$

If $\underline{q}_i$ is the displacement at the node with position (x_i,y_i,z_i) then in order that $\underline{u} (x_i,y_i,z_i) = \underline{q}_i$ we choose the N_i such that

$$N_i (x_i,y_i,z_i) = 1$$

and $$N_j (x_i,y_i,z_i) = 0 \quad j \neq i$$

A further desirable property is that the displacements along an edge of an element should be the same as those calculated from the adjacent element. Such elements are called conforming elements and certainly would appear to model reality more closely than non-conforming elements. The elements will be conforming if the displacement at any point on a side is determined only by the nodes which lie on that side (since these nodes are in both the adjacent elements).

Two further criteria must be satisfied to ensure convergence (Zienkiewicz (1977), pp 32-34). These are that:

a) a rigid body displacement of the nodes should give a rigid body displacement throughout the element, and not produce any strain,

b) nodal displacements compatible with constant strain should in fact produce constant strain in each element.

It can be shown that if the elements are conforming and that the conditions (a) and (b) are met then the finite element formulation will be convergent, in the sense that if finer and finer subdivisions of the finite element net are used then the displacements so obtained will converge on the true solution.

2.2 Shape Functions for a triangle

In this study the basic element is the simplest possible of all possible 2-dimensional elements and it certainly meets the above convergence criteria. The element consists of a triangle with nodes at the vertices, and the displacement at any point in the triangle is found from the nodal displacements assuming a linear displacement model. This element is illustrated in Fig. 2.1.

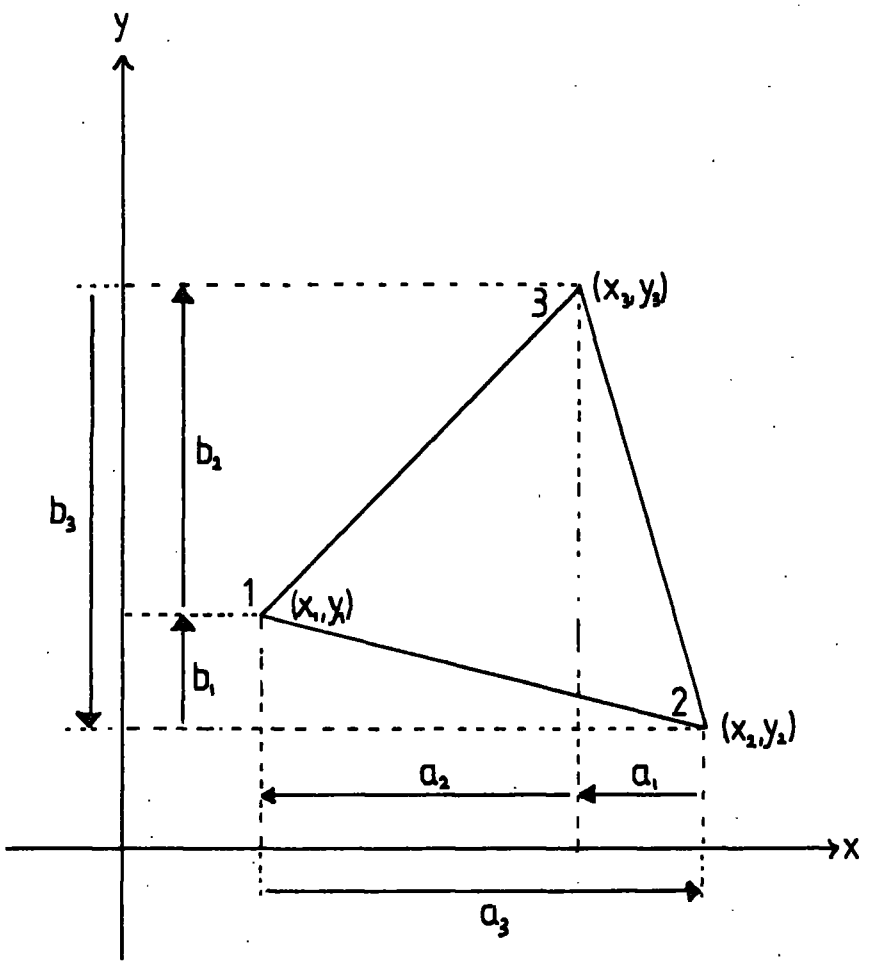

Fig. 2.1 Triangular element co-ordinates.

Let the co-ordinates of the nodes be (x_1,y_1), (x_2,y_2), (x_3,y_3), the displacements at these nodes be (u_1, v_1), (u_2,v_2), (u_3,v_3), and the displacements at an interior point (x,y) be (u,v). Then a linear displacement model assumes that there are constants $\alpha_1, \alpha_2,\alpha_3, \beta_1,\beta_2,\beta_3$ such that

$$u = \alpha_1 + \alpha_2 x + \alpha_3 y \quad \text{and} \quad v = \beta_1 + \beta_2 x + \beta_3 y$$

Since we know the x-displacements at the nodes, we can determine the values of α_1, α_2 and α_3.
In fact we can write

$$\begin{aligned} u_1 &= \alpha_1 + \alpha_2 x_1 + \alpha_3 y_1 \\ u_2 &= \alpha_1 + \alpha_2 x_2 + \alpha_3 y_2 \\ u_3 &= \alpha_1 + \alpha_2 x_3 + \alpha_3 y_3 \end{aligned}$$

or $$\begin{bmatrix} u_1 \\ u_2 \\ u_3 \end{bmatrix} = [A] \begin{bmatrix} \alpha_1 \\ \alpha_2 \\ \alpha_3 \end{bmatrix} \quad \text{where} \quad [A] = \begin{bmatrix} 1 & x_1 & y_1 \\ 1 & x_2 & y_2 \\ 1 & x_3 & y_3 \end{bmatrix}$$

and so $$\begin{bmatrix} \alpha_1 \\ \alpha_2 \\ \alpha_3 \end{bmatrix} = [A]^{-1} \begin{bmatrix} u_1 \\ u_2 \\ u_3 \end{bmatrix}$$

Therefore the displacement of an interior point can be written

$$u = [1 \; x \; y] \begin{bmatrix} \alpha_1 \\ \alpha_2 \\ \alpha_3 \end{bmatrix} = [1 \; x \; y] \; [A]^{-1} \begin{bmatrix} u_1 \\ u_2 \\ u_3 \end{bmatrix} \qquad 2.2.1$$

We are seeking shape functions, N_i, such that

$$u = N_1 u_1 + N_2 u_2 + N_3 u_3 = [N_1\ N_2\ N_3] \begin{bmatrix} u_1 \\ u_2 \\ u_3 \end{bmatrix} \qquad 2.2.2$$

Comparing 2.2.1 and 2.2.2, and using the fact that they must hold for any values of the nodal displacements u_i, we find that the shape functions are given by

$$[N_1\ N_2\ N_3] = [1\ x\ y]\,[A]^{-1} \qquad 2.2.3$$

It can be verified that

$$[A]^{-1} = \frac{1}{2A} \begin{bmatrix} x_2y_3 - x_3y_2 & x_3y_1 - x_1y_3 & x_1y_2 - x_2y_1 \\ b_1 & b_2 & b_3 \\ a_1 & a_2 & a_3 \end{bmatrix}$$

where $a_1 = x_3 - x_2$ $\quad b_1 = y_2 - y_3$

$a_2 = x_1 - x_3$ $\quad b_2 = y_3 - y_1$

$a_3 = x_2 - x_1$ $\quad b_3 = y_1 - y_2$

and $A = \frac{1}{2}\left|[A]\right| = \frac{1}{2}\,(a_3b_2 - a_2b_3)$ = area of triangle

Thus

$$
\begin{aligned}
N_1(x,y) &= \frac{1}{2A}\,(x_2y_3 - x_3y_2 + b_1x + a_1y) \\
N_2(x,y) &= \frac{1}{2A}\,(x_3y_1 - x_1y_3 + b_2x + a_2y) \\
N_3(x,y) &= \frac{1}{2A}\,(x_1y_2 - y_2y_1 + b_3x + a_3y)
\end{aligned}
\qquad 2.2.4
$$

It will be seen that

$$N_i(x_i,y_i) = 1$$

and $N_i(x_j,y_j) = 0 \quad i \neq j$ as required.

The y-displacements will yield exactly the same shape functions, and we can combine them with the x-displacements in the single matrix equation

$$\begin{bmatrix} u \\ v \end{bmatrix} = [N]\,[q]$$

where $[q] = \begin{bmatrix} u_1 \\ v_1 \\ u_2 \\ v_2 \\ u_3 \\ v_3 \end{bmatrix}$ and $[N] = \begin{bmatrix} N_1 & 0 & N_2 & 0 & N_3 & 0 \\ 0 & N_1 & 0 & N_2 & 0 & N_3 \end{bmatrix}$

2.3 Stress and strain for a finite element

The stress and strain at any point in a body are determined by the stress tensor σ_{ij} and the strain tensor e_{ij}. These are related by Hooke's law

$$\sigma_{ij} = \lambda e_{kk} \delta_{ij} + 2\mu e_{ij}$$

where λ and μ are Lame's constants, δ_{ij} is the Kroneker delta function and the summation convention is used. With this notation the strain energy density is given by

$$U = \tfrac{1}{2} \sigma_{ij} e_{ij}$$

Since σ_{ij} and e_{ij} are both symmetric, they have only six independent components, and we can rewrite U in the form

$$U = \tfrac{1}{2} [\sigma]^T [e] \qquad 2.3.1$$

where

$$[\sigma] = \begin{bmatrix} \sigma_{11} \\ \sigma_{22} \\ \sigma_{33} \\ \sigma_{12} \\ \sigma_{13} \\ \sigma_{23} \end{bmatrix} \quad \text{and} \quad [e] = \begin{bmatrix} e_{11} \\ e_{22} \\ e_{33} \\ 2e_{12} \\ 2e_{13} \\ 2e_{23} \end{bmatrix}$$

We can also write Hooke's law using $[\sigma]$ and $[e]$ in the form

$$[\sigma] = [D][e] \qquad 2.3.2$$

where

$$[D] = \begin{bmatrix} \lambda+2\mu & \lambda & \lambda & 0 & 0 & 0 \\ \lambda & \lambda+2\mu & \lambda & 0 & 0 & 0 \\ \lambda & \lambda & \lambda+2\mu & 0 & 0 & 0 \\ 0 & 0 & 0 & \mu & 0 & 0 \\ 0 & 0 & 0 & 0 & \mu & 0 \\ 0 & 0 & 0 & 0 & 0 & \mu \end{bmatrix}$$

In the 2-dimensional case of plane strain equation 2.3.2 reduces to the form

$$\begin{bmatrix} \sigma_{11} \\ \sigma_{22} \\ \sigma_{12} \end{bmatrix} = \begin{bmatrix} \lambda+2\mu & \lambda & 0 \\ \lambda & \lambda+2\mu & 0 \\ 0 & 0 & \mu \end{bmatrix} \begin{bmatrix} e_{11} \\ e_{22} \\ 2e_{12} \end{bmatrix} \qquad 2.3.3$$

The constitutive matrix $[D]$ can be rewritten using Young's modulus, E, and Poisson's ratio ν in which case it takes the form

$$[D] = \frac{E}{(1+\nu)(1-2\nu)} \begin{bmatrix} 1-\nu & \nu & 0 \\ \nu & 1-\nu & 0 \\ 0 & 0 & \frac{1}{2}(1-2\nu) \end{bmatrix} \qquad 2.3.4$$

The strain tensor is related to the displacements by the relation

$$e_{ij} = \frac{1}{2}\left(\frac{\partial u_i}{\partial x_j} + \frac{\partial u_j}{\partial x_i}\right)$$

which enables us to write, in the 2 dimensional case,

$$[e] = \begin{bmatrix} \frac{\partial u}{\partial x} \\ \\ \frac{\partial v}{\partial y} \\ \\ \frac{\partial u}{\partial y} + \frac{\partial v}{\partial x} \end{bmatrix} \qquad 2.3.5$$

Now, for the interior of a finite element,

$$\frac{\partial u}{\partial x} = \frac{\partial N_1}{\partial x} u_1 + \frac{\partial N_2}{\partial x} u_2 + \frac{\partial N_3}{\partial x} u_3$$

and $$\frac{\partial v}{\partial x} = \frac{\partial N_1}{\partial x} v_1 + \frac{\partial N_2}{\partial x} v_2 + \frac{\partial N}{\partial x} v_3$$

with similar equations for $\frac{\partial u}{\partial y}$ and $\frac{\partial v}{\partial y}$;

and so we have the relation

$$[e] = [B]\ [q] \qquad 2.3.6$$

where

$$[B] = \begin{bmatrix} \frac{\partial N_1}{\partial x} & 0 & \frac{\partial N_2}{\partial x} & 0 & \frac{\partial N_3}{\partial x} & 0 \\ 0 & \frac{\partial N_1}{\partial y} & 0 & \frac{\partial N_2}{\partial y} & 0 & \frac{\partial N_3}{\partial y} \\ \frac{\partial N_1}{\partial y} & \frac{\partial N_1}{\partial x} & \frac{\partial N_2}{\partial y} & \frac{\partial N_2}{\partial x} & \frac{\partial N_3}{\partial y} & \frac{\partial N_3}{\partial x} \end{bmatrix}$$

For the particular triangular element we are considering, the derviatives of the shape functions are particularly simple and we arrive at, using 2.2.4

$$[B] = \frac{1}{2A} \begin{bmatrix} b_1 & 0 & b_2 & 0 & b_3 & 0 \\ 0 & a_1 & 0 & a_2 & 0 & a_3 \\ a_1 & b_1 & a_2 & b_2 & a_3 & b_3 \end{bmatrix} \qquad 2.3.7$$

We see that in this case the strain matrix $[e]$ has constant components, and so this element is called a constant strain triangle (CST). However, for any element, there will be a relationship of the form $[e] = [B][q]$ where $[q]$ is the vector of nodal displacements, and $[B]$ is a matrix determined by derivatives of the shape functions for that element.

From equations 2.3.1., 2.3.2 and 2.3.6 we obtain

$$[\sigma] = [D][B][q] \qquad 2.3.8$$

and $U = \frac{1}{2} [q]^T [B]^T [D][B][q]$

remembering that $[D]^T = [D]$

2.4 Finite Element Formulation of the Equations of Motion

We are now in a position to determine the equation of motion of an element in terms of matrices $[B]$ and $[C]$, which we will do using Hamilton's principle. This requires the evaluation of the Lagrangian.

$$L = K - X + W$$

where K is the Kinetic energy, X is the strain energy and W is the work done by the applied loads. The following analysis is quite general and is not specific to the triangular element we were considering above.

If the body has a density ρ and occupies a volume V with displacements u_i throughout the body, then the Kinetic energy

$$K = \frac{1}{2} \int_V \rho \dot{u}_i \dot{u}_i \, dV$$

where the dot denotes differentiation with respect to time, and the integral is over the volume of the body (and the summation convention is in effect). The strain energy will be the integral of the strain energy density and so

$$X = \tfrac{1}{2} \int_V \sigma_{ij}\, e_{ij}\, dV$$

The work done by the applied loads is made up of two parts. The body forces F_i will have a contribution $\int_V F_i\, u_i\, dV$ and the surface tractions will have a contribution $\int_S {}^{n}\sigma_i\, u_i dS$

where ${}^{n}\sigma_i$ is the stress vector at the surface with respect to a plane perpendicular to the normal to the surface, and the integral is carried out over the surface S which bounds the volume V. Thus

$$L = \tfrac{1}{2}\int_V \rho \dot{u}_i\, \dot{u}_i\, dV - \tfrac{1}{2}\int_V \sigma_{ij}\, e_{ij}\, dV + \int_V F_i\, u_i\, dV + \int_S {}^{n}\sigma_i\, u_i\, dS$$

To rewrite this in matrix form we let

$$[u] = \begin{bmatrix} u_1 \\ u_2 \\ u_3 \end{bmatrix} \quad [F] = \begin{bmatrix} F_1 \\ F_2 \\ F_3 \end{bmatrix} \quad [T] = \begin{bmatrix} {}^{n}\sigma_1 \\ {}^{n}\sigma_2 \\ {}^{n}\sigma_3 \end{bmatrix}$$

and $[\sigma]$ and $[e]$ are defined in 2.3. Then

$$L = \tfrac{1}{2}\int_V \rho\, [\dot{u}]^{T} [u]\, dV - \tfrac{1}{2}\int_V [\sigma]^{T} [e]\, dV$$

$$+ \int_V [u]^{T} [F]\, dV + \int_S [u]^{T} [T]\, dS$$

Now $[u] = [N][q]$, $[e] = [B][q]$ and $[\sigma] = [D][e]$ as shown above. Substituting these in the equation for L leads to

$$L = \tfrac{1}{2}[\dot{q}]^T[M][q] - \tfrac{1}{2}[q]^T[K][q] + [q]^T[Q]$$

where $[M] = \int_V \rho[N]^T[N]\,dV$, $[K] = \int_V [B]^T[D][B]\,dV$

and $[Q] = \int_V [N]^T[F]\,dV + \int_S [N]^T[T]\,dS$

Hamilton's principle requires that we miminise the functional

$$\int_{t_1}^{t_2} L\,dt \qquad \text{where} \qquad L = L\,(t, [q], [\dot{q}]\,)$$

The theory of the calculus of variations shows that for this it is necessary that L satisfy the Euler equation

$$\frac{\partial L}{\partial [q]} - \frac{d}{dt}\left(\frac{\partial L}{\partial [\dot{q}]}\right) = 0$$

These terms are easily evaluated from the expression for L given above. Remembering that if x is a column vector, then

$$\frac{\partial}{\partial [x]}\left([x]^T[A][x]\right) = 2[A][x] \text{ and } \frac{\partial [x]^T}{\partial [x]} = [I]$$

Thus

$$\frac{\partial L}{\partial [q]} = -[K][q] + [Q] \quad \text{and} \quad \frac{\partial L}{\partial [\dot{q}]} = [M][\dot{q}]$$

and the Euler equation reduces to

$$[M][\ddot{q}] + [K][q] = [Q]$$

This is the equation of motion for an element and so strictly should be rewritten with a notation such as

$$[M_e][\ddot{q}_e] + [K_e][q_e] = [Q_e]$$

However if all the nodal degrees of freedom are numbered for the whole grid then $[q_e]$ can be expanded with the zeros to a $2n$ x 1 column vector, where N is the number of nodes with 2-degrees of freedom at each node. $[\ddot{q}_e]$ and $[Q_e]$ are expanded similarly, and $[M_e]$ and $[K_e]$ are expanded to $2n$ x $2n$ matrices. The equations of motion of each element can then be added together to give a single matrix equation of motion for the whole grid. The details of this assembly process are in any text on the finite element method, e.g. Desai and Abel (1972) pp. 183-188.

It is also possible to include in the above analysis the effect of frictional damping forces. If it is assumed that these are of a simple linear type proportional to velocity, then they produce additional forces per unit volume of $\mu\dot{u}$ (where μ is some constant).

It is shown by Zienkiewicz (1977) pp. 530-531 that this leads to an additional term in the equation of motion leading to final form

$$[M]\,[\ddot{q}] + [C]\,[\dot{q}] + [K]\,[q] = [Q] \qquad 2.4.1$$

The load vector $[Q]$ is evaluated from the applied loads $[F]$ and surface tractions $[T]$ using

$$[Q] = \int_V [N]^T [F]\, dV + \int_S [N]^T [T]\, dS \qquad 2.4.2$$

The stiffness matrix $[K]$ is determined by the element geometry and elastic properties by

$$[K] = \int_V [B]^T [D][B]\, dV \qquad 2.4.3$$

The matrices $[M]$ and $[C]$ have the forms

$$[M] = \int_V \rho[N]^T [N]\, dV \quad \text{and} \quad [C] = \int_V [N]^T [\mu][N]\, dV$$

and are often termed the consistent mass and consistent damping matrices respectively.

2.5 Consistent and lumped matrices for a constant strain triangle

In order to evaluate the expression $[M] = \int_V \rho\, [N]^T [N]\, dV$ for a constant strain triangular element it is easiest to use natural (or areal) co-ordinates.

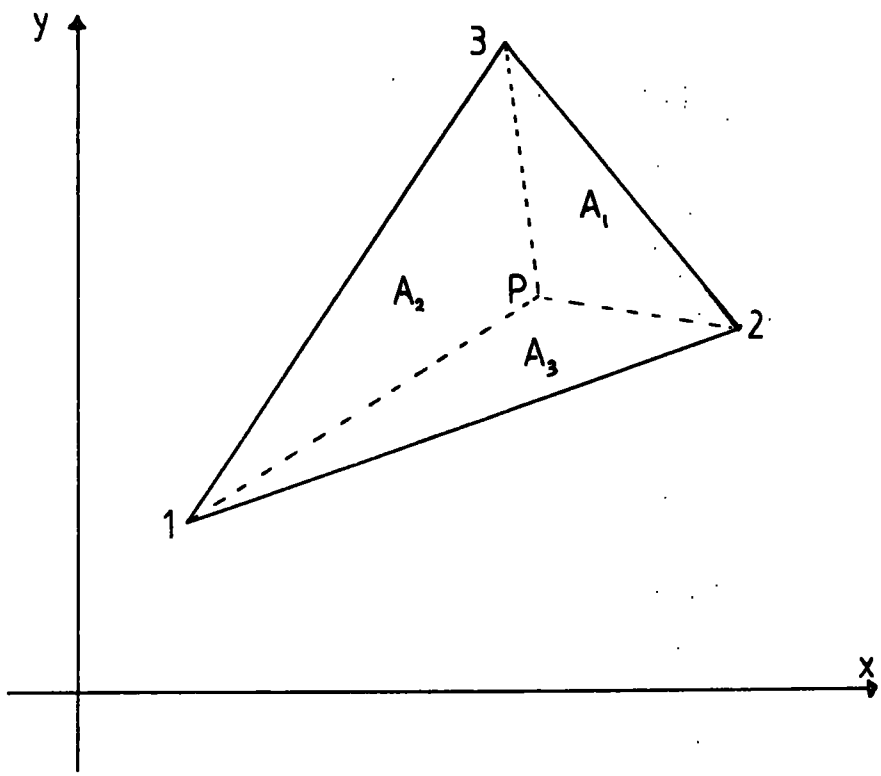

Fig 2.2 Natural co-ordinates for a triangle.

The triangular element has nodes $1,2,3$ with co-ordinates (x_1,y_1) (x_2,y_2), (x_3,y_3) and the co-ordinates of any interior point P are (x,y). The natural co-ordinates (L_1,L_2,L_3) of P are defined by

$$L_1 = \frac{A_1}{A}, \quad L_2 = \frac{A_2}{A}, \quad L_3 = \frac{A_3}{A}$$

where A_i is the area of the triangle made by P and the side jk, and A is the area of the element. This is shown in Fig. 2.2.

$L_1 = 1$ at node 1 and $L_1 = 0$ along side 23 and so the contours L_1 = constant are lines parallel to the side 23 varying linearly between the value 0 along 23, to the value 1 through node 1. Similar considerations apply to the contours of L_2 and L_3, which implies that the co-ordinates of P must be related to the co-ordinates of the nodes by the relations

$$x = L_1x_1 + L_2x_2 + L_3x_3$$
$$y = L_1y_1 + L_2y_2 + L_3y_3$$

These two relations, together with the obvious relation

$$L_1 + L_2 + L_3 = 1$$

can be written

$$\begin{bmatrix} 1 \\ x \\ y \end{bmatrix} = \begin{bmatrix} 1 & 1 & 1 \\ x_1 & x_2 & x_3 \\ y_1 & y_2 & y_3 \end{bmatrix} \begin{bmatrix} L_1 \\ L_2 \\ L_3 \end{bmatrix}$$

Taking the transpose of both sides yields

$$\begin{bmatrix} 1 & x & y \end{bmatrix} = \begin{bmatrix} L_1 & L_2 & L_3 \end{bmatrix} \begin{bmatrix} 1 & x_1 & y_1 \\ 1 & x_2 & y_2 \\ 1 & x_3 & y_3 \end{bmatrix}$$

It is seen that this equation has exactly the same form as equation 2.2.3 and so the equality of the natural co-ordinates and the shape functions N_1, N_2, N_3 is established.

The advantage of the natural co-ordinates is that we can use the following integration formula (Eisenberg M.A. & Malvern L.E.(1973)) :-

$$\int_A L_1^a L_2^b L_3^c \, dA = \frac{2A a!b!c!}{(a+b+c+2)!} \qquad 2.5.1$$

where a, b, c are non-negative integers, and the integration is over the area of the triangle.

Thus for a triangle of constant density ρ and thickness h

$$[M] = \rho h \int_A [N]^T [N] \, dA$$

$$= \rho h \int_A \begin{bmatrix} L_1 & 0 \\ 0 & L_1 \\ L_2 & 0 \\ 0 & L_2 \\ L_3 & 0 \\ 0 & L_3 \end{bmatrix} \begin{bmatrix} L_1 & 0 & L_2 & 0 & L_3 & 0 \\ 0 & L_1 & 0 & L_2 & 0 & L_3 \end{bmatrix} dA$$

Using $N_i = L_i$

Use of 2.5.1 gives

$$[M] = \frac{\rho h A}{12} \begin{bmatrix} 2 & 0 & 1 & 0 & 1 & 0 \\ 0 & 2 & 0 & 1 & 0 & 1 \\ 1 & 0 & 2 & 0 & 1 & 0 \\ 0 & 1 & 0 & 2 & 0 & 1 \\ 1 & 0 & 1 & 0 & 2 & 0 \\ 0 & 1 & 0 & 1 & 0 & 2 \end{bmatrix}$$

This, then is the consistent mass matrix for a constant strain triangle.

An alternative approach, but without the theoretical justification of the above method, is to use for the N_i not the true shape functions for this element, but functions

ψ_i which are defined as equal to *1* over a part of the element adjacent to node i, and equal to *0* elsewhere. If the parts chosen are non-overlapping thirds of the triangular element then

$$\int_V \rho \psi_i \psi_j \, dV = \begin{cases} \frac{\rho h A}{3} & i = j \\ 0 & i \neq j \end{cases}$$

This then leads to a mass matrix

$$[M] = \frac{\rho h A}{3} \begin{bmatrix} 1 & 0 & 0 & 0 & 0 & 0 \\ 0 & 1 & 0 & 0 & 0 & 0 \\ 0 & 0 & 1 & 0 & 0 & 0 \\ 0 & 0 & 0 & 1 & 0 & 0 \\ 0 & 0 & 0 & 0 & 1 & 0 \\ 0 & 0 & 0 & 0 & 0 & 1 \end{bmatrix}$$

This matrix has effectively placed *1/3* of the mass of the element at each of its nodes, and accordingly is called the lumped mass matrix. The fact that it is diagonal commends if for numerical work, but such a matrix does not seem to reflect the continuous distribution of matter that actually exists. However Zienkiewicz (1977) p. 531 writes

> "Many practitioners are today using such [i.e. lumped] matrices exclusively showing often an improvement of accuracy"

and again on pp. 536-37 writes

> "Thus any lumping which preserves the total mass will lead to convergent results. Key... and others have experimented successfully with various procedures which give not only acceptable

but often improved results over those attainable with consistent mass matrices".

Accordingly, this study uses lumped mass matrices rather than consistent ones.

The question of how best to evaluate the damping matrix is even more uncertain. What values should be given to the damping coefficients $[\mu]$ are not known (Zienkiewicz (1977) p. 532). Certain schemes, such as chosing $[C] = \alpha[M] + \beta[K]$ with α,β determined empirically, have been tried. In this study, however, in view of the premium on computer storage space it was decided that provision would be made only for a lumped damping matrix. As will be detailed in Appendix A the stiffness matrix $[K]$ is of banded form and does not require the storage space that might have been at first envisaged. Thus a grid with 1000 nodes has 2000 degrees of freedom, and would seem to imply a stiffness matrix of 2000x 2000. In practice this needs to be only 2000 x bandwidth, where the bandwidth might typically be 100. If the consistent forms of $[M]$ and $[C]$ were to be used, then these would be banded in the same way as $[K]$ and require identical storage space. It can thus be appreciated that using the lumped forms,requiring as it does only a storage space of 2000, not only keeps the storage down to almost a third of what it would have been but also in consequence reduces the time spent in any operation involving these matrices by a factor of the order of the bandwidth (i.e. about 100).

2.6 Formulation of stiffness matrix for grid elements

The stiffness matrix for an element is found from equation 2.4.3,

$$[K] = \int_V [B]^T [D][B]\, dV$$

For a constant strain triangle, the matrices $[B]$ and $[D]$ are both constant throughout the element, and so

$[K] = Ah\,[B]^T[D][B]$ where h is the element thickness

$$= \frac{hE}{4A(1+\nu)(1-2\nu)} \begin{bmatrix} b_1 & 0 & a_1 \\ 0 & a_1 & b_1 \\ b_2 & 0 & a_2 \\ 0 & a_2 & b_2 \\ b_3 & 0 & a_3 \\ 0 & a_3 & b_3 \end{bmatrix} \begin{bmatrix} 1-\nu & \nu & 0 \\ \nu & 1-\nu & 0 \\ 0 & 0 & \tfrac{1}{2}(1-2\nu) \end{bmatrix} \begin{bmatrix} b_1 & 0 & b_2 & 0 & b_3 & 0 \\ 0 & a_1 & 0 & a_2 & 0 & a_3 \\ a_1 & b_1 & a_2 & b_2 & a_3 & b_3 \end{bmatrix} \qquad 2.6.1$$

using equations 2.3.4 and 2.3.7.

It will be seen that since $[D]$ is symmetric, $[K]$ will be a 6×6 symmetric matrix.

In order to provide more flexibility in the construction of the grids the finite element program used also accepts quadrilateral elements. These elements are however composed of four constant strain triangles formed by the four vertices of the quadrilateral together with a common vertex at the centroid of the quadrilateral. This added internal node

is then eliminated by a process known as condensation, which is explained below. Another important advantage of using quadrilateral elements is that it eliminates an arbitary skew in the results which tends to occur when only triangles are used, particularly if they all slope in the same direction.

2.7. Condensation of an internal node

If an element has loads $[Q]$ acting at its nodes, producing equilibrium displacements of $[q]$, then these will be related by

$$[K]\,[q] = [Q]$$

where $[K]$ is the stiffness matrix. (If there are 2 degrees of freedom at each node, and there are n nodes, then $[K]$ is $2n$ x $2n$ and $[q]$ and $[Q]$ are each $2n$ x 1).

Let this matrix equation be partitioned as follows

$$\begin{bmatrix} [K_{11}] & [K_{12}] \\ [K_{22}] & [K_{22}] \end{bmatrix} \begin{bmatrix} [q_1] \\ [q_2] \end{bmatrix} = \begin{bmatrix} [Q_1] \\ [Q_2] \end{bmatrix} \qquad 2.7.1$$

where $[K_{11}]$ is now p x p and $[K_{22}]$ is r x r $(p + r = 2n)$; $[q_1]$ and $[Q_1]$ are p x 1; $[q_2]$ and $[Q_2]$ are r x 1. Also we can imagine that the rows have been ordered so that the displacements $[q_2]$ are those belonging to the node (or nodes) that we wish to eliminate.

It is straight forward to verify that

$$\begin{bmatrix} [K_{11}] & [K_{12}] \\ [K_{21}] & [K_{22}] \end{bmatrix}^{-1} = \begin{bmatrix} [P]^{-1} & [P]^{-1}\,[K_{12}]\,[K_{22}]^{-1} \\ -[K_{22}]^{-1}\,[K_{22}]\,[P]^{-1} & [K_{22}]^{-1}([I] + [K_{22}][P]^{-1}[K_{12}][K_{12}]^{-1}) \end{bmatrix}$$

where $[P] = [K_{11}] - [K_{12}]\,[K_{22}]^{-1}\,[K_{21}]$

assuming that all appropriate matrices are non-singular.

Thus equation 2.7.1 can be solved as

$$[q_1] = [P]^{-1}[Q_1] - [P]^{-1}\,[K_{12}]\,[K_{22}]^{-1}\,[Q_2]$$

$$[q_2] = -[K_{22}]^{-1}\,[K_{21}][P]^{-1}\,[Q_1] + [K_{22}]^{-1}([I] + K_{22}]\,P]^{-1}\,[K_{12}][K_{22}]^{-1})[Q_2]$$

The first of these can be written

$$([K_{11}] - [K_{12}]\,[K_{22}]^{-1}\,[K_{21}])[q_1] = [Q_1] - [K_{12}][K_{22}]^{-1}\,[Q_2]$$

and it will be seen that this has the form

$$[\bar{K}][\bar{q}] = [\bar{Q}] \qquad 2.7.2$$

with
$$[\bar{q}] = [q_1]$$
$$[\bar{K}] = [K_{11}] - [K_{12}] [K_{22}]^{-1} [K_{21}]$$
$$[\bar{Q}] = [Q_1] - [K_{12}] [K_{22}]^{-1} [Q_2] \qquad 2.7.3$$

These equations determine the displacements of the nodes of the element except for those at the nodes we wish to eliminate, and it tells us how to form the appropriate modifications to the stiffness matrix and load vector. It will be noticed that if m nodes are eliminated by this method then, as expected, $[\bar{K}]$ is $2(n-m)$ x $2(n-m)$ and $[\bar{q}]$ and $[\bar{Q}]$ are each $2(n-m)$ x 1.

For most applications the nodes that are to be eliminated are internal nodes and do not have any loads, and so $[Q_2] = 0$ and the modified load vector just consists of the vector of loads at the nodes not eliminated. Also, when $[Q_2] = 0$ the displacements of the eliminated nodes are given by

$$\begin{aligned}[q_2] &= -[K_{22}]^{-1} [K_{21}] [P]^{-1} [Q_1] \\ &= -[K_{22}]^{-1} [K_{21}] [q_1]\end{aligned} \qquad 2.7.4$$

The following procedure is thus adopted to form the stiffness matrix of a quadrilateral element.

First, its centroid is calculated from the co-ordinates of its vertices, splitting the element into four triangles.

Second, the stiffness matrix of each triangle *(6 x 6)* is found using equation 2.6.1.

Third, the four matrices found so far are assembled into a *10 x 10* matrix, being the stiffness matrix of the quadrilateral including the node at the centroid.

Fourth, the modified stiffness matrix $[\bar{K}]$, *(8 x 8)* is found using equation 2.7.3.

Fifth, the modified stiffness matrices for each quadilateral element, together with the stiffness of any triangular elements, are all assembled to give the global stiffness matrix of the grid.

2.8. Note on the centroid of a quadrilateral

In the computer code published in Desai & Abel (1972) p.453 the centroid is calculated using $\frac{1}{4}(\underline{r}_1 + \underline{r}_2 + \underline{r}_3 + \underline{r}_4)$ where the position vector of vertex i is given by $\underline{r}_i$. This is however incorrect (as can be seen from the special case $\underline{r}_3 = \underline{r}_4$ which should reduce to a triangle). This error is not of great importance since there is no necessity for the internal node to be the centroid; however, by choosing the true centroid the triangular elements formed are less obtuse and there should be some improvement in accuracy (at least no

loss). So the program used in this study does calculate the true centroid, which can be shown to be given by

$$\underline{\bar{r}} = 1/3\ (\underline{r}_1 + \underline{r}_2 + \underline{r}_3 + \underline{r}_4 - \underline{r}_5)$$

where $\underline{r}_1$ to $\underline{r}_4$ are the position vectors of the vertices, and $\underline{r}_5$ is that of the intersection of the diagonals. $\underline{r}_5$ is determined from $\underline{r}_1$ to $\underline{r}_4$, and a little algebra gives the following formulas, which are convenient for computation.

$$\bar{x} = \frac{\sum_{i=1}^{4} y_i(x_j - x_l)\ (x_l + x_i + x_j)}{3\sum_{i=1}^{4} y_i(x_j - x_l)} \qquad \bar{y} = \frac{\sum_{i=1}^{4} x_i(y_j - y_l)(y_l + y_i + y_j)}{3\sum_{i=1}^{4} x_i(y_j - y_l)}$$

where $\underline{\bar{r}} = (\bar{x}, \bar{y})$, $\underline{r}_i = (x_i, y_i)$

and i,j,k,l are assumed to be in cyclic order $1,2,3,4$.

2.9 Calculation of load vector for an element

The load vector is given by equation 2.4.2

$$[Q] = \int_V [N]^T [F]\, dV + \int_S [N]^T [T]\, dS$$

There are four special cases which will be of use in this study, which will now be considered separately.

a) The loads consist of concentrated forces applied directly at the nodes. The above equation is not really needed in this case since what we are given are the components of Q that we seek.

b) The loads consist of the gravitational force on each element. Thus for a *CST* equation 2.4.2 will have the form

$$[Q] = \int_V [N]^T \begin{bmatrix} 0 \\ -\rho g \end{bmatrix} dV$$

$$= -h\rho g \int_A \begin{bmatrix} L_1 & 0 \\ 0 & L_1 \\ L_2 & 0 \\ 0 & L_2 \\ L_3 & 0 \\ 0 & L_3 \end{bmatrix} \begin{bmatrix} 0 \\ 1 \end{bmatrix} dA$$

where h is the thickness of the triangle, A is area, and L_1 etc. are the natural co-ordinates introduced in section 2.5. The integration is performed using 2.5.1., giving

$$[Q] = \frac{-h\rho gA}{3} \begin{bmatrix} 0 \\ 1 \\ 0 \\ 1 \\ 0 \\ 1 \end{bmatrix}$$

c) The sides of the element have a surface traction, which varies linearly along the side.

Consider the *CST* in Fig. 2.3 with a traction along side *23* (the other sides being free)

Using natural co-ordinates, we note that on side *23* $L_1 = 0$ and $L_3 = 1 - L_2$, with $L_2 = 0$ at node *3* and $L_2 = 1$ at node *2*. If l is measured along *23* from node *3* and s is the length of this side then $l = L_2 s$ and $dl = s dL_2$. Equation 2.4.2 thus has the form

$$[Q] = hs \int_0^1 [N]^T [T] \, dL_2 \qquad 2.9.1$$

If the stress vector at node *3* is $\begin{bmatrix} p_x \\ p_y \end{bmatrix}$ and at node *2* is $\begin{bmatrix} q_x \\ q_y \end{bmatrix}$ then the assumption of a linearly varying traction gives

$$[T] = \begin{bmatrix} p_x \\ p_y \end{bmatrix} + L_2 \begin{bmatrix} q_x - p_x \\ q_y \quad p_y \end{bmatrix} \qquad 2.9.2$$

$$\text{Also } [N]^T = \begin{bmatrix} 0 & 0 \\ 0 & 0 \\ L_2 & 0 \\ 0 & L_2 \\ 1-L_2 & 0 \\ 0 & 1-L_2 \end{bmatrix} \qquad 2.9.3$$

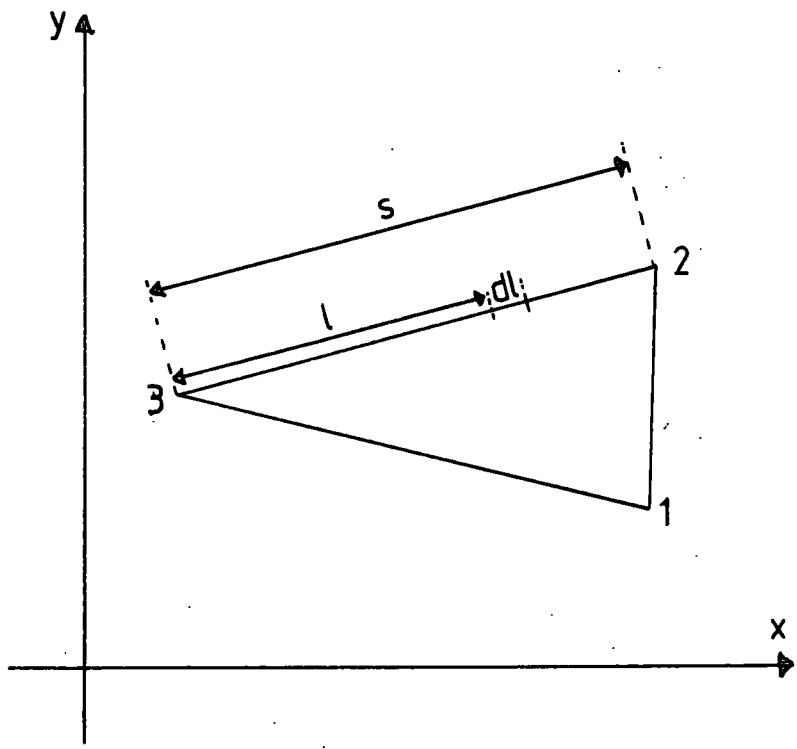

Fig 2.3

Substituting 2.9.2 and 2.9.3 into 2.9.1. and carrying out the integrations gives

$$[Q] = \frac{hs}{6}\begin{bmatrix} 0 \\ 0 \\ p_x + 2q_x \\ p_y + 2q_y \\ 2p_x + q_x \\ 2p_y + q_y \end{bmatrix} \qquad (2.9.4)$$

The above load vector is that produced by a traction along side 23 only. If there were tractions along the other sides then each of these would give a corresponding load vector, and the three vectors would have to be added to give the load vector for that element. The final contribution to the load vector for the whole grid for a particular node will, of course, be the sum of all the contributions to that node that any element containing that node makes.

d) Hydrostatic pressure. This is just a special case of (c).

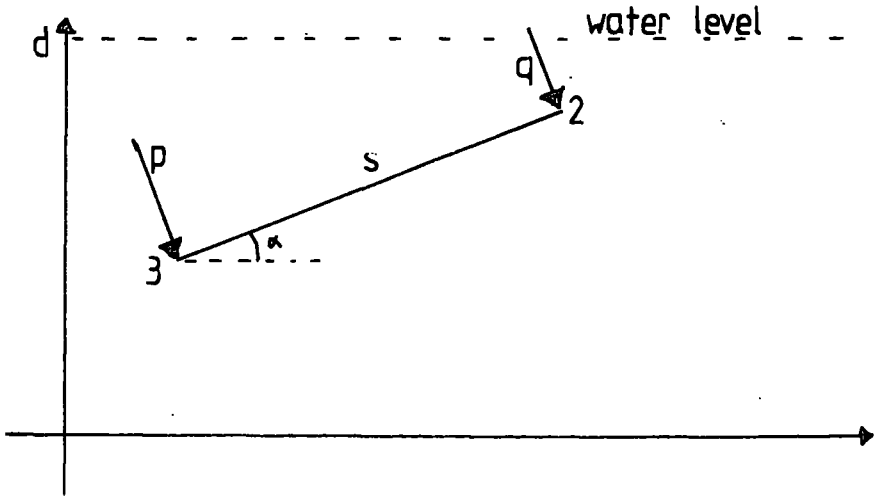

Fig 2.4

Let the side 23 be inclined at angle α (see Fig. 2.4). The stress vector due to the hydrostatic pressure will be normal to the side, and let it have magnitude p at node 3 and q at node 2. If the water surface is at $y=d$, and the co-ordinates of nodes 2 and 3 are (x_2,y_2), (x_3,y_3), then

$$p = (d - y_3)\rho g \qquad q = (d-y_2)\rho g$$

$$p_x = \rho \sin \alpha \qquad q_x = q \sin \alpha$$

$$p_y = - \rho \cos \alpha \qquad q_y = -q \cos \alpha$$

$$\sin \alpha = (y_2 - y_3)/s \qquad \cos \alpha = (x_2 - x_3)/s$$

Thus, using 2.9.4, we obtain for the contribution to the load vector for node 2 due to the hydrostatic pressure over side 23

$$(3d - y_3 - 2y_2) \frac{\rho g h}{6} \begin{bmatrix} y_2 - y_3 \\ x_3 - x_2 \end{bmatrix}$$

Similarly the contribution for node 3.3 is

$$(3d - y_2 - 2y_3) \frac{\rho g h}{6} \begin{bmatrix} y_2 - y_3 \\ x_3 - x_2 \end{bmatrix}$$

2.10 Calculation of stress in a quadrilateral element

Fig. 2.5. shows a general quadrilateral element.

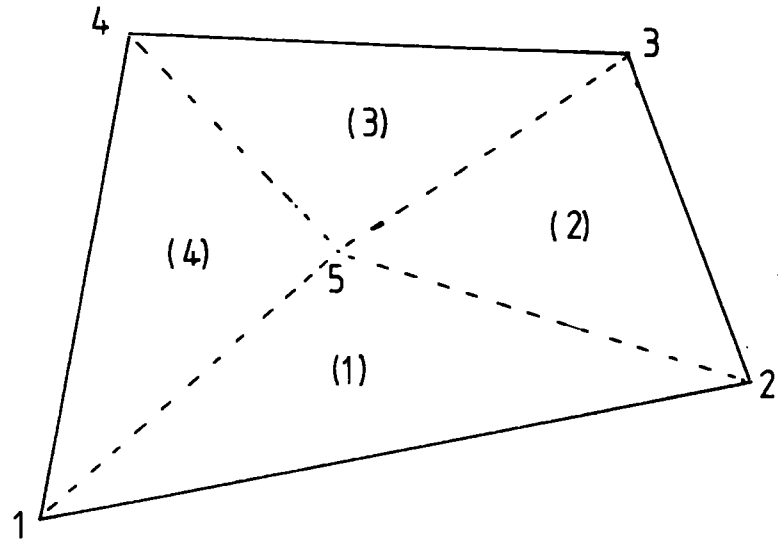

Fig 2.5 Quadrilateral element.

If the displacements at the vertex nodes, $1,2,3,4$, have been calculated by solving the equations of motion 2.4.1 then the displacement of the "condensed" node 5 is found using equation 2.7.4. The stress of each of the four constituent *CST's* can then be found using equation 2.3.8. Thus the stress of element (1) is

$$[\sigma_1] = [D] \begin{bmatrix} \beta_1^1 & 0 & \beta_2^1 & 0 & \beta_3^1 & 0 \\ 0 & \alpha_1^1 & 0 & \alpha_2^1 & 0 & \alpha_3^1 \\ \alpha_1^1 & \beta_1^1 & \alpha_2^1 & \beta_2^1 & \alpha_3^1 & \beta_3^1 \end{bmatrix} \begin{bmatrix} q_1 \\ q_2 \\ q_3 \\ q_4 \\ q_9 \\ q_{10} \end{bmatrix} \qquad 2.10.1$$

where D is the consitutive matrix (2.3.4), and B of 2.3.7 has been written with α_i^1 for $a_i/2A$ and β_i^1 for $b_i/2A$. (The superscript is to indicate element 1). Also the displacement of node j is given as $\begin{bmatrix} q_{2j-1} \\ q_{2j} \end{bmatrix}$

The stress for the whole element is then taken to be the average over the constituent *CST's*.

$$[\sigma] = \tfrac{1}{4}([\sigma_1] + [\sigma_2] + [\sigma_3] + [\sigma_4]) \qquad 2.10.1$$

For the purpose of computation this is found by expanding the [B] matrix of 2.10.1 into a *3* x *10* matrix, and the displacement vector a *1* x *10* column vector consisting of the displacements at all five nodes. The four stresses of 2.10.1 can now be easily added together to give

$$[\sigma] = \tfrac{1}{4} [D][G][q]$$

where

$$[G] = \begin{bmatrix} \beta_1^1+\beta_2^4 & 0 & \beta_2^1+\beta_1^2 & 0 & \beta_2^2+\beta_1^3 & 0 & \beta_1^4+\beta_2^3 & 0 & \beta_3^1+\beta_3^2+\beta_3^3+\beta_3^4 & 0 \\ 0 & \alpha_1^1+\alpha_2^4 & 0 & \alpha_2^1+\alpha_1^2 & 0 & \alpha_2^2+\alpha_1^3 & 0 & \alpha_1^4+\alpha_2^3 & 0 & \alpha_3^1+\alpha_3^2+\alpha_3^3+\alpha_3^4 \\ \alpha_1^1+\alpha_2^4 & \beta_1^1+\beta_2^4 & \alpha_2^1+\alpha_1^2 & \beta_2^1+\beta_1^2 & \alpha_2^2+\alpha_1^3 & \beta_2^2+\beta_1^3 & \alpha_1^4+\alpha_2^3 & \beta_1^4+\beta_2^3 & \alpha_3^1+\alpha_3^2+\alpha_3^3+\alpha_3^4 & \beta_3^1+\beta_3^2+\beta_3^3+\beta_3^4 \end{bmatrix}$$

and $[q]^T = [q_1\ q_2\ q_3\ q_4\ q_5\ q_6\ q_7\ q_8\ q_9\ q_{10}]$

This method of calculating the stresses clearly has a certain smoothing effect, and it is found to give consistent directions for the principle stresses over a grid, eliminating the skewness in direction produced by a grid of triangles only (as evident for example in Mithen (1980) Figs. 4.3 and 4.4.). Some trials carried out by

G.D. Waghorn (private communication) indicate that quadrilateral elements as used here give displacements and stresses very close to those given by six-noded triangular elements using quadratic shape functions.

Chapter 3. Integration of the equations of motion

3.1 Introduction

The finite element formulation of the dynamic behaviour of an elastic continuum has the effect of reducing the solution of a partial differential equation to the solution of a set of ordinary second order differential equations, namely the set 2.4.1 derived in the previous chapter:-

$$[M][\ddot{q}] + [C][\dot{q}] + [K][q] = [Q(t)] \qquad 3.1.1.$$

The matrices $[M]$, $[C]$ and $[K]$ are determined by the properties of the grid, and $[Q(t)]$ is the given time history of the applied loads. For a static problem the first two terms of the equation vanish and the solution consists of inverting $[K]$, or some equivalent procedure. Other than numerical rounding errors this can be done exactly, and so with due computing care a solution of required accuracy can be found. The errors in a static problem thus lie in the finite element formulation rather than its solution. With the dynamic problem we are however faced with the difficulty of being unable to give an exact solution to a set such as 3.1.1 (unless it happens to be a very small set and the elements of $[Q(t)]$ are simple functions). Some numerical method, with its own inherent inaccuracies, has to be adopted for the solution of equation 3.1.1.

3.2. Choice of Method

There is a considerable literature concerning the time integration schemes that are in current use. See, for instance the references at the end of chapter 21. Zienkiewicz (1977) or the bibliography given in Zienkiewicz (1980?). An elegant method of deriving such schemes is given by Zienkiewicz (1977) p 570-593, giving as special cases certain well known methods such as those known by the names of Newmark, Houbolt and Wilson-θ. Methods may differ in that they are explicit or implicit, unconditionally stable or conditionally stable, single-step or multi-step. In an explicit algorithm the values at the new time-step can be found by a single calculation rather than by the solution of a set of simultaneous equations as in an implicit method. However all explicit methods are conditionally stable (that is,if a time-step greater than a certain critical value is used then the values diverge), but certain implicit methods are unconditionally stable. A single-step method requires values at the previous time value only, whereas multi-step methods require values at several previous time-steps. It may be possible to give an algorithm in two equivalent forms, one of which is single-step and the other multi-step, as shown in Wood (1981) where the Newmark method is given in both single-step and two-step forms.

Some writers consider unconditional stability all important; for instance Brusu & Nigro (1980) state "In order to filter the high frequency modal contributions out of the solution, unconditionally stable methods must be used". This same paper, however, compares the results of a new method proposed by its authors with the Wilson-θ

method, Houlbolt's method and the trapezoidal rule by testing the single equation

$$\ddot{y} + y = 2 \qquad y(0) = 3 \quad \dot{y}(0) = 0.$$

Their results are given in Fig 3.1, which are for a time-step of $\pi/6$, and show the predictions of the various methods and the exact solution for the range 36 to 48 time-steps. It will be seen that all the methods suffer to varying degrees amplitude loss, and, with the exception of the method proposed by Brusu and Nigro, phase shift as well. When the Runge-Kutta algorithm, described in section 3.3, was used on this same initial value problem using the same time-step the predictions of the algorithm were indistinguishable from the exact solution of $y = 2 + \cos t$ over the time-step range of Fig 3.1. In fact the exact solution and the Runge-Kutta prediction differed by only 10^{-3} after 72 time-steps.

In this study an explicit Runge-Kutta procedure is used, to eliminate the long calculations that would be required with an implicit scheme. It also has the advantage of being single step and so only requiring the initial values in order to start. Runge-Kutta methods do not appear to be widely discussed in the journals covering structural dynamics, but such a method was used by W.D. Smith (1975). This method was selected after some preliminary trials, and comparisons with some unpromising results using the version of the Wilson-θ procedure as given by Desai and Abel (1972) pp 25-26.

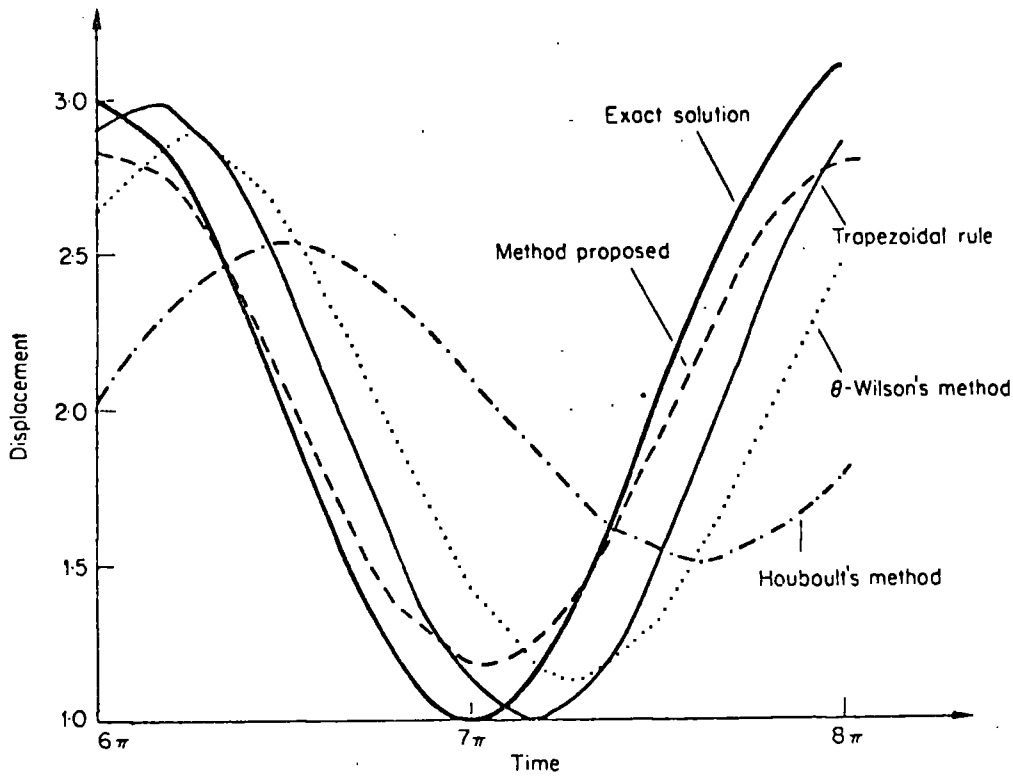

Fig. 3.1 Accuracy of different integration schemes.
"Method proposed" is that of Brusu and Nigro.
The exact solution and the Runge-Kutta algorithm are indistinguishable.
From Brusu and Nigro (1980).

3.3. The Runge-Kutta algorithm

By letting $[\dot{q}] = [s]$ the set of equations 3.1.1 can be rewritten as a set of first order equations:-

$$\begin{aligned} [\dot{q}] &= [s] \\ [\dot{s}] &= [M]^{-1}\left([Q(t)] - [C][s] - [K][q] \right) \end{aligned} \qquad 3.3.1$$

The algorithm calculates $[q(t+h)]$ and $[s(t+h)]$ given the values $[q(t)]$ and $[s(t)]$ for a given time-step of length h. In otherwords it advances our knowledge of position and velocity one time-step at a time. The routine is a fourth order one (in that it is equivalent to using a Taylor series up to terms in h^4), and is taken from Fox and Mayers (1968) p 202, except that the single variables are replaced with the vectors $[q]$ and $[s]$.

It is first necessary to compute eight subsidiary vectors:-

$$[\Delta_1] = h[s(t)]$$

$$[\Gamma_1] = h[M]^{-1}\left([Q(t)] - [C][s(t)] - [K][q(t)] \right)$$

$$[\Delta_2] = h\left([s(t)] + \tfrac{1}{2}[\Gamma_1]\right)$$

$$[\Gamma_2] = h[M]^{-1}\left\{ [Q(t+\tfrac{h}{2})] - [C]\left([s(t)] + \tfrac{1}{2}[\Gamma_1]\right) - [K]\left([q(t)] + \tfrac{1}{2}[\Delta_1]\right)\right\}$$

$$[\Delta_3] = h\left([s(t)] + \tfrac{1}{2}[\Gamma_2]\right)$$

$$[\Gamma_3] = h[M]^{-1}\left\{ [Q(t+\tfrac{h}{2})] - [C]\left([s(t)] + \tfrac{1}{2}[\Gamma_2] - [K]\left([q(t)] + \tfrac{1}{2}[\Delta_2]\right)\right)\right\}$$

$$[\Delta_4] = h\left([s(t)] + \tfrac{1}{2}[\Gamma_3]\right)$$

$$[\Gamma_4] = h[M]^{-1}\left\{ [Q(t+h)] - [C]\left([s(t)] + [\Gamma_3] - [K]\left([q(t)] + [\Delta_3]\right)\right)\right\}$$

The values of $[q(t+h)]$ and $[\dot{q}(t+h)]$ are given by

$$[q(t+h)] = [q(t)] + \frac{1}{6}([\Delta_1] + 2[\Delta_2] + 2[\Delta_3] + [\Delta_4])$$

$$[\dot{q}(t+h)] = s(t+h)] = [\dot{q}(t)] + \frac{1}{6}([\Gamma_1] + 2[\Gamma_2] + 2[\Gamma_3] + [\Gamma_4])$$

Although this scheme is lengthy to write out it is convenient for purposes of computation as it involves only the addition and multiplication of matrices, except for the evaluation of $[M]^{-1}$. But if a lumped mass matrix is used (as in this study), even that difficulty disappears. The routine requires the knowledge of the applied force vector $[Q]$ at t, $(t+\frac{h}{2})$, and $(t+h)$. In this study the value at $(t+\frac{h}{2})$ is taken as the average of the values at t and $(t+h)$.

3.4 Stability of the Runge-Kutta algorithm

If a set of differential equations may be written in the form

$$[\dot{x}] = [A][x] \qquad 3.4.1$$

then it can be shown (Lapidus and Seinfeld (1977) pp 120-131) that a 4th order Runge-Kutta algorithm when applied to this set will be stable if

$$\left| 1 + h\lambda + \frac{1}{2}h^2\lambda^2 + \frac{1}{6}h^3\lambda^3 + \frac{1}{24}h^4\lambda^4 \right| < 1 \qquad 3.4.2$$

where h is the time-step employed in the routine, and λ is the eigenvalue of $[A]$ with the greatest modulus.

Since λ may be complex, let $h\lambda = a + ib$. The case λ real then leads to the condition

$$\left| 1 + a + \frac{1}{2}a^2 + \frac{1}{6}a^3 + \frac{1}{24}a^4 \right| < 1$$

which is true for $-2.78 < a < o$

Similarly the case λ purely imaginary gives $o < b < 2\sqrt{2} = 2.83$

The precise values of $h\lambda$ which gives stability is a rather complicated region of the complex plane, but stability is assured if the condition $h|\lambda|_{max} < 2.6.$ is satisfied. 3.4.3

The homogeneous set of second order equations

$$[M][\ddot{q}] + [C][\dot{q}] + [K][q] = o$$

can be reduced to the type 3.4.1 by letting

$$\begin{bmatrix} q_1 \\ \cdot \\ \cdot \\ \cdot \\ \cdot \\ q_n \end{bmatrix} = \begin{bmatrix} x_1 \\ \cdot \\ \cdot \\ \cdot \\ \cdot \\ x_n \end{bmatrix} \quad \text{and} \quad \begin{bmatrix} \dot{q}_1 \\ \cdot \\ \cdot \\ \cdot \\ \cdot \\ \dot{q}_n \end{bmatrix} = \begin{bmatrix} x_{nt1} \\ \cdot \\ \cdot \\ \cdot \\ \cdot \\ x_{2n} \end{bmatrix}$$

This gives the set

$$\dot{x}_1 = x_{n+1}$$

$$\vdots$$

$$\dot{x}_n = x_{2n}$$

$$\begin{bmatrix} \dot{x}_{n+1} \\ \vdots \\ x_{2n} \end{bmatrix} = -[M]^{-1}[K] \begin{bmatrix} x_1 \\ \vdots \\ x_n \end{bmatrix} - [M]^{-1}[C] \begin{bmatrix} x_{n+1} \\ \vdots \\ x_{2n} \end{bmatrix}$$

or

$$[\dot{x}] = \begin{bmatrix} [O] & [I_n] \\ -[M]^{-1}[K] & -[M]^{-1}[C] \end{bmatrix} [x]$$

which is of the form $[\dot{x}] = [A][x]$

The eigenvalues are given by

$$\left| [A] - \lambda [I_{2n}] \right| = 0$$

i.e.

$$\begin{vmatrix} -\lambda [I_n] & [I_n] \\ -[M]^{-1}[K] & -M]^{-1}[C] - \lambda [I_n] \end{vmatrix} = 0$$

which reduces to

$$\begin{vmatrix} \lambda[I_n] & [0] \\ [M]^{-1}[K] & \lambda[M]^{-1}[C] + \lambda^2[I_n] + [M]^{-1}[K] \end{vmatrix} = 0$$

and hence $$\left| \lambda^2[M] + \lambda[C] + [K] \right| = 0 \qquad 3.4.4.$$

This is called the auxiliary of the equation set.

An analysis of some simple cases shows that we might expect instability if there are large damping coefficients.

The simplest possible case is

$$\ddot{q} + c\dot{q} + kq = 0 \qquad k>0, \quad c \geq 0 \qquad 3.4.5$$

which has auxiliary equation

$$\lambda^2 + c\lambda + k = 0$$

with roots

$$\lambda = \frac{-c \pm \sqrt{(c^2-4k)}}{2} = \frac{\sqrt{k}}{2}\left\{ -\alpha \pm \sqrt{(\alpha^2-4)} \right\}$$

where

$$c = \alpha\sqrt{k} \qquad (\alpha \geq 0)$$

It is easy to see that for $0 \leq \alpha \leq 2$

$$|\lambda|_{max} = \sqrt{k}$$

and for $\alpha \geq 2$

$$|\lambda|_{max} = \frac{\alpha\sqrt{k}}{2} \left\{ 1 + \sqrt{\left(1 - \frac{4}{\alpha^2}\right)} \right\}$$

This is illustrated in Fig 3.2.

Thus for $\alpha<2$ (i.e. $c<2\sqrt{k}$) $|\lambda|_{max} = \sqrt{k}$ and stability is assured if $h < \frac{2.6}{\sqrt{k}}$

But for larger values of α, $|\lambda|$ max $\doteq \alpha\sqrt{k} = c$, and so for stability we would require the time-step to be less than $(2.6/c)$. Above a certain value the stability depends almost entirely on the values of the damping coefficient and the time-step required is inversely proportional to that coefficient.

Another case that can be analysed is

$$\begin{bmatrix} 1 & 0 \\ 0 & 1 \end{bmatrix} \begin{bmatrix} \ddot{q}_1 \\ \ddot{q}_1 \end{bmatrix} + \begin{bmatrix} c & 0 \\ 0 & c \end{bmatrix} \begin{bmatrix} \dot{q}_1 \\ \dot{q}_2 \end{bmatrix} + \begin{bmatrix} k & \beta k \\ \beta k & k \end{bmatrix} \begin{bmatrix} q_1 \\ q_2 \end{bmatrix} = 0 \qquad 3.4.6$$

We assume that $c \geq 0$, $k>0$ and $0 \leq \beta < 1$

The auxiliary equation is

$$\begin{vmatrix} \lambda^2 + c\lambda + k & \beta k \\ \beta k & \lambda^2 + c\lambda + k \end{vmatrix} = 0$$

$$\{ \lambda^2 + c\lambda + k(1-\beta) \} \{ \lambda^2 + c\lambda + k(1+\beta) \} = 0 \qquad 3.4.7$$

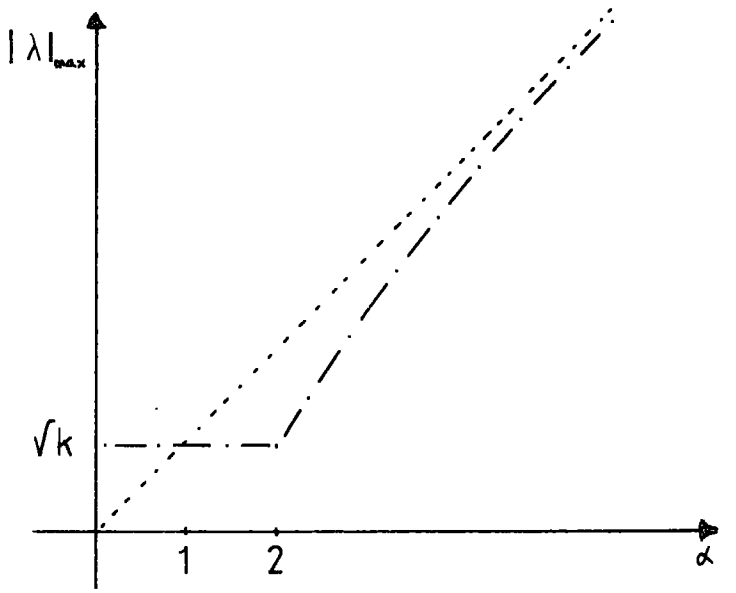

Fig. 3.2 Magnitude of maximum eigenvalue against damping for equation 3.4.5 $\alpha = c/\sqrt{k}$

Again we let $c = \alpha\sqrt{k}$

The first bracket of the equation 3.4.7 gives

$$|\lambda_1|_{max} = \begin{cases} \sqrt{k(1-\beta)} & \alpha \leq 2\sqrt{(1-\beta)} \\ \frac{\alpha\sqrt{k}}{2}\left\{1 + \sqrt{\left(1 - \frac{4(1-\beta)}{\alpha^2}\right)}\right\} & \alpha > 2\sqrt{(1-\beta)} \end{cases}$$

and the second bracket gives

$$|\lambda_2|_{max} = \begin{cases} \sqrt{k(1+\beta)} & \alpha \leq 2\sqrt{(1+\beta)} \\ \frac{\alpha\sqrt{k}}{2}\left\{1 + \sqrt{\left(1 - \frac{4(1+\beta)}{\alpha^2}\right)}\right\} & \alpha > 2\sqrt{(1+\beta)} \end{cases}$$

We require whichever is the greater of these two, which can be seen to be

$$|\lambda|_{max} = \begin{cases} \sqrt{k(1+\beta)} & \alpha \leq \frac{2}{\sqrt{(1+\beta)}} \\ \frac{\alpha\sqrt{k}}{2}\left\{1 + \sqrt{\left(1 - \frac{4(1-\beta)}{\alpha^2}\right)}\right\} & \alpha > \frac{2}{\sqrt{(1+\beta)}} \end{cases}$$

These results are illustrated in Fig. 3.3.

The general pattern is similar to the analysis of equation 3.4.5, but two points are worth noting.

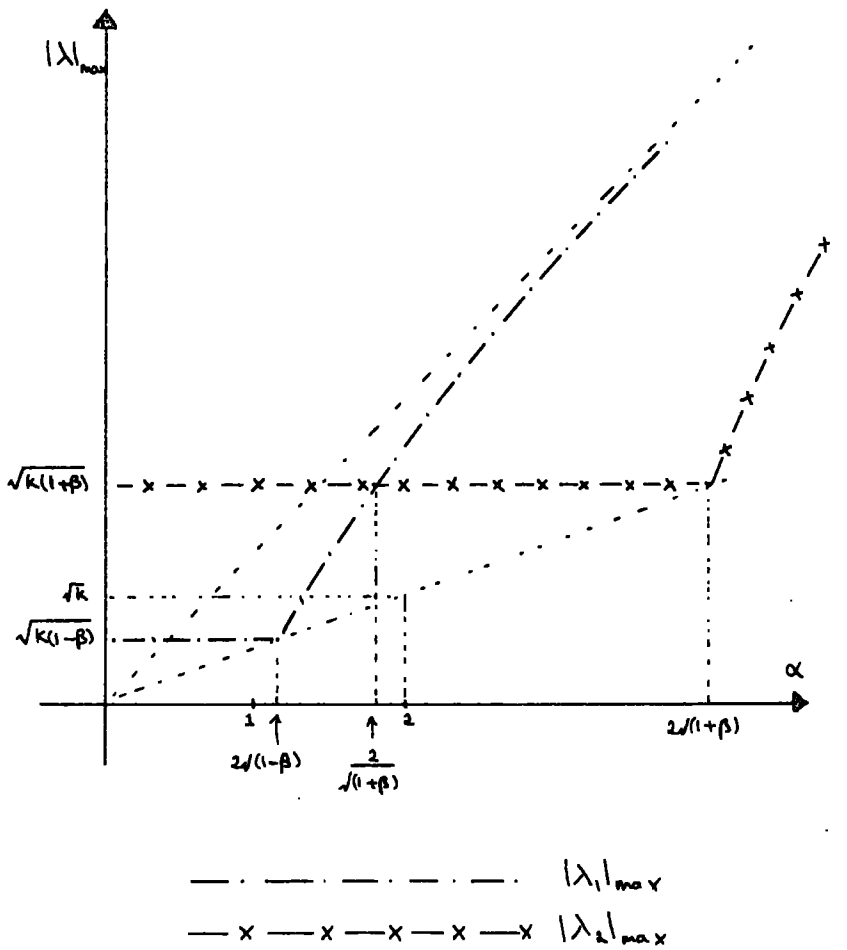

Fig. 3.3 Magnitude of maximum eigenvalue against damping for equation 3.4.6 $\alpha = c/\sqrt{k}$.
The maximum eigenvalue is given by the upper of the two curves for $|\lambda_1|_{max}$ and $|\lambda_2|_{max}$

i) Even with no damping ($\alpha=0$), the fact that the equations are coupled ($\beta>0$) leads to a raising of $|\lambda|_{max}$, and hence requiring a smaller time-step to satisfy the condition 3.4.3, than was required by equation 3.4.5.

ii) As before, for α greater than a certain critical value the size of the damping is the major factor, but the coupling makes this critical value lower, and the values of $|\lambda|_{max}$ higher than they were in the first example.

It is possible to go one stage further and consider the set of 3 equations of this type:-

$$\begin{bmatrix} 1 & 0 & 0 \\ 0 & 1 & 0 \\ 0 & 0 & 1 \end{bmatrix} [\ddot{q}] + \begin{bmatrix} c & 0 & 0 \\ 0 & c & 0 \\ 0 & 0 & c \end{bmatrix} [\dot{q}] + \begin{bmatrix} k & \beta k & 0 \\ \beta k & k & \beta k \\ 0 & \beta k & k \end{bmatrix} [q] = 0 \qquad 3.4.8$$

This has an auxiliary equation in factored form

$$(\lambda^2 + c\lambda + k)(\lambda^2 + c\lambda + k(1-\beta\sqrt{2})(\lambda^2 + c\lambda + k(1+\beta\sqrt{2})) = 0 \qquad 3.4.9$$

which is similar to 3.4.7, and consequently leads to a very similar analysis, with all the same conclusions. The auxiliary equation of the set of 4 equations of this type does not factor so neatly, but there seems no reason to doubt that in this case also $|\lambda|_{max}$ will be of the order of the damping coefficient provided it is above a certain value.

For a set of equations with little or no damping the value of $|\lambda|_{max}$ is determined by the values of $[K]$, and, as illustrated in the examples above and in section 3.5, will be of the order of the value of the maximum frequency of all the components that form the exact solution to the given set. The condition $|\lambda|_{max}\ h < 2.6$ thus can be written

i) for equations with dominant damping coefficients

$$h < \frac{2.6}{c}$$

where c is the order of the damping coefficients

ii) for equations with little or no damping

$$h < 0.4T$$

where T is the period of the mode of highest frequency.

3.5 An example

The method was tested on a set of 3 equations of the form of 3.4.8, with $c = 2$, $k = 4$, and $\beta k = \sqrt{2}$. Writing these equations out, with dependent variable $[y]$, we have

$$\begin{aligned} \ddot{y}_1 + 2\dot{y}_1 + 4y_1 + \sqrt{2}y_2 &= 0 \\ \ddot{y}_2 + 2\dot{y}_2 + \sqrt{2}y_1 + 4y_2 + \sqrt{2}y_3 &= 0 \\ \ddot{y}_3 + 2\dot{y}_3 + \sqrt{2}y_2 + 4y_3 &= 0 \end{aligned} \qquad 3.5.1$$

The auxiliary equation in factored form is then

$$(\lambda^2 + 2\lambda + 2)\ (\lambda^2 + 2\lambda + 4)\ (\lambda^2 + 2\lambda + 6) = 0$$

giving the possible eigenvalues

$$\lambda = -1 \pm i,\ -1 \pm i\sqrt{3},\ -1 \pm i\sqrt{5}$$

for which $|\lambda|_{max} = 2.45$

and hence the critical time-step is when $h = 1.1$

If to 3.5.1 we attach the initial conditions

$$y_1 = 1 \qquad y_2 = 0 \qquad y_3 = -1$$
$$\dot{y}_1 = 0 \qquad \dot{y}_2 = \sqrt{2} \qquad \dot{y}_3 = 6$$

then it can be shown that the exact solution is

$$y_1 = e^{-t}\left\{\frac{2}{\sqrt{5}}\sin\sqrt{5}t + \cos\sqrt{3}t - \frac{2}{\sqrt{3}}\sin\sqrt{3}t + \sin t\right\}$$

$$y_2 = e^{-t}\left\{\frac{2}{\sqrt{5}}\sin\sqrt{5}t - \sin t\right\}$$

$$y_3 = e^{-t}\left\{\frac{2}{\sqrt{5}}\sin\sqrt{5}t - \cos\sqrt{3}t + \frac{2}{\sqrt{3}}\sin\sqrt{3}t + \sin t\right\}$$

In this example the value of $|\lambda|_{max}$ is determined largely by the highest frequency component (which has a period of 2.8) rather than the damping coefficients.

Fig. 3.4 - 3.6 gives plots of the values of y_1, y_2 and y_3 for different values of time-step, together with the exact solution. For $h = 0.05$ the algorithm gives values which are indistinguishable from the exact solution even after 100 timesteps. For $h = 0.5$ the accuracy is still quite good. However, since in this example the amplitudes of all the frequency components are the same order, any time-step larger than 0.5 , no matter how accurate, hardly gives a good picture of the exact solution. For an example like this the critical value of the time-step is no limitation. It is not possible to plot the behaviour of the routine for time-steps greater than the critical value since the instability is quite spectacular. For example, with $h = 2.0$, y_1,y_2 and y_3 all have values of order 10^9 after only 8 time-steps. Such extreme instability is all to the good, since if instability is going to occur it is best that the algorithm user is given a clear indication of it if he inadvertently selects a too large value for the time-step.

3.6 Modification of equation of motion to include constraints.

The vector $[Q(t)]$ of equation 3.1.1 contains the known values throughout time of the external loads acting at each node. Nodes which have no applied forces, and are free to move in any direction, simply have zero for the elements of $[Q(t)]$ that correspond to the degrees of freedom of that node. However there will also be nodes which are not constrained by an applied force, but by an applied displacement. A particular case of this is a node which is fixed

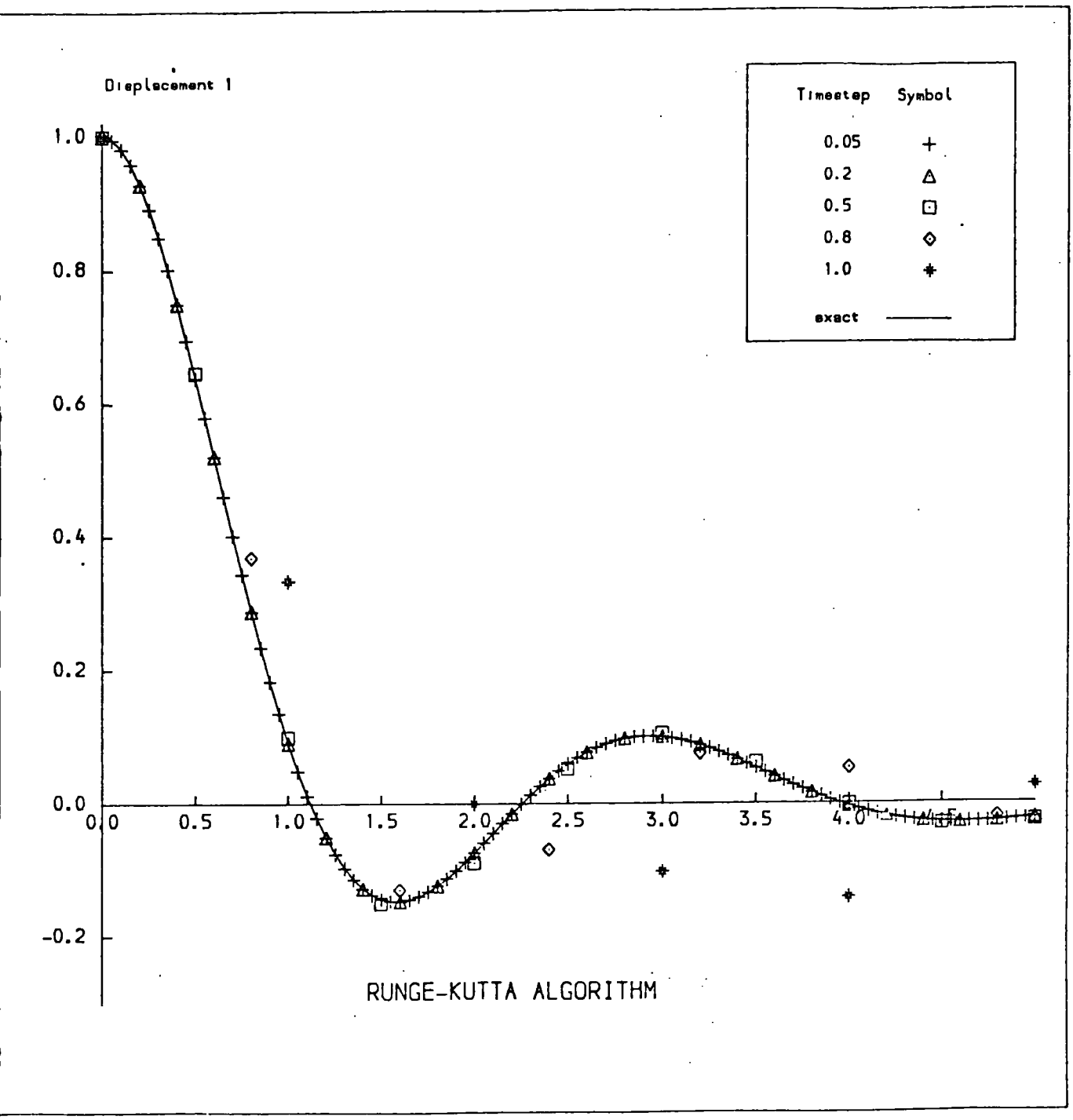
Displacement 1
Timestep Symbol
0.05
0.2
0.5
0.8
1.0
exact
1.0
0.8
0.6
0.4
0.2
0.0
-0.2
0.0
0.5
1.0
1.5
2.0
2.5
3.0
3.5
4.0
RUNGE-KUTTA ALGORITHM

Fig. 3.4

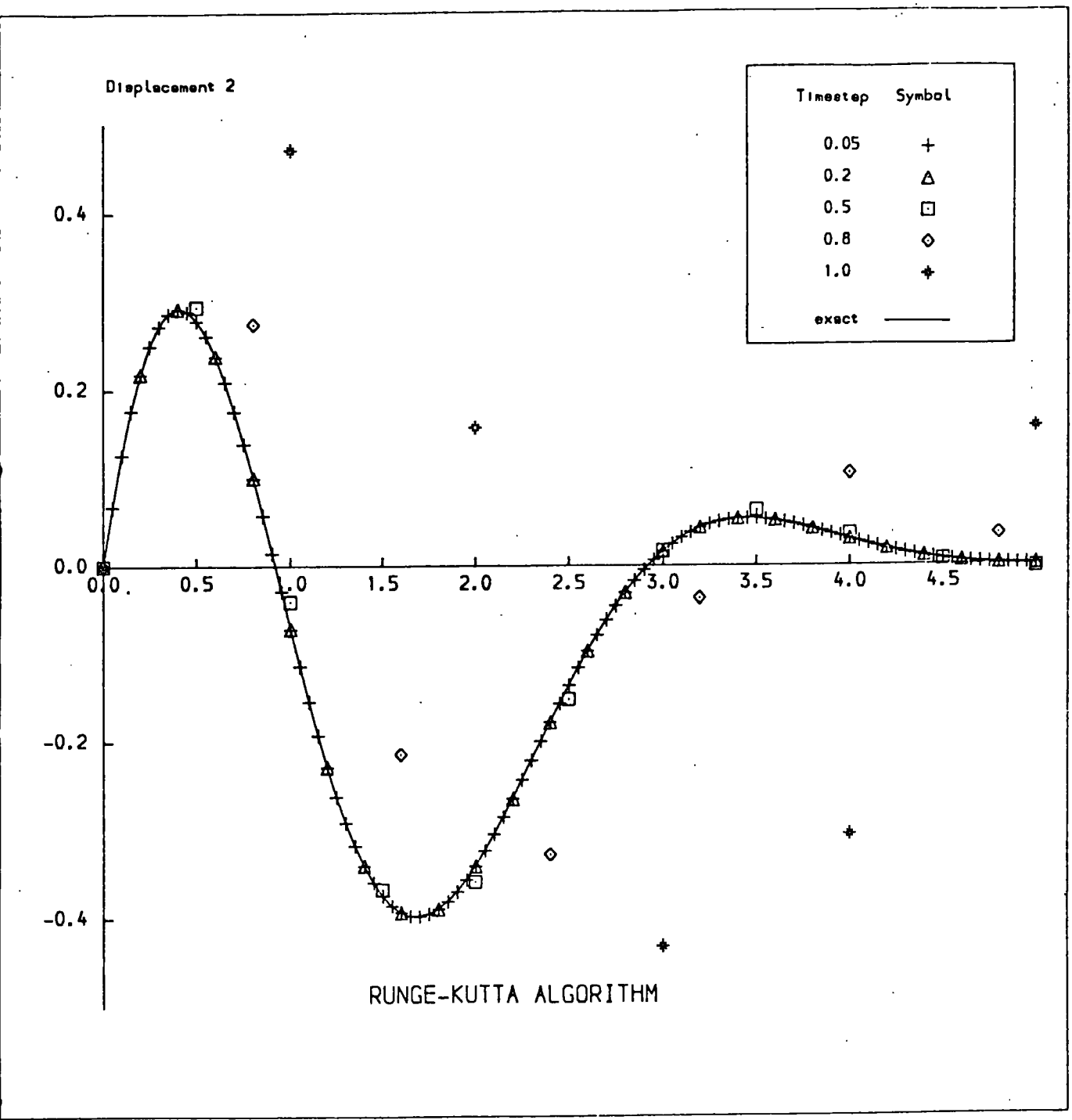
Displacement 2
Timestep Symbol
0.05
0.2
0.5
0.8
1.0
exact
0.4
0.2
0.0
-0.2
-0.4
0.0
0.5
1.0
1.5
2.0
2.5
3.0
3.5
4.0
4.5
RUNGE-KUTTA ALGORITHM

Fig. 3.5

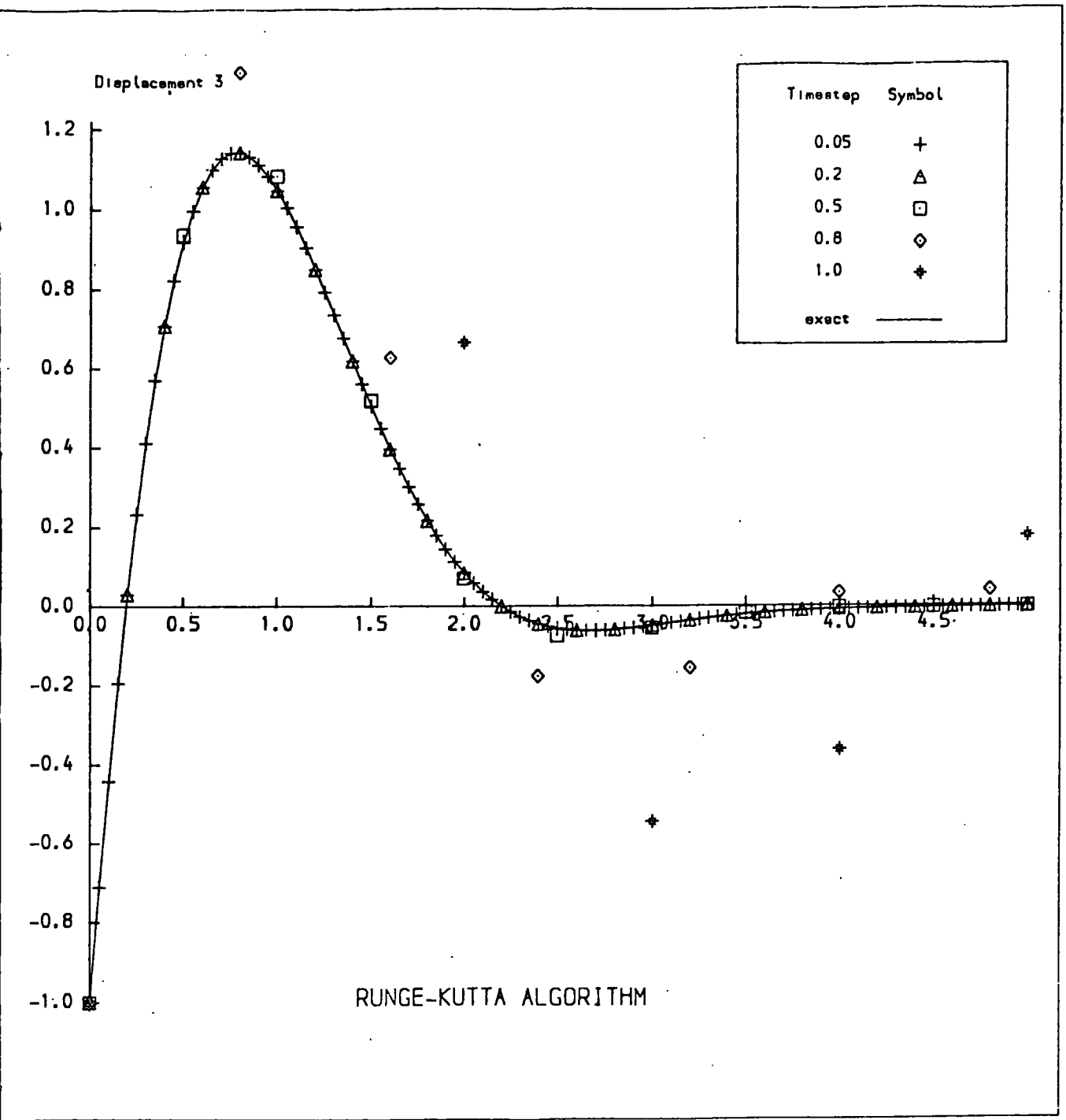
Displacement 3
Timestep Symbol
0.05
0.2
0.5
0.8
1.0
exact
1.2
1.0
0.8
0.6
0.4
0.2
0.0
-0.2
-0.4
-0.6
-0.8
-1.0
0.0
0.5
1.0
1.5
2.0
2.5
3.0
3.5
4.0
4.5
RUNGE-KUTTA ALGORITHM

Fig. 3.6

throughout time. In order that this possibility can be accommodated it is necessary to modify the equations of motion 3.1.1. Smith (1975) states that rigid nodes were simulated by setting to zero the corresponding elements of $[M]^{-1}$, which is equivalent to infinite masses at those nodes. It is not clear however how he provided for nodes moving in time. A different, and rather more realistic procedure, is adopted in this study.

Suppose that m degrees of freedom are constrained by applied loads, and n are constrained by applied displacements. Thus

($m + n$ = number of equations = 2 x number of nodes).

The equations of motion may be partitioned

$$\begin{bmatrix} [\ddot{q}_m] \\ [\ddot{q}_n] \end{bmatrix} = \begin{bmatrix} [\mu_m] & [0] \\ [0] & [\mu_n] \end{bmatrix} \left\{ \begin{bmatrix} [Q_m] \\ [Q_n] \end{bmatrix} - \begin{bmatrix} [C_{mm}] & [C_{mn}] \\ [C_{nm}] & [C_{nn}] \end{bmatrix} \begin{bmatrix} [\dot{q}_m] \\ [\dot{q}_n] \end{bmatrix} - \begin{bmatrix} [K_{mm}] & [K_{mn}] \\ [K_{nm}] & [K_{nn}] \end{bmatrix} \begin{bmatrix} [q_m] \\ [q_n] \end{bmatrix} \right\} \quad 3.6.1$$

In this equation the matrix $[M]^{-1}$ has been written as $\begin{bmatrix} [\mu_m] & [0] \\ [0] & [\mu_n] \end{bmatrix}$

where it is to be understood that the sub-matrices $[\mu_m]$ and $[\mu_n]$ consist only of non zero elements on their leading diagonals. This is justified since as was stated in 2.5 the mass matrix is of lumped form and so its inverse also consists of a diagonal matrix. Clearly the non-zero elements of $[\mu_m]$ and $[\mu_n]$ are simply the reciprocals of the corresponding elements of $[M]$.

Since the displacements of the last n degrees of freedom are the given constraints, $[q_n]$ and $[\dot{q}_n]$ are known. To emphasize that these are not unknown displacements and velocities call them $[r_n]$ and $[\dot{r}_n]$. So effectively what has to be solved is the first m equation of 3.6.1.

$$[\ddot{q}_m] = [\mu_m] \left\{ [Q_m] - [C_{mm}][\dot{q}_m] - [C_{mn}][\dot{r}_n] - [K_{mm}][q_m] - [K_{mn}][r_n] \right\}$$

However, instead of attempting to extract just this set of equations - which would involve forming the new matrices $[K_{mm}]$, $[K_{mn}]$ etc., - it is easier to modify the already assembled matrices $[K]$and $[C]$ to form the following set of equations

$$\begin{bmatrix} [\ddot{q}_m] \\ [\ddot{q}_n] \end{bmatrix} = \begin{bmatrix} [\mu_m] & [0] \\ [0] & [\mu_n] \end{bmatrix} \left\{ \begin{bmatrix} [Q_m] \\ [r_n] \end{bmatrix} - \begin{bmatrix} [C_{mm}] & [C_{mn}] \\ [0] & [0] \end{bmatrix} \begin{bmatrix} [\dot{q}_m] \\ [\dot{q}_n] \end{bmatrix} - \begin{bmatrix} [K_{mm}] & [K_{mn}] \\ [0] & [I] \end{bmatrix} \begin{bmatrix} [q_m] \\ [q_n] \end{bmatrix} \right\} \qquad 3.6.2$$

This modification is quite easy to do on the computer. It requires that the load vector $[Q]$ consists of the applied displacements $[r_n]$ for those degrees of freedom which are so constrained, that the rows of the damping matrix $[C]$ are all zeros for those degrees of freedom, and the corresponding rows of$[K]$ also consist of zeros except the diagonal element which is unity.

In this modified form it will be seen that the last n equations of 3.6.2 are now uncoupled, and all have the form

$$\dot{q} = \mu \left\{ r(t) - q(t) \right\}$$

If we solve this equation using the Runge-Kutta routine given in section 3.3, and taking

$$\begin{aligned} q(t_o) &= r(t_o) \\ \dot{q}(t_o) &= s(t_o) = \frac{1}{h} \left\{ r(t_o + h) - r(t_o) \right\} \end{aligned} \qquad 3.6.3$$

and $$r(t_o + \frac{h}{2}) = \frac{1}{2} \left\{ r(t_o + h) + r(t_o) \right\}$$

we find that

$$\Delta_1 = \Delta_2 = \Delta_3 = \Delta_4 = r(t_o + h) - r(t_o)$$

and

$$\Gamma_1 = \Gamma_2 = \Gamma_3 = \Gamma_4 = 0$$

giving

$$q(t_o+h) = r(t_o+h)$$

and

$$\dot{q}(t_o+h) = \frac{1}{h} \left\{ r(t_o+h) - r(t_o) \right\} = \dot{q}(t_o)$$

Thus by using this linear approximation to the velocity and displacement of the constraint nodes during the interval t_o to (t_o+h) we get the correct value of the displacements of those nodes at the end of the interval. The last n equations of the modified set of equations of motion therefore yield under the Runge-Kutta routine the correct applied displacements, and hence when the set of equations 3.6.2 are solved using 3.6.3 for the constrained nodes the correct values of the displacements and velocities q_m and $q_{m'}$ of the unconstrained nodes will be found.

It will be noted that it was essential for this method of modifying the equations that the mass matrix be diagonal - for otherwise the last m equations would not have been uncoupled - but that the damping matrix did not have to be so constrained. But, for the reasons given in sections 2.5 and 2.3 the computer program that has been written to carry out this Runge-Kutta solution assumes that both $[M]$ and $[C]$ are diagonal.

3.7. Summary

The Runge-Kutta algorithm is an accurate, efficient and easy to use procedure for solving sets of equations of the type 3.1.1. Its main drawback is that it is conditionally stable. The critical time-step condition, $h|\lambda|_{max} < 2.6$, is however better than that of some other methods in use. For instance of the eight integration procedures illustrated by Zienkiewicz (1977) p.583, five are conditionally stable, and of those five only one has a better time-step condition. The poorest is a 'central explicit' method, with $h|\lambda|_{max} < 2$. The method with a more favourable condition is unnamed, but which Zienkiewicz refers to as a "popular scheme", and has $h|\lambda|_{max} < 3.5$. It is however a two step implicit scheme, and so without the main advantages of the Runge-Kutta algorithm. Indeed if an extension in the region of stability is required a user might do well to consider a fifth order Runge-Kutta process, such as that proposed by Lawson (1966) for which $h|\lambda|_{max} < 5.7$.

The stability criterion will be most troublesome for equation sets that have damping coefficients, or high frequency components. For cases of high frequency components of significant amplitudes, as in the example of section 3.5., the stability criterion is not really a limiting factor, since in order to get a solution which satisfactorily displays such components a small enough time-step must be used. For equation sets whose solution is dominated by low frequency components, and only comparatively small amplitudes of the high frequency components, the Runge-Kutta method will not be so satisfactory, as a time-step which caters for the high frequencies will have to be used even though they are of little interest.

Such a situation will however be ideally suited to the method of mode superposition discussed in section 1.3. In the present study, which models a considerable extent of substructure, in addition to the region of interest, it will be the high modes of vibration that are the significant ones as far as determining the displacements of the structure are concerned. The Runge-Kutta algorithm should be an effective tool in these circumstances. For models containing high damping coefficients but only significant low frequency components the mode superposition method will also be valid; but for models with both high damping and significant high frequencies neither mode superposition nor the Runge-Kutta procedure will be appropriate. In such a case resort would have to be to an unconditionally stable scheme, with all the increased call on computer resources that that entails.

Although the computer program written for this study does allow for a damping matrix in diagonal form, in view of this difficulty with damping coefficients, and also because little can be said about reasonable numerical values for them, none of the models in this study include values for damping coefficients.

Chapter 4. Testing of the finite element programs

4.1. Introduction

Computer programs based on the theory given in chapters 2 and 3 were written, to cater for a two dimensional plane strain model. The region to be studied is modelled by a grid of elements of either triangular or quadrilateral shape, with a variety of material properties. The nodes of the grid can be left free, or can be given a time history of applied loads or displacements, and the programs determine the displacements of all the nodes, and the stresses in each element at each time-step. The details of the structure of these programs, how they are used and a listing are given in Appendix A.

That the finite element method will introduce approximations is of its very nature, but quite what effect these approximations will have, especially in a dynamics problem, is not so clear. In the case of a statics problem we know that, as mentioned in Section 2.1, for certain types of element we will have as close an approximation to the continuum solution as we please provided small enough elements are used. For a dynamics problem both the spatial and time dimensions are divided into discrete sections. The use of a time-step may be expected to lead to aliasing difficulties if too large a value is used, whereas the division of space into regions with discontinuities in strain along their boundaries must lead to problems of dispersion.

If too coarse a mesh were to be used then we might expect each node to behave something like a point source. A finite element model will thus only be able to give a reasonable representation of, say, a plane wave, if, in the manner of Huygens' principle, we have nodes sufficiently close together so that when they are considered as point sources their secondary wavelets do sum to a plane wave within an acceptable tolerance.

The tests described in this chapter form a comparison between known analytic solutions for certain propagation problems and finite element models for these problems, so that a clear idea of the necessary criteria for the use of the finite element method can be formed. The formulation of these criteria and a discussion of their implications is given in Chapter 5.

4.2. Description of test grid and pulse

For the purpose of the tests a rectangular grid of 28 x 14 elements was used, each element being a square of side 15m. This grid is illustrated in Fig. 4.1.

The nodes along the base were given various time displacements, and the displacements of all the nodes were calculated at all time-steps. From these values two forms of display were examined:

a) displacement time graphs of certain selected nodes (usually nodes on the line $x = 0$)

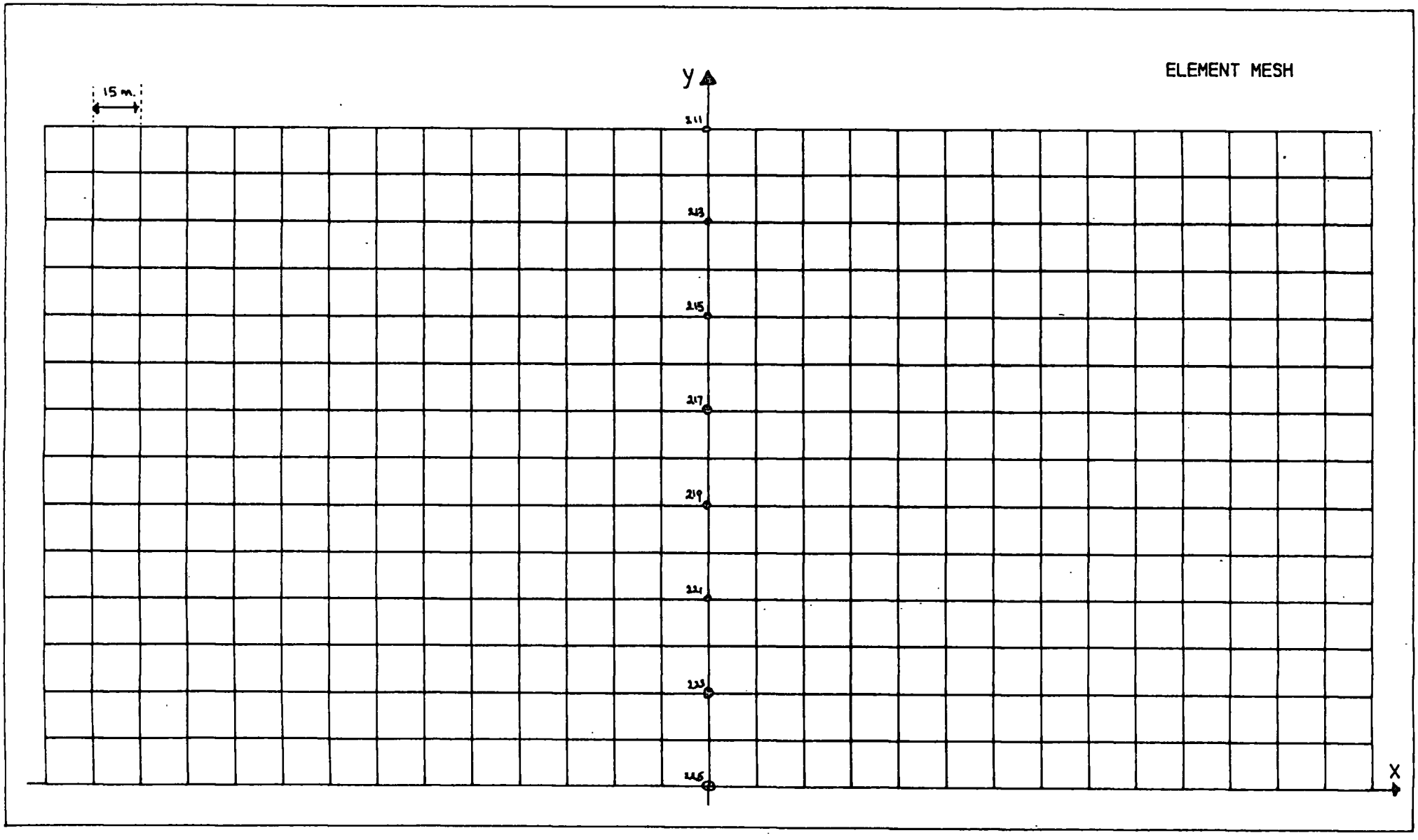

Fig. 4.1

b) plots of the principal stresses in each element at certain selected time-steps. This was either for a selected part of the whole grid, or for the whole grid.

To follow the propagation of a pulse the input at the base was based on a pulse consisting of 1 period of a cosine wave

$$\text{displacement} = \begin{cases} 0 & t<0 \\ a(1 - \cos \frac{2\pi t}{T}) & 0 \leq t \leq T \\ 0 & t > T \end{cases}$$

Thus to simulate a P-wave progressing up the y-axis the above displacement was applied in the y direction to all the nodes along $y=0$ simultaneously, whereas for an S-wave progressing up the y-axis the same displacement was applied to all nodes simultaneously but in the x-direction.

For the general case of a plane wave incident at an angle θ to the y-axis, consider the x-axis and suppose that the disturbance at $x = 0$ begins at $t = 0$.

The disturbance at P will begin after a time $t' = \frac{x \sin \theta}{c}$, where c is the velocity of propagation and x is the distance of P from O. This is illustrated in the diagram overleaf.

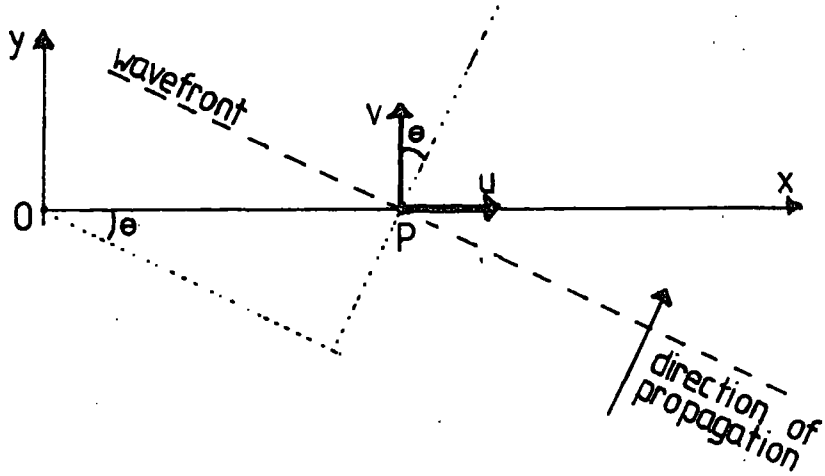

The disturbance at P is therefore equal to

$$a\left\{1 - \cos\frac{2\pi}{T}(t-t')\right\} \qquad 0<t-t'<T$$

and zero otherwise.

Thus for a P-wave the components of displacement (u,v) at P are

$$u = a\sin\theta\left\{1 - \cos\frac{2\pi}{T}(t-t')\right\}$$

$$v = a\cos\theta\left\{1 - \cos\frac{2\pi}{T}(t-t')\right\} \qquad \text{for} \qquad 0<t-t'<T$$

where $t' = \dfrac{x\sin\theta}{\alpha}$ (α = velocity of P-waves)

Similarly if β is the velocity of S-waves, then for S-wave propagation we have the displacements

$$u = a\cos\theta\left\{1 - \cos\frac{2\pi}{T}(t-t')\right\}$$

$$v = a\sin\theta\left\{1 - \cos\frac{2\pi}{T}(t-t')\right\} \quad \text{for} \quad 0<t-t'<T$$

where $t' = \frac{x \sin\theta}{\beta}$

The program INPUT was used to create a date file based on these formulas in the format required by the subroutine LOAD 2 in the program TIMESTEP.

4.3. Description of tests

Test Run A

Boundary Conditions		
Top surface free	Sides zero x-displacements	Base plane wave pulse

Pulse parameters		Type P-wave			
Period	0.06 s.	Timestep	0.01 s.	Amplitude	0.1 m.
Angle	0.0^{o}	Frequency	16.6 Hz.	Timestep per period	6

Material Properties						
Young's modulus $n.m.^{-2}$	Poisson's ratio	Density $kg.\ m.^{-3}$	Velocities $m.s^{-1}$		Wave-length m.	Elements per wavelength
			P-wave	S-wave		
8×10^{9}	0.25	2400	2000	1155	120	8

The graphs of y-displacements against time are illustrated in Fig. 4.2 for 10 nodes from base to surface along the centre of the grid.

The form of the pulse is displayed by the graph for node 225, and it will be noted that after t=0.06 this node is kept with zero displacement. The progression of the wave to the surface (node 211) is clearly seen, where it is reflected, without change of phase since it is a free surface, back into the grid. This reflected wave returns to the base at 0.21s. where it is again reflected, this time with a change of phase since the base is fixed, and we can follow the wave again to the surface.

From the graph of the time taken for the peak of the wave to travel as it first rises through the grid an average speed of 1900m.s^{-1} is determined, agreeing quite well with the theoretical value of 2000m.s^{-1}. On the other hand it can be seen from the time displacement graphs of the nodes that the exact shape of the pulse is not preserved. The onset of the disturbance is a little earlier than it should be, the pulse develops a little ripple in its tail and there is some loss of amplitude.

These characteristics of dispersion of the pulse are the sort of errors that we would expect from a process which discretises the information. Stress plots at various time-steps were also produced - but they are not reproduced here, since they are similar to those of the next run. However it is worth remarking that since stress is a function of the spatial derivatives of displacement, any inaccuracies in the calculation of displacements as a result of the finite element approximations is likely to lead to rather worse errors in the stresses.

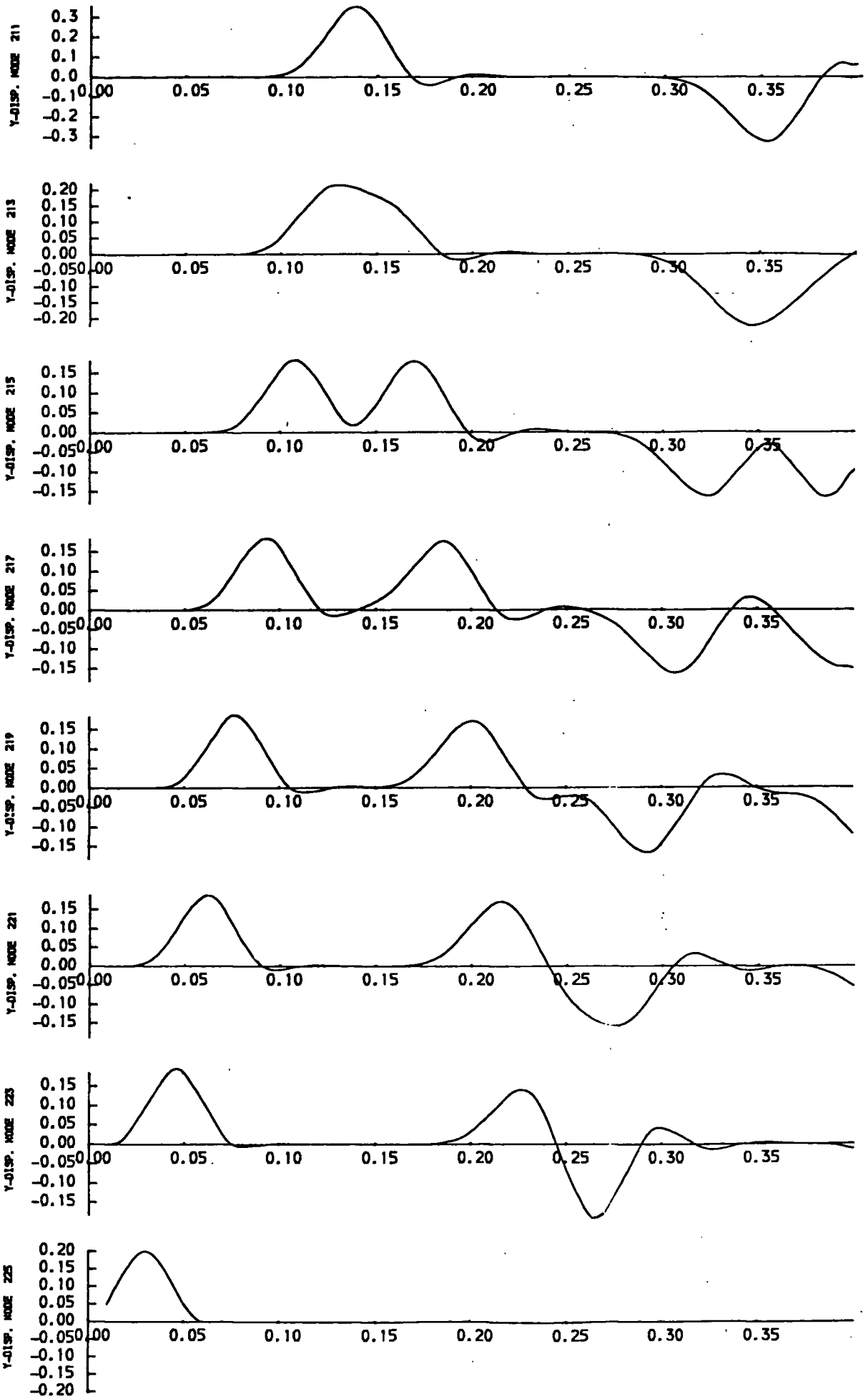

Fig. 4.2 Test Run A y-displacements.

Test Run B

Boundary Conditions						
Top surface free		Sides zero x-displacements			Base plane wave pulse	
Pulse parameters		Type P-wave				
Period	0.06 s.	Timestep	0.005 s.		Amplitude	0.1 m.
Angle	0.0^{o}	Frequency	16.7 Hz.		Timestep per period	12

Material Properties						
Young's modulus $n.m.^{-2}$	Poisson's ratio	Density $kg.\ m.^{-3}$	Velocities $m.s^{-1}$		Wave-length m.	Elements per wavelength
			P-wave	S-wave		
8×10^{9}	0.25	2400	2000	1155	120	8

Graphs of y-displacements against time are illustrated in Fig. 4.3 for the same nodes as in A. These graphs have an almost identical appearance as those nodes for run A, and measurements of the progress of the first peak give the same velocity. However the loss in amplitude is not so great. For instance the displacement of the node on the free surface should be twice that at the base, i.e. 0.4m. In the case of A the graphs give a figure of 0.35m.,whereas the B graphs give 0.39m.

Also illustrated for this run in Figs. 4.4-4.7 are plots of principal stresses for the central section of the grid at various times. The principal stresses are worked out for each element and plotted at the centre of the element.

For the case of a P-wave applied at the base one would expect the x and y displacements (u,v) for a general point to be given by

$$u(x,y,t) = 0$$

$$v(x,y,t) = \begin{cases} a\left\{1 - \cos\frac{2\pi}{T}\left(t - \frac{y}{\alpha}\right)\right\} & \frac{y}{\alpha} < t < T + \frac{y}{\alpha} \\ 0 \text{ for all other } t \text{ until the first reflection arrives} \end{cases}$$

where α is the velocity of P-waves, and provided the point is not within half a wavelength of the free surface.

Using the relations 2.3.5 and 2.3.3 we derive for the stress at a point

$$\sigma_{11} = \lambda\frac{\partial v}{\partial y} = -\lambda\frac{2\pi a}{T\alpha}\sin\frac{2\pi}{T}\frac{(t-y)}{\alpha}$$

$$\sigma_{22} = (\lambda + 2\mu)\frac{\partial v}{\partial y} = -(\lambda + 2\mu).\ \frac{2\pi a}{T\alpha}\sin\frac{2\pi(t-y)}{T\alpha}$$

$$\sigma_{12} = 0$$

The principal stresses are therefore

$$\sigma_1 = \sigma_{11} \text{ and } \sigma_2 = \sigma_{22}$$

and directed along the x and y axes respectively.

The ratio of the principal stresses will be at all times

$$\frac{\sigma_1}{\sigma_2} = \frac{\lambda}{\lambda+2\mu} = \frac{\nu}{1-\nu}$$

$$= \frac{1}{3} \quad \text{when } \nu = \frac{1}{4}$$

Also $|\sigma_2|_{max} = |\sigma_{22}|_{max}$

$$= (\lambda + 2\mu). \frac{2\pi a}{T\alpha} = \alpha^2 \rho \frac{2\pi a}{T\alpha}$$

$$= \frac{2\pi a \alpha \rho}{T}$$

With the parameter's of this trial we get

$$|\sigma_2|_{max} = 5.03 \times 10^7 \text{ Pa.}$$

and $|\sigma_1|_{max} = 1.68 \times 10^7$ Pa.

Measurements from the plots give values

a) on the front half of the pulse maximum compressive stresses of 4.4×10^7 Pa. and 1.5×10^7 Pa. for in the y and x directions respectively.

b) on the back half of the pulse maximum tensional stresses of 4.9×10^7 Pa. and 1.67×10^7 Pa.

It will be seen that these values, especially in the case (b), agree well with the theoretically expected values. Also there did appear to be a slight improvement in the stress plots of run B, compared to those of A.

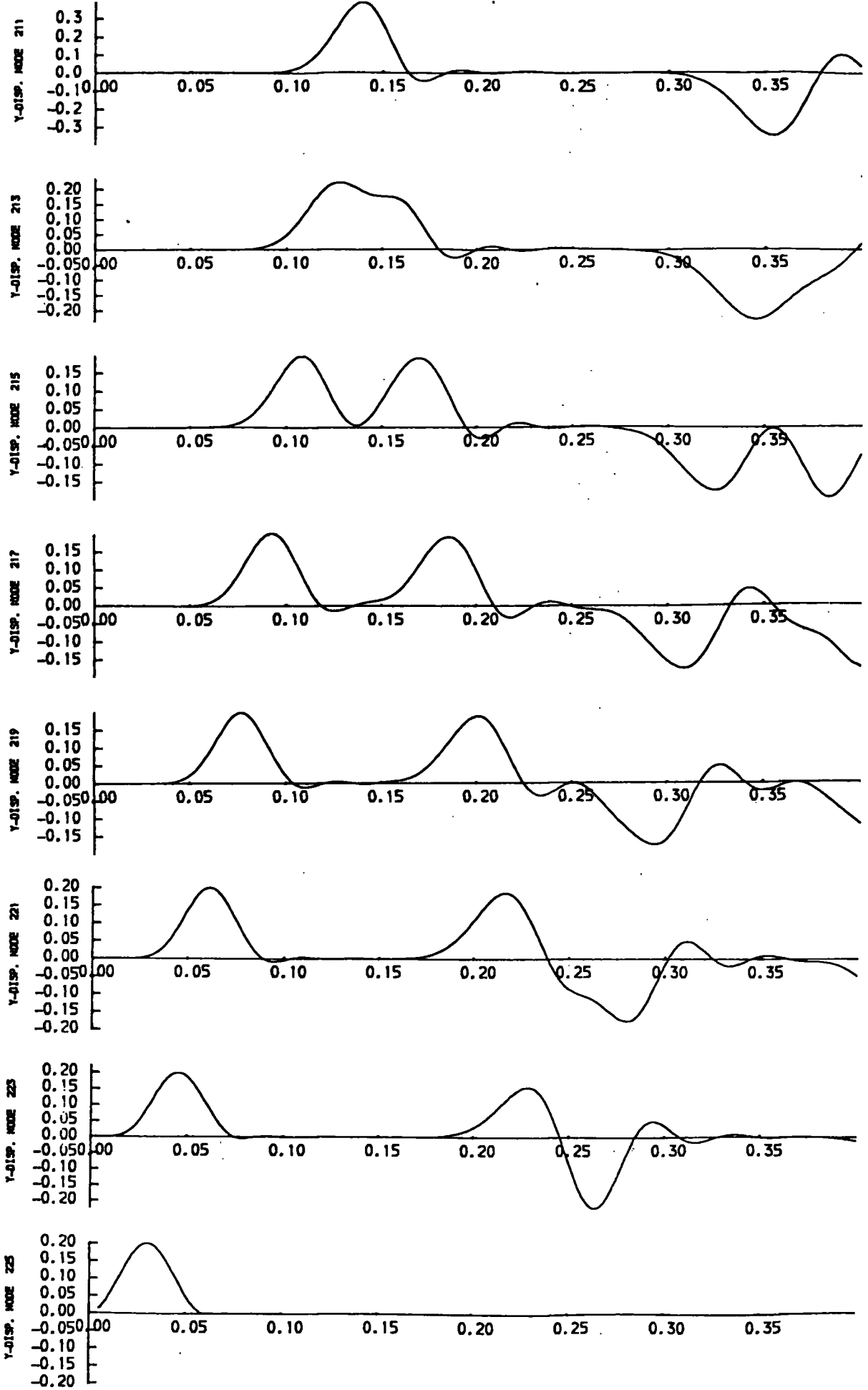

Fig. 43 Test Run B. y-displacements.

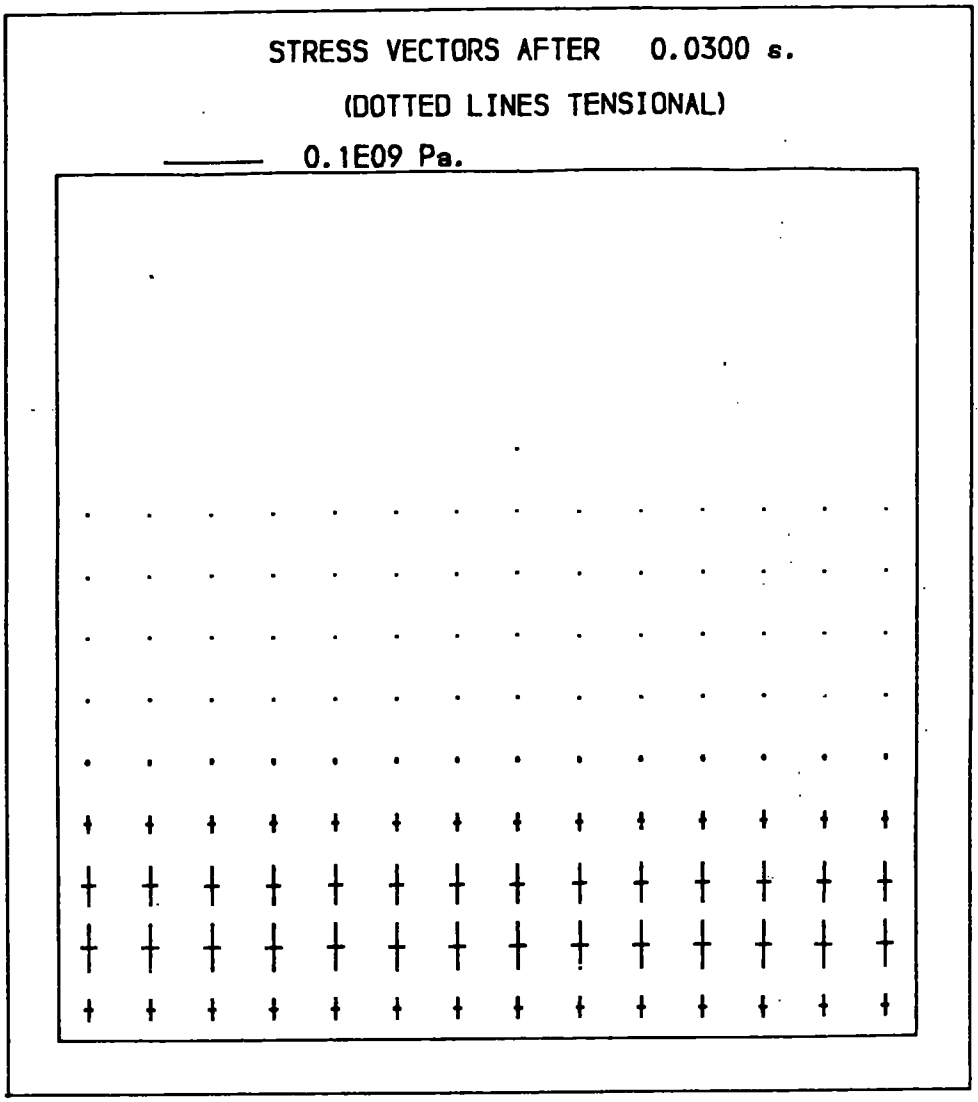
STRESS VECTORS AFTER 0.0300 s.
(DOTTED LINES TENSIONAL)
0.1E09 Pa.

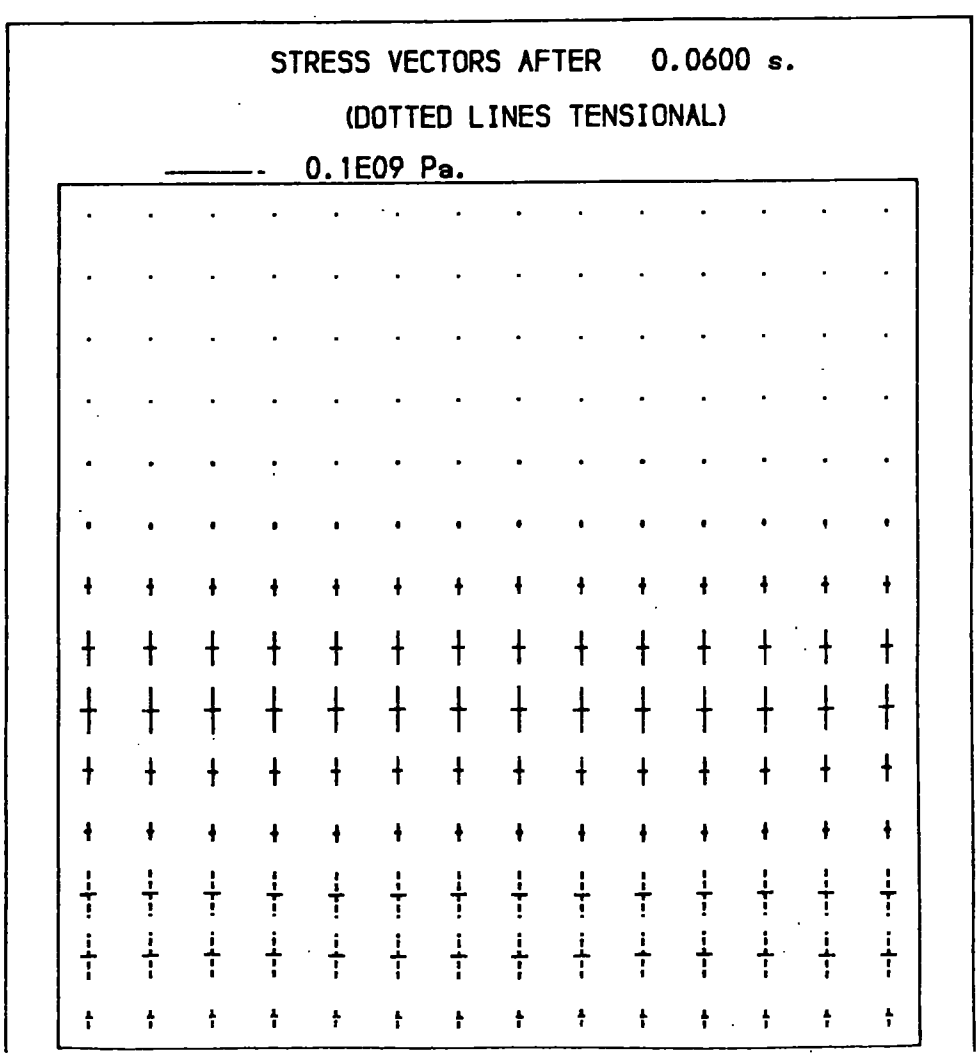
STRESS VECTORS AFTER 0.0600 s.
(DOTTED LINES TENSIONAL)
0.1E09 Pa.

Fig. 4.4

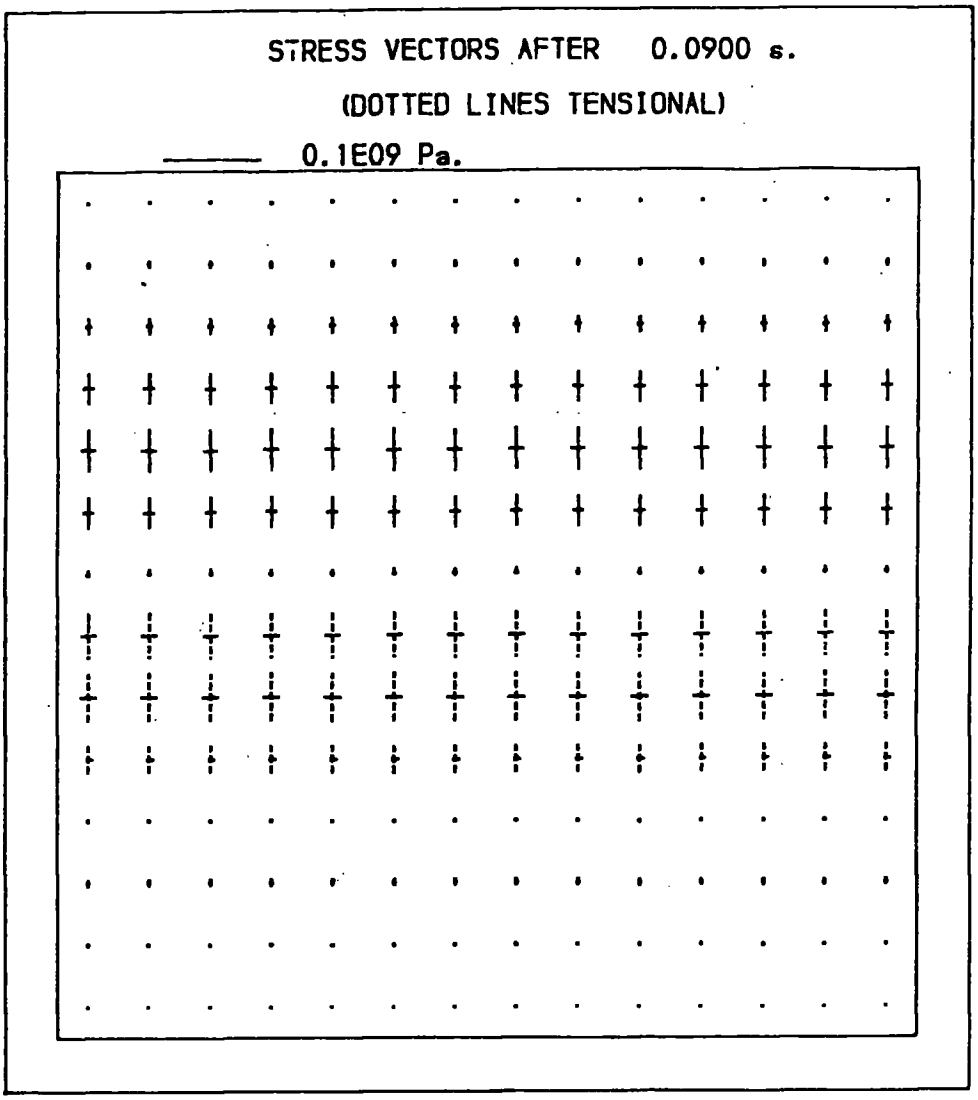
STRESS VECTORS AFTER 0.0900 s.
(DOTTED LINES TENSIONAL)
0.1E09 Pa.

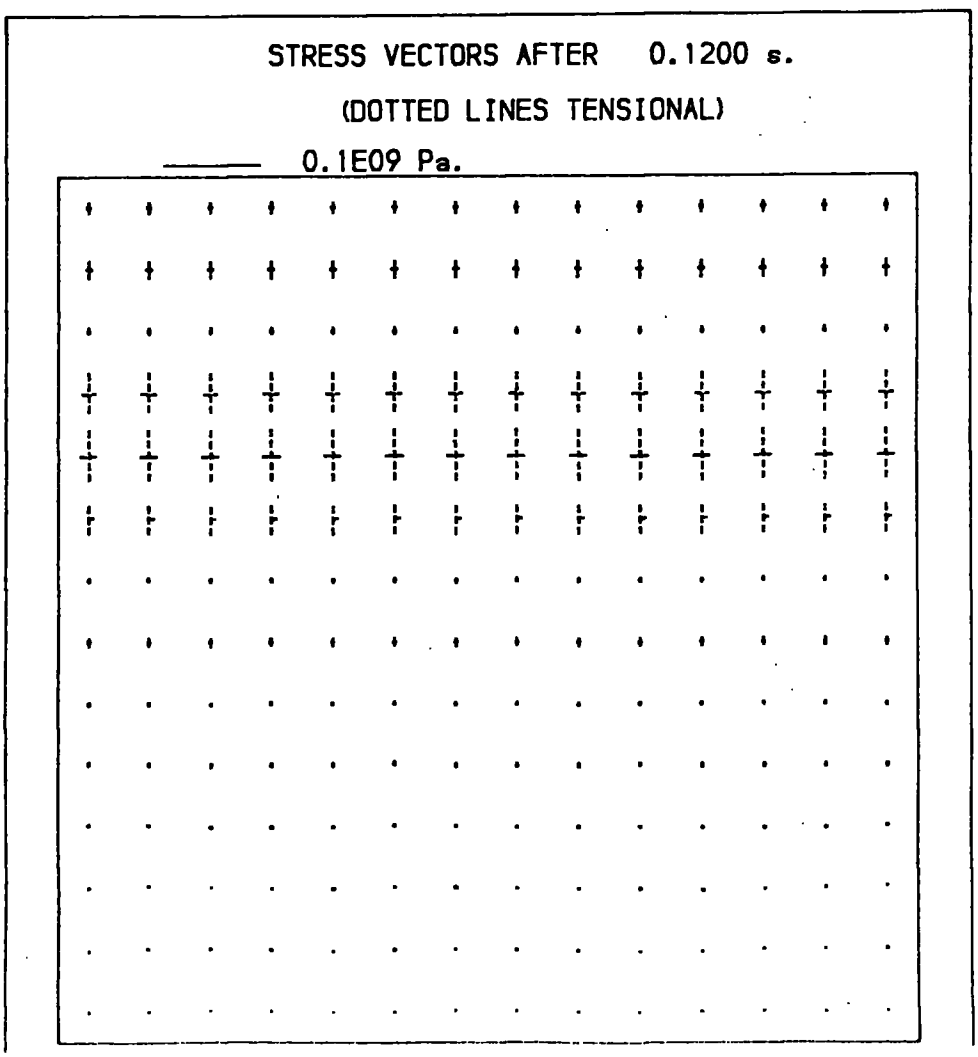
STRESS VECTORS AFTER 0.1200 s.
(DOTTED LINES TENSIONAL)
0.1E09 Pa.

Fig. 4.5

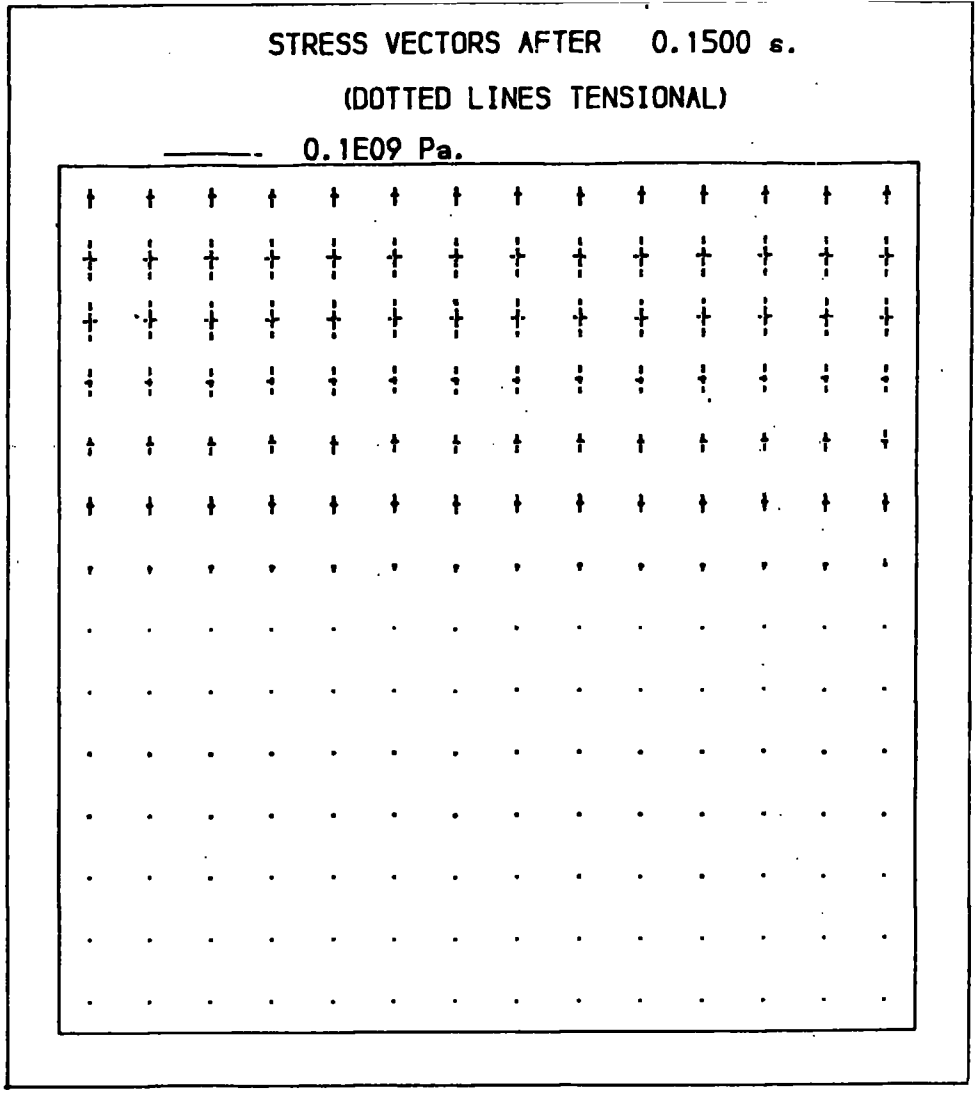
STRESS VECTORS AFTER 0.1500 s.
(DOTTED LINES TENSIONAL)
0.1E09 Pa.

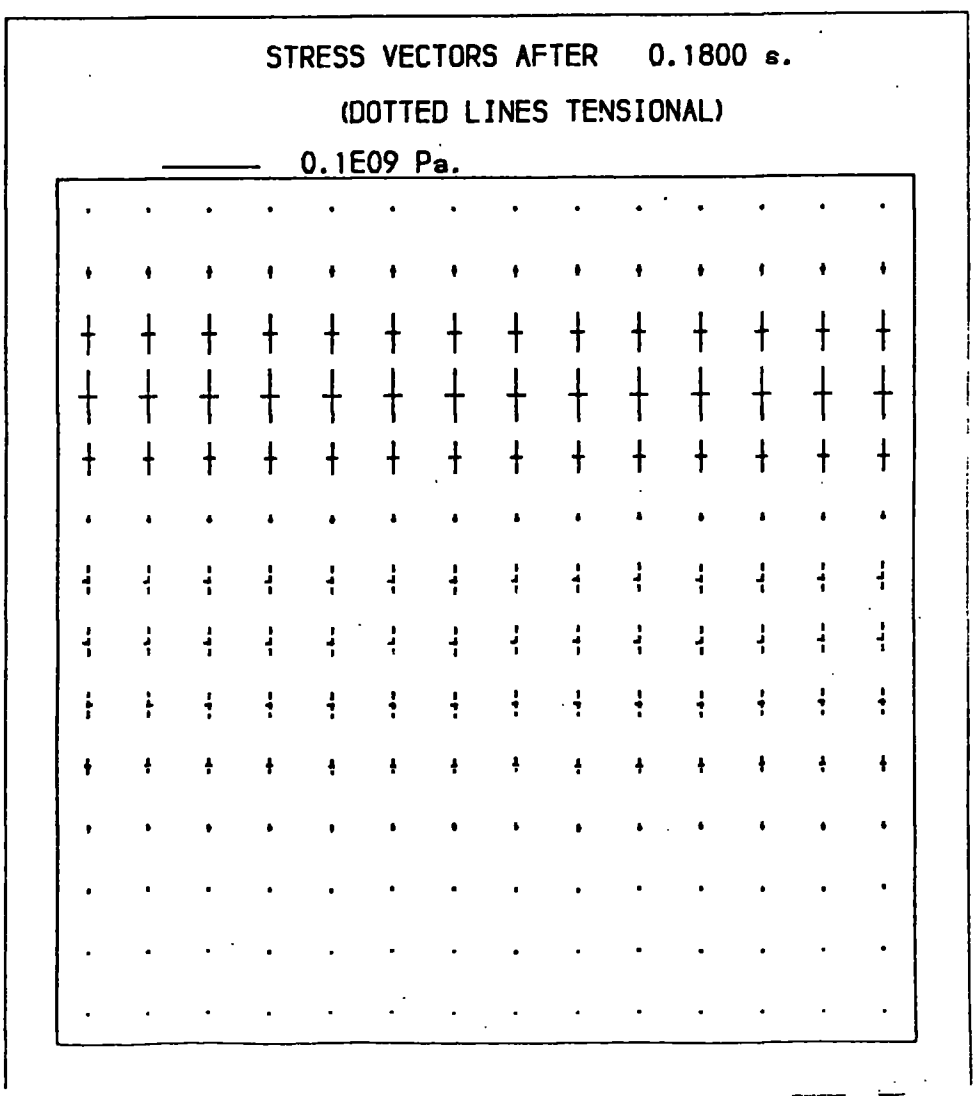
STRESS VECTORS AFTER 0.1800 s.
(DOTTED LINES TENSIONAL)
0.1E09 Pa.

Fig. 4.6

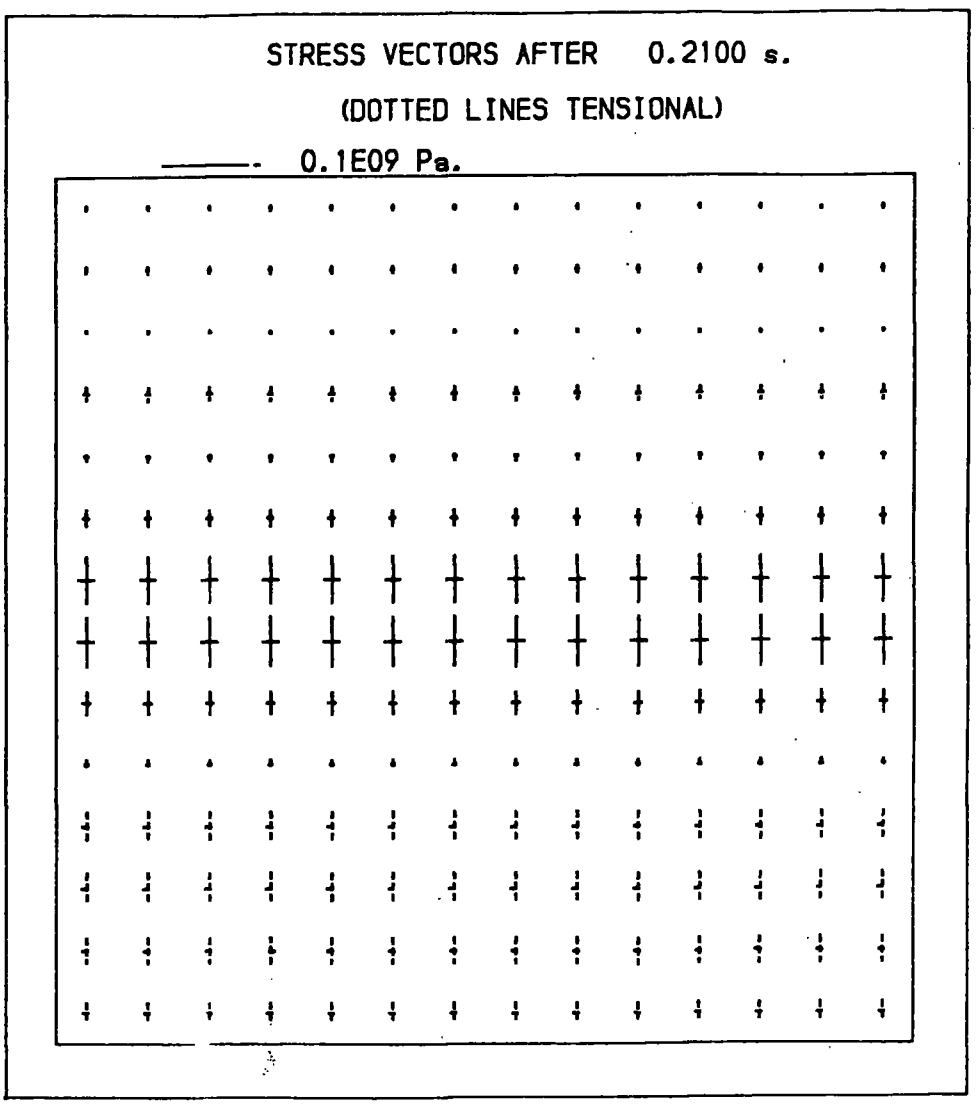
STRESS VECTORS AFTER 0.2100 s.
(DOTTED LINES TENSIONAL)
0.1E09 Pa.

Fig. 4.7

Test Run C

Boundary Conditions						
Top Surface free	Sides zero x-displacement				Base plane wave pulse	
Pulse parameters	Type P-wave					
Period 0.03s.	Time step 0.0025s.				Amplitude 0.1m.	
Angle 0.0^{o}	Frequency 33.3 Hz.				Timesteps per period 12	
Material Properties						
Young's modulus $n.m.^{-2}$	Poisson's ratio	Density $kg.m.^{-3}$	Velocities $m.s^{-1}$		Wave-length m.	Elements per wavelength
			P-Wave	S-wave		
8×10^{9}	0.25	2400	2000	1155	60	4

This run has the same number of time-steps in each period as run B but has only half the number of elements per wavelength. This is achieved on the same grid by using half the period. From the graph, Fig. 4.8., the time taken by the first peak to travel a given distance as the wave first propagates along the y-axis gives a velocity of 1850 $m.s.^{-1}$ (slightly worse than that obtained in runs A and B). However the dispersion of the wave is significantly worse than in either of the previous runs. This is shown by the loss in amplitude of the wave, even within two elements of the base; and at the free surface the amplitude is 0.28 instead of the expected 0.4. Also the pulse develops a marked ripple in its tail. These ripples seriously affect the stress plots (which are not given). On these the front of the wave is quite clear, but within a short time spurious stresses appear in the wake of the pulse.

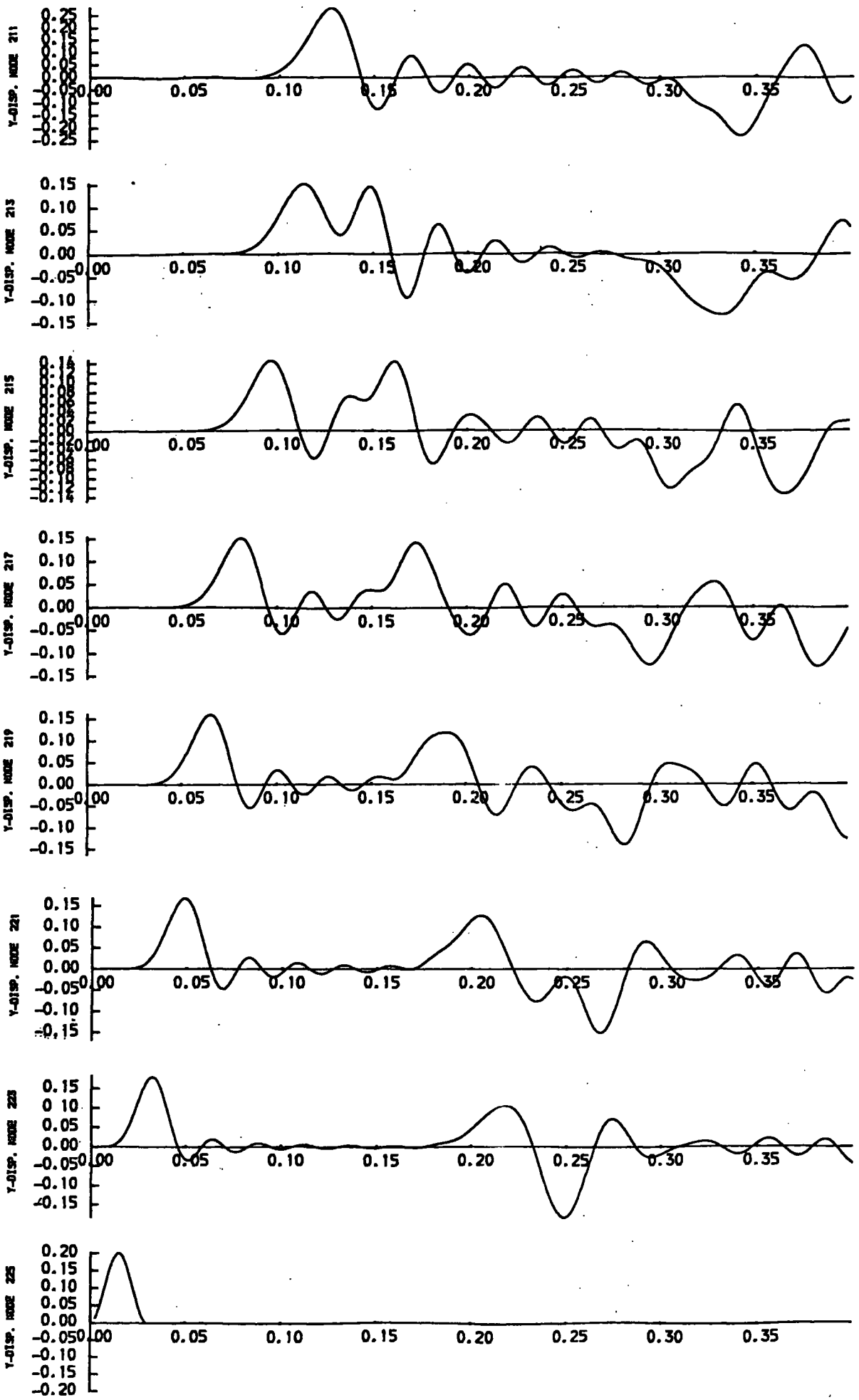

Fig. 4.8 Test Run C y-displacements.

Test Run D

Boundary Conditions						
Top surface free		sides zero y-displacement			Base plane wave pulse	
Pulse parameters			Type S-wave			
Period	0.06s.	Timestep	0.005s.		Amplitude	0.1m.
Angle	0.0^{o}	Frequency	16.7 Hz.		Timesteps per period	12
Material Properties						
Young's modulus $n.m.^{-2}$	Poisson's ratio	Density $kg.\ m.^{-3}$	Velocities $m.s^{-1}$ P-wave	S-wave	Wave-length m.	Elements per wavelength
8×10^{9}	0.25	2400	2000	1155	69.3	4.6

The graphs of x-displacement against time Fig. 4.9 are given for the same nodes as in previous examples. The velocity of progression of the the first peak is found from the graph to be $1070 m.s.^{-1}$, which compares quite well with the theoretical value of $1155 m.s.^{-1}$, for the velocity of S-waves in this medium.

Since this is an S-wave the theoretical displacements for points not within half a wavelength of the surface are

$$u(x,y,t) = \begin{cases} a\left\{1 - \cos\frac{2\pi}{T}\left(t-\frac{y}{\beta}\right)\right\} & \frac{y}{\beta} < t < \frac{y}{\beta}+T \\ 0 \quad \text{for other } t, \text{ until first reflection arrives} \end{cases}$$

$$v(x,y,t) = 0$$

Hence $\sigma_{11} = \sigma_{22} = 0$

and $$\sigma_{22} = \mu \frac{\partial u}{\partial y} = \frac{\mu 2\pi a}{T\beta} \sin\frac{2\pi}{T}\left(t-\frac{y}{\beta}\right)$$

The principal stresses therefore have magnitudes

$$\sigma_1 = \sigma_{12} \quad \text{and} \quad \sigma_2 = -\sigma_{12}$$

but with σ_2 inclined at an angle θ to the x-axis given by

$$\tan 2\theta = \frac{2\sigma_{12}}{\sigma_{11}-\sigma_{22}}$$

Since $\sigma_{11} - \sigma_{22} = 0$ this is satisfied by $\theta = \frac{\pi}{4}$

It will be seen that as the shear wave propagates along the y-axis, σ_1 will initially be negative (i.e. compressive) and σ_2 will be positive (i.e. tensional). This behaviour is observed on the stress plots for the first time-steps. Furthermore the magnitude of both σ_1 and σ_2 will have a maximum value

$$|\sigma_1|_{max} = \frac{\mu 2\pi a}{T\beta} = \frac{2\pi a \beta \rho}{T}$$

For the parameters of this run this has the value 2.9×10^8 Pa. The graphs of the stress plots, Figs. 4.10-4.11 give a maximum principal stress of 1.5×10^8 Pa. on the front of the pulse, and 2.7×10^8 Pa. on the back of the pulse.

However the low number of elements in each wavelength produce an unsatisfactory degree of dispersion as is readily seen on the displacement time graphs, with a corresponding deterioration of the stress plots with increasing time.

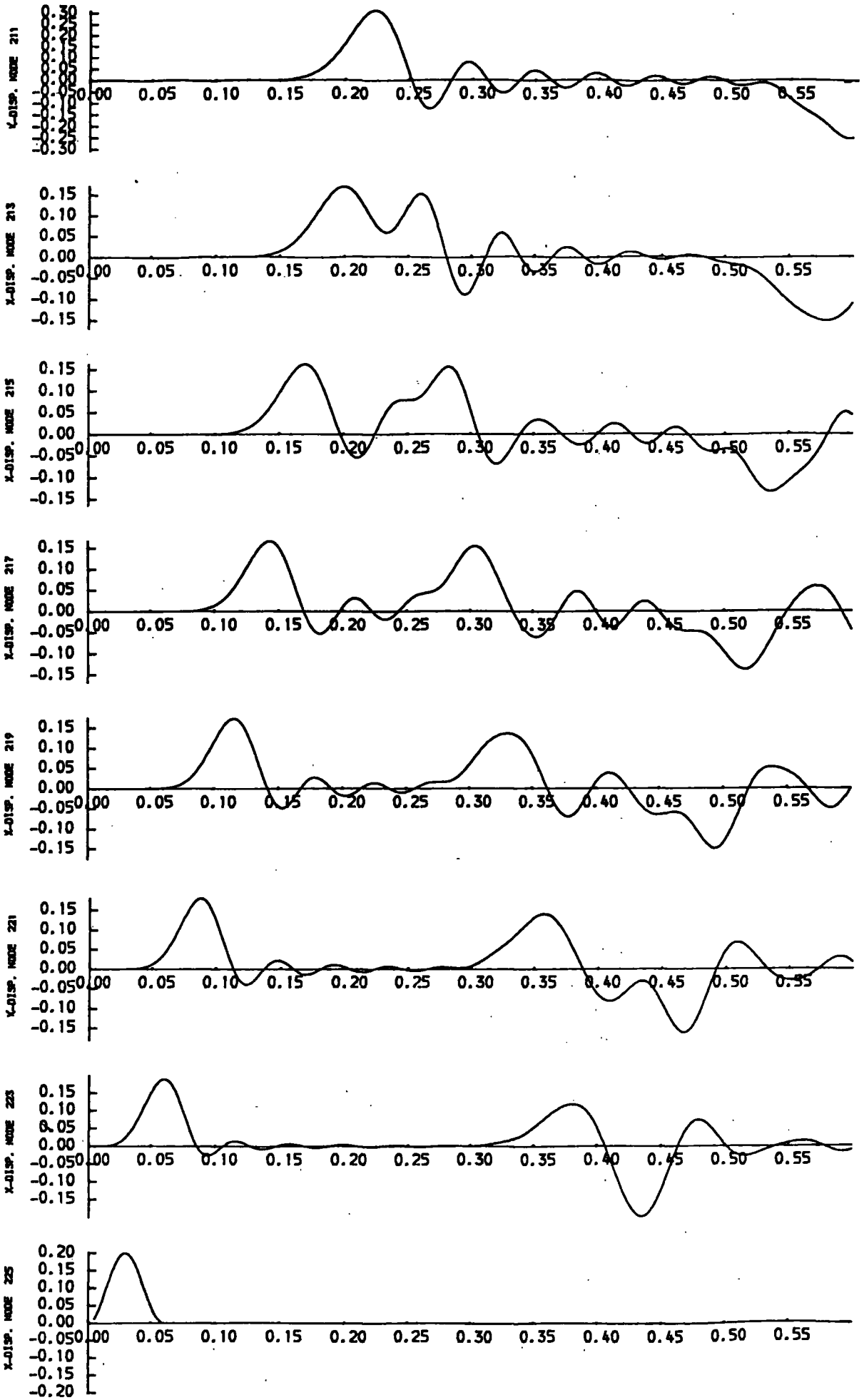

Fig. 4.9 Test Run D x-displacements.

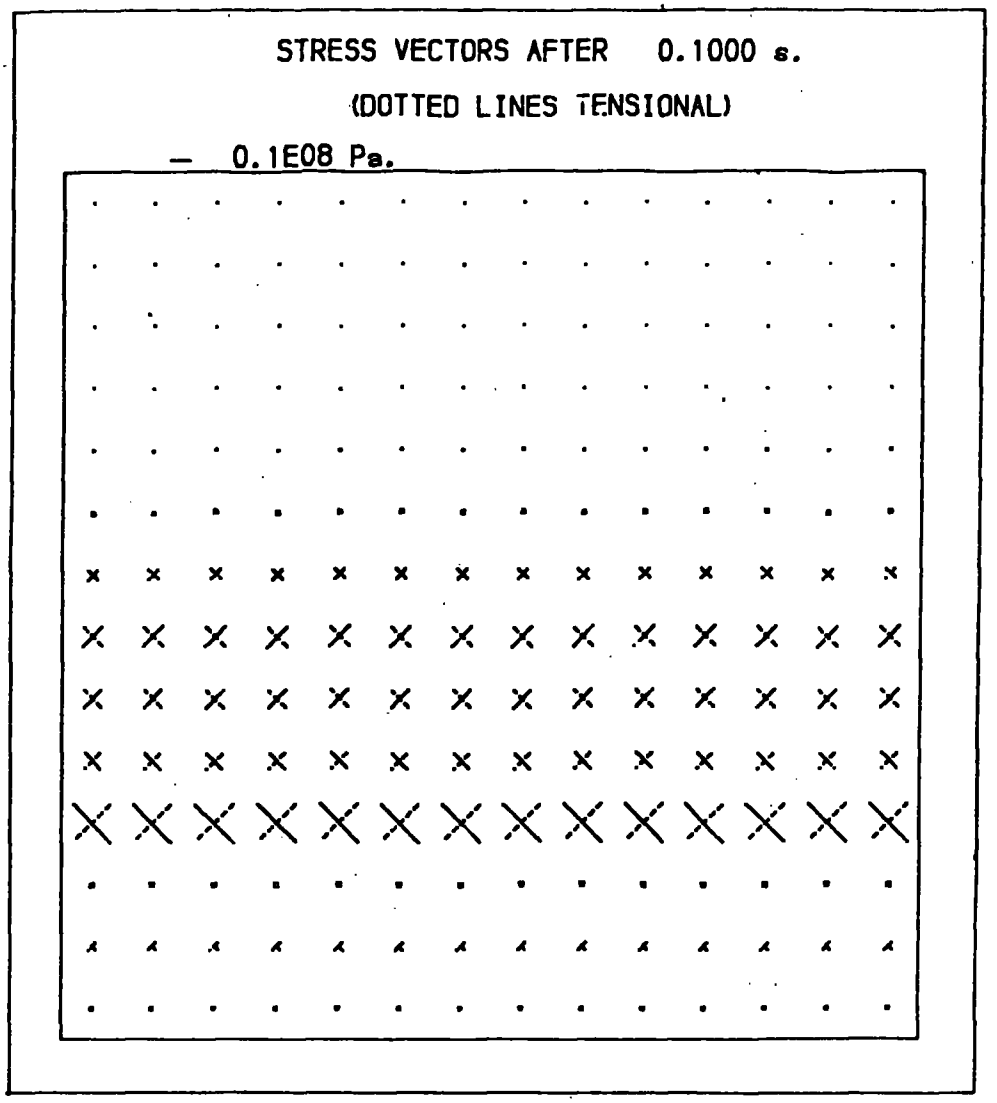
STRESS VECTORS AFTER 0.1000 s.
(DOTTED LINES TENSIONAL)
— 0.1E08 Pa.

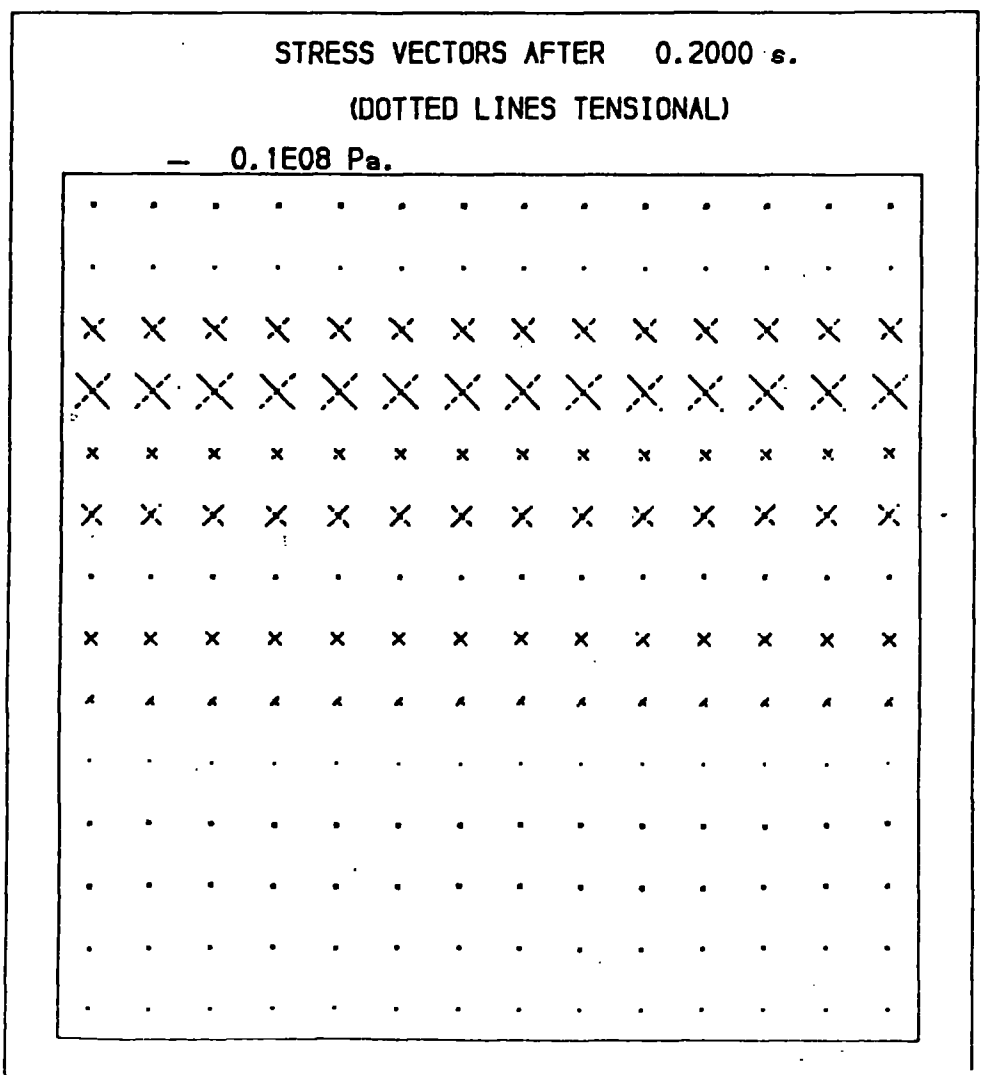
STRESS VECTORS AFTER 0.2000 s.
(DOTTED LINES TENSIONAL)
— 0.1E08 Pa.

Fig. 4.10

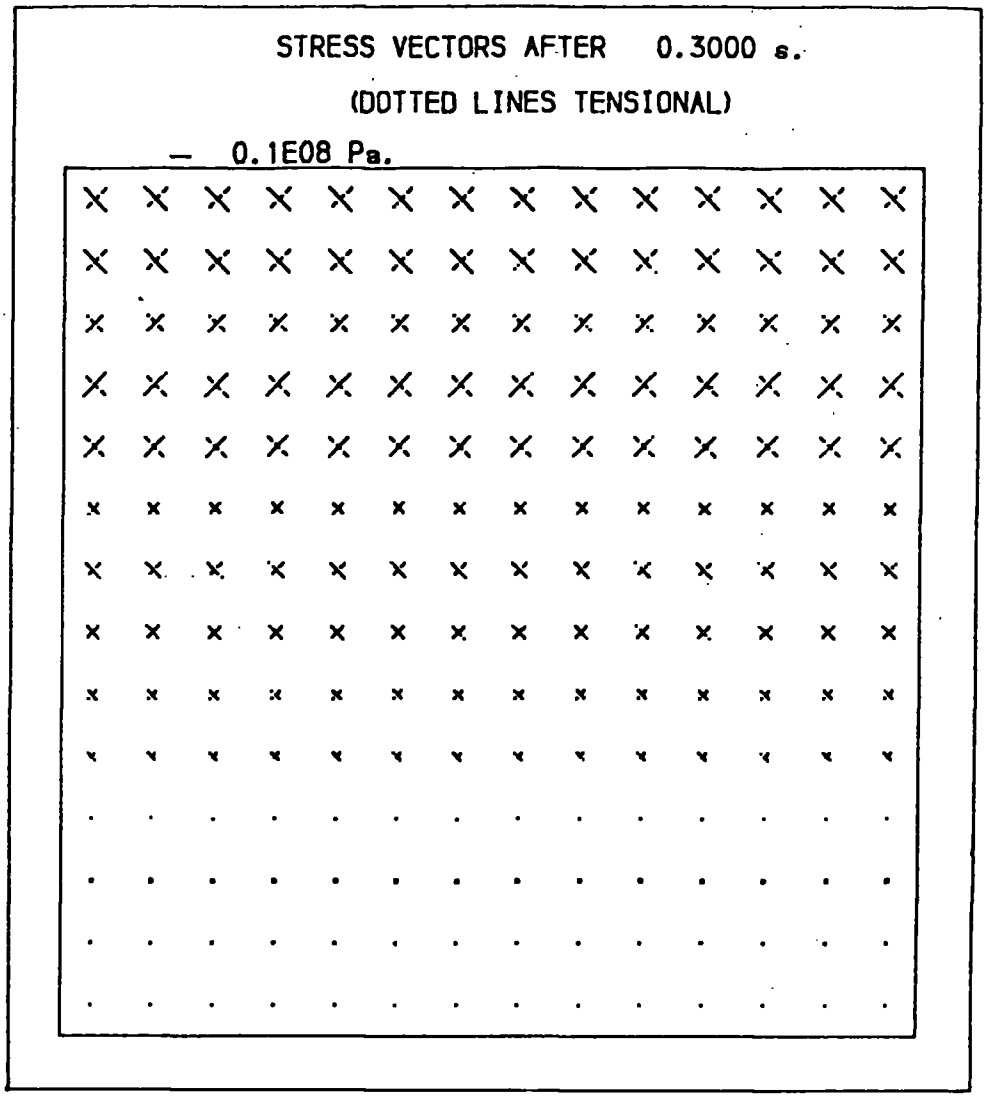
STRESS VECTORS AFTER 0.3000 s.
(DOTTED LINES TENSIONAL)
— 0.1E08 Pa.

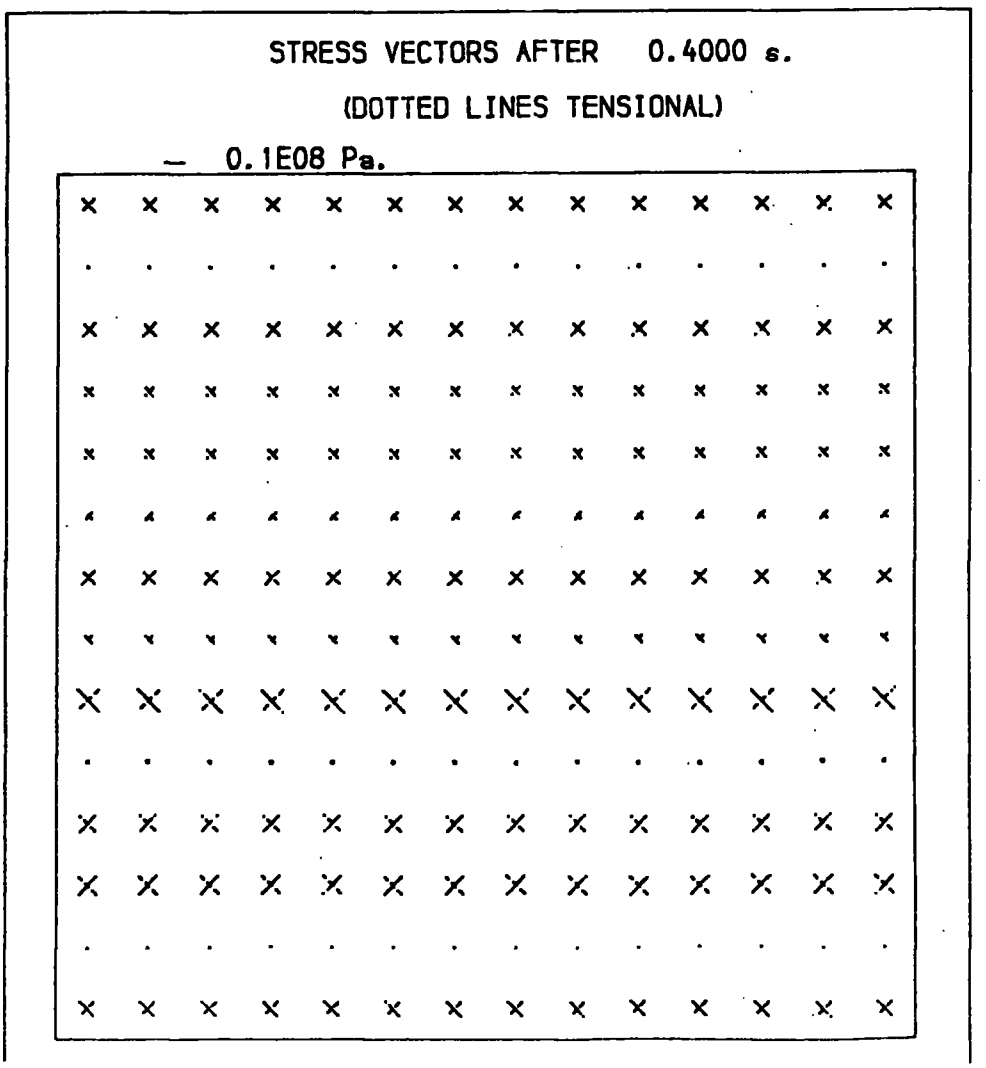
STRESS VECTORS AFTER 0.4000 s.
(DOTTED LINES TENSIONAL)
— 0.1E08 Pa.

Fig. 4.11

Test Run E

Boundary Conditions						
Top surface free		Sides zero y-displacement			Base plane wave pulse	
Pulse parameters		Type S-wave				
Period 0.13s.		Timestep 0.004s.			Amplitude 0.1m.	
Angle 0.0^0		Frequency 7.7 Hz.			Timesteps per period 32.5	
Material Properties						
Young's modulus $n.m.^{-2}$	Poisson's ratio	Density $kg.\ m.^{-3}$	Velocities $m.s^{-1}$ P-wave	Velocities $m.s^{-1}$ S-wave	Wave-length m.	Elements per wavelength
8×10^9	0.25	2400	2000	1155	150	10

This run is similar in nature to run D, but with a lower frequency. The time-displacement graphs, Fig. 4.12, give 1133 ms^{-1} for the velocity of the progression of the first peak, which compares very well with theoretical value of 1155 ms^{-1}. The amplitude of the pulse is 0.2 for all nodes near the base, and attains the expected value of 0.4 at the free surface both at its first and second arrivals.

The graphs of the stress plots, Fig. 4.13-4.14, also agree well with theory. The maximum stress is found to be 1.36×10^7 Pa. on both the front and back part of the pulse. The theoretical value is 1.34×10^7 Pa.

The time-displacement graphs show very little dispersion, and this is reflected in the stress plots, where a spurious stress cannot be found until time 0.36 (i.e. after 90 time steps) where a small stress can be detected in the wake of the downgoing wave after the first reflection. Another indicator of the satisfactory nature of the runs are the time-displacement graphs for some nodes in the y-direction, Fig. 4.15.

These displacements should be zero, and the graphs give maximum values of 8×10^{-5}m. compared with the 0.4m. in the x-direction. The y-displacements are fairly random and are certainly no more than you would expect simply from round off errors - all the calculations are carried out in single precision.

DURHAM UNIVERSITY
- 5 AUG 1982
SCIENCE LIBRARY

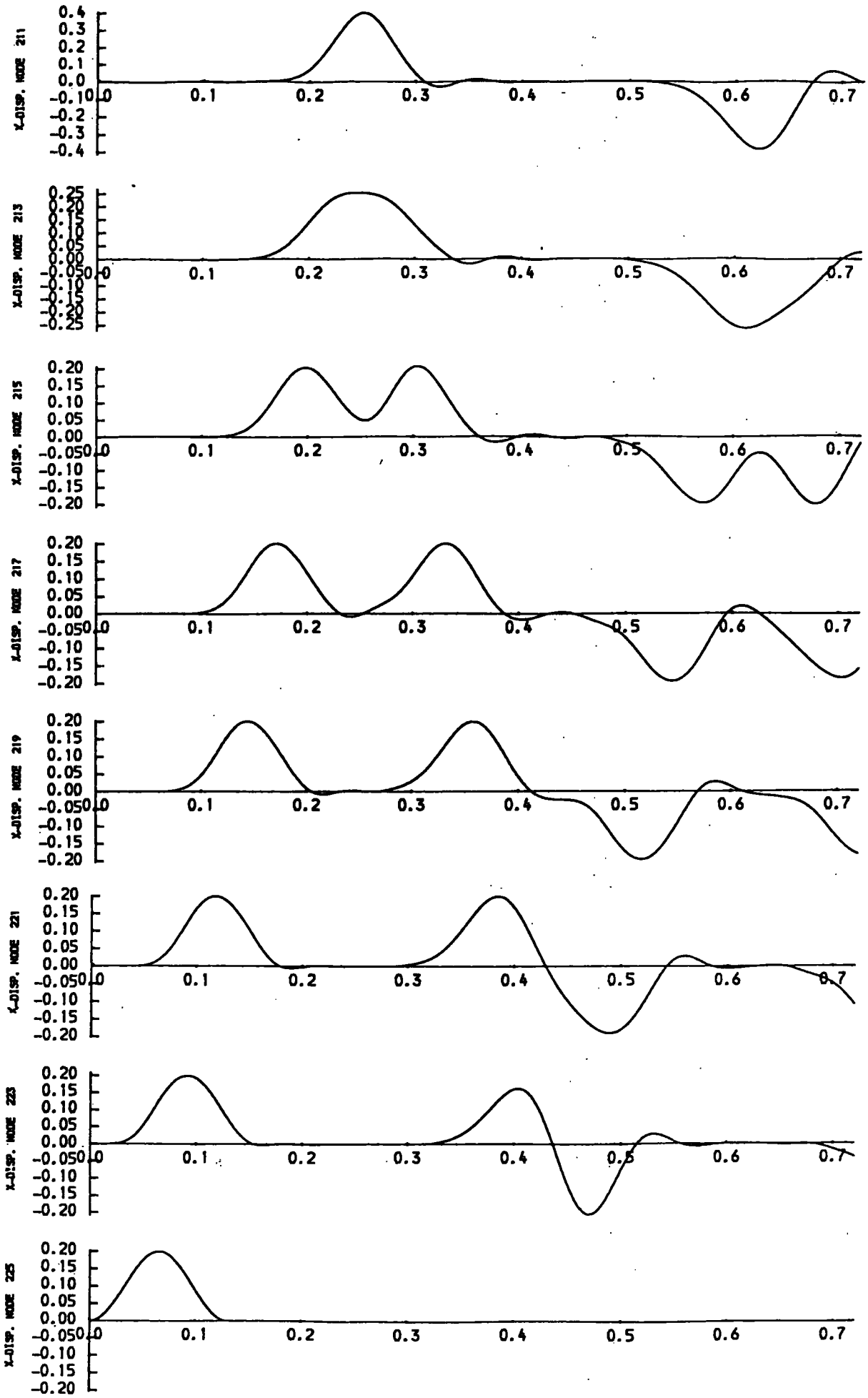

Fig. 4.12 Test Run E x-displacements.

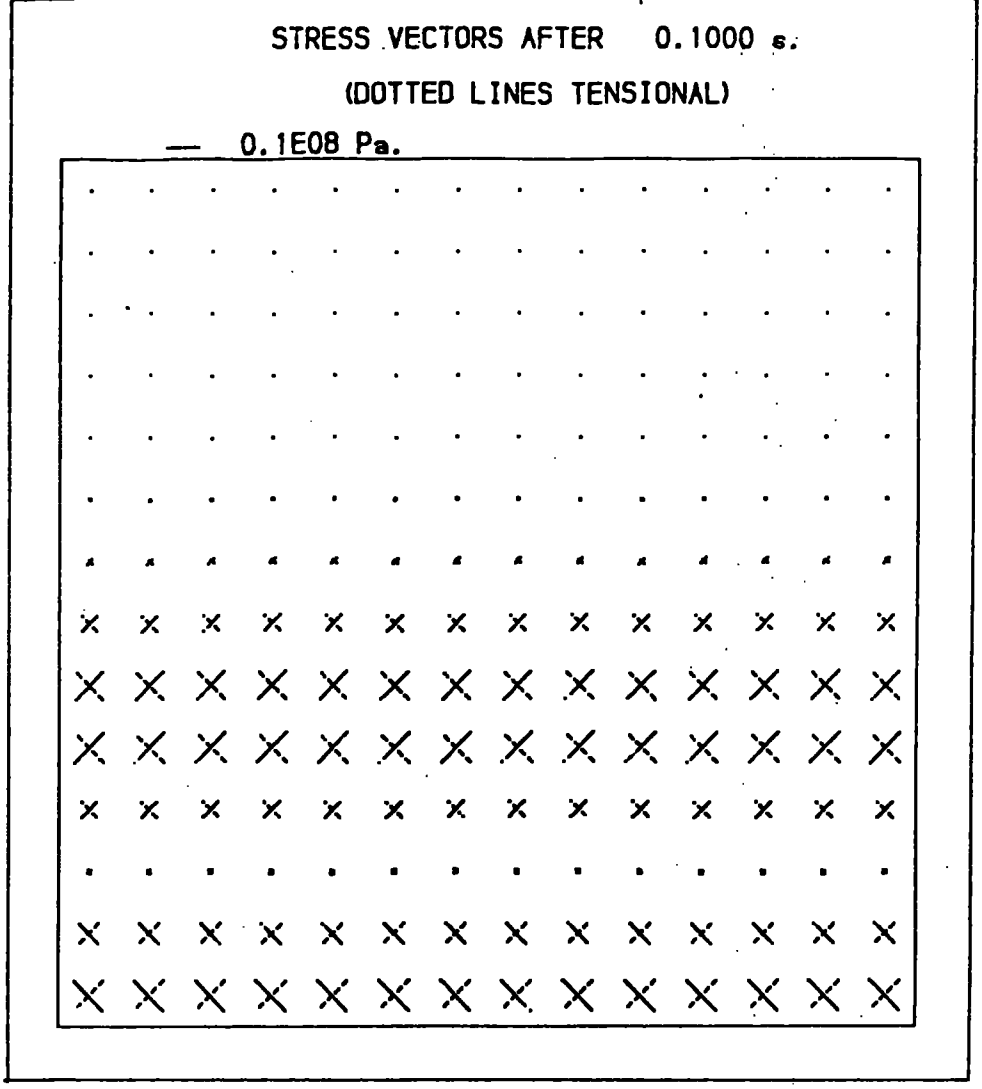
STRESS VECTORS AFTER 0.1000 s.
(DOTTED LINES TENSIONAL)
— 0.1E08 Pa.

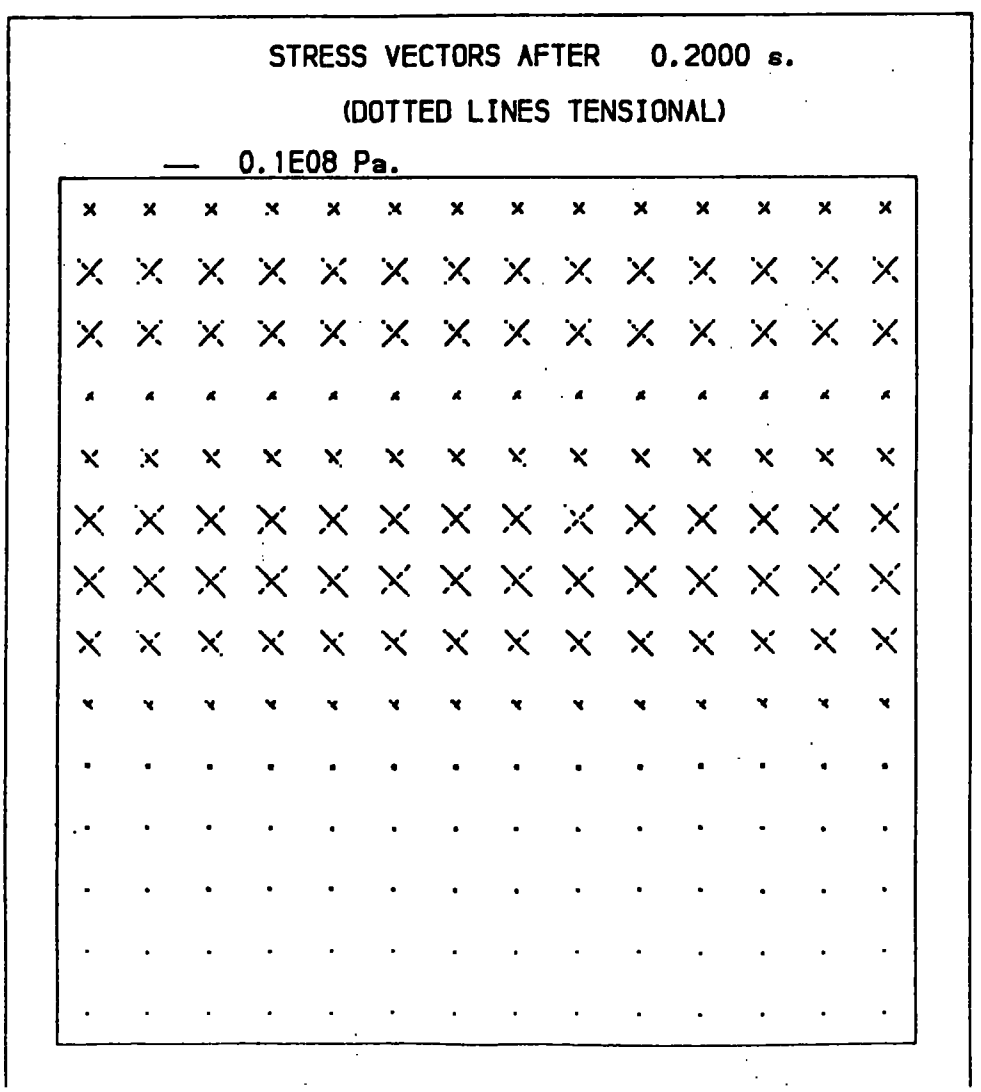
STRESS VECTORS AFTER 0.2000 s.
(DOTTED LINES TENSIONAL)
— 0.1E08 Pa.

Fig. 4.13

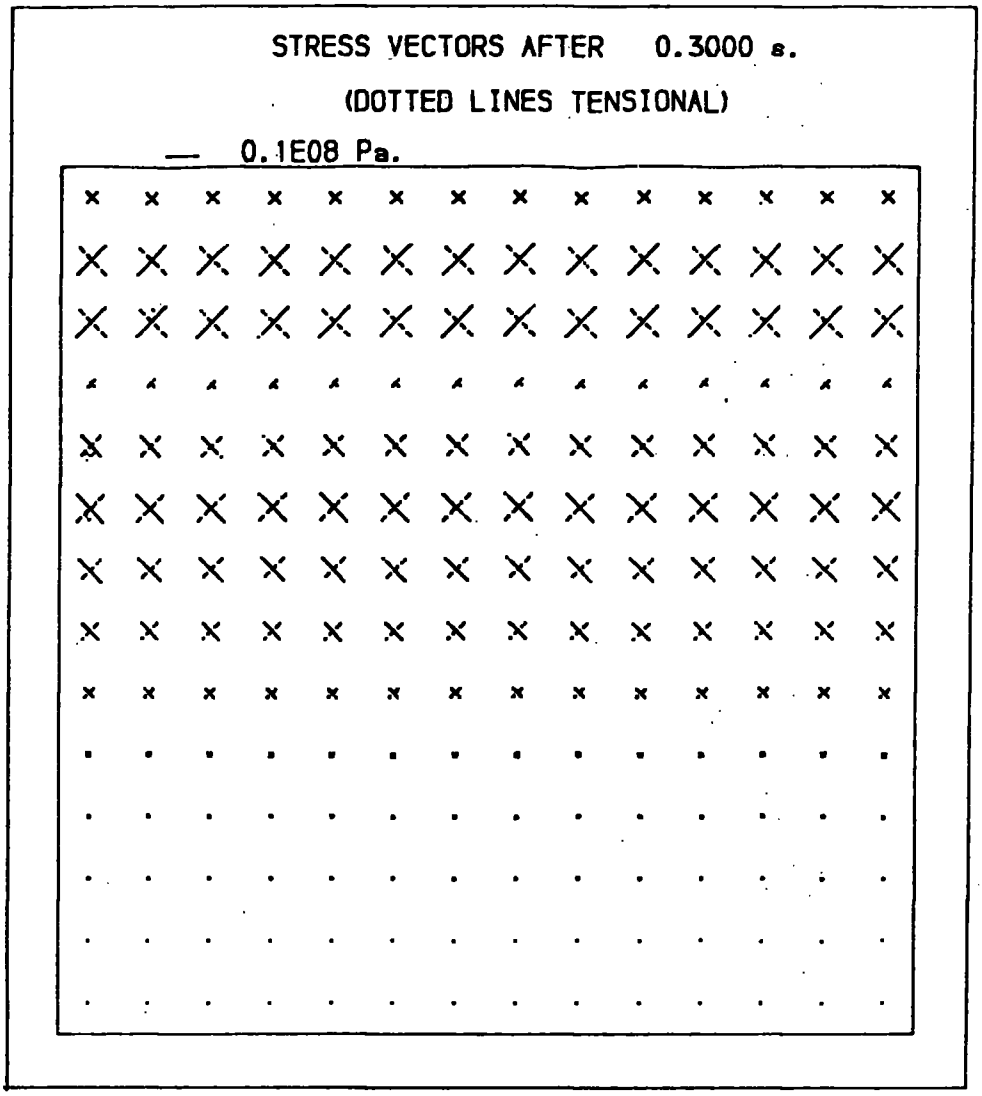
STRESS VECTORS AFTER 0.3000 s.
(DOTTED LINES TENSIONAL)
— 0.1E08 Pa.

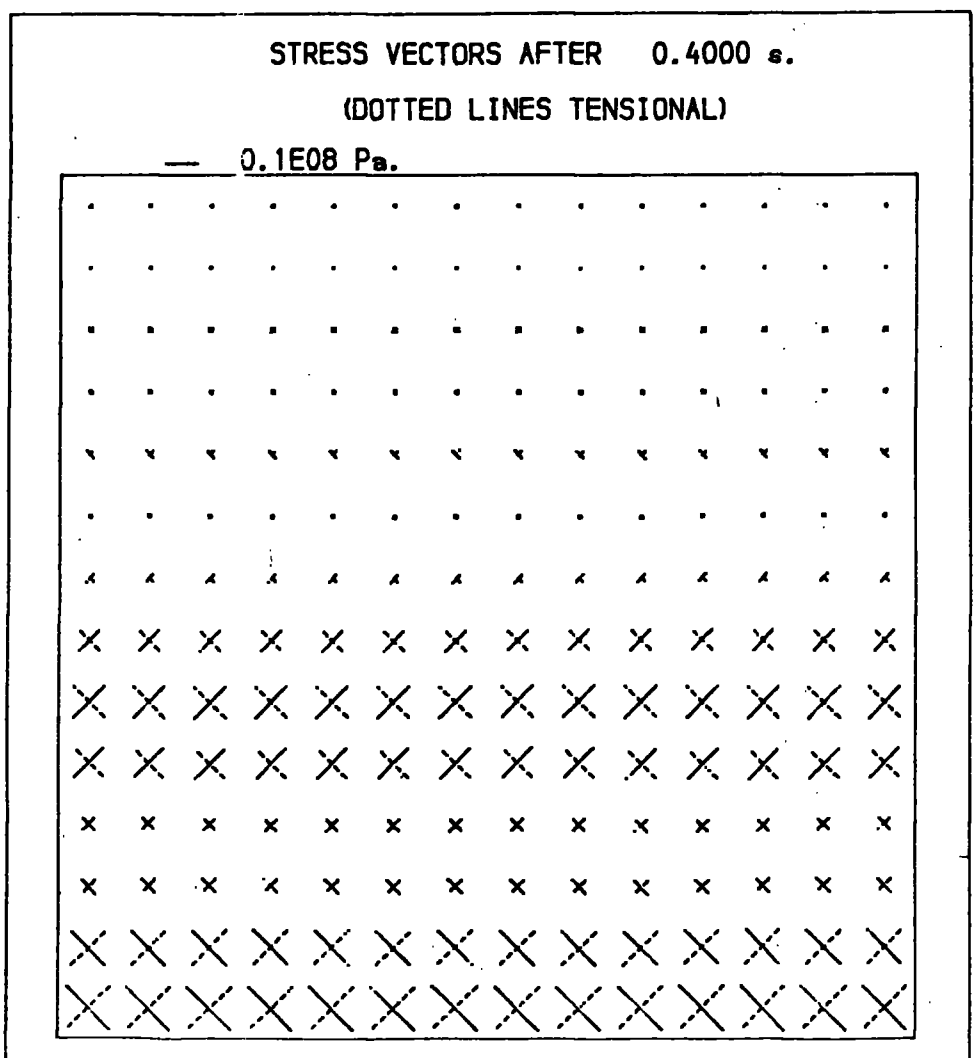
STRESS VECTORS AFTER 0.4000 s.
(DOTTED LINES TENSIONAL)
— 0.1E08 Pa.

Fig. 4.14

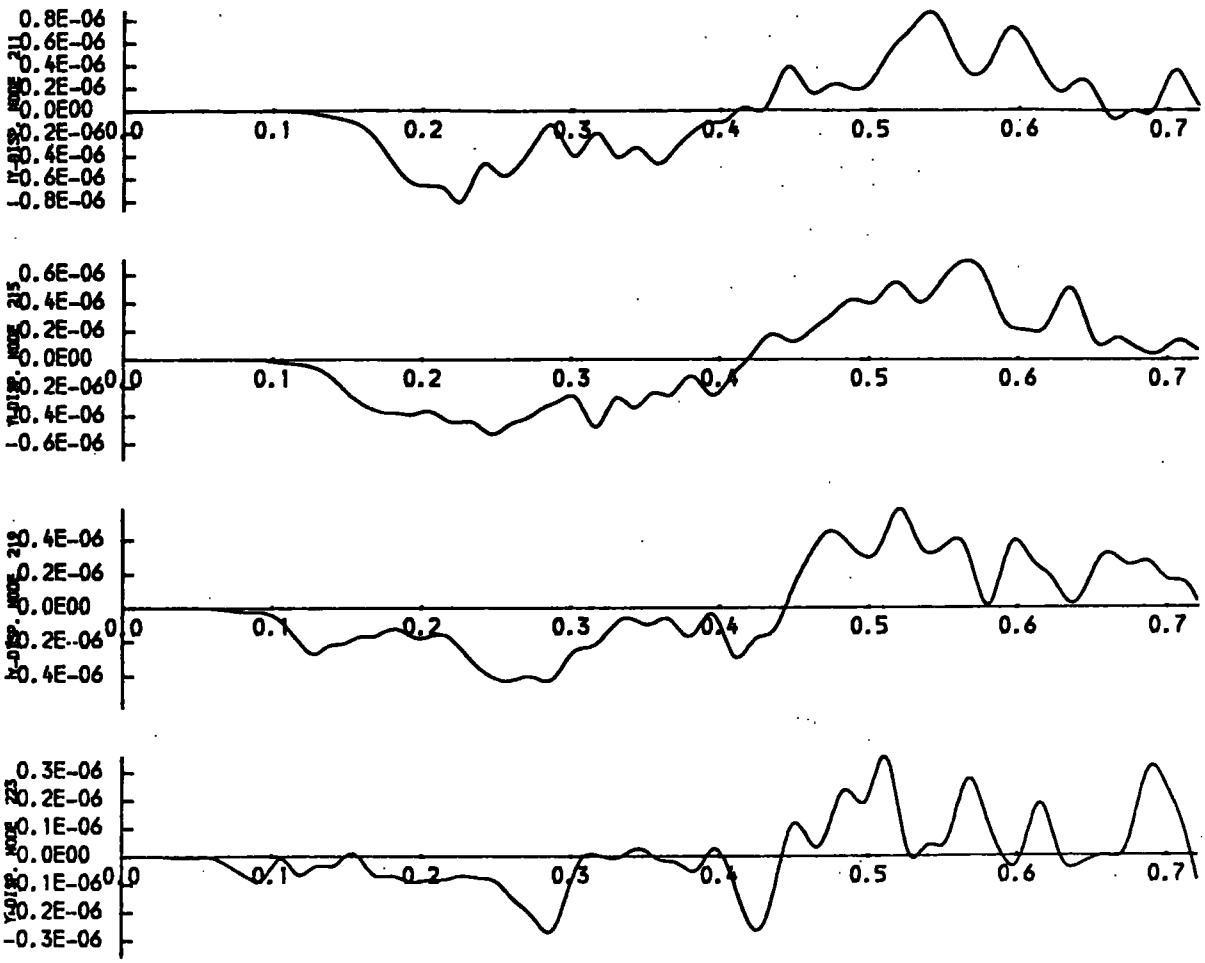

Fig. 4.15 Test Run E y-displacements.

Test Run F

Boundary Conditions							
Top surface nodes free		Sides nodes free		Base plane wave pulse			
Pulse parameters		Type P-wave					
Period 0.1s.		Timestep 0.001s.		Amplitude 0.1m.			
Angle 45^{o}		Frequency 10 Hz.		Timesteps per period 100			
Material properties		2 layers					
	Young's Modulus $n.m.^{-2}$	Poisson's Ratio	Density $kg.m.^{-2}$	Velocity		Wave-length m.	Elements per wavelength
				P-wave $m.s^{-1}$	S-wave $m.s^{-1}$		
layer 1	1.8×10^{10}	0.25	2400	3000	1730	300	20
layer 2	4.05×10^{10}	0.25	2400	4500	2600	450	30

This run has the grid divided into two layers of different materials as shown in Fig. 4.16.

In this trial the wavelength is large compared to the mesh size and there is no detectable dispersion in the time displacement graphs, Figs 4.18-4.19, and the stress plots, Figs 4.20-4.23, at successive time-steps vary smoothly from one pattern to another, even though the pattern after 120 time-steps is quite complex. From the stress plots the progress of the incoming P-wave at 45^{o} is clearly seen, and then its subsequent refraction at the boundary between the two layers, which is half way down the grid. Measurements from the stress plots at 0.08s give the angle of the wave as 43^{o} in the bottom layer, and 30^{o} to the vertical after refraction.

The exact nature of the refraction is quite complicated, with both P and SV components in both layers. The theoretical results are derived in Aki and Richards (1980) pp. 133-152. Fig. 4.17 gives the expected angles of these components and the % of energy in each component for the parameters of this trial.

We would thus expect to see primarily a refracted P-wave at about 30^{o} to the vertical, which is in agreement with the results.

However, this example is not only complicated by the nature of the refraction and reflection at the boundary between the layers, but also, since the input wave is not parallel to the sides, it includes reflections from the sides almost as soon as the input pulse begins. Thus the refraction at the boundary between the layers can only be observed at the leading edge of the incoming pulse. Behind this there quickly develops an exceedingly complicated stress pattern which is a result of the combined displacements due to the incoming P-wave, and reflected and/or refracted P and SV waves from the sides, top, bottom and interface.

If this grid were being used to model a finite region of the dimensions of the grid subject to the boundary conditions and input which we used, then, since the elements per wavelength and time-steps per period are both very favourable there seems no reason to suppose that the stress plots obtained are not good representations of reality. Unfortunately, however, the region to be modelled in this study is not finite, but infinite in breadth and depth. In such a case all the reflections from the sides and base are unwanted. This presents a severe restriction on the finite element method for the study of transient wave propagation problems. This is discussed at greater length in section 5.5.

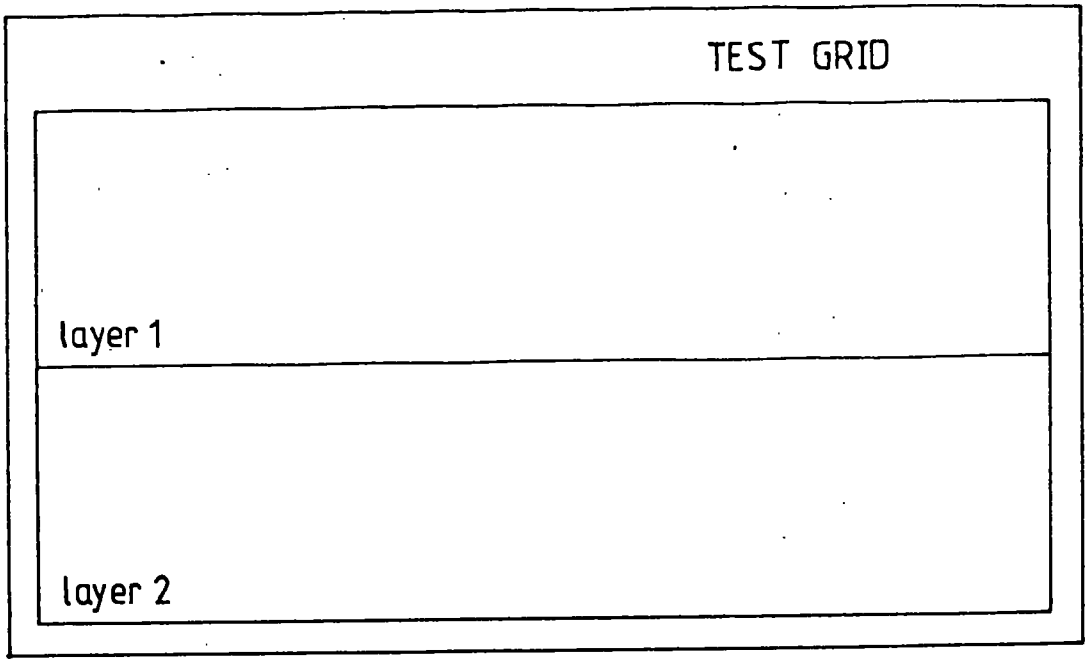

Fig. 4.16

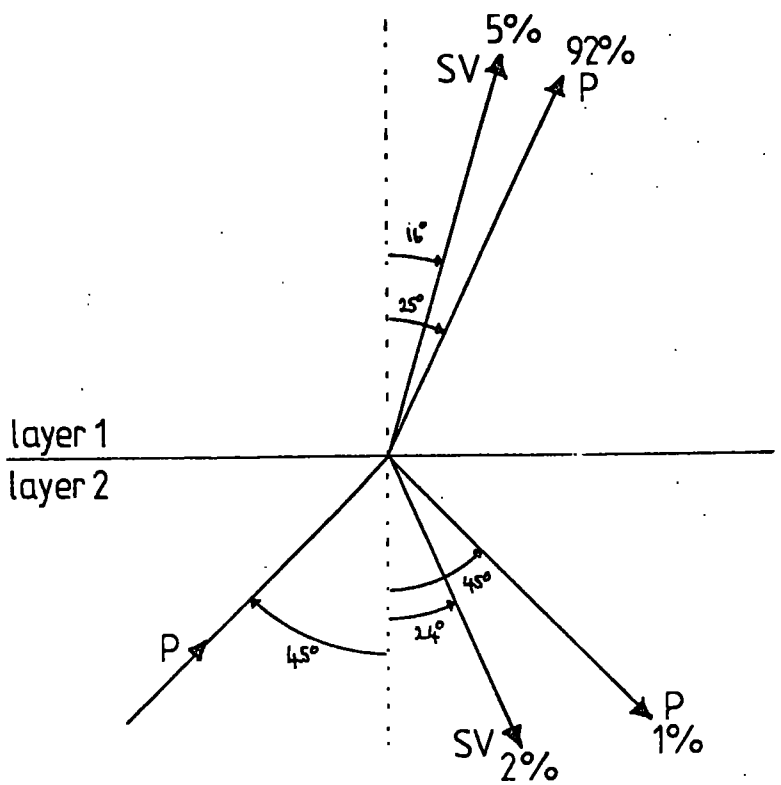

Fig. 4.17 Mode conversion of incident P-wave.

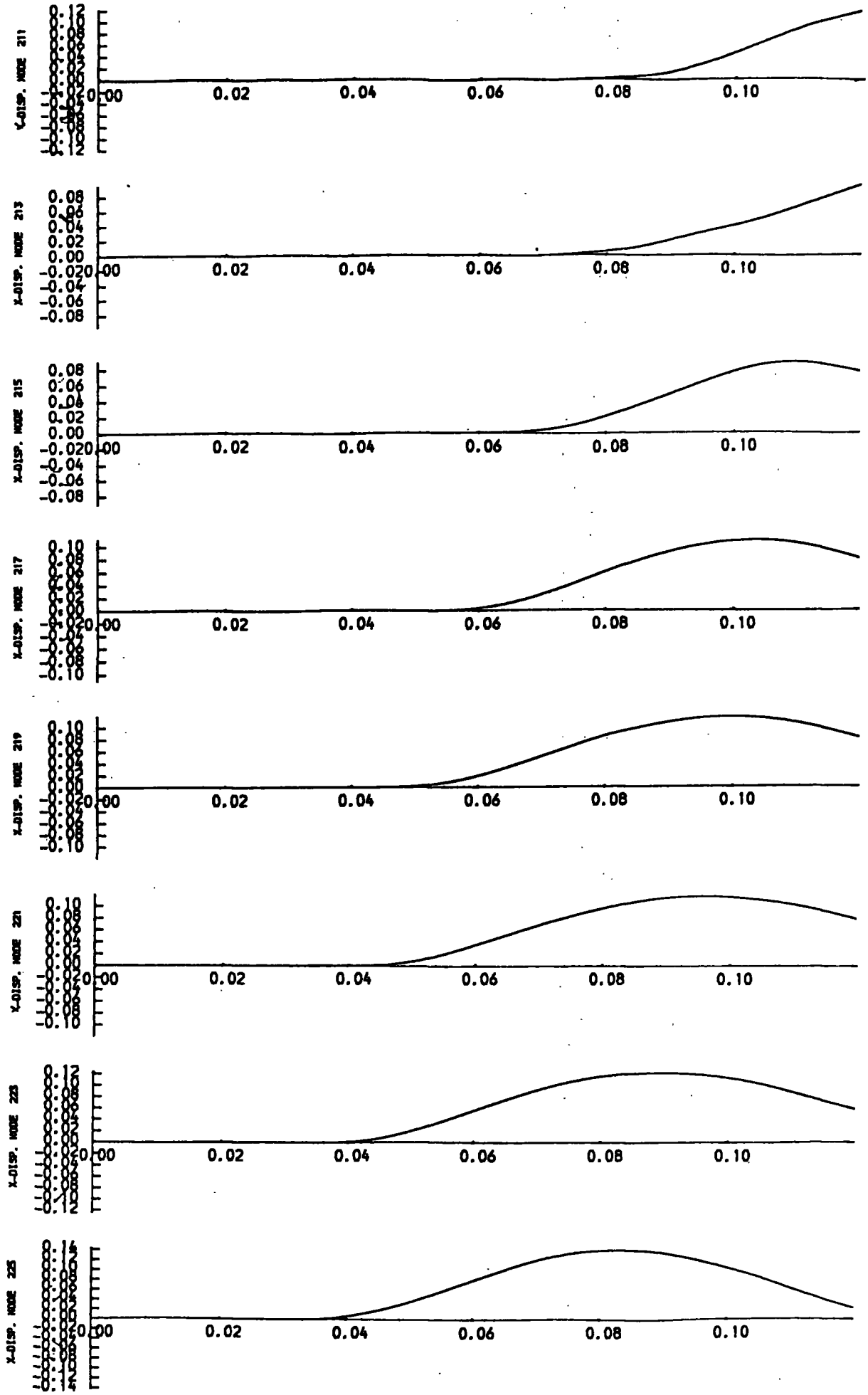

Fig. 4.18 Test Run F x-displacements.

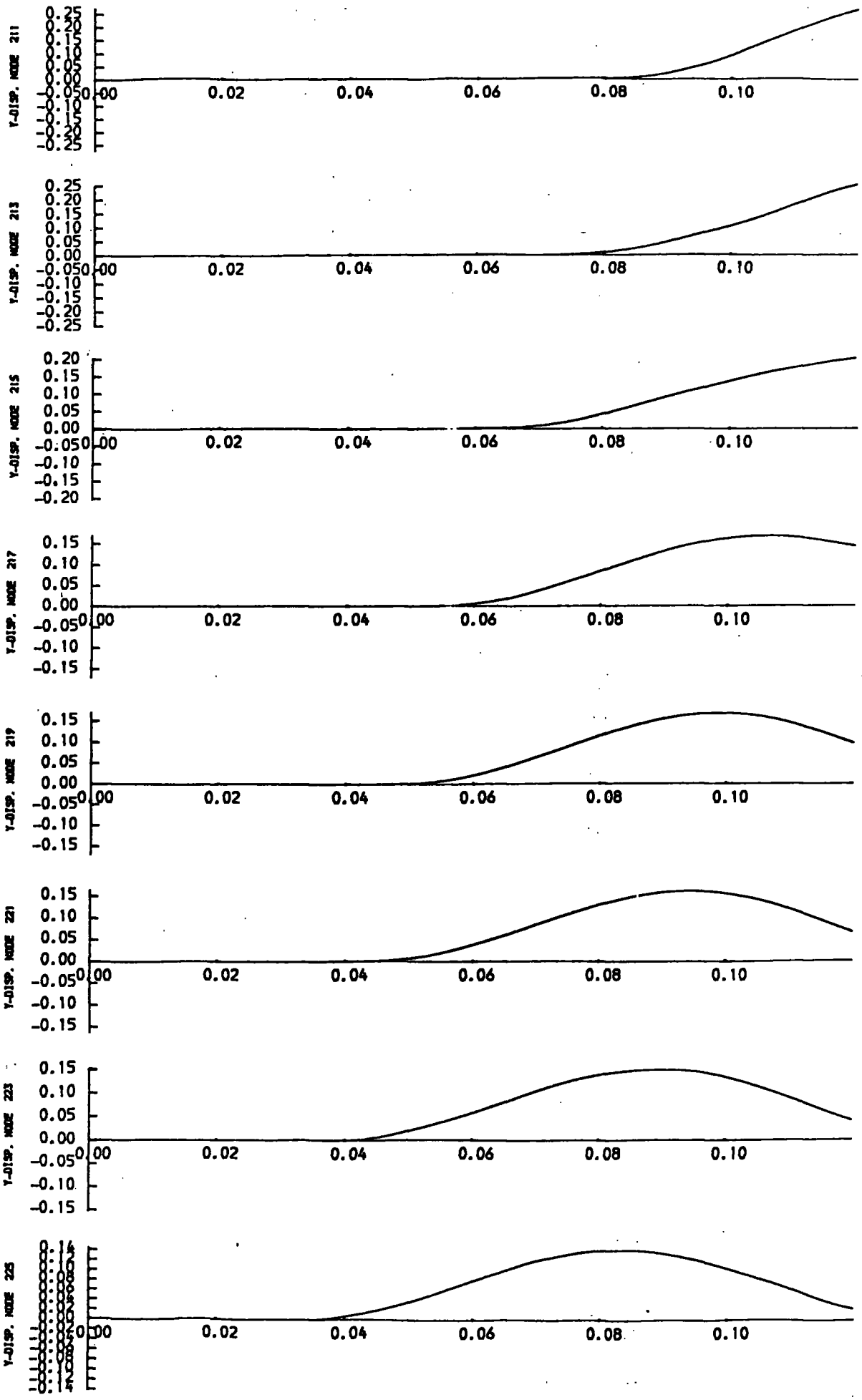

Fig. 4.19 Test Run F y-displacements.

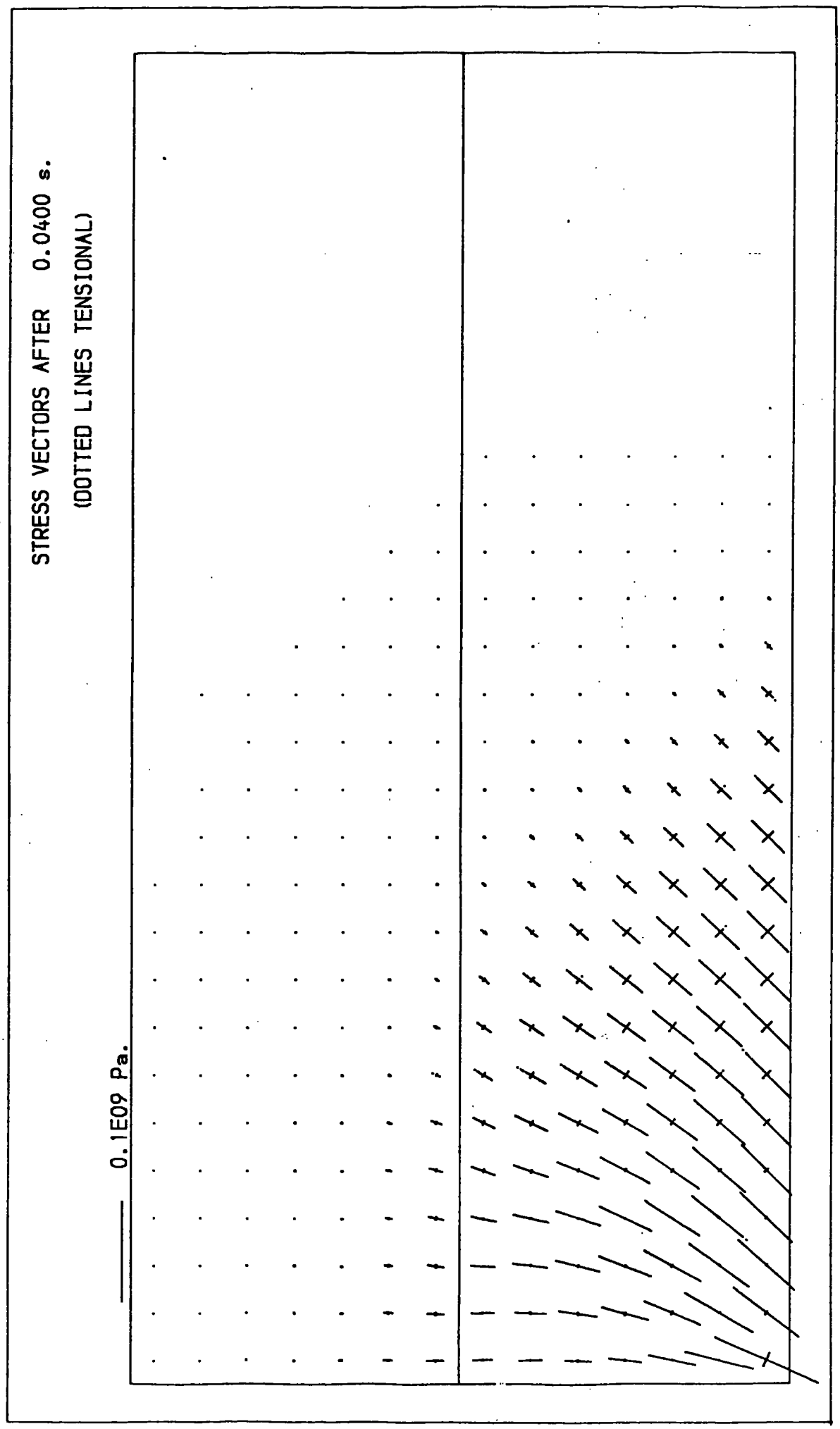
STRESS VECTORS AFTER 0.0400 s.
(DOTTED LINES TENSIONAL)
0.1E09 Pa.

Fig. 4.20

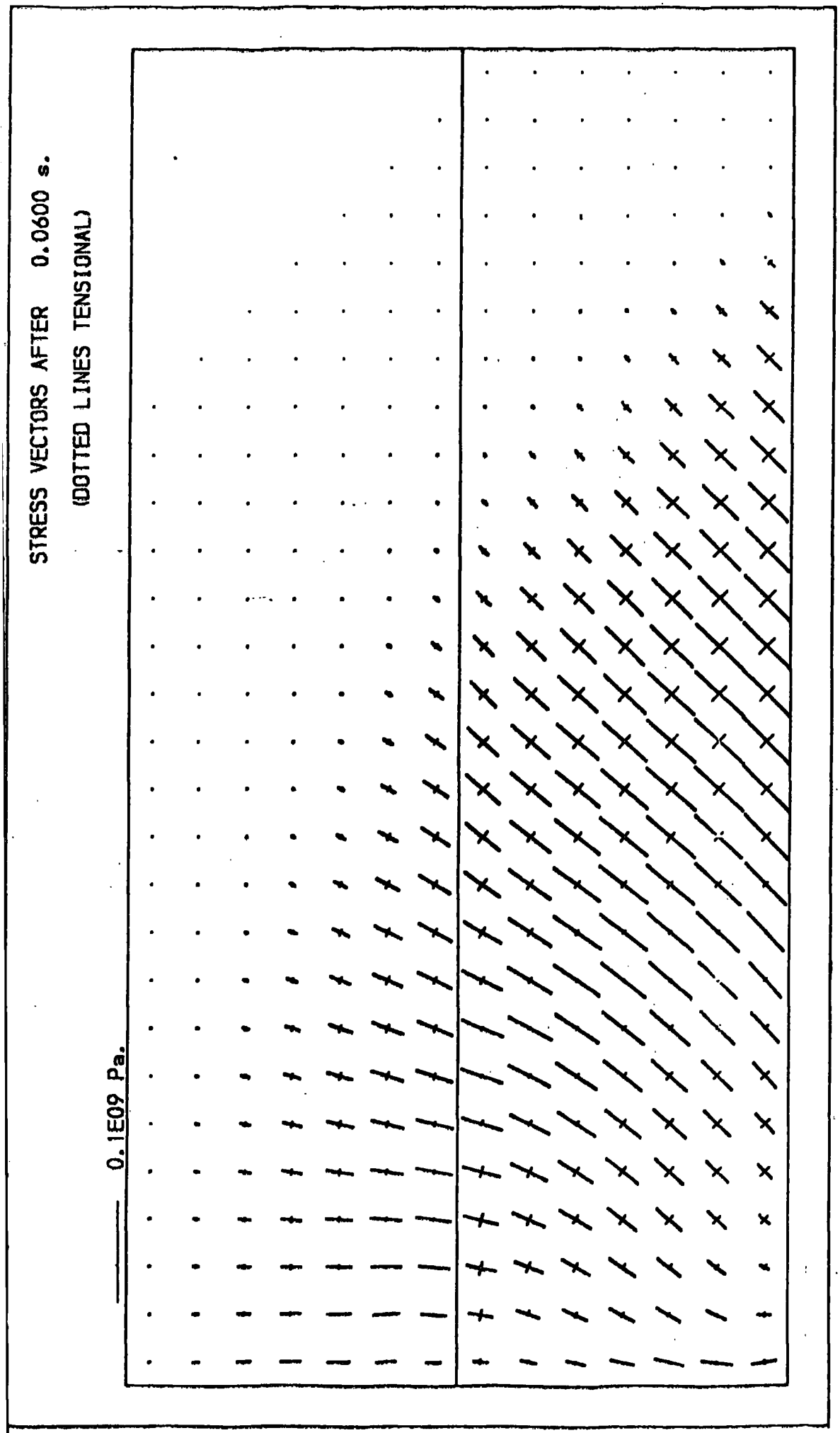
STRESS VECTORS AFTER 0.0600 s.
(DOTTED LINES TENSIONAL)
0.1E09 Pa.

Fig. 4.21

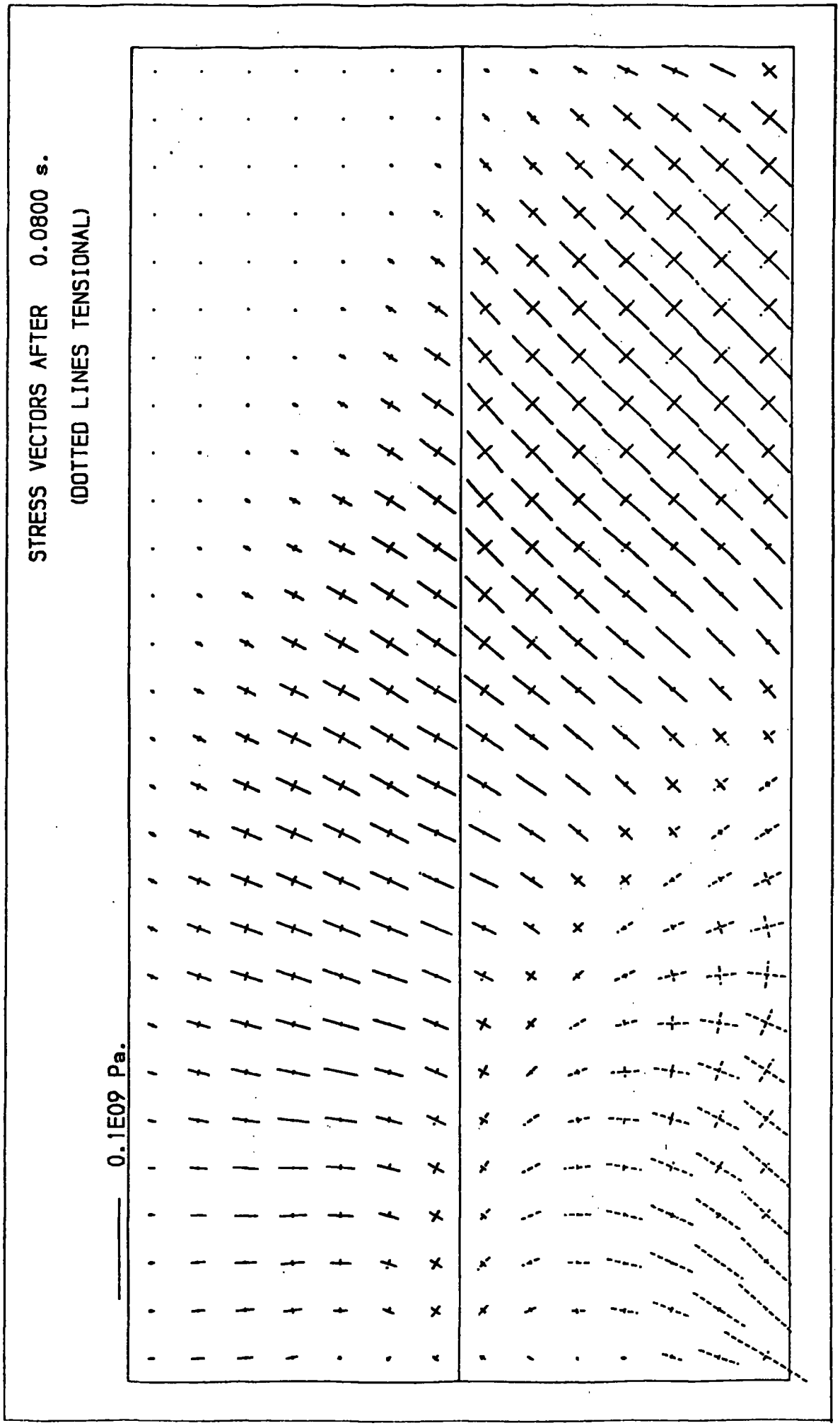
STRESS VECTORS AFTER 0.0800 s.
(DOTTED LINES TENSIONAL)
0.1E09 Pa.

Fig. 4.22

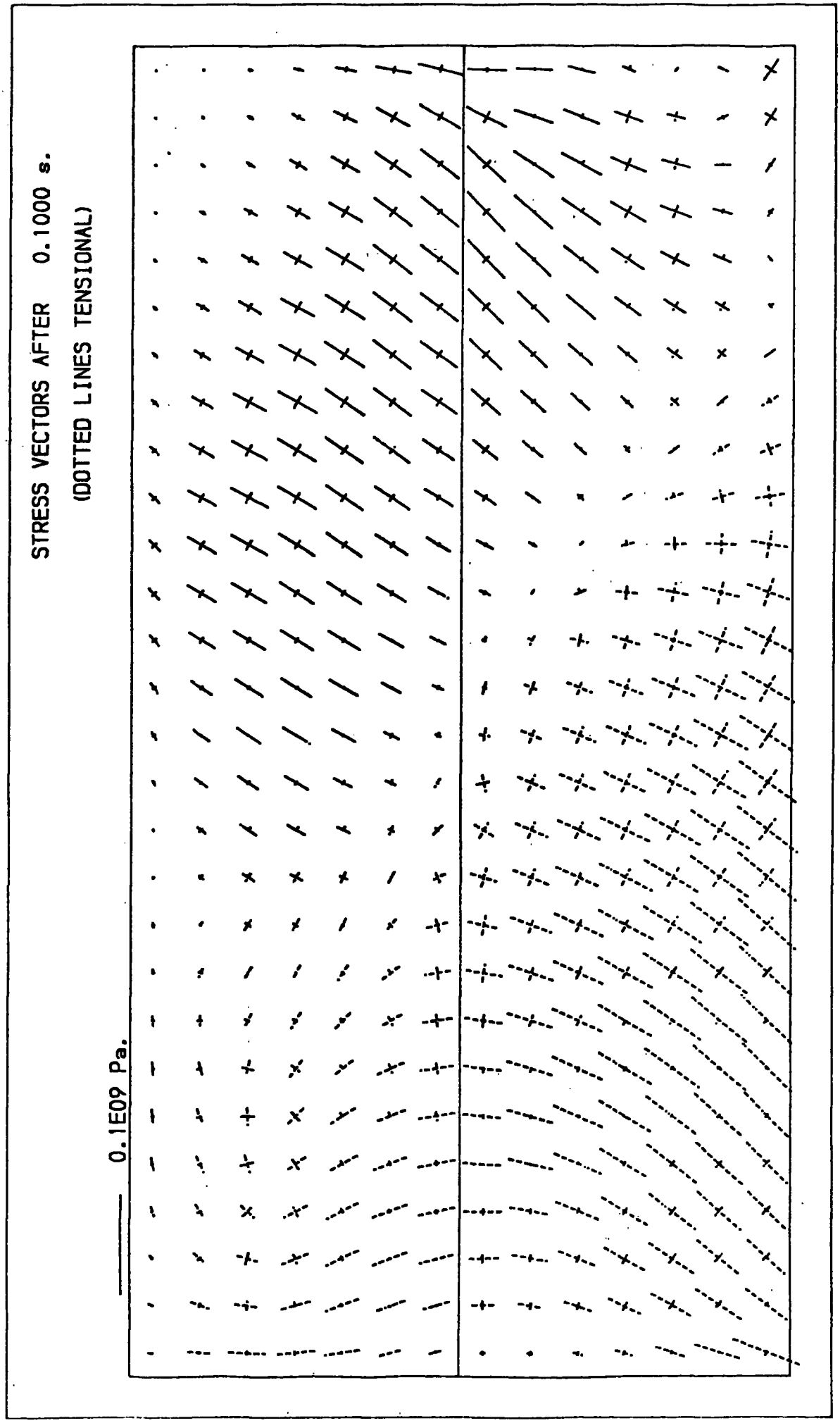
STRESS VECTORS AFTER 0.1000 s.
(DOTTED LINES TENSIONAL)
0.1E09 Pa.

Fig. 4.23

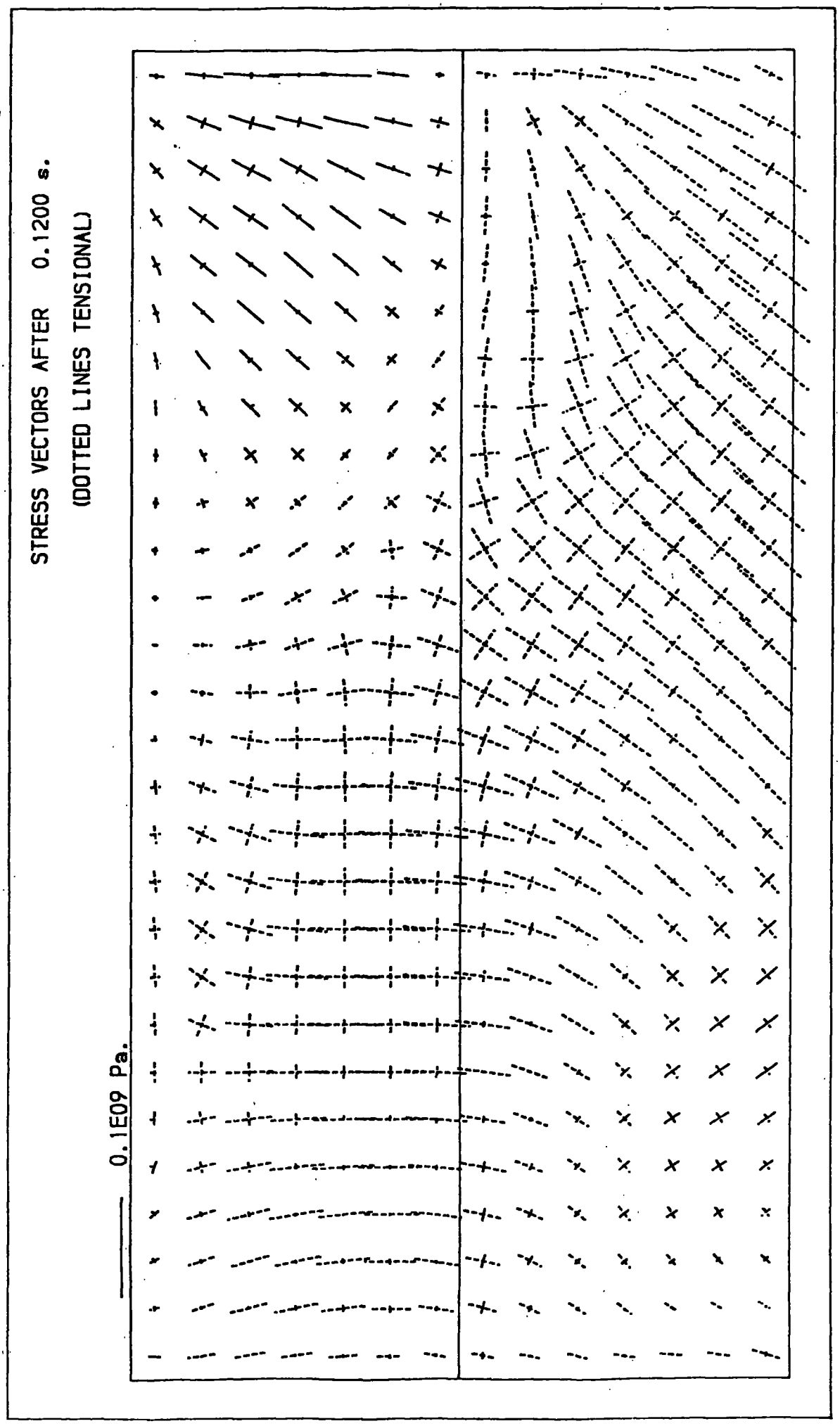
STRESS VECTORS AFTER 0.1200 s.
(DOTTED LINES TENSIONAL)
0.1E09 Pa.

Fig. 4.24

4.4. Summary

The trials described in the previous sections are summarised in the following table.

RUN	P or S wave	Timesteps per period	Elements per wavelength	Acceptability
A	P	6	8	good
B	P	12	8	very good
C	P	12	4	bad
D	S	12	4.6	bad
E	S	32.5	10	excellent
F	P	100	30	excellent

The "acceptability" is a judgement based on the features discussed in the previous section - namely the lack of dispersion of the time-displacement graphs, the maintenance of amplitude, the accuracy of the velocity of propagation, the accuracy of the principal stresses and the absence of artefacts from the stress plots.

Chapter 5. Limitations of the finite element method

5.1. Introduction

The test runs previously described in chapter 4 show that it is possible to model effectively the propagation of elastic waves provided that certain criteria are met. What these criteria are, and what their implications are, will be discussed in this chapter.

5.2. Restriction on time-step size

As explained in detail in chapter 3 there is a critical time-step size whenever a Runge-Kutta algorithm is used. This critical value is determined solely by the left handside of the equations of motion (3.1.1.), and is in no way affected by the nature of the forcing term $[Q(t)]$. There are thus two separate questions:-

a) Is the time-step small enough to avoid instability?

b) Is the time-step small enough to give a realistic model for a given forcing term?

The answer to (a) is a property of the grid being used, and is found empirically in the sense that if too large a time-step is used then the instability will be manifest.

The test runs revealed that 6 time-steps for each period of the forcing function gave satisfactory results, and that if other factors such as mesh size are kept the same, a decrease in the time-step size produced some improvement, but not one which was marked. Thus it is possible to adopt as a criterion for step size, h,

$$h < \frac{1}{6f} \qquad 5.2.1$$

where f is the frequency of the forcing term.

It is also interesting to note that for the test runs, whenever this criterion was met there was no difficulty in meeting the stability condition. There is, of course, no necessity for this to be the case as the two criteria depend on entirely independent things. However, this happy circumstance also prevailed in the later models to be discussed in chapter 7. Also, in order to give a detailed picture of the progression of an elastic wave it was usually decided to use a time-step size smaller than that required by 5.2.1.

5.3. Restriction on mesh size

The test runs revealed that the mesh size compared with the wavelength of the propagating wave is a severe restriction on the applicability of the finite element method. It was found that for

too coarse a mesh the energy of the propagation wave is dispersed leading to both loss in amplitude of the wave, and, more seriously, the development of ripples in the wake of the wave. This in turn leads to quite unsatisfactory predictions of principal stress. A comparison of predicted displacements, velocities, and stress values with theoretical values, and a visual interpretation of time-displacement graphs suggested that for satisfactory results there should be at least 8 elements in each wavelength of the propagating wave. Exactly the same figure is suggested by Smith (1975), whereas Fedock and Schreyer (1981) suggests a value of 6 elements in each wavelength. In this study the more restrictive figure was used in the criterion to be met, which may be stated as

$$l < \frac{\lambda}{8} \qquad 5.3.1$$

where l is the element size needed to satisfactorily propagate a wave with wavelength λ.

This rule can be regarded as a limitation on the possible waves that can be modelled, either in velocity or frequency. For a given velocity of propagation, v, 5.3.1., gives an upper limit to frequencies, f, given by

$$f < \frac{v}{8l} \qquad 5.3.2.$$

If the frequency is given then the rule gives a lower limit to possible velocities. For example, for the grid, described in chapter 6, which

is used to model embankment dams, the mesh size is 8m. (or less). So for waves with a propagation velocity of 1000 $m^{-1}s$ the maximum frequency is 15.6 Hz. Alternatively, if the frequency is given as 10Hz, then the velocity must exceed 640 ms^{-1}.

5.4. Restriction on possible input signals

The limitations imposed by the condition 5.3.1 have quite far reaching implications. In a study such as this it might be thought desirable to use as in input signal an actual strong motion record such as the San Fernando record of 1971. This suffers from the criticisms, already made in section 1.2., that the record of one locality may not be applicable to a different locality, nor even to the same locality at a different time. A more general approach, suggested by Smith (1975), is to use as input an impulse function and use the finite element method to determine the impulse response of the structure. The response of the structure to any input function, whether it be an actual strong motion record or a theoretically derived seismogram, is then found by convolving the input function with the impulse response. But a strong motion record is an extremely complex time series containing a wide range of frequencies, and an impulse function contains all frequencies. So if either of these were used as an input to a finite element model they would fall foul of the condition 5.3.1. Furthermore this criticism applies equally to all finite element formulations, such as mode superposition, since the

limitation results from the finite element approximation itself, and not from the procedure for solving the equations of motion. The tests of chapter 4 have shown that if the input function contains frequencies greater than that permitted by 5.3.2., then the predicted displacements will contain artefacts in the form of unwanted ripples. These ripples seriously affect the calculation of stresses, and the tests suggest that an input function that at all approached an impulse would yield stresses so corrupted by artefacts as to render them of little value. Indeed in the paper of Smith (1975) he remarks on a "ringing" in the predicted displacements which he filters out before presentation. It is perhaps significant that he does not calculate stresses.

The approach adopted in this study is rather more simplistic. If a high frequency in the output cannot be realistically modelled by the grid, why put it in in the first place? So, instead, this study uses idealised inputs consisting of a pulse of known frequency which complies with the requirement 5.3.2 - by 'pulse' is meant, not an impulse, but one complete cycle of a sinusoid wave, as used in the tests. Whilst the results obtained with such an input will be correspondingly idealised, at least we can be reasonably confident that any component of an actual earthquake source with the frequency of the pulse will behave as predicted. The limitations of this approach cannot be denied, but the results obtained should be meaningful.

5.5. The finite size of grids

A limitation to the applicability of the finite element method that is quite different from those discussed in the previous sections of this chapter, though which was raised in the discussion of Test Run F, is that imposed by the finite size of the grid. This is, of course, no problem when the region being modelled is itself finite. Even for static problems which involve an infinite half-space a reasonable representation of the boundary conditions at infinity may be simulated by using large elements at the edges, or better still by using some such artifice as the "infinite elements" proposed by Bettess (1977 and 1980).

In the case of dynamic problems this limitation is much more serious, since the fictitious edges of the grid (that is, those edges which do not correspond to an actual boundary in reality) will act as reflecting boundaries, returning into the grid energy which properly should not be there. In the early stages of this study three methods were tested in an attempt to overcome this problem, for which it can only be reported there was complete lack of success. The first attempt put the boundaries at a large distance by making the elements round the edge very large; however as far as propagating waves were concerned they did not act as though they had any greater dimension than the conventionally sized elements. The same was true of the "infinite elements" of Bettess. It has also been pointed out by Belytschko and Mullen (1978) that variation of size of elements is undesirable anyway in wave propagation problems because of attendent dispersive properties.

A third approach was to use damping elements around the edge. In this case it was possible to reduce the amount of reflected energy - but not to an acceptably low level. However it required much trial and error to find suitable damping coefficients, even with very simple trial grids. Furthermore, as discussed in chapter 3, the inclusion of damping coefficients in the equations of motion leads to instability problems with the Runge-Kutta routine.

Another method, proposed by Smith (1974), uses a summation of two solutions with different boundary conditions along the edges which has the effect of cancelling out the reflected wave. For an acoustic wave the boundary must be free for one solution, and fixed in the other. Since the reflected waves in these two cases are 180^{o} out of phase they cancel each other. However the summation of several solutions is required to eliminate any multiple reflections, and the method fails, as pointed out in a later paper by Smith (1975), when there are waves propagating parallel to a boundary. It is also not clear how the method can be used for any boundary which is being forced in time, such as the base of all the models considered in this study. For these reasons, and in view of the more than doubling of computer time needed, it was decided not to use this method. A survey of this whole problem is contained in Zienkiewicz, Kelly and Bettess (1979), where they do report some progress but admit that their results at the time of writing were inconclusive. A simple resolution of this problem, if indeed one is possible, would be a major breakthrough for the applicability of the finite element method for this type of dynamic problem.

The approach used in this study is the naive one of using a grid large enough so that the area of interest can be studied for long enough before the unwanted reflected waves begin to arrive. This either means that a very large grid has to be used or the time span that can be studied is severely restricted. The size of the grid is limited by the capabilities of the computer, which therefore becomes the overriding constraint.

5.6. Summary

We are now able to assess the use of the finite element method for the solution of dynamic problems. As expected, the modelling of a continuum by a set of ordinary differential equations (3.1.1) has brought its limitations. These limitations are the consequences of three separate problems.

First, given the equations of motion 3.1.1., are we able to find an accurate solution to them? If we use a direct integration method then this puts a limitation on the time-step that we can use. The tests gave the rule 5.2.1 as a condition that has to be met by a stepsize in order to give a satisfactory modelling of a propagating wave with frequency f. It should be emphasised that this condition is imposed by the forcing term of 3.1.1., and <u>not</u> by the particular integration method used. In addition to this condition on stepsize there are the limitations inherent in the integration method, which for the Runge-Kutta algorithm proved to be less restrictive than 5.2.1.,

when the model contained no damping. If mode superposition is used as a means of solving the equations of motion then the accuracy of the solution will depend on the number of modes used.

A second, and more fundamental problem, is how well do the equations of motion 3.1.1., model the continuum at all? That is, even if we were able to find an analytic solution to the set 3.1.1., how close would it be to propagation of a wave through a continuum? In order that there should be a satisfactory fit the tests of chapter 4 suggested the rule 5.3.1., relating the internodal distance of the mesh to the wavelength of the propagation. For given material properties this is a condition between mesh size and frequency of the wave (5.3.2). No ingenuity in the method of solving the equations of motion can overcome this limitation. For instance, if mode superposition were being used, and even if all modes were being calculated, the predictions would still be in error if the mesh size was not fine enough for the frequency of wave being propagated. The severe consequences for possible input signals to any finite element model have been discussed in section 5.4.

The third major limitation of the finite element method is the extent to which it can model an infinite, or semi-infinite, region. As detailed in section 5.5., the reflections of waves from fictitious boundaries make this a severe limitation for dynamics problems.

The finite element method when applied to dynamics problems must therefore be used with full knowledge of its limitations, and with steps taken to ensure that those limitations are not exceeded.

Chapter 6. The representation of an embankment dam by a finite element model

6.1. The forms of embankment dam

It is hardly surprising that no two dams are the same, each being built to meet the specific conditions of the site chosen. It is therefore necessary to look at several examples to see which broad features should be included in any model.

The diagrams of Fig. 6.1-6.6 illustrate some of the variety of embankment dams. Fig. 6.1. is an example of the simplest type, constructed largely from a homogeneous material. It has a height of 45m. and slopes about 1 in 3. The El Isiro dam of Fig. 6.2. has a height of about 30m, and was built with a central core. This dam was built with a curved longitudinal axis (radius of curvature 212m. convex upstream). A dam with a more complex central core is illustrated in Fig. 6.3. This dam has a height of about 90m. and a crest length of 400m., and its more complex construction enables slopes of 1 in 1.6 to be used. The Mammoth Pool Dam (Fig. 6.4), with a height of about 110m. and a crest length of 250m, has neither a central core, nor with its variety of material types could be termed homegeneous. The 112m. high Djatiluhur Dam shown in Fig. 6.5, has a more complex structure, with a sloping core and is built adjoining a first stage cofferdam. Another central core dam is shown in Fig. 6.6., the Nurek Dam, U.S.S.R., which has a height of 312m., illustrating the kind of height that

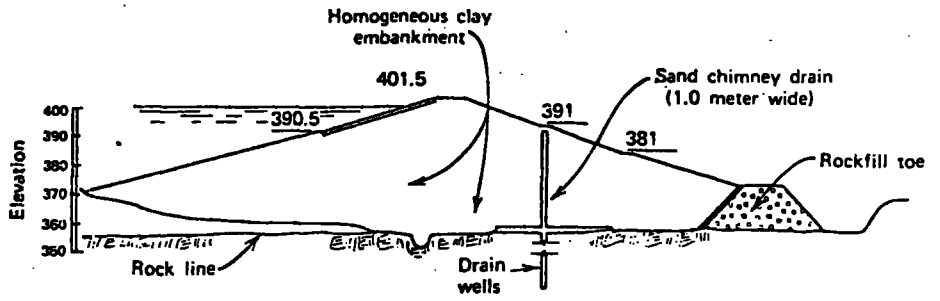

Fig. 6.1 Vigario Dike, Brazil. Homogeneous clay embankment. From Sherard (1973).

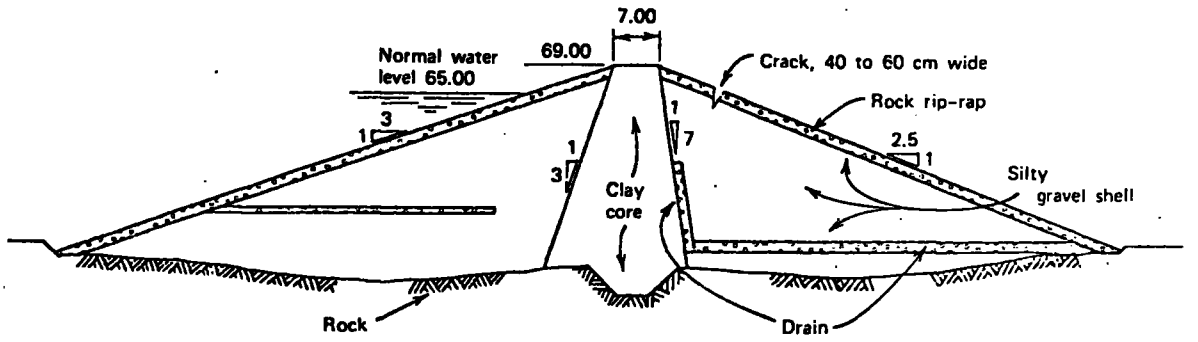

Fig. 6.2 El Isiro Dam. Clay core embankment. From Sherard (1973).

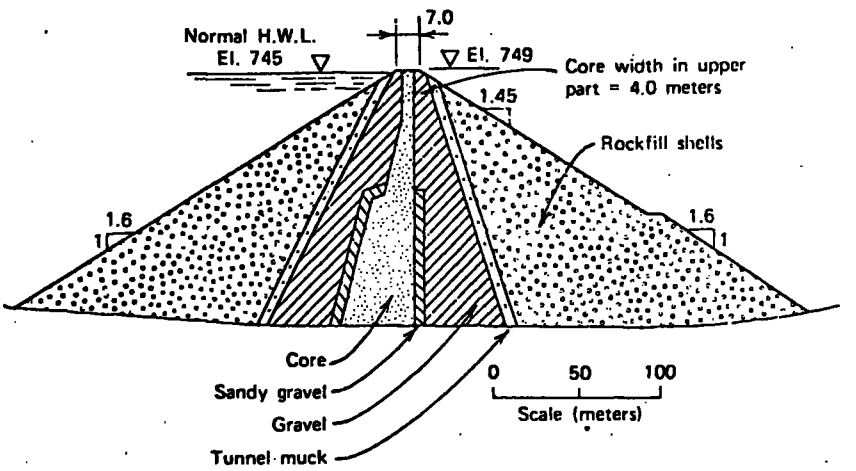

Fig. 6.3 Hyttejuvet Dam. Central core embankment. From Sherard (1973).

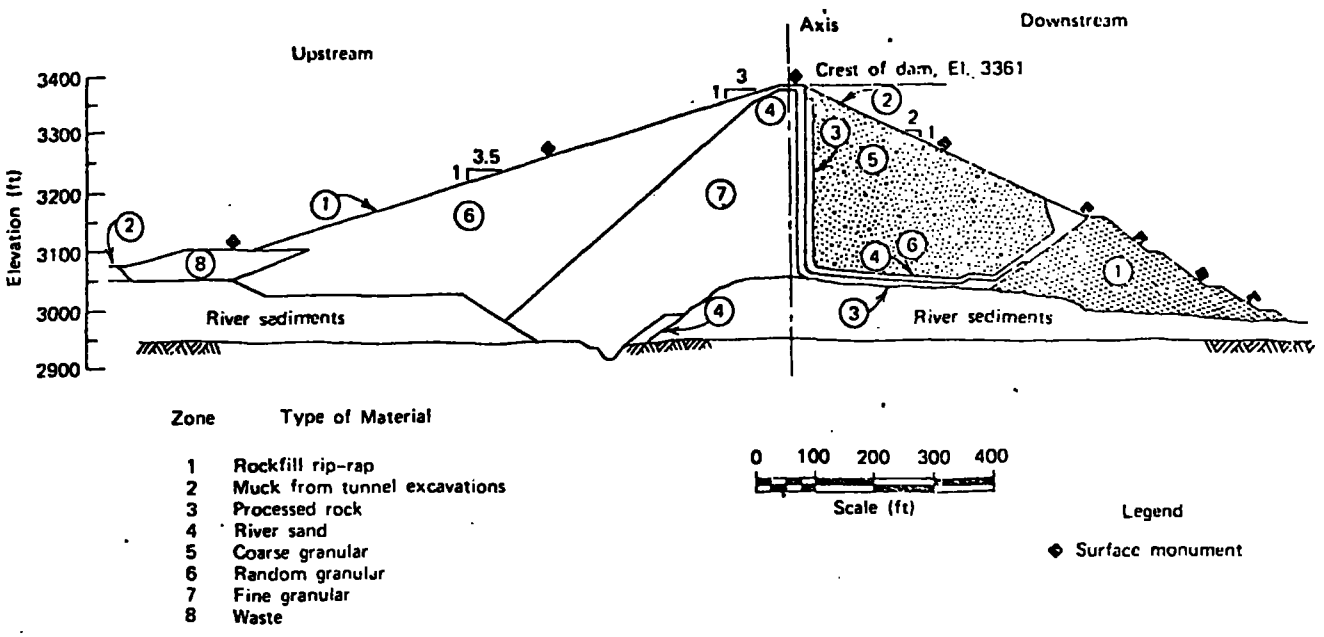

Fig. 6.4 Mammoth Pool Dam. From Wilson (1973).

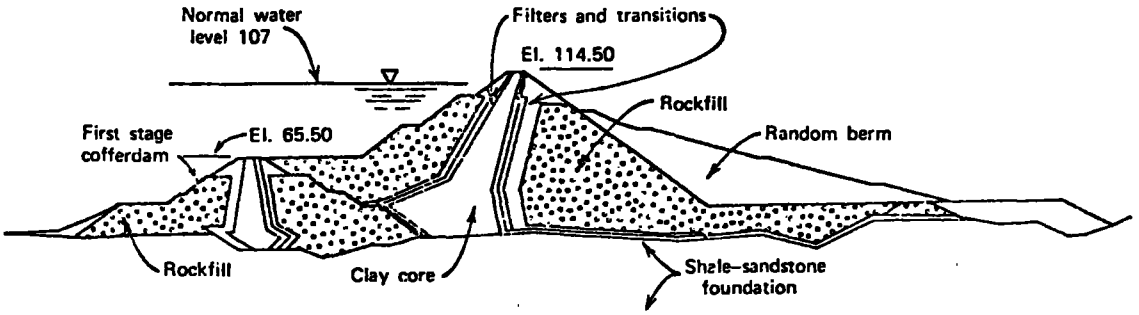

Fig. 6.5 Djatiluhur Dam, Indonesia. From Sherard (1973).

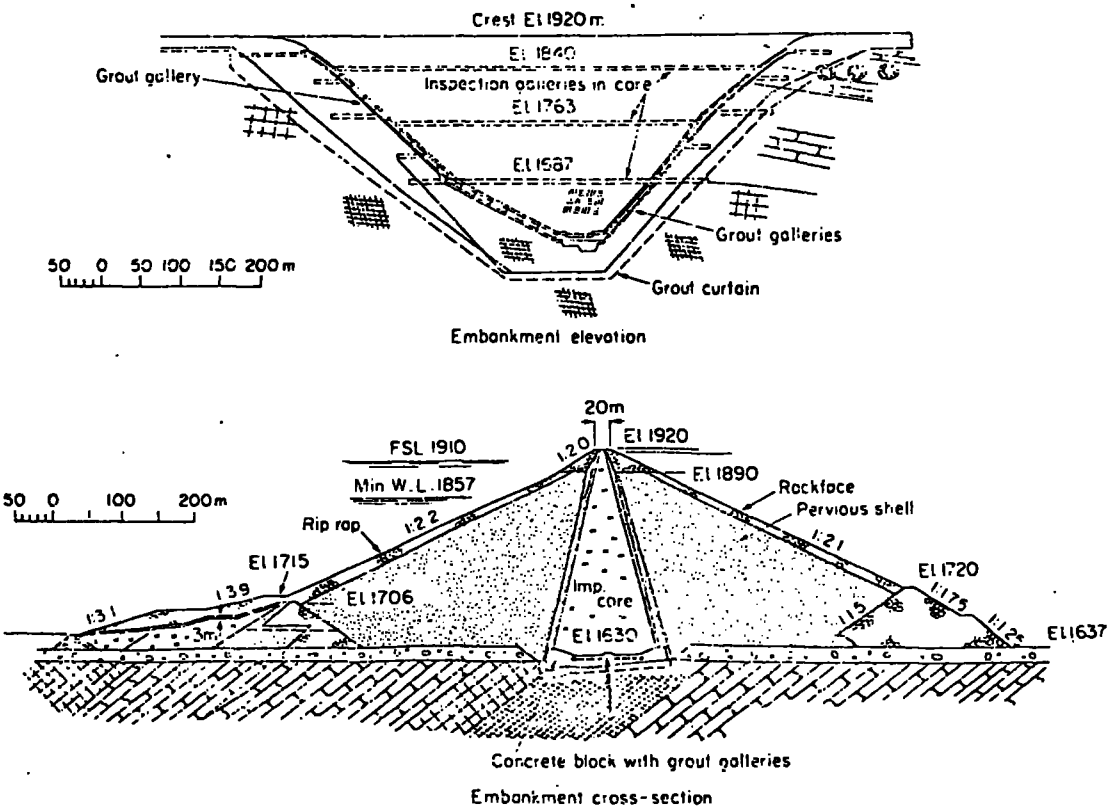

Fig. 6.6 Nurek Dam, U.S.S.R. From Thomas (1976).

can be achieved by modern construction techniques. For this dam both a cross-section longitudinal elevation are given. The latter is a reminder to us that embankment dams are three-dimensional structures with a cross-section varying throughout their length.

A broad classification of types is given by Thomas (1976), and is illustrated in Fig. 6.7. together with typical slopes.

A feature that is, of course, quite specific to each dam is the surrounding geology. Fig. 6.8. gives a sketch in longitudinal elevation of the geology of the Parangana Dam, Australia, and it illustrates the probably common feature of a dam built between the solid rock sides of a steep ravine but over a base of drift or other loosely consolidated material.

6.2. The features of an embankment dam model

The finite element method is ideally suited to modelling most of the features mentioned in section 6.1. Complex geometries and differing material types are quite easily incorporated. A decision has to be made whether the model is to be a three-dimensional or two-dimensional one. A two-dimensional plane strain model may well be an adequate representation for the central sections of a long embankment dam (Lefebvre et al (1973)), but the limitations of a two-dimensional model were recently forcefully expressed by Prof. Severn (Dams and Earthquake (1981), p. 244). A two-dimensional model will completely fail to represent the longitudinal vibrations in a dam. The finite element method is suited to a 3-dimensional model

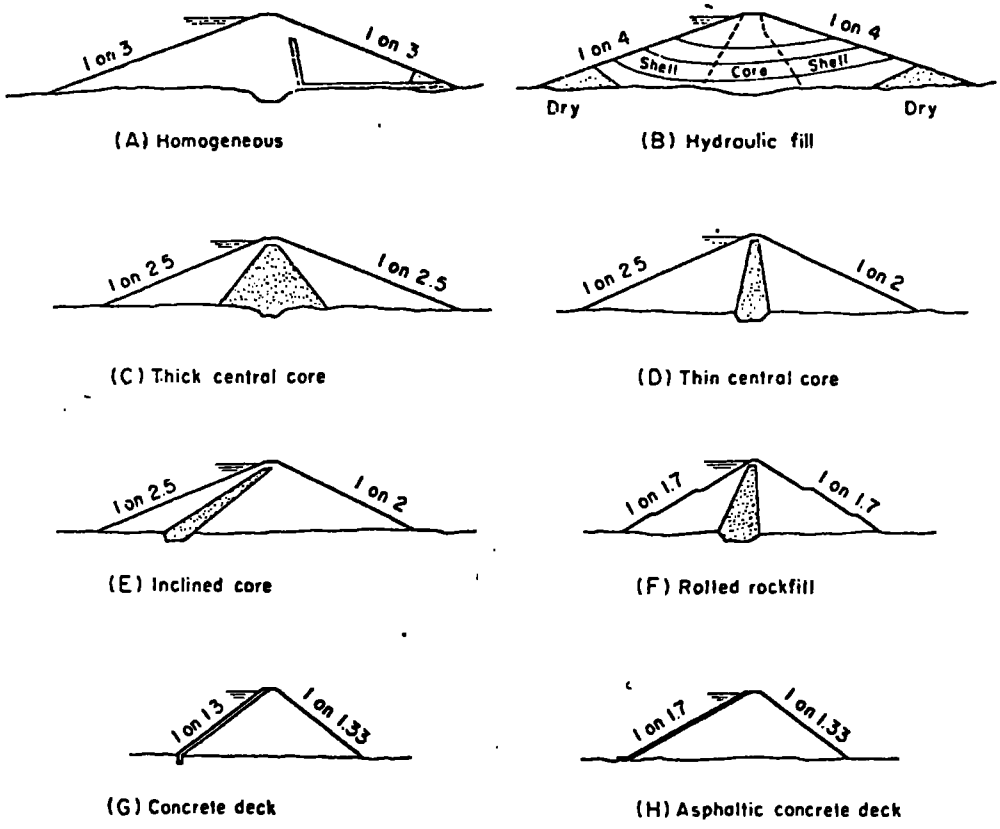

Fig. 6.7 Types of embankment dams.
From Thomas (1976).

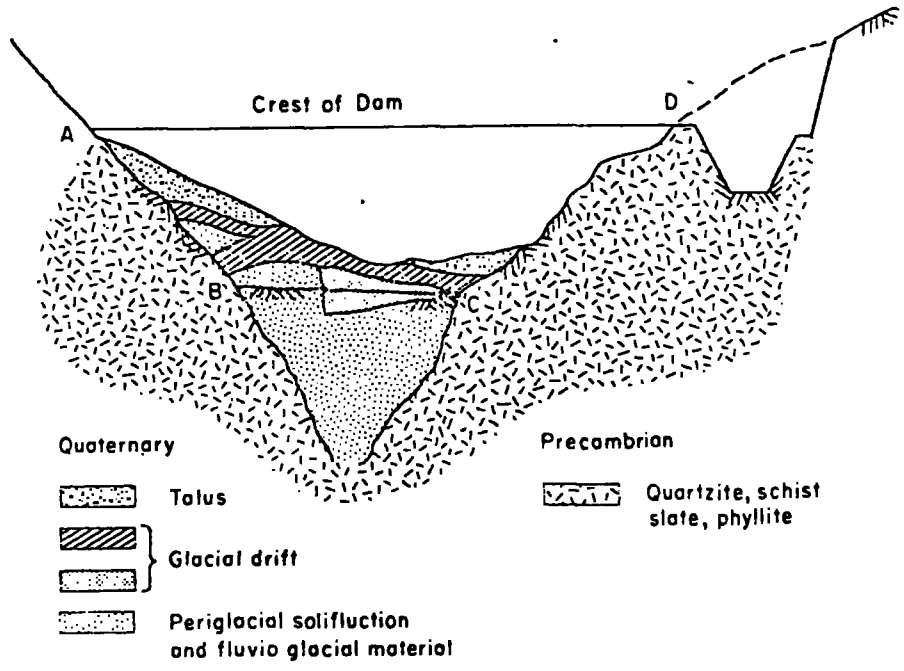

Fig. 6.8 Underlying geology of Parangana Dam, Australia.
From Thomas (1976).

except for the rapid increase in the number of nodes as the size of the model is increased. Thus for the grid that was used in this study, which had of order 1200 nodes and a base length of 90 nodes, an extension to three-dimensions with a square base would have required of order 10^5 nodes. Such a figure is beyond the computing possibilities available at the moment, and so in this study only a two-dimensional method was considered. It is not difficult with a finite element method to take account of the variety of material types that may be used. This is especially easy if the materials are elastic, but it is possible to incorporate materials with non-linear properties also. A greater difficulty is perhaps the determination experimentally of the best parameters that should be used to characterise the actual materials used.

It is with these considerations in mind that this study has chosen to concentrate on a very idealised model. If we are to gain some understanding of how the outline geometry of an embankment affects the propagation of elastic waves entering at various angles, perhaps it is best, at least initially, not to consider a model cluttered up with the fine detail of a realistic model. Since what is of interest is how the reflections from the sloping sides, and the refractions and mode conversions at interfaces, affect the wave progression and consequent stresses, it was decided to model just the broad features of an embankment dam. For this purpose the homogeneous dam type was taken as a basis, such as illustrated in Fig. 6.1 and Fig. 6.7(A).

6.3. Choice of element size

Since our aim is to give a reasonable model for the propagation of seismic waves we will require elements small enough for that to be achieved. The condition that has to be met is the relation 5.3.2., namely

$$f < \frac{v}{8l} \qquad 6.4.1$$

where l is the mesh size and f,v are the frequency and velocity of the propagating wave. We can therefore regard the mesh size as being determined by the material of the region, which fixes v, and the frequency of the seismic source. From 6.4.1. we can see that if this relation is satisfied for a certain velocity then it is satisfied for all greater velocities; likewise if it is satisfied for a given frequency, then all lower frequencies will be adequate. In order to settle on the mesh size we therefore have to determine a minimum velocity, v_{min}, and a maximum frequency f_{max}. Given these, the mesh size l, must be chosen so that

$$l < \frac{v_{min}}{8f_{max}} \qquad 6.4.2$$

For v_{min} we must choose a value sufficiently small to account for the low velocity materials that make up the embankment. For this study a value of 600m.s.$^{-1}$ has been chosen, but even this value could be too high, especially for the speed of propagation of S-waves in materials of high Poisson's ratio, (see Watanabe (1975), p. 760). For this study Poisson's ratio was 0.25 throughout. Clearly,

if this method were to be used for the seismic response of an actual dam, the mesh size could not be decided upon until experimental data were available for the velocities of the materials.

The justification for choosing a value for f_{max} comes from the study of the spectra of earthquakes. Fig. 6.9. is a response spectrum for the El Centro earthquake, plotting velocity ratios against frequency for different damping factors. For this spectrum the velocity ratio is greatest in the range 0.3 - 3.0 Hz., with a sharp cut off outside this range. The velocity ratio at 10 Hz. is about 1/10th the value at 3 Hz. Fig. 6.10 is taken from the Pacoima Dam strong motion record of the San Fernando earthquake and gives peak velocity over a narrow band of frequencies for selected frequencies from 0.5 Hz. to 10 Hz. A spectrum is given for each of the horizontal records and the vertical record. For these records the highest velocities are in the 0.5 - 2 Hz. range, and the peak velocities fall by 1/5th from 2 to 10 Hz.

If we assume that it is the energy of a seismic disturbance that causes the damage to a structure, then, since energy is proportional to velocity squared, it is to the velocity spectrum that we should look to see which frequencies are the most important as far as structural damage is concerned. The sharp fall in the velocity spectra over a certain frequency thus justifies the idea of a cut-off frequency. For this study f_{max} was taken as 10 Hz., and the spectra of Fig. 6.9-6.10 suggest that this is a reasonable value.

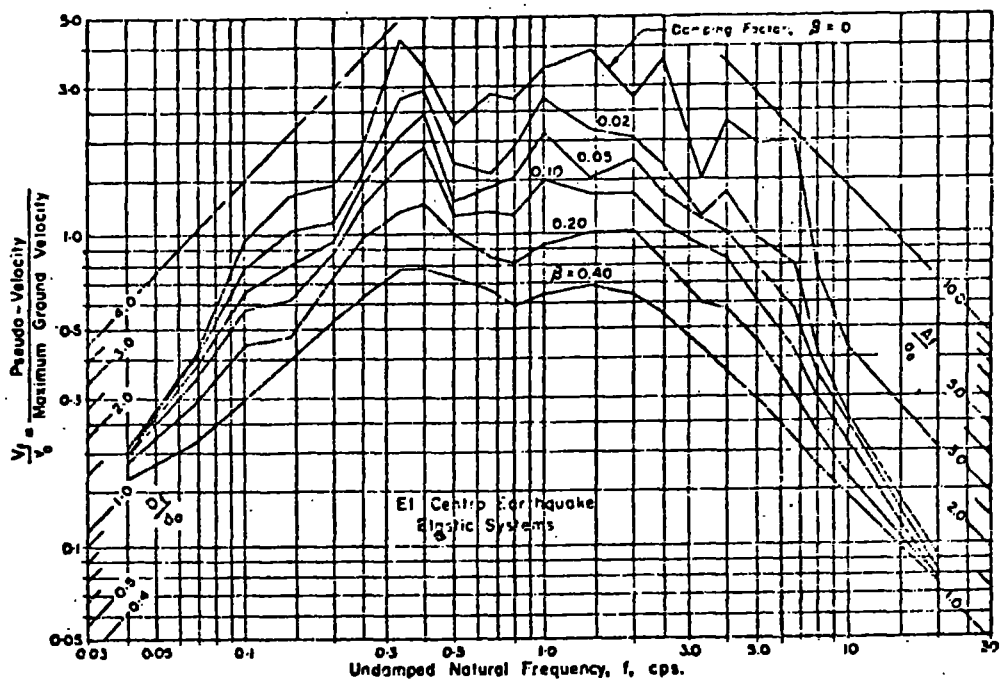

Fig. 6.9 Response spectra for elastic systems subjected to the El Centro earthquake. From Newmark (1965).

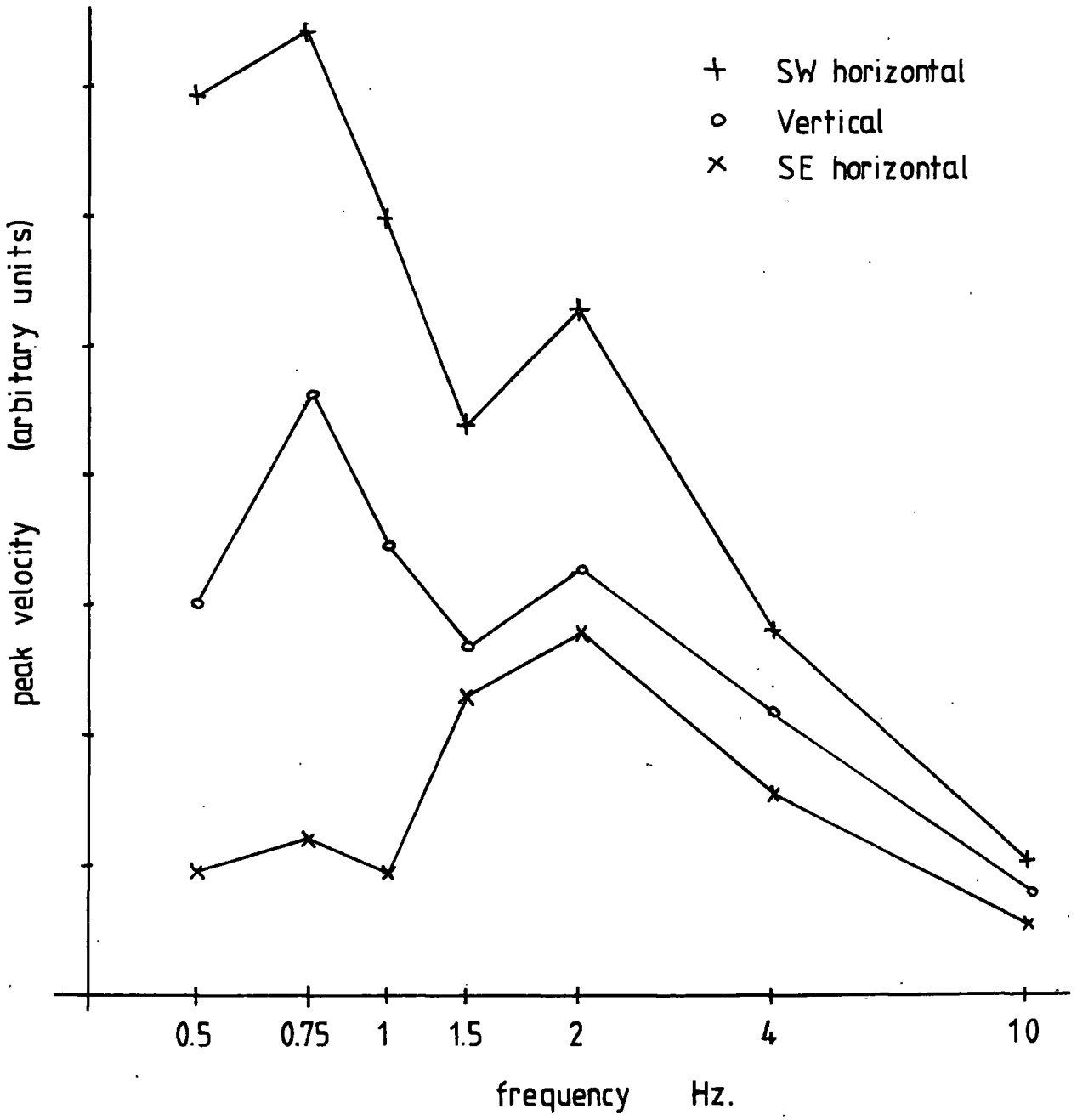

Fig. 6.10 Velocity spectra. San Fernando earthquake. Based on Bolt (1972).

If it is thought that the displacement spectrum is the more significant one, as far as structural damage is concerned, then the cut-off with higher frequencies is even more marked, as can be seen in Fig. 6.9, where the displacement spectrum can be read using the diagonal lines marked on the right side of the graph.

The values chosen here for v_{min} and f_{max} give, using 6.4.2., a value of 7.5m. for l. It should be noticed that the values used, whilst acceptable, are not generous. The choice of a cut-off value for the earthquake spectrum is a somewhat arbitary one, especially since we cannot be certain that it is the appropriate one for some future earthquake; and certainly there may be cases when the materials of a embankment demand a lower value for v_{min}. A value for the mesh size of around 8 m. is therefore a forced choice for dynamic problems with dams subject to earthquake.

It could be argued that we need not be so restrictive on mesh size in regions of the model which are composed of higher velocity materials. This is true; but there are two disadvantages. First, as has already been referred to in section 5.5., a variation in element size is undesirable as it tends to produce dispersion of waves (Belytshko and Mullen (1978)). Second, a grid with element sizes chosen to match the material properties of each element would be inflexible, especially in a general study such as this, for studying a variety of embankment dam models. The value of 8m. was therefore adopted for the size of the elements throughout the grid.

6.4. Examples of finite element grids

Many finite element grids have been published for dam studies. Most of these have been for static analyses, but a number have been proposed for dynamic studies. One of the earliest was that used by Clough and Chopra (1966), and is reproduced in Fig. 6.11. This models an idealised dam about 91m. high with slopes of 1 in 1.5., using elements of order 18m.

The grids illustrated in Figs. 6.12-6.13 were designed to model actual dams. That in Fig. 6.12 was designed by Watanabe (1975) to model the Kisenyama dam, and has a height of 95m. with slopes of about 1 in 1.25. The mesh size varies from about 5m. at the crest to 30m. at the base. The grid of Fig. 6.13 was designed by Seed, Duncan and Idriss (1975) for the Upper San Leandro dam. This is a homogeneous dam with slopes of around 1 in 3, rising to 61m., and has a mesh size of order 9m.

Another example, Fig. 6.14, due to Seed (1973) was used to analyse the failure due to earthquake of the Sheffield dam in 1925. This dam would not be considered a large dam, having a height of only 7.6m. The grid was designed with a mesh size of order 2.5m. This dam is one of the few examples of a catastrophic failure as a result of earthquake, and from his analysis Seed concluded that the failure was most probably due to progressive liquefaction along the base of the dam.

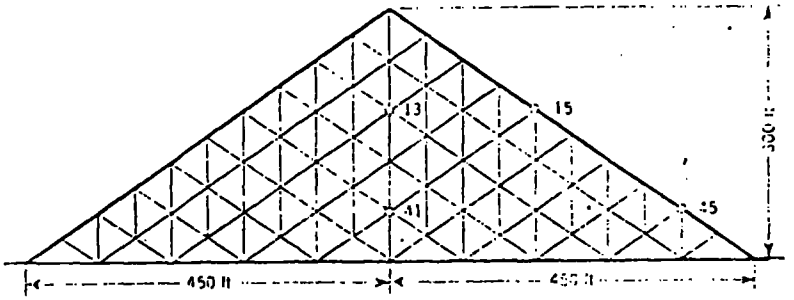

Fig. 6.11 Finite element idealisation for an earth dam.
From Clough and Chopra (1966).

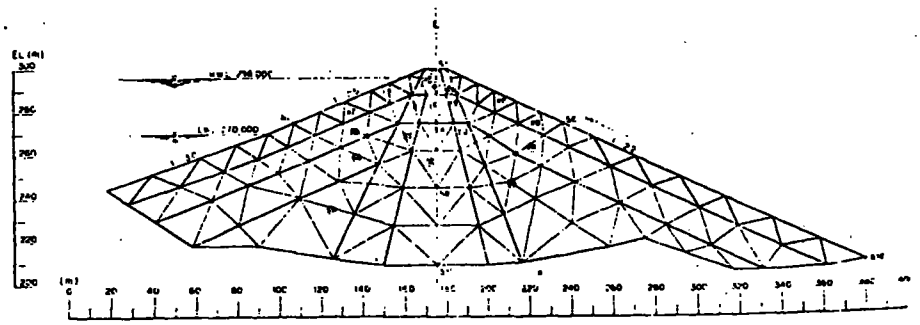

Fig. 6.12 Finite element grid for Kiseyama dam.
From Watanabe (1975)

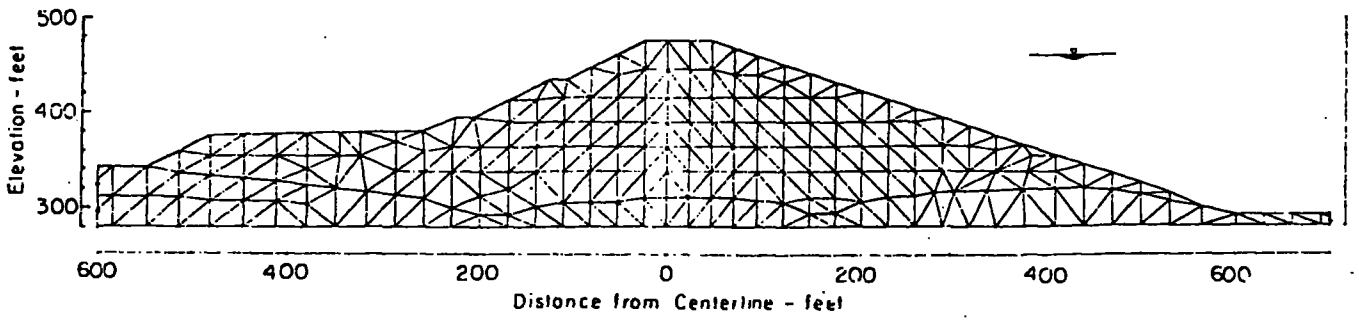

Fig. 6.13 Finite element grid for Upper San Leandro dam.
From Seed, Duncan and Idriss (1975).

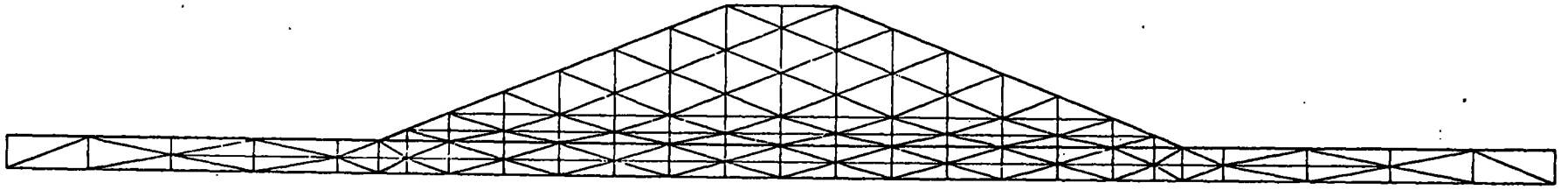

Fig. 6.14 Finite element grid for Sheffield dam.
From Seed (1973).

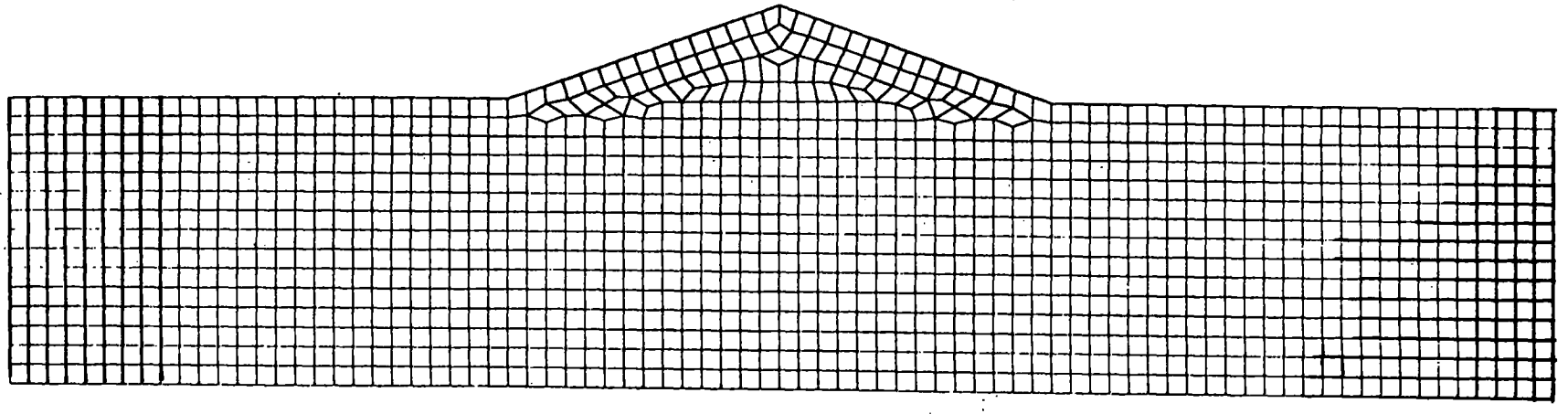

Fig. 6.15 Finite element grid for an idealised embankment.
From Smith (1975)

Smith (1975) used a finite element grid to model, not an embankment dam, but an idealised mountain. Furthermore this grid (Fig. 6.15) includes a considerable amount of the underlying halfspace. The dimensions of the grid are such that a horizontal extent of 6.4 km, to a depth of 1.2 km below the ground surface, is modelled, together with a mountain of height 420 m. above ground level and slopes of 20^{o}. The mesh size is of order 80 m.

The parameters of these grids are summarised in the Fig. 6.16.

Finite element grid	Slope	Height m.	Mesh size m.	Height/ mesh size
Clough and Chopra	34^{o}	91	18	5
Watanabe Kiseyama Dam	39^{o}	95	5 - 30	6
Seed et al. San Leandro Dam	20^{o}	61	9	7
Seed Sheffield Dam	22^{o}	7.6	2.5	3
Smith	20^{o}	420	80	5

Fig. 6.16

It will be noticed that of these grids only those by Seed meet the mesh size requirement of 6.4.2. In the case of the grid of Smith it could be argued that since it was to model a mountain rather than a dam the velocity of the material would be higher. However for the mesh size of 80m. to meet 6.4.2 would require v_{min} to be 6400m.s.$^{-1}$ which is certainly not a realistic value.

The fact that the ratios of height to mesh size are similar for all these grids, despite the wide range in absolute dimensions, suggest that their designers were largely influenced by the geometric shape of the region to be modelled. Whilst it is clear that any grid must be designed so that it adequately represents the geometric complexities of the dam, what has been shown is that this is by no means the only criterion that must be satisfied. It must be concluded that any results which use grids that do not meet the requirement of mesh size given by 6.4.2., should be treated with caution. As the tests of chapter 4 showed this is especially true for any deductions concerning stress rather than just displacement.

6.5 Design of a finite element grid for an embankment

The grid illustrated in Fig. 6.15 (Smith (1975)), contains features that fitted the needs of this study, in that of models an embankment with slopes of 20^{o} together with a considerable amount of the underlying half-space, and it uses uniformly sized elements of quadrilaterals together with some triangles. For the dimensions that Smith used it fails completely to meet the all important mesh size requirement. However this requirement could be met by a rescaling, and this would reduce the embankment height to 40m.

In the early stages of this study the grid of Fig. 6.15 was used, scaled to a height of 100m. It was the unsatisfactory results, especially in the values of stress, that were obtained from this grid that prompted the tests of chapter 4, leading to the conclusions on mesh size stated in chapter 5. It was therefore decided to design a new grid able to meet these conditions. A further point is this. A mesh size of 8m., implies, by the relation 5.3.1., that the wavelengths that can be modelled must be longer than 64m. If the magnitude of the structure is much less than the wavelength of an incident seismic wave then we would expect the structure to move as an entity without significant production of strains. It is only when the magnitude of the structure is of the same order as, or greater than, the incident wavelength that we would expect the production of strains across the structure. It is thus the larger dams that are more at risk from seismic disturbance. So the grid to be designed, besides having a mesh size of order 8m., should be as large as possible.

Fig. 6.17 is a sketch of an outline for a grid such as that used by Smith (1975). The first problem is to determine suitable values for the dimensions a, b, c, h.

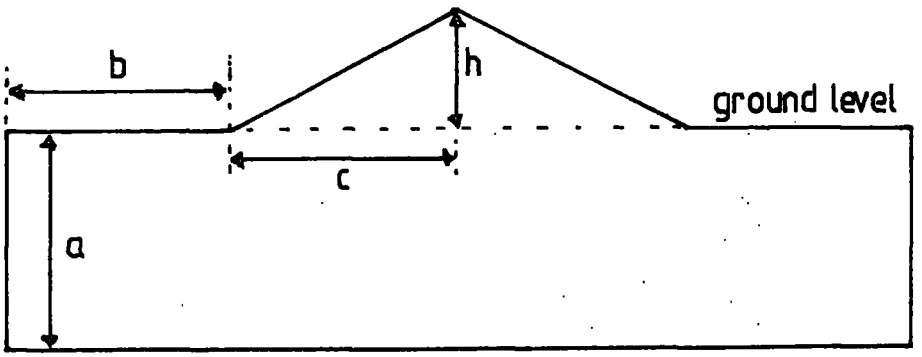

Fig. 6.17

To model a homogeneous dam the embankment slope should be about 1 in 3 (18^{o}). This requires $c = 3h$.

The values of a and b must be chosen to minimise the problem of unwanted reflections, as discussed in section 5.5. A minimum requirement for a was determined by demanding that a vertical incident wave originating at the base would travel to the top of the dam and down again to ground level before the first unwanted reflections from the base arrive back at ground level. Assuming uniform velocity this gives

$$3a \geq a + 2h \quad \text{or} \quad a \geq h \qquad 6.5.1$$

If we further require that a diffracted wave originating at a base corner should arrive at the bottom of the dam slope no earlier than it takes a vertically incident wave to arrive at ground level after a reflection from the top of the dam, we get a condition for b,

$$\sqrt{(a^2 + b^2)} \geq a + 2h \qquad 6.5.2.$$

So that the structure will be of the order of the wavelength we take h = 60m. and c = 180m. With these values 6.5.1 and 6.5.2 imply that $a \geq$ 60m. and $b \geq$ 170m.

If we take $a = h$, and $b = \sqrt{8}h$ to just meet with the requirements of 6.5.1 and 6.5.2., then the area of the grid of Fig. 6.7 will be 17.65 h^2. For a mesh size of 8m. this would require N elements to cover it, where

$$N \simeq 0.275h^2 \qquad 6.5.3$$

The number of elements for various dam heights is given in Fig. 6.18.

Height of dam (m)	No. of elements needed
50	690
60	990
70	1350
80	1760
90	2230
100	2750

Fig. 6.18

At this stage the choice of dimensions becomes limited by the size of the computer to be used. The major storage requirement in the finite element program is the stiffness matrix, and it requires an array of (no. of degrees of freedom x bandwidth). The degrees of freedom are $2n$, where n is the number of nodes, and the bandwidth is $(4d + 3)$ where d is the maximum difference in nodal numbering for any one element throughout the grid. The IBM 360/168 at NUMAC allows a maximum of 1 megabyte of storage for any one array (i.e. 2^{20} bytes). With single precision, 4 bytes are required for each real number, and so we need

$$2n(4d+3) < 2^{18}$$

This can be rewritten

$$d < \left[\frac{32768}{n} - \frac{3}{4} \right] \qquad 6.5.4.$$

where the square brackets indicate "nearest integer to".

We can express 6.5.4. as a table, as is done in Fig. 6.19.

Number of nodes	Maximum nodal difference
1000	32
1100	29
1200	26
1300	24
1500	21
2000	15

Fig. 6.19

Experience showed that it was difficult to achieve the nodal difference requirement with over 1100 nodes. The number of nodes is a little larger than the number of elements, so the table in Fig. 6.18 suggested a maximum height of dam between 60 and 70m.

With all these factors in mind a grid was designed with a = 64m., b = 170m., c = 180m., a height of dam between ground level and crest of 60.8m., and slopes of 1 in 3. These values just meet the requirements of 6.5.1 and 6.5.2. The large part of the grid was divided up into 8m. squares, but with two layers of 4m. squares along the slopes of the dam, so that more accurate values would be given of the stresses close to the slope surfaces. Some triangular and irregular quadrilateral elements were required to complete the grid using a total of 1140 elements and 1184 nodes. This grid is shown in Appendix B, the accompanying portfolio.

The numbering of a grid to achieve a small maximum nodal difference is something of an art. In the present case a numbering by hand achieved a value for d of 29, whereas the storage requirement 6.5.4. was for a d of 26. The necessary reduction in bandwidth was done using the bandwidth reduction program given in Appendix A. This program is not very efficient, and the necessary result was only achieved after many iterations of the program, with a judicious varying of the arbitary parameters that enter into the program. The original node numbering is shown in Appendix B, since all the input data is given with respect to that numbering, and the improved nodal numbering obtained by the bandwidth reduction program need never concern the user.

6.6. Summary

The design of any grid to model the dynamic behaviour of an embankment must first and foremost meet the mesh size requirement 6.4.2. Certainly some of the published girds do not meet this, and so cannot be considered satisfactory for use in dynamics problems, particularly if the aim is to calculate stresses.

The problem of reflections from the fictitious boundaries imposes further geometrical restrictions on the overall size of the grid. When these restrictions are combined with the limitations of the available computer storage we are left with a very small range of satisfactory grids.

More ingenuity of design could possibly reduce the bandwidth of a grid, but this is a very time consuming process and would not give a significant improvement in the grid given in Appendix B. To achieve even larger grids would require another dimension in computing ingenuity - such as storing the stiffness matrix in more than one array, or, better still the elimination of storage of all the zero elements in the matrix.

Chapter 7. Stresses in embankments produced by P and S waves

7.1. Introduction

Our analysis has carried us to a point where we have designed a grid (Appendix B. Fig.B.1) which we know will be able to model wave propagations for certain specific velocities and frequencies. In particular we know that the calculated displacements will be accurate enough for stresses to be calculated without the introduction of artefacts. We are thus in a position to be able to calculate the stresses in an embankment as a result of an idealised seismic input, and see if they are of the form likely to cause failure. Before these stress distributions are discussed we shall first review the stress conditions that are necessary for failure.

7.2. Conditions for failure

The simplest, but most often used, condition for failure is the Coulomb criteria (Jaeger and Cook (1969), pp 87-91). It states that a shearing failure will occur in a plane if the magnitude of the shear stress along the plane, τ, is related to the normal stress across the plane, σ, by

$$|\tau| > \alpha + \mu\sigma \qquad 7.2.1.$$

where α is called the adherence and μ the coefficient of internal

friction. (Here, as is usual in soil mechanics positive stresses are compressional). a and μ are properties of the material, which would have to be determined experimentally. If the total stress at any point has major and minor principal stresses σ_1 and σ_2 (i.e. $\sigma_1 > \sigma_2$), then the maximum shear stress has magnitude $\frac{1}{2}(\sigma_1 - \sigma_2)$ and acts along lines at 45^0 to the principle stresses. However it can be shown that $|\tau| - \mu\sigma$ reaches its maximum value along lines at angle β to the minor principle stress, where $\tan 2\beta = -1/\mu$. Thus by 7.2.1. these are the possible directions of shear fracture. For $\mu=0$, $\beta=45^0$ and 135^0; whereas for $\mu>0$ the two values of β lie in the range 45^0 to 135^0 and are symmetric about the major principal stress. This is illustrated in Fig. 7.1.

Some further analysis gives the condition for shear fracture 7.2.1. as

$$\sigma_1 > b^2 \sigma_2 + 2ab \qquad 7.2.2.$$

where $b = \mu + \sqrt{(\mu^2 + 1)}$

The relation 7.2.2. will hold only if σ_2 is not so negative (i.e. the minor principal stress being a tension) that the material breaks with extension fracture. If the tensile strength is T_0, then we can expect extension fracture for $\sigma_2 > -T_0$. These results are summarised in Fig. 7.2.

Fig. 7.2. shows that it is necessary to know the three material properties characterised by the constants T_o, a and μ, if a prediction

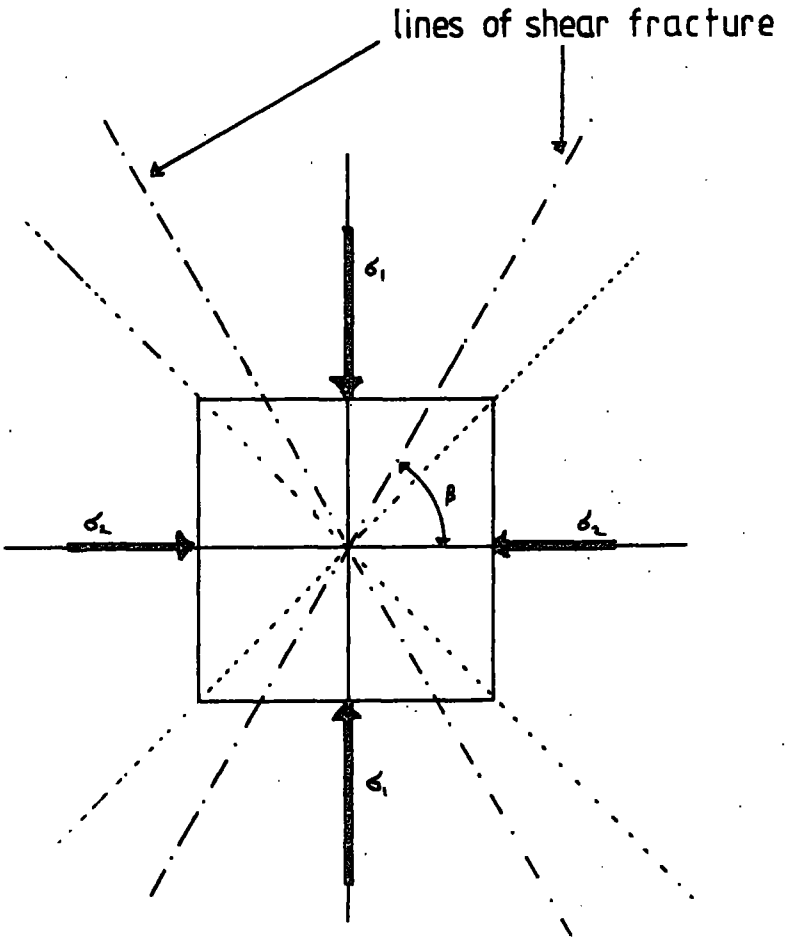

Fig. 7.1 Lines of shear fracture in a soil subject to major and minor principal, σ_1 and σ_2. For internal friction greater than zero the angle β is greater than 45°

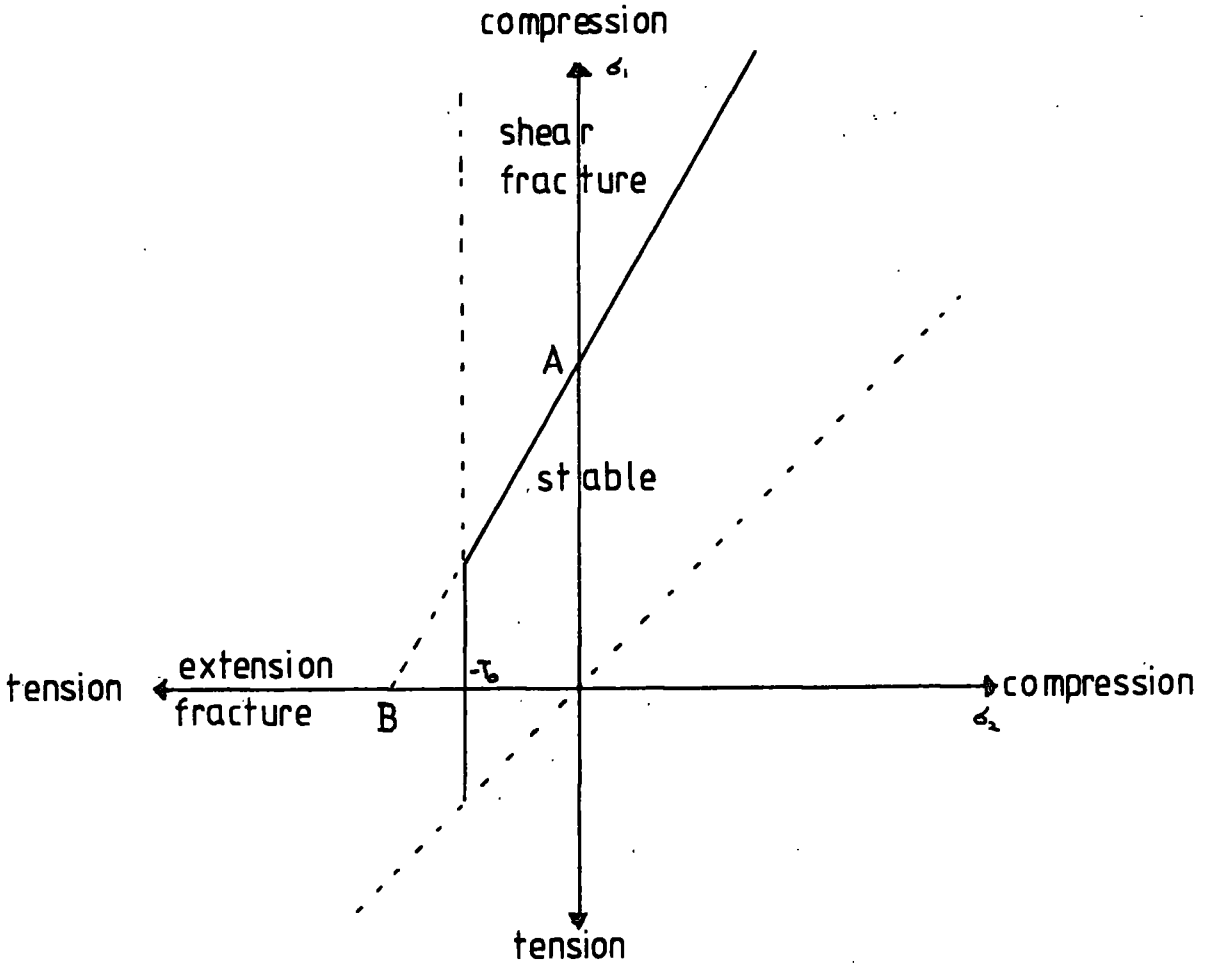

At A $\sigma_1 = 2ab$

B $\sigma_2 = -2a/b$

Fig.7.2 Principal stress diagram, showing regions of stability and failure.

is to be made of the type of failure from a knowledge of the principal stresses. However certain general points can be made from this diagram. First, it is not possible to obtain shear fracture if both principal stresses are tensional - either the material is stable, or there is extension fracture with cracks normal to the minor principal stress. Second, if the tensile strength T_0 is small - and this is likely for the materials of an embankment - then if the minor principal stress is tensional, extension fracture is the most likely form of failure. Third, if the internal friction, μ, is reduced - such as by wetting of the material - the possibility of shear fracture is increased.

The static distribution of stresses of an embankment does not include any tensions (see, for example Appendix B), and so we would not expect any extension fractures. The usual form of analysing the stability of a slope is to look for possible shear fracture along certain critical surfaces. That shear failures do take place in embankment dams is well documented (Newmark (1965), Seed (1970)), and they take the form of slumping along surfaces of approximately circular cross-section, stretching from some point near the top of the slope, going into the body of the dam and emerging near the bottom of the slope. Such a slope is illustrated in Fig. 7.3.

If values for the material properties are given, then from any stress pattern a search can be made for any surface along which the condition 7.2.2. holds, and so would be liable to shear fracture. This may be

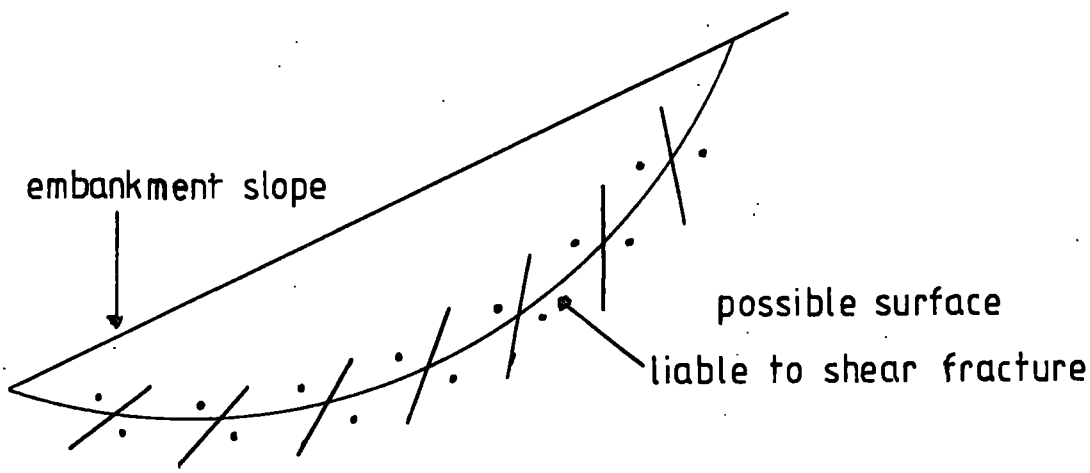

Fig. 7.3 Possible slumping surface, together with principal stresses.

done using the generalised procedure of slices, comprehensive details of which are given by Janbu (1973). The process is a lengthy one since several trial surfaces may have to be considered before a critical one is found. However we can see the sort of stress patterns that would be needed for this kind of failure, and these are drawn on Fig. 7.3. They are drawn with the convention that is used for the stress plots in Appendix B, that is with two dots to indicate a tensional stress. However it is not necessary for one of the stresses to be in tension and the other in compression, only that the difference between the principal stresses is large enough to meet the condition 7.2.2. and so would be plotted in the shear fracture region of Fig. 7.2. What is important is the orientation of the stresses. Since any shear will take place close to a line bisecting the principal stresses (at least for low values of internal friction), in order to get shear along the proposed slumping surface it is necessary for the stresses to show the variation in orientation that is illustrated in Fig. 7.3. Whenever, therefore, we notice a steady rotation of the principal stresses along a curved line (and provided they are not close to equality) we may suspect this to be a region of possible slumping failure; but a confirmation of this would require the analysis such as that given by Janbu (1973).

Besides the existence of slumping surfaces, since we are considering a dynamics problem, there is the possibility that for some regions tensional stresses will appear, even if only for a limited time. These might be in the form of one stress compressional, and the other tensional - like those given in Fig. 7.3. Since these could produce

a shear the term "region of shear" will be applied to any area where this kind of principal stress occurs. Another possibility is that both principal stresses might be tensional, and such an area will be termed a "region of tension". In a similar way if both principal stresses are compressional the term "region of compression" may be used. It should be noted that these terms are only convenient labels, and it must not be forgotten that shear fracture is not confined to regions of shear, but might well occur in regions of compression; likewise extension fracture could occur in a region of shear as well as a region of tension.

In view of the likely low value for the tensile strength of the materials used in an embankment both regions of tension and regions of shear must be considered likely areas where extension fracture might occur. For a completely dry embankment composed of a material such as sand we might expect no tensile strength at all, and the effect of tensile stresses would be to produce a crumbling of the embankment. However with the compacted clays that are typical of embankments there will be some tensile strength, at least in the short term (see Janbu (1973) p. 62) , and in this case tensile stresses would produce cracking.

Once a crack has began to develop, the further history of the dam would require a separate analysis. Since we shall see that tensions that are produced are only maintained for a short period of time it might be that the succeeding period of compression would heal the

crack before significant development had taken place. This might be particularly true of the interior of the dam. However it must be borne in mind that if a crack does begin to develop then there is a redistribution of stresses to account for the newly created free surface. In particular this will lead to stress concentration at the crack tip which will enhance its propagation, and the following phase of compression will be altered quite significantly if the crack has developed to some size.

7.3. Description of models

The grid developed in chapter 6, and illustrated in Appendix B Fig. B.2., was used in two forms, (a) as a homogeneous grid of one material type and (b) as a layered grid of three material types. The regions of each layer for case (b) are also indicated in Appendix B Fig. B.2. The material properties for both cases are given in Fig. 7.4.

Model			Young's Modulus $N.m^{-2}$	Poisson's ratio	Density $kg.m.^{-3}$	P-wave velocity $m.s.^{-1}$	S-wave velocity $m.s.^{-1}$
D1	Homogeneous embankment and substructure		$2.0x10^{9}$	0.25	2400	1000	577
D2	Layered Model	Layer 1	$1.6x10^{10}$	0.25	2500	2771	1600
		Layer 2	$3.84x10^{9}$	0.25	2400	1386	800
		Layer 3	$8.4x10^{8}$	0.25	2100	693	400

Fig. 7.4. Table of material properties.

The values of the material properties are not those of any particular embankement dam, but are chosen as representative values. By considering the two models, homogeneous (D1) and layered (D2), it should be possible to differentiate between those effects that are primarily due to the geometry of the embankment and the angle of incidence of the seismic wave, and those effects that are produced by layers of low velocity material over high velocity material.

For both D1 and D2 the static distribution of stresses due to the body forces was calculated. To do this the same finite element formulation as for the dynamic problem was used, except that, instead of an equation of motion, an equilibrium equation

$$[K][q] = [Q] \qquad 7.3.1.$$

is formed, where $[K]$ is the stiffness matrix, $[Q]$ the vector applied loads and $[q]$ the vector of nodal displacements. Equation 7.3.1. is solved using the routine given in Desai and Abel (1972) p. 456. The vector $[Q]$ is formed using the results of 2.9(b). The stress distributions for body forces are given in Appendix B Fig. B.4 and Fig. B.6 for the models D1 and D2.

In addition to the body forces due to the weight of the embankment materials it is possible to include the effect of the weight of impounded water on one side of the dam. This is done by including within $[Q]$ components due to the effect of hydrostatic pressure along

certain edges of the grid, using the results of 2.9(d). The inclusion of these hydrostatic forces for model D1 is also illustrated in Appendix B, Fig B.5.

For each of the two embankment models, D1 and D2, a number of dynamic examples were calculated. Each of these examples consisted of an excitation along the base of the grid in the form of a sinusoidal pulse of one period, in exactly the same way as was used in the tests of chapter 4. The pulse was applied either as a P-wave or an S-wave and for waves entering at a variety of angles of incidnece. In order to meet the mesh size requirement 5.3.2., the frequency of the P-waves were taken as 10Hz., and for S-wave as 6Hz. For these frequencies the number of elements per wavelength for the various materials of the models are given in Fig. 7.5.

Model		P-waves at 10 Hz.		S-waves at 6 Hz.	
		Wavelength m.	Elements per wavelength	Wavelength m.	Elements per wavelength
D1		100	12.5	96	12.0
D2	layer 1	277	34.6	267	33.3
	layer 2	139	17.3	133	16.7
	layer 3	69	8.7	67	8.3

Fig. 7.5

It will be seen that there are a number of parameters that can be varied. A plane wave can be varied in frequency, amplitude, angle of incidence and mode (P or S). Variations in embankment slope and crest width could also be considered. The examples presented were

chosen so that a study could be made of the affects of P and S-waves at a variety of angles fairly close to the vertical. Also two different amplitudes were used corresponding to base accelerations of g and $\frac{1}{2}g$.

The parameters of each of the fifteen examples which are illustrated in Appendix B are given in Fig. 7.6. Each example is given a designation, such as D2/3. This designation is sometimes extended to include the wave type, the angle of incidence and the base acceleration. Thus D2/3; P 10; g shows that example D2/3 is a P-wave at 10^{o} to the vertical with a base acceleration of g.

For each of these examples Appendix B displays two forms of results.

(a) Time-displacement graphs.

These are given for selected nodes along the top surface of the grid, which are the numbered nodes in Appendix B, Fig. B1 and Fig. B.3. These give displacements in meters due to the progagating wave (but not including the static displacements) both in the x and y directions for the complete length of the run. It should be noted when comparing one with another that the displacement scale has been adjusted so that the maximum displacement has always the same dimension on the graph.

Designation	Wave Type	Frequency Hz.	Angle of incidence	Amplitude at base m.	Max. accel. at base $m.s^{-2}$	Timestep s	Run-time s
D1 /1	P	10	0^o	0.0024	g	0.002	0.3
D1 /2	P	10	20^o	0.0024	g	0.002	0.4
D1 /3	S	6	0^o	0.0069	g	0.0025	0.4
D1 /4	S	6	20^o	0.0069	g	0.0025	0.525
D2 /1	P	10	0^o	0.0024	g	0.002	0.3
D2 /2	P	10	0^o	0.0012	$\frac{1}{2}$g	0.002	0.3
D2 /3	P	10	10^o	0.0024	g	0.002	0.3
D2 /4	P	10	20^o	0.0024	g	0.002	0.4
D2 /5	P	10	20^o	0.0012	$\frac{1}{2}$g	0.002	0.4
D2 /6	S	6	0^o	0.0069	g	0.0025	0.375
D2 /7	S	6	0^o	0.00345	$\frac{1}{2}$g	0.0025	0.4
D2 /8	S	6	10^o	0.0069	g	0.0025	0.4875
D2 /9	S	6	20^o	0.0069	g	0.0025	0.6
D2 /10	S	6	20^o	0.00345	$\frac{1}{2}$g	0.0025	0.6
D2 /11	S	6	30^o	0.0069	g	0.0025	0.6

Fig. 7.6. Table of parameters for different models.

(b) Stress distributions

These are given for only a section of the complete grid. This section is illustrated in Appendix B. Fig. B.3. On each stress plot only an outline of the section is given, with, in the case of D2 examples the interface drawn between layers 2 and 3. The plot consists of two orthogonal vectors intersecting at the centroid of each element having the magnitude and direction of the principal stresses of that element. For compressive stresses the vector is given by a solid line, whereas for tensional stresses the vector is represented by dots at its ends. The plots are given for a selection of times from the length of the run, usually ten time-steps apart. For these plots the stresses include the stress distribution due to the body forces.

7.4. Discussion of the time-displacement graphs

The smooth shape of the time-displacement graphs without the appearance of extraneous ripples except possibly towards the end of the run confirms the use of the criteria established in chapter 5. There are two features of these graphs that are worth noticing.

(a) In all cases there is an amplification of the displacement between the ground level and the crest, which confirms the conclusions of Bouchon (1973) etc., already cited in chapter 1. The table of Fig. 7.7. gives the amplification factors for the examples. The ground level displacement was measured at node 100 in each case.

Designation	Type	Angle of incidence	Amplification factors displacement at crest/displacement at ground	
			x-components	y-components
D1/1	P	0^o	-	1.1
D1/2	P	20^o	1.6	1.1
D1/3	S	0^o	1.8	-
D1/4	S	20^o	1.9	1.5
D2/1	P	0^o	-	1.5
D2/2	P	0^o	-	1.5
D2/3	P	10^o	1.5	1.6
D2/4	P	20^o	2.0	1.7
D2/5	P	20^o	2.0	1.7
D2/6	S	0^o	3.0	-
D2/7	S	0^o	3.0	-
D2/8	S	10^o	3.0	3.0
D2/9	S	20^o	3.1	3.0
D2/10	S	20^o	3.1	3.0
D2/11	S	30^o	3.3	2.1

Fig. 7.7. Amplification factors

These magnification factors point to a conclusion which will be evident also from a study of the stressplots, namely that the effect of the seismic disturbance is greater for any, or all, of the following conditions. (i) S-waves, (ii) layered model, (iii) non-vertical incidence.

(b) For examples D1/2 and D1/4 which are at 20^{o} incidence the disturbance starts later and later as we traverse the surface from left to right. The ground level nodes on the L.H. side are the first to move, followed by those nodes of the dam, and finally the R.H. side nodes at ground level. For all the examples of angled waves in D2 models there is a marked contrast. In these examples the R.H. side ground nodes (numbers 987 and 1077), far from being the last, in fact start moving only shortly after the wave has entered the dam at the L.H. side. Furthermore the disturbances at nodes 987 and 1077 start at almost the same time. This effect is due in part to the low velocity of the dam material, slowing down the progress of the wave when it enters the dam. However, the almost simultaneous start to the displacements at nodes 987 and 1077 (and the same is observed of the L.H. side ground nodes, numbers 100 and 190), indicates that the wave is travelling close to vertical incidence. This must be due to the refraction at the interface between the two layers that make up the substructure in model D2. Since the velocity across this interface is halved, the angle of incidence is approximately halved for waves that are refracted without mode conversion. For a conversion from P to S-waves at the interface the angle of refraction is approximately a quarter of the angle of incidence; but for an S to P conversion the reduction in angle is by a factor of approximately 0.8.

7.5. Discussion of the stress distributions

The stress plots are illustrated from the time when the disturbance begins to modify the body force stress distribution, and in all cases the progression of a wave through the dam can be clearly seen Rather than give a description of each of the examples, this discussion will centre round certain points which they bring out.

(a) Regions of tension and regions of shear appear in nearly all the examples, sometimes to a considerable extent. The only examples which are tension free are D2/2; P; 0; ½g and D2/5; P; 20; ½g. D1/1; P; 0; g has only a small region of tension near the crest at 0.18s. It could be argued that the tensions are produced only because of the high accelerations at the base, but it must be noted that D2/7; S; 0; ½g and D2/10; S; 20; ½g, both develop tensions parallel to the slopes of the dam, even though they have the lower acceleration.

There are thus many examples which we could consider as potential places for tensional cracking; e.g. D2/4; P; 20; g at 0.2-0.225, D2/8; S; 10; g at 0.325-0.35.

(b) The rotation of principle stress of the kind illustrated on Fig. 7.3. and characteristic of slumping failure can be seen in several examples, especially in those involving D2 and S-waves. The example D2/8; S; 10; g at 0.35s, already mentioned may serve as an illustration. As already explained in section 7.2., slumping

failure does not require tensional stresses. An example of a rotation of stress along a possible slumping surface, without tensions, is D2/10; S; 20; ½g at 0.35-0.4s at the lower left side of the dam.

(c) The effect of S-waves is certainly more dramatic. This is seen by comparing any two examples at which one is P and the other S, and the other parameters the same. For example D1/2; P; 20; g produces some quite large changes to the static compressional stresses, but barely produces any regions of tension or shear, whereas D1/4; S; 20; g is characterised by a large region of shear which travels across and up the embankment, with the shear stresses quite deep into the structure.

(d) Perhaps the most significant gleaning from these results are the differences between the homogeneous and layered models. A comparison of D1/1; P; 0; g and D2/1; P; 0; g makes this very clear. In D1/1 a compression followed by a rarefraction moves up the dam, just producing tensions at 0.18s at the crest. The wave is reflected from the surface of the dam and passes down and out from the region of the dam at 0.3s, when the stresses are returning to the static distribution. For D2/1 near vertical tensions first appear at the toes of the dam at 0.08s, which then travel up the slopes behind a compression producing a considerable region of tension at the crest at 0.16s. The history then departs even more from its counterpart D1/1, with the dam region dividing up into regions of compression and tension. A similar comparison can be made between D1/3; S; 0; g and D2/6; S; 0; g. Here again

the patterns begin broadly the same, but with more exaggerated distortions of the static stress distribution in the D2 example. Towards the end of the run the D2 example divides into regions of tension and compression.

As already observed from the time-displacement graphs there is a marked difference between the angled waves when comparing D1 models with D2 models. This was because the layering of the substructure tends to bring the wave closer to vertical incidence. A comparison of D1/4; S; 20; g and D2/9; S; 20; g shows that the effects of layering for the angled S-waves is quite considerable. In the D1 model a wave is seen to enter from the L.H. side and progress across and up the dam, giving quite a large region of shear near the crest at 0.5s. At no point is the R.H. side ever in tension. For the D2 model regions of shear enter both the left and right toes of the dam at about the same time, (indeed, for D2/8 model which is at 10^{o} the shears begin at the R.H. side). These two regions of shear both reach the crest around 0.4s, giving substantial tensions deep into the dam structure. The dam then, as in the other D2 models discussed, divides up into smaller regions of compression and tension, as the energy is reflected from the base interface back into the dam.

7.6. The stress distributions and their physical explanation

The considerable variety of stress distributions that are produced by the variations in wave type, angle of incidence and embankment model,

that make up examples of this study are as a result of certain well known physical properties of elastic wave propagation, namely reflection, refraction, mode conversion and diffraction. At each interface a propagating wave will suffer one or more of these properties, which even with a quite simple geometry, rapidly increases the number of wavefronts. As these wavefronts begin to interfere with each other the nature of the displacement pattern takes on an increasingly complex form.

The kind of complexities that we might expect with the models D1 and D2 are illustrated in Fig. 7.8 and Fig. 7.9. Fig 7.8. illustrates an S-wave, incident to the vertical, entering the homogeneous model D1, and gives the types of wave that will be produced after one reflection from the top surface. The angles of the rays are only suggestive, and are not drawn to scale, but they are easily calculated using Snell's law. The amplitude ratios of each component to the incident amplitude are not given, but could be calculated from formulas derived in seismological texts (e.g. Aki and Richards (1980) pp 144-151). Also, indicated in Fig. 7.8., by circular wave fronts, are the diffracted waves that would originate at the discontinuities in slope.

Fig. 7.9 is a similar diagram for part of model D2. It will be seen that the introduction of two interfaces increases very considerably the number of wave fronts that will be produced in a given time.

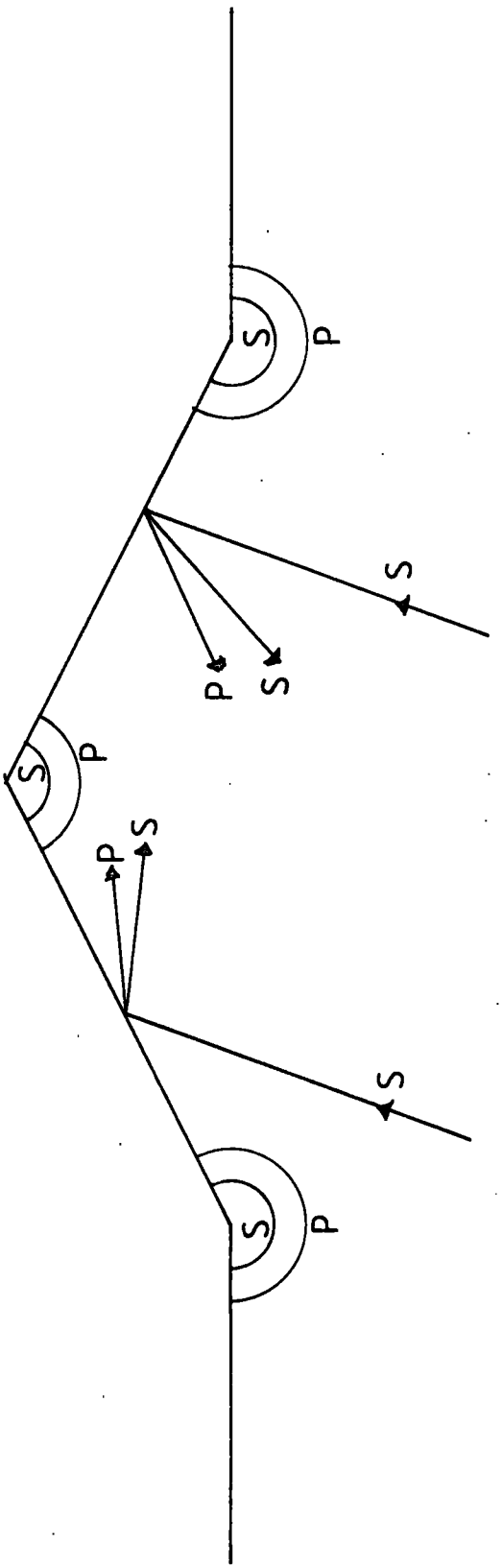

Fig. 7.8 Diagram showing forms of waves produced in model D1 by an incident S-wave.

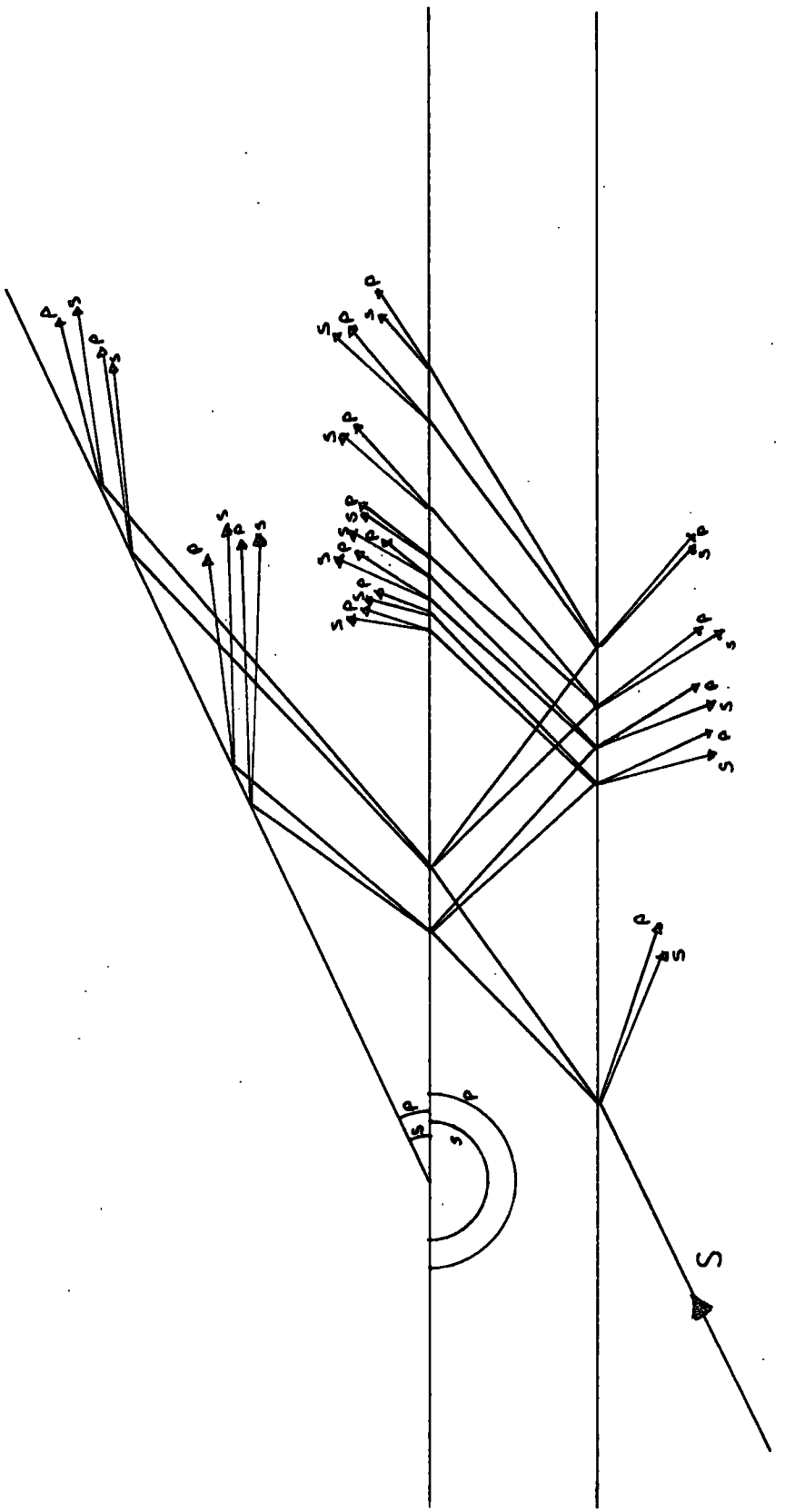

Fig. 7.9 Diagram showing forms of waves produced in model D2 by an incident S-wave.

The fact that the incident wave in these diagrams is S is not significant; the same sort of splitting of the wave into a variety of types would occur with an incident P-wave, but with differences in some of the angles.

It is not easy to disentangle these different wave fronts from each other in the stress distributions in Appendix B. However there are some examples where we can see these processes taking place.

(a) Reflection

This is well issustrated by the examples D1/1; P; 0; g and D1/2; 20; g. A sketch of the expected P wavefront for D1/1 is given in Fig. 7.10. The reflected compression waves from the dam slopes are clearly identifiable, coinciding in the central region of the dam at about 0.24s, and having passed through each other by 0.3s.

A similar series of sketches is given in Fig. 7.11 which give the progress of a compression wave incident at 20^{o} as in D1/2.

The same effect is not so easily seen in the cases of D1/3 and D1/4 since these are S-waves, and the exact position of an S-wave is not readily seen when it is overlain (as in all the examples) with the compressive stresses of the static forces. However in D1/3; S; 0; g there are clear regions of shear which

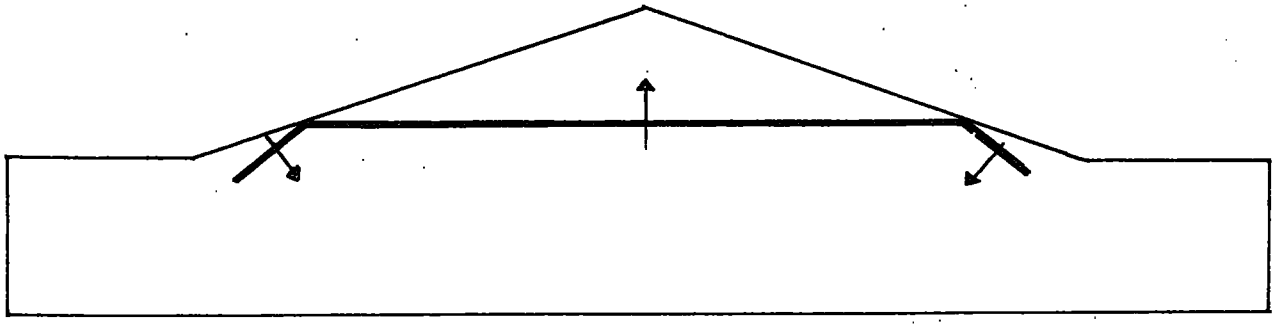

0·12s

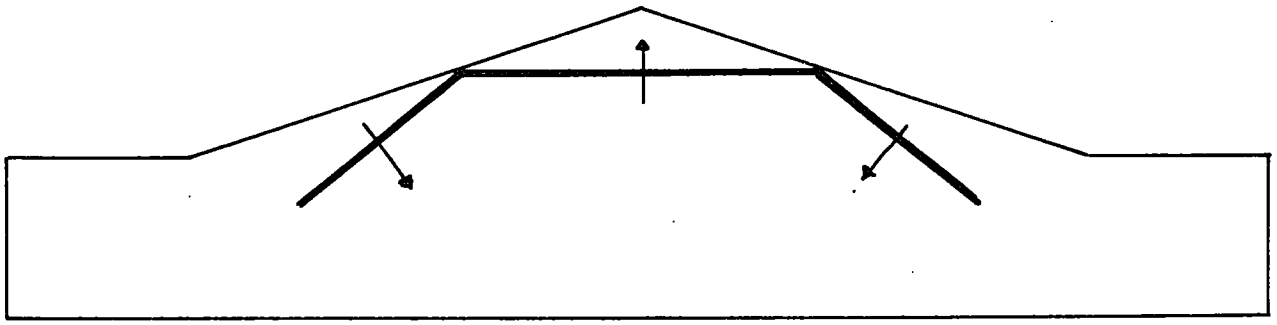

0·18s

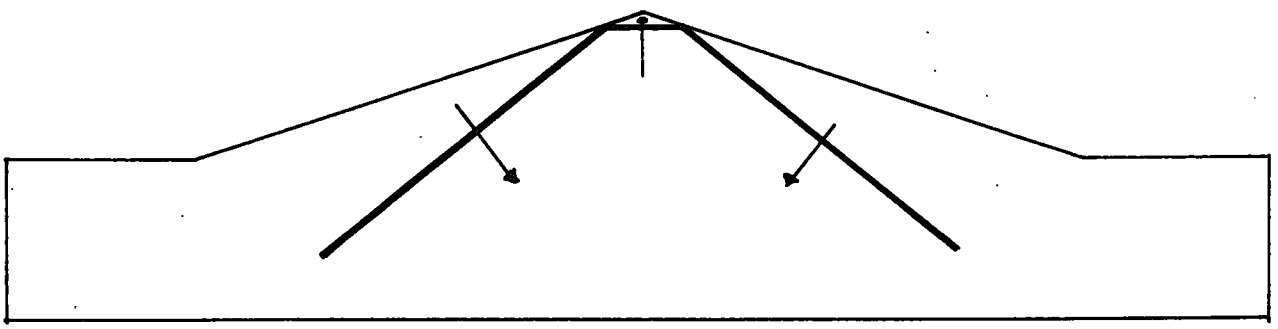

0·22s

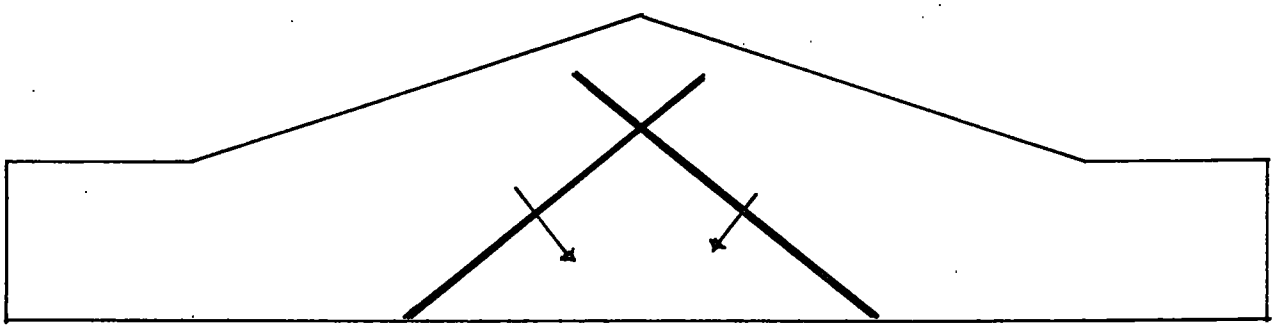

0·24s

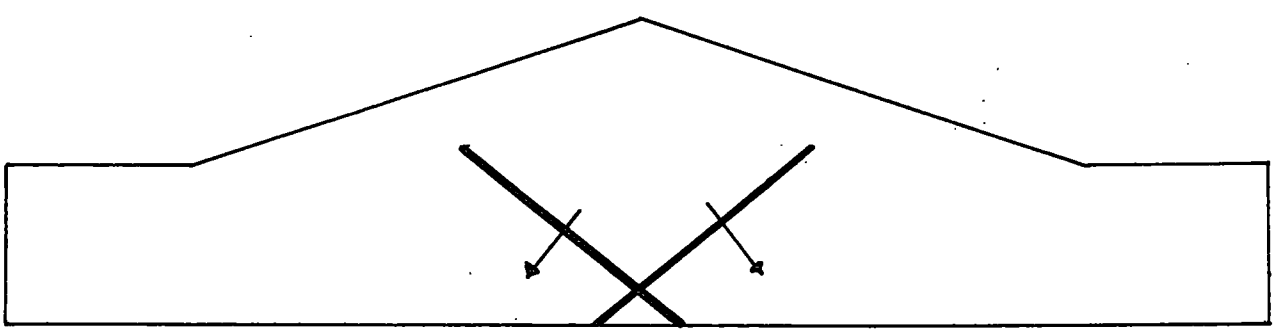

0·3s

Fig. 7.10 Progression of a compression wave in D1/1.

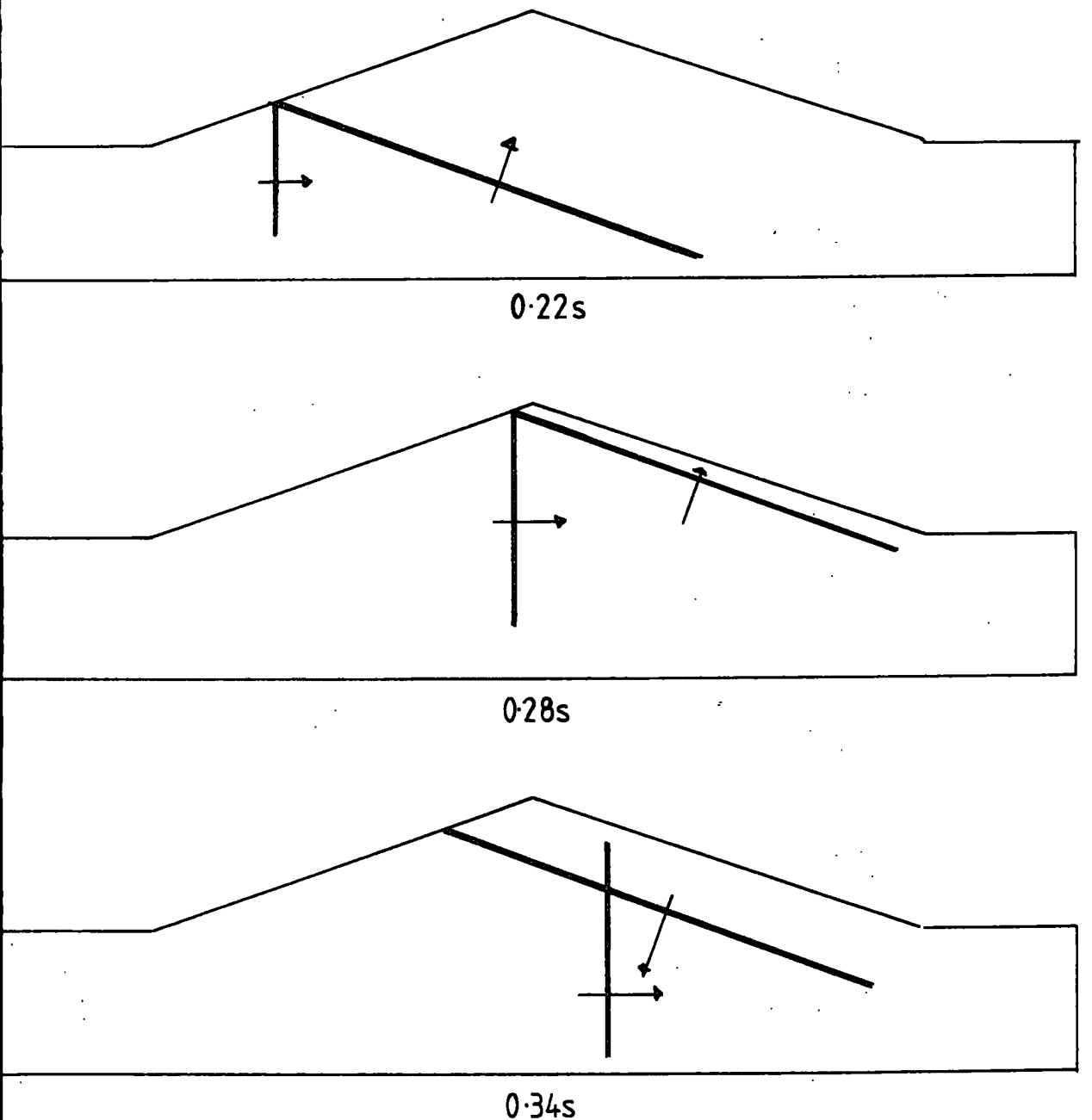

Fig. 7.11 Progression of a compression wave in D1/2.

move from the slopes towards the centre (e.g. at 0.25s on the R.H. side), which will be the result of interference of the reflected wave with the latter portion of the upgoing wave. In a similar way in D1/4;S; 20; g, a region of shear is observed to travel from left to right across the body of the embankement from 0.3s to 0.5s, being the result of reflection from the left slope.

(b) Refraction

This has already been inferred from the time displacement graphs, where it was observed that the waves incident at an angle arrive at the ground surface almost at the same time along its whole length. The effect of this refraction becomes evident in the stress plots with the early arrival of a wave at the R.H. toe of the embankment. In the case of D2/4; P; 20; g this is seen at 0.12s and 0.14s., and is sketched in Fig. 7.12, showing the position of maximum compression at these times.

(c) Mode conversion

The stress distributions do not give any direct evidence of mode conversion, but we have no reason to doubt its importance. Perhaps the best evidence they give for its cumulative effect is a comparison of D2/1; P; 0; g and D2/6; S; 0; g. The early

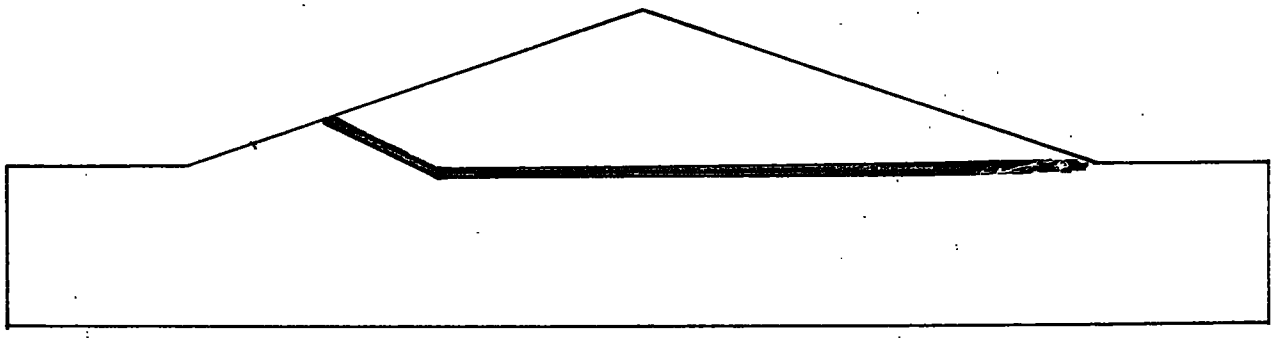

0·12s

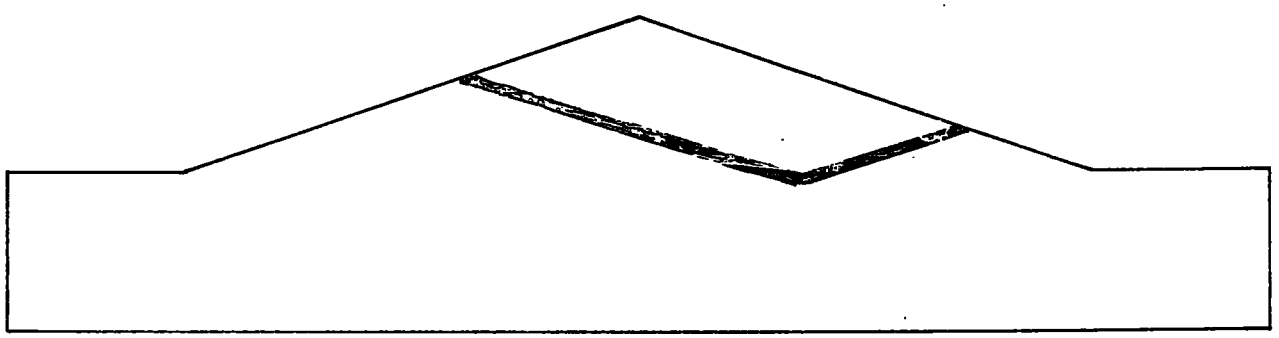

0·14s

Fig. 7.12 Bending of a compression wave due to refraction in D2/4.

parts of the examples show distinctly the patterns of P and S waves respectively, but by the end of their runs, they begin to show similarities, particularly in the breaking up of the embankment into regions of compression and tension. The eventual similarity is to be expected from the continual splitting into P and S waves at each reflection within the region of the embankment.

(d) Diffraction

Diffraction will occur at any discontinuity in a free surface or of an interface. Any plane wave reflected by a surface with a break in slope will be split into sections; the "shadow" zone between these sections will not be free from disturbances, but will contain circular wave fronts of both P and S types originating at the discontinuity. This is illustrated in the sketch Fig. 7.13.

The position illustrated in Fig. 7.13 would occur on D1/1 at about 0.18s (using the compressive part of the wave as indicator). There is no clear evidence of a circular wave front in the region of the corner, suggesting that the diffraction effect is small. In a similar way, in none of the examples are there obvious indications of circular wavefronts propagating from the crest.

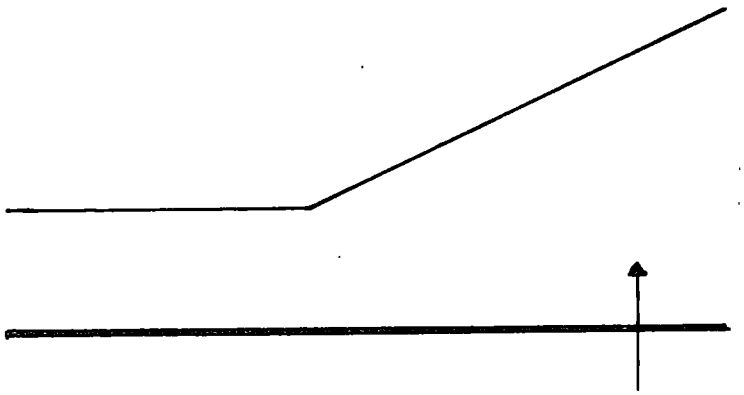

(a) Vertically incident P-wave approaching slope corner.

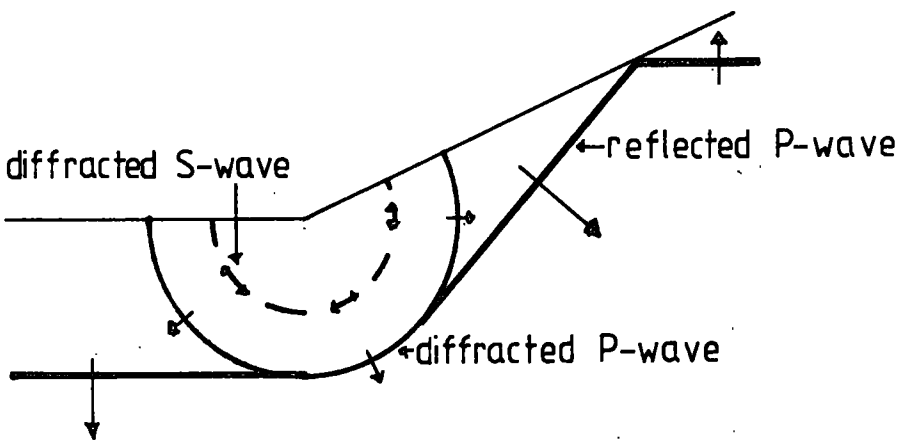

(b) Reflected and diffracted waves after incidence.

Fig.7.13

In D2 examples the junction of an interface (which is itself somewhat irregular) with the break of slope at the toe of the embankment could be expected to enhance diffraction effects; and this region does develop into one of high stresses with considerable variation in stress in time. However it is also the region where reflection, refraction, and mode conversion are occurring most frequently. It is not, therefore, possible to ascribe the detail of this region to diffraction in particular, and in view of lack of evidence of it elsewhere it can be concluded that it is most likely a subsidiary factor in determining the stress distributions.

The above discussions show that the well known physical properties of reflection, refraction, mode conversion, and, to a lesser extent, diffraction, are able to qualitatively explain some of the more simple stress patterns; and that they are not able to explain immediately the more complex stress distributions is only because the observed effect is a sum of so many different components. This raises the possibility that a straightforward ray theory approach carried through systematically might be able to give as good predictions of stress patterns as are given here. This approach would require not only a careful accounting of all the generated wave fronts, but also the calculation of the amplitude and phase of each wave. The total displacement at each point would be then found by summing the displacements of all the generated waves that pass that point at each moment in time. It would seem feasible that such a programme could be carried out

for incident plane waves, at least for geometries of the complexity of D1 and D2. The great advantage of this approach, if it were successful, is that there would be no need to introduce the artificial boundaries that are needed by the finite element method. The calculations could be carried out over a genuine half-space. The difficulties would seem largely to be computing ones, in which a system of book-keeping would be needed to keep account of the history of each wave from the time that it is generated.

7.7. The Stress distributions and natural modes of vibration

The evidence of the stress distributions for the layered model is that much of the incident energy becomes trapped in the embankment. If this trapping of energy were total then the form of model used in a mode superposition analysis, which has a rigid base, would be valid. In the present model some re-radiation of energy to the substructure takes place. The question may be asked whether the need to model this re-radiation is significant, particularly if there is a large velocity contrast between the embankment and its substructure. It might be argued that the embankment as a result of the inhomogeneities is largely isolated from the substructure, and that, even though some of the input energy will be re-radiated, the form of vibration will be essentially that of the natural modes of vibration of the embankment fixed to a rigid base. Such an argument is implicit in some methods of design, for example the "Simplified Approach", proposed as a preliminary design method by Chopra and Corns (1979) for concrete

gravity dams and which is discussed by Alitnisk and Severn (1981) An evaluation of this hypothesis can be had from an examination of the stress distributions.

Fig. 7.14 gives the first six mode shapes for an idealised embankment. They were derived by Clough and Chopra (1966) for the dam section already illustrated in Fig. 6.11.The embankment of the grid of this study would have different frequencies, but the order of magnitude would be similar (1-4 Hz), and the pattern of the mode shapes would be almost the same. Certain of these shapes may be seen in the stressplots, albeit only for a short period of time. For example D2/6; S; 0; g at 0.3s has an antisymmetric distribution about the central vertical with each slope divided into a region of compression and one of tension. Mode 3 of Fig 7.14 would correspond to this. However this mode shape is certainly not maintained, for by 0.375s the slopes are divided into four distinct regions alternating between compression and tension. However this may be the shape of mode 4 of Fig. 7.14 (or possible, a mode higher than those illustrated). Likewise for D2/1; P; 0; g, the position at 0.18s corresponds to the shape of mode 2, and later at 0.3s we have a distribution that would fit mode 6.

The examples with vertical incidence do not therefore contradict the hypothesis that, the forms of stress distribution could be obtained by a consideration of the natural modes of vibration, but using higher modes with increase in time. However this hypothesis can no longer be held in the case of the stress distributions produced by waves incident to the vertical. In all the D2 models which have

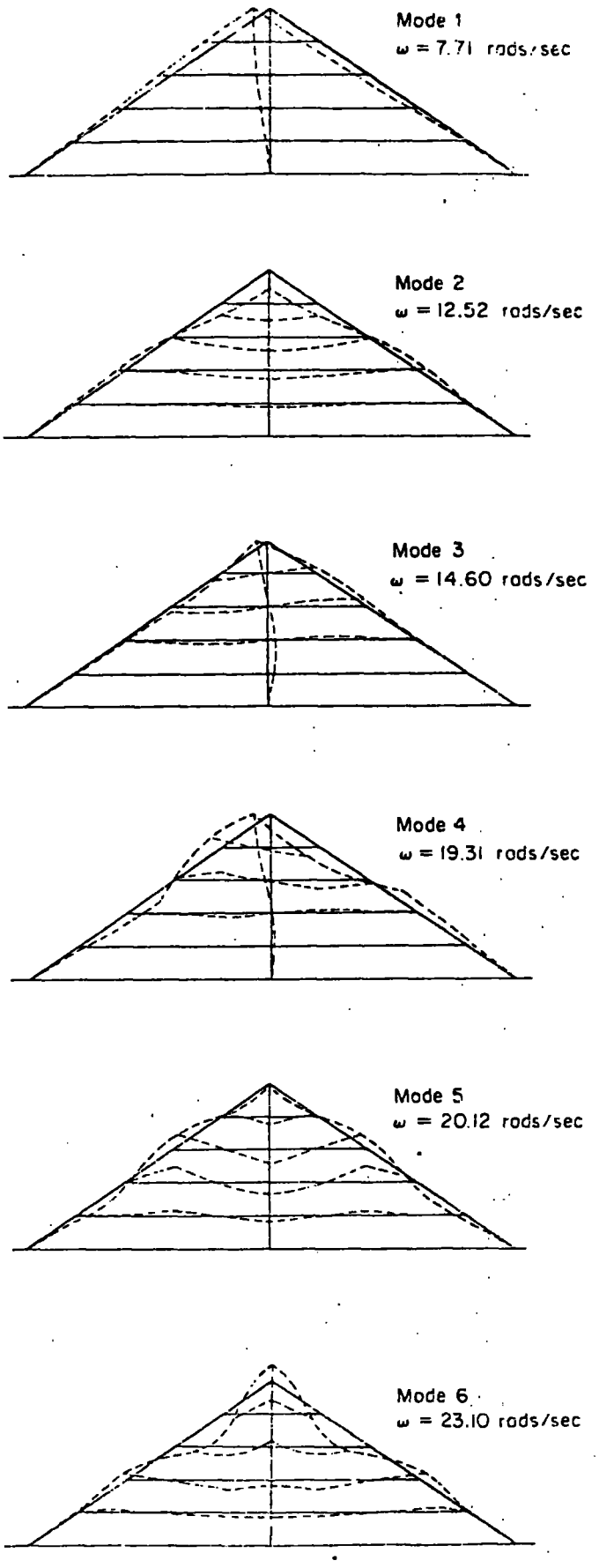

Fig. 7.14 Natural mode shapes and frequencies for the finite element grid of Fig. 6.11. From Clough and Chopra (1966).

waves incident at an angle there is a tendency as time progresses for the stresses to break into smaller regions of either tension or compression. An important feature of these examples is that the number of regions is always more on the left side. For example in D2/11; S; 30; g at 0.525 we can count 5 alternative regions of compression and tension on the left side as opposed to 3 on the right. The same is equally true of P-wave examples, e.g. D2/4; 20; g which has at 0.4s a similar 5 regions on the left and 3 on the right. This is a feature which is clearly dependent on the side from which the wave approaches and so cannot be explained by a suitable combination of natural modes. The mode shapes for a symmetric body must be either symmetric or antisymmetric - that is if an origin is placed on the line of symmetry, the displacement at the point $(-x,y)$ will have the same components as that at (x,y), but with possibly a change of sign in either or both of the components. This behaviour is seen in all the illustrated modes of Fig. 7.14, and means that the numbers of alternating regions of compression and tension down each slope will be the same. A combination of mode shapes could possible destroy this symmetry, but we should then see an alternation of the stresses from one side of the embankment to the other.

It must be concluded that the persistent division of the left slope into more regions of alternating, tension and compression than on the right slope is a reflection of the side from which the wave enters. Such stress patterns as these, cannot, therefore be even approximated by a combination of natural modes, but must be formed by a consideration of the original nature of the forcing function, as has been done in this study.

7.8. Conclusion

The idealised seismic inputs used in the examples have shown that considerable distortions of the static stress distribution may be produced, and that this may be done with considerable variety by a variation of the input parameters and whether the model is homogeneous or layered. This variety is not surprising when the physical processes of reflection, refraction, mode-conversion and diffraction are considered. Indeed, on the stress plots it is possible to discern some of these processes, though this is not so readily done as time progresses and the stress distribution becomes a summation of the many waves that have been generated.

Both the time-displacement graphs and the stress plots confirm that the displacement amplitudes and stress distortions are greater in the cases of (a) S-waves, (b) layered model (c) angled incidence. Of these, perhaps, the inhomogeneity is the most important factor. The trapping of energy in the low-velocity embankment is quite evident and even in the case of a P-wave the mode conversion at each reflection and refraction produces in time a stress distribution with similarities to that from an S-wave.

Many of the stress distributions, even with the lower base acceleration, are suggestive of failure. In addition to the possibility of slumping surfaces, there are many instances that would suggest tension fracture, notably near the crest.

The stress patterns from waves incident at an angle contain permanent features that clearly are consequences of the directional nature of the wave. It is therefore not possible to construct a simplified model in these cases based on natural modes. An analysis in terms of only natural modes would imply source independence. The examples of angled incidence show that this is not tenable.

Chapter 8. Summary

The object of this study has been to study the effect of elastic waves from a seismic source on an embankment dam. The concern has been to evaluate the displacements and stresses generated in an embankment when it is subjected to waves which have the characteristics of seismic waves. Since there is ample field evidence of the effect of the surrounding topography and geology of the substructure on seismic waves, this study takes as a starting point that the embankment should not be considered in isolation, but that any proposed model should include as much of the underlying substructure as possible.

Of the possible numerical approaches to this problem the finite element method is one that has much to commend it, and to a great extent this study is an evaluation of its applicability. The feature of the finite element method that is so attractive is its great flexibility in modelling regions of both geometric complexity and variation in material properties. Since these were the sort of features to be modelled the finite element method was selected rather than a finite difference approach.

The use of finite elements for dynamics problems consist of two distinct phases. First there is the formulation of the equations of motion, which consist of a coupled set of second order differential equations. This formulation involves the construction of matrices

which reflect the inertial, elastic and damping properties of the whole region being studied, together with a time varying vector that records the history of any external forces or displacements that are applied to the region. The assembly of these matrices is a standard procedure. The theoretical details are given in chapter 2, based substantially on the text of Desai and Abel (1972). For this assembly the user has the choice of a variety of element types, but the simplicity of the constant strain triangle still makes it very popular. Its shortcomings may not always be fully realised, especially when used for the calculations of stresses where it appears that the orientation of the triangle can affect the orientation of the stress vectors. The quadrilateral elements, which were the main elements used in this study, each formed out of four CST's, do not show this defect. An area which could be investigated is the performance of higher order elements. It is known that for static problems higher order elements can significantly reduce the number of nodes needed to obtain a certain accuracy. Whether such elements give similar advantages to dynamics problems could be determined, but there would appear to be some doubt about this in view of the critical nature of the internodal distance for the propagation problems which is emphasised in this study.

The second phase of a finite element solution to a dynamics problem is the solution of the equations of motion. For this there are currently two quite different approaches - mode superposition and direct integration. Mode superposition is effective for a dynamical

system which is governed predominantly by the lower modes of vibration. This may be reasonable for a structure attached to a rigid base, but not for the study of the displacements (and even more so stresses) in a structure which is attached to a substructure which is itself vibrating. It was therefore neccesary for this study to use a method of direct integration.

There are many methods of integration that can be used. Methods which are explicit and self-starting have great computational advantages. Of these a Runge-Kutta fourth order algorithm was chosen and extensively tested. Its accuracy is greatly superior to some other methods recommended in the literature and it gave good results even after 200 time-steps. It is straightforward to program, since it involves only addition and multiplication of vectors and matrices. To advance a set of almost 2400 equations forward by 1 time-step required approximately 3 c.p.u. seconds. Whether any other methods are significantly faster than this is not known; but the length of time for computation was not the most restrictive of the limitations encountered in this study. The main disadvantage of the Runge-Kutta algorithm is its instability if too large a time-step is used. It was discovered empirically that this instability was more likely to occur if the equations contained damping coefficients, and this observation was confirmed theoretically for some simple cases. The determination of the critical time-step for a given set of equations is theoretically possible, but for large systems presents a formidable computing task in itself. Fortunately, if in practice too large a time-step is chosen, the instability is dramatic leaving the user in no doubt

that a smaller step must be used. A time-step of half the critical value gave, for the test example, a good result. The Runge-Kutta algorithm therefore proved to be a very satisfactory integration method for problems without damping.

A series of tests on some simple wave propagation problems revealed the capability of a finite element mesh to give accurate predictions for both displacement, stresses and speed of propagation. As would be expected, it was found that for satisfactory predictions there had to be both limitations on both the time-step of integration and the size of the elements. From the tests a value of six time-steps in each period of the propagating wave was found as a lower limit. The restriction on mesh size was fixed by the tests at eight elements per wavelength.

This latter restriction is of fundamental importance. It implies for a certain material, and hence a known propagating velocity, that there is a relation between the element size and the maximum frequency that can be modelled by that grid. It is therefore no use activating a finite element grid with anything like an impulse. For earthquake studies we can rationally settle on a cut-off frequency for our input. Given the material properties of the dam this fixes our element size, and the grid must be designed accordingly. It would appear from some of the published grids that this fact has not always been realised. Failure to meet the grid size requirement will lead to poor predictions of displacement but after only a few time-steps useless predictions of stress. It is

worth emphasising that this is a limitation of the finite element model, and not the method of solving the equations of motion. It therefore applies equally to other integration algorithms, and to the method of mode superposition.

Care was taken in this study to design a grid that meets with the mesh size limitation. An unwanted feature of a finite element grid when used to model an infinite space is the reflective nature of its artificial boundaries. Whether this defect can be eliminated is not certain, but the grid used in this study overcame the problem only to the extent that its boundaries were placed as far away as possible. The size of grid was finally determined by the limitations of the computer storage available.

Again, it is worth pointing out that mode superposition does not escape from unwanted reflections. Since it is used with the input given along the base of the embankment, the predictions it gives are those that result from waves originating at the base which will be internally reflected in the embankment back to the base again, at which point they will be reflected from the base. At least in the model of this study the first fictitious surface that may act as a reflector is placed some way down into the half-space beneath the embankment.

The fact that a finite element model can only cope with frequencies below a certain level means that it is not possible to use an actual strong motion record as an input. This study used single pulses at a known frequency. These have the advantage of simplicity, and are

suitable for a study whose aim is insight into the broad features of wave propagation in embankments. A more realistic source would be to use a strong motion record filtered at the cut-off frequency. However the use of such an input would require a solution to the problem of reflections from the artificial boundaries, so that the model could be run for the full duration of the seismic record.

Certain other limitations of the model used in this study should be noted.

(a) The model is two dimensional. This is a serious weakness, since modes of vibration along the length of an embankment dam, which have been observed, fail to be modelled. However the extension of three dimensions of the method as formulated here, whilst posing no new theoretical problems, would require a large increase in the number of nodes. A two dimensional model with N nodes, if extended to a three dimensional model of similar extent would require of order $N^{1.5}$ nodes. For the 2400 degrees of freedom of the model of this study, this becomes approximately 125,000 degrees of freedom.

(b) The materials are assumed to be linearly elastic. The visco-elastic properties of the embankment materials will produce a modification of the static stress distribution due to the body forces, but their effect on short term events such as seismic waves might not be large. However it would be possible to extend the method used in this study to investigate this.

(c) The effects of any impounded water have been ignored. The static stresses due to the weight of impounded water on one side was calculated, and is illustrated in Appendix B, but this is not included in any of the dynamic examples, except in some trial examples that have not been included in this study. However the weight of water is not a large addition to the body forces, and so would not give a radically different stress pattern for dynamic problems. There are however other effects that the impounded water may have, which have not been considered at all. First the boundary on the upstream side will be an interface between an elastic medium and an acoustic medium, with transmission of energy across it. To include this in a finite element model would require dividing the water up into elements with the appropriate properties (Saini et al. (1978)). Second the presence of water will affect the properties of the embankment materials by the addition of a pore pressure. This relates to the limitation (b) already discussed. A third effect that impounded water might have is the generation of water waves on the surface of the resevoir as a result of an earthquake. This is a different kind of problem to that considered in this study, and would require a separate analysis.

The models used for the examples of chapter 7 were based on a grid which was designed to meet the requirements of mesh size. The predicted stress distributions are therefore reliable. Grids which have been used in the past, such as those given in chapter 6, which fail to meet the mesh requirement can only be regarded as poor predictors of displacement and worthless predictors of stress distribution.

The examples of chapter 7 illustrate the variety of stress distributions that are possible, and they emphasise the importance of S-waves, angled incidence and inhomogenity. Various forms of failure are indicated as possibilities, especially slumping failures and tensional cracking near the crest.

The physical nature of the wave propagation can be seen to give a qualitative explanation of the predicted stress patterns. Reflection, refraction and mode conversion play important parts in determining the stress distributions, but diffraction effects, at least in the examples presented, are not noticeable. There seems to be the possibility that results comparable to those of this study could be obtained by a quantitive application of ray theory. If successful, this may provide a means of avoiding the problem of fictitious boundaries which is inherent in finite element methods.

The examples with angled incidence show that an analysis based on natural modes can never be sufficient. The form of the forcing function, in particular the direction of the incident energy, has

a persistent effect, showing that the stress distributions are not independent of the nature of the source. This indicates that the use of an actual strong motion record as input for a test has a further limitation, since it is the record at a point which has a specific directional relationship to the source; a dam under design may be more likely to receive seismic waves from a different direction. For dams which are built close to faults which may be the site of an earthquake, no single record would be sufficient. This is because, even if the seismic waves could be approximated by plane waves, the movement along the fault producing the earthquake implies that we should, at least, have to consider these waves as approaching from different directions.

This last point reinforces the need for an integrated model which includes both the seismic source and the embankment, as mentioned in section 1.7. However, the overriding requirement of a sufficiently small mesh size that is established in this study, suggests that a straightforward extension of the finite element method as used here, to achieve such a model, would be impracticable.

REFERENCES

AKI, K. (1968). Seismic displacement near a fault. J. geophys. Res., 73, 5359-5376.

AKI, K. and RICHARDS, P.G. (1980). Quantitative Seismology: Theory and models, Freeman, San Francisco, 2 vols, 932 pp.

ALTINISIK, D. and SEVERN, R.T. (1981). Natural frequencies and response characteristics of gravity dams. In Dams and Earthquake, pp. 205-312, Thomas Telford, London.

ANDERSON, J.G. and RICHARDS, P.G. (1975). Comparison of strong ground motion from several dislocation models. Geophys. J.R. astr. Soc., 42, 347-373.

BELYTSCHKO, T. and MULLEN, R. (1978). On dispersive properties of finite element solutions. In Modern Problems in Elastic Wave Propagation, pp. 67-82, edited by Miklowitz, J. and Achenback, J.D., Wiley Interscience, New York.

BETTESS, P. (1977). Infinite elements. Int. J. Numer. Meth Eng., 11, 53-64.

BETTESS, P. (1980). More on infinite elements. Int. J. Numer Meth. Eng., 15, 1613-1626.

BOLT, B.A. (1972). San Fernando rupture mechanism and the Pacoima strong-motion record. Bull. seism. Soc. Am., 62, 1053-1061.

BOORE, D.M. (1973). The effect of simple topography on seismic waves : implications for the accelerations recorded at Pacoima dam, San Fernando valley, California. Bull. seism. Soc. Am., 63, 1603-1609.

BOUCHON, M. (1973). Effect of topography on surface motion. Bull. seism. Soc. Am., 63, 615-632.

BOUCHON, M. (1980a). The motion of the ground during an earthquake. 1. The case of a strike slip fault. J. geophys. Res., 85, 356-366.

BOUCHON, M. (1980b). The motion of the ground during an earthquake. 2. The case of a dip slip fault. J. geophys. Res., 85, 367-375.

BRUSU, L. and NIGRO, L. (1980). A one step method for direct integration of structural dynamic equations. Int. J. Numer. Meth Eng., 15, 685-699.

CHOPRA, A.K. and CORNS, C.F. (1979). Dynamic method for earthquake resistant design and safety evaluation of concrete gravity dams. I.C.O.L.D., 13th Congress, New Delhi, Q51, R6.

CLOUGH, R.W. and CHOPRA, A.K. (1966). Earthquake stress analysis in earth dams. J. Engng. Mech. Div. Am. Soc. civ. Engrs. 92 (EM2), 197-211.

DAMS AND EARTHQUAKE, (1981). Proceedings of a conference, Institution of Civil Engineers, London, 1-2 Oct. 1980. Thomas Telford, London, 313 pp.

DESAI, C.S. and ABEL, J.F. (1972). Introduction to the finite element method : a numerical method for engineering analysis, Van Nostrand, New York, 477 pp.

EISENBERG, M.A. and MALVERN, L.E. (1973). On finite element integration in natural co-ordinates. Int. J. Numer. Meth. Eng., 7, 574-575.

FEDOCK, J.J. and SCHREYER,H.L. (1981). Effect of earth media on the seismic motion of embedded rigid structures. Earthquake Eng & Struct.Dyn., 9, 311-327.

FOX, L. and MAYERS, D.F. (1968). Computing methods for scientists and engineers, Clarendon Press, Oxford, 255 pp.

GROOMS, H.R. (1972). Algorithm for matrix bandwidth reduction. J. struct. Div. Am. Soc. civ. Engrs., 98 (STI), 203-214.

GUTIERREZ, J.A. and CHOPRA, A.K. (1978). A substructure method for earthquake analysis of structures including structure-soil interaction. Earthquake Eng. & Struct. Dyn.,6,51-69.

HANSTEEN, O.E. and BELL, K. (1979). On the accuracy of mode superposition analysis in structural dynamics. Earthquake Eng. & Struct. Dyn, 1, 405-411.

HAWS, E.T. and REILLY, N. (1981). Dams, natural and induced earthquakes and the environment. In Dams and Earthquake, pp.253-260, Thomas Telford, London.

ILAN, A., BOND, L.J. and SPIVACK, M. (1979). Interaction of a compressional impulse with a slot normal to the surface of an elastic half space. Geophys. J.R. astr. Soc., 57, 463-477.

ISRAEL, M. and KOVACK, R. (1977). Near field motions from a propagating strike slip fault in an elastic half space. Bull. seism. Soc. Am., 67, 977-994.

JAEGER, J.C. and COOK, N.G.W. (1969). Fundamentals of rock mechanics, Chapman and Hall, London, 515 pp.

JANBU, N. (1973). Slope stability computations. In Embankment-dam engineering : Casagrande volume, pp. 47-86, edited by Hirschfeld, R.C. and Poulos, S.J., John Wiley, New York.

LAMB, H. (1904). On the propagation of tremors over the surface of elastic solid. Phil. Trans. R. Soc., Series A, 203, 1-42.

LAPIDUS, L. and SEINFELD, J.H. (1971). Numerical solution of ordinary differential equations, Academic Press, New York.

LAWSON, J.D. (1966). An order five Runge-Kutta process with extended region of stability. SIAM J. Numer. Anal., 3, 593-597.

LEFEBVRE, G., DUNCAN, J.M. and WILSON, E.L. (1973). Three dimesional finite element analyses of dams. J. Soil Mech. Fdns. Div. Am. Soc. Civ. Engrs., 99 (SM10), 849-862.

LONG, R.E. (1981) Optimum seismic input in the design of large structures. In Dams and Earthquake, pp. 3-8, Thomas Telford, London.

MITHEN, D.F. (1980). Numerical investigation into the mechanism of graben formation.. Ph.D. Thesis. University of Durham.

MURPHY, J.R., DAVIS, A.H. and WEAVER, N.L. (1971). Amplification of seismic body waves by low-velocity surface layers. Bull. seism. Soc. Am., 61, 109-145.

NEWMARK, N.M. (1965). Effects of earthquakes on dams and embankments. Géotechnique, 15, 139-159.

PARK, M.J.M. (1981). Numerical analysis of deformation in the upper part of subduction zones. Ph.D Thesis. University of Durham.

RODGERS, A.M., KUTZ, J.J. and BENNETT, T.J. (1974). Topographic effects on ground motion for incident P waves: A model study. Bull. seism. Soc. Am., 64, 437-456.

SAINI, S.S., BETTRESS, P. and ZIENKIEWICZ, O.C. (1978). Coupled hydrodynamic response of concrete gravity dams using finite and infinite elements. Earthquake Eng. & Struct. Dyn., 6, 363-374.

SEED, H.B. (1970). Earthslope stability during earthquakes. In Earthquake engineering, pp. 383-401, edited by Wiegel, R.L., Prentic Hull, Eaglewood Cliffs N.J.

SEED, H.B. (1973). Stability of earth and rockfill dams during earthquakes. In Embankment-dam engineering : Casagrande volume, pp. 239-269, edited by Hirschfeld, R.C. and Poulos, S.J., John Wiley, New York.

SEED, H.B., DUNCAN, J.M. and IDRISS, I.M. (1975). Criteria and methods for static and dynamic analysis of earthquakes. In Criteria and assumptions for numerical analysis of dams, pp.564-588, edited by Naylor, D.J., Stagg, K.G. and Zienkiewicz, O.C., University College Department of Civil Engineering, Swansea.

SHERARD, J.L. (1973). Embankment dam cracking. In Embankment-dam engineering : Casagrande volume, pp.271-353, edited by Hirschfeld, R.C. and Poulos, S.J., John Wiley, New York.

SMITH, W.D. (1974). A nonreflecting plane boundary for wave propagation problems. J. Comput. Phys., 15, 492-503.

SMITH, W.D. (1975). The application of finite element analysis to body wave propagation problems. Geophys. J.R. astr. Soc., 42, 747-768.

THOMAS, H.H. (1976). The engineering of large dams, Wiley, London, 2 vols., 777 pp.

WATANABE, H. (1975). A numerical method of seismic analysis for rock and earthfill dams and verification of its reliability through both model test and observation of earthquake on an actual dam. In Criteria and assumptions for numerical analysis of dams, pp 746-765, edited by Naylor, D.J., Stagg, K.G. and Zienkiewicz, O.C., University College Department of Civil Engineering, Swansea.

WILSON, S.D. (1973). Deformation of earth and rockfill dams. In Embankment-dam engineering : Casagrande volume, pp. 365-417, edited by Hirschfeld, R.C. and Poulos, S.J., John Wiley, New York.

WOOD, W.L. (1981). Numerical integration of structural dynamics equations including natural damping and periodic forcing terms. Int. J. Numer. Meth. Eng., 17, 281-289.

ZIENKIEWICZ, O.C. (1977). The finite element method, 3rd. expanded and revised edition of The finite element method in engineering science, McGraw Hill, London, 787 pp.

ZIENKIEWICZ, O.C. (1980?). Finite elements in the time domain, contribution to "state of the art" survey by the Committee in Computing in Applied Mechanics of the American Society of Mechanical Engineers, Naval Postgraduate School, Monterey, California, 79 pp.

ZIENKICWICZ, O.C., KELLY, D.W. and BETTESS, P. (1979). The Sommerfeld (radiation) condition on infinite domains and its modelling in numerical procedures. In Lecture notes in mathematics, pp.169-203, edited by Dold, A. and Eckmann, B., Springer Verlag, Berlin.

Appendix A. Computer Programs

1. Function

The computer programs listed at the end of this appendix have been written to perform the finite element fomulation given in chapters 2 and 3. There are three main programs:-

(a) ASSEMBLY.

This reads in the grid data and forms the stiffness, mass and damping matrices of the equation of motion 2.4.1. For a static problem it calculates the displacements as a result of given loads.

(b) TIMESTEP.

This advances the displacements and velocities by a set number of time-steps using the Runge-Kutta algorithm.

(c) PLOTS.

This produces graphical displays of displacement with time for selected nodes, and distripution of stress at selected times.

These programs are run with the help of four minor programs:-

(d) REDUCE.

This reduces the bandwidth of a grid.

(e) INPUT.

This forms the input data for TIMESTEP for different plane waves.

(f) FILESUM.

This adds the displacements due to static forces to those from the dynamic problem.

(g) DISPLAY.

This allows the user to select the required display options of PLOTS.

The program ASSEMBLY is based on the published code in Desai and Abel (1972) pp. 447-457, though it has undergone considerable modification and extension.

Some of the subroutines of PLOTS which perform the plotting of the stress vectors are based on routines contained in Park (1981).

2. Structure

Each program reads from and writes to devices, labelled in the program by numbers. Numbers 1 to 5 are used for input devices and 6 to 10 for output. Some of the programs have a small degree of user interaction via a terminal, in which case 5 and 6 are used for input and output and must therefore be attached to the terminal rather than a file. A flow diagram illustrating the relation of each program to its input and output files is given in Fig. A.1.

The main programs, ASSEMBLY, TIMESTEP and PLOTS, are composed of many subroutines. Figs A2, A3 and A4 give flow charts for the order in which the subroutines are called by the main program (which in all cases is just a calling program). Subroutines which input or output data are indicated by lines to device numbers, which are the same as those in Fig. A.1. The function of each subroutine is described in the comment cards of the program listings, given at the end of this appendix.

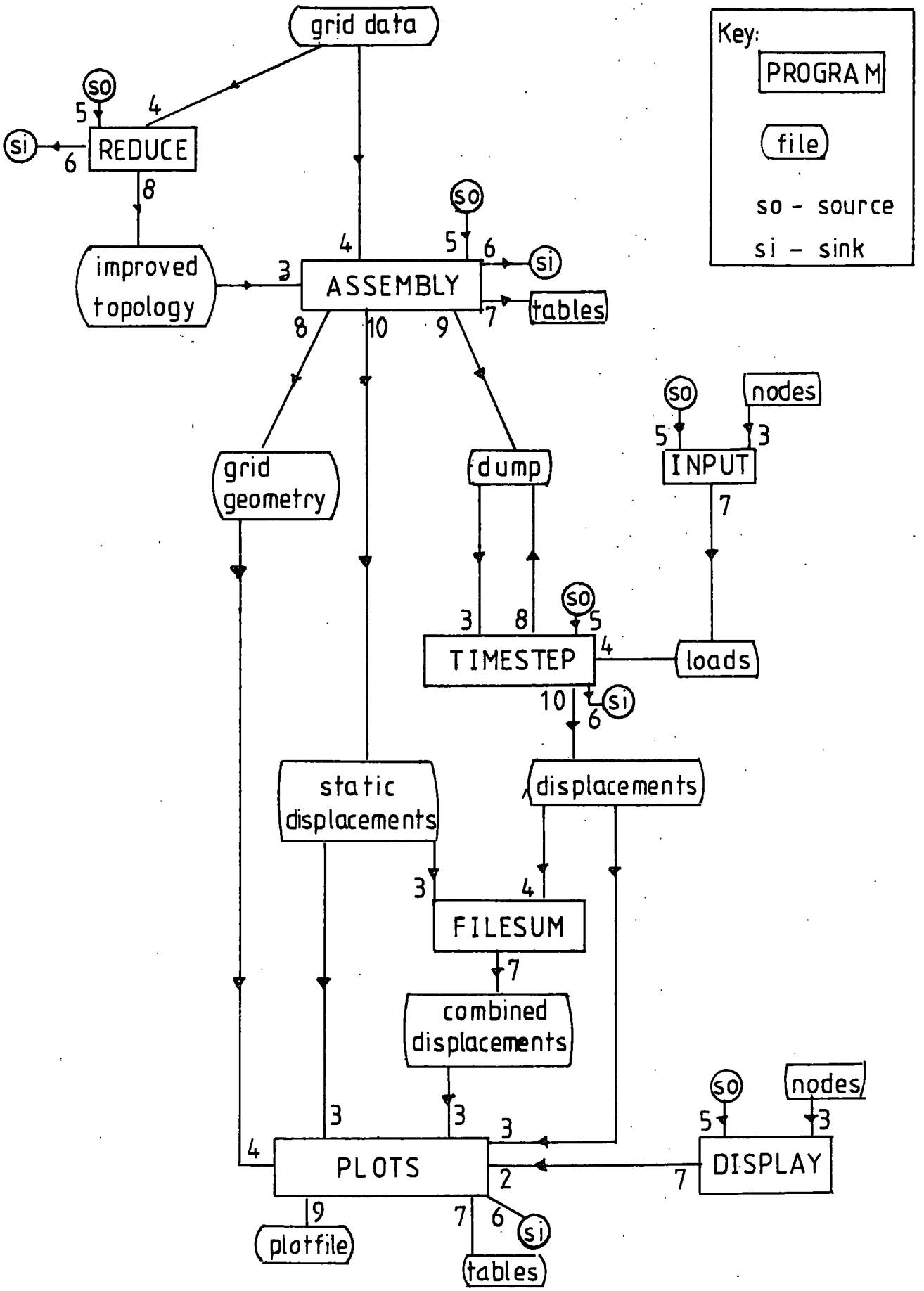

Fig. A1 Interrelation of programs. Numbers are device numbers for the adjoining files.

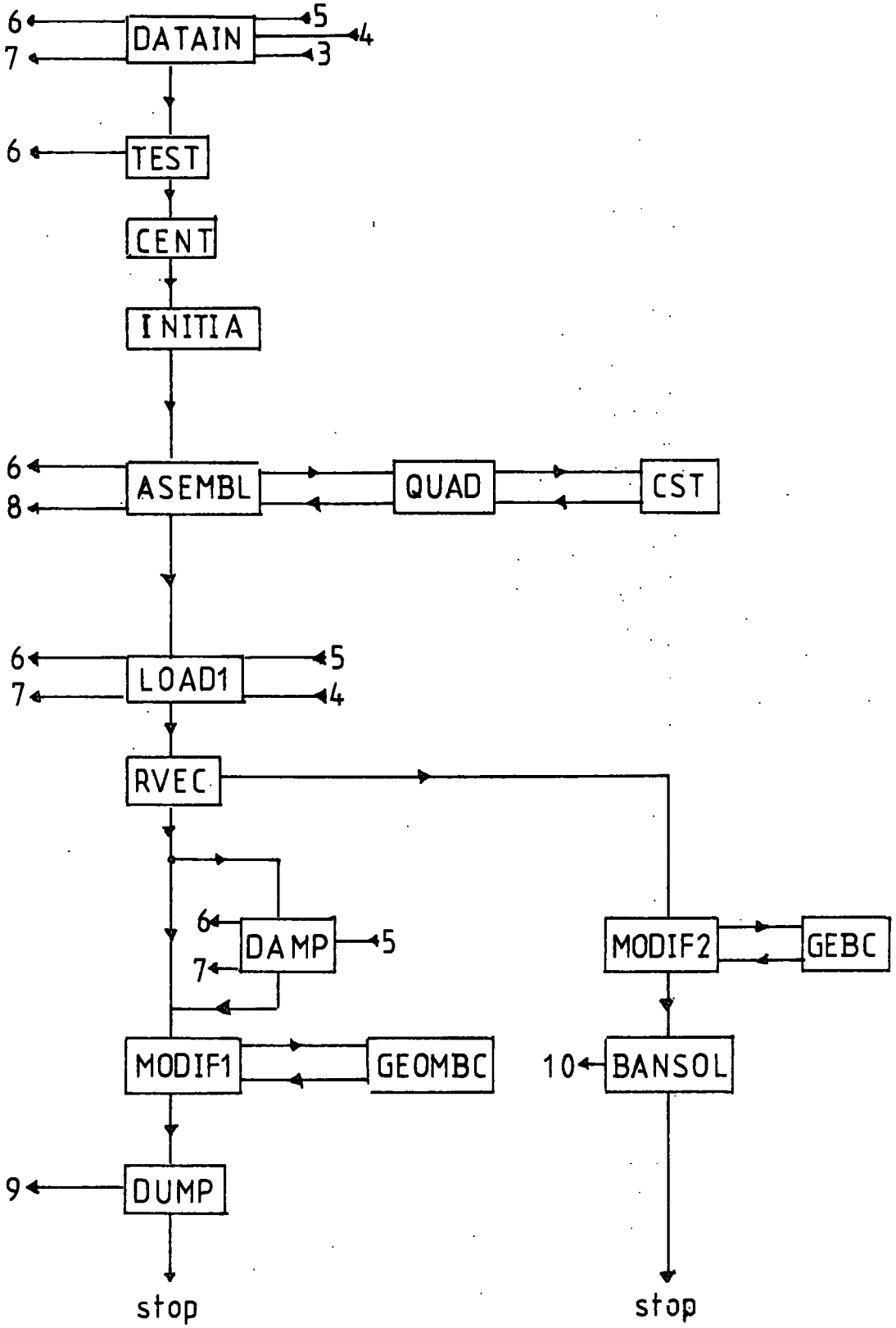

Fig. A.2 Subroutines of ASSEMBLY with input/output device numbers.

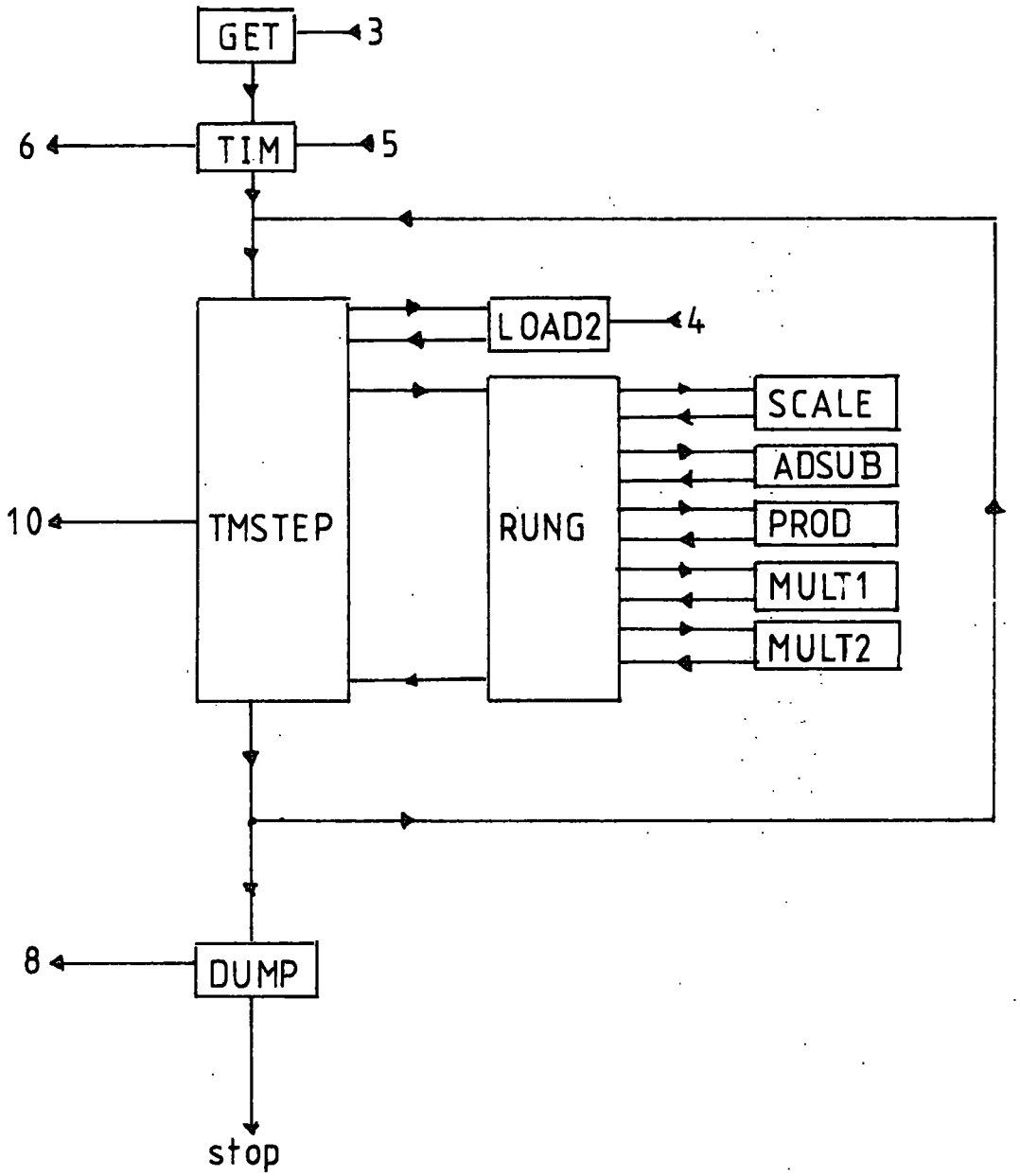

Fig. A.3 Subroutines of TIMESTEP
with input/output device numbers.

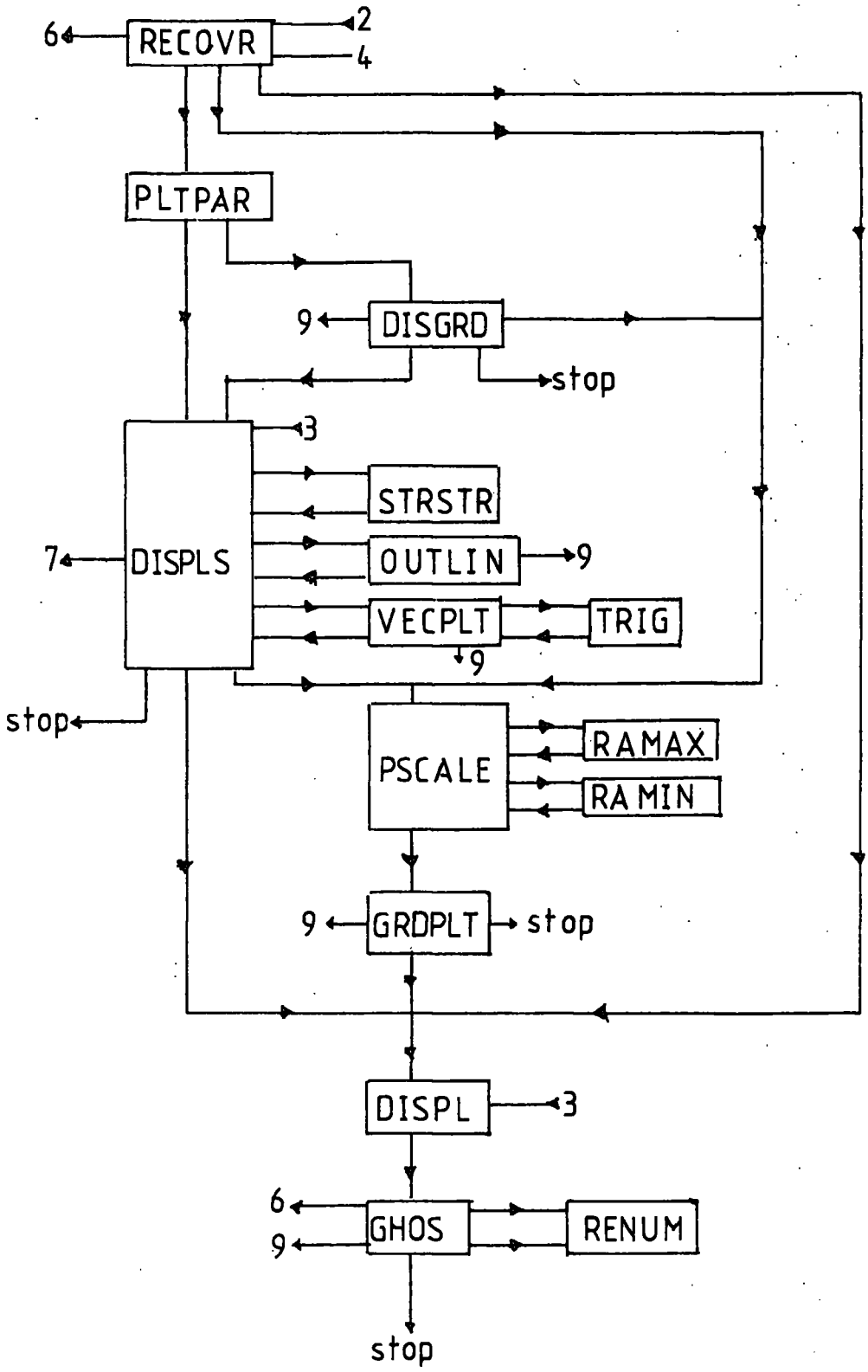

Fig. A.4 Subroutines of PLOTS
with input/output device numbers.

3. Some notes

(a) ASSEMBLY

The main task of data preparation has to be carried out for this program, which is read in the subroutines DATAIN and LOADI. A useful subroutine, TEST, was devised to help in eliminating errors from the grid data file. An error in a co-ordinate of a node or in a node number is very likely to lead to a non-convex quadrilateral element. Using the notation of Fig. A.5 the component along the Z-axis of the vector $(\underline{r}_3 - \underline{r}_2) \times (\underline{r}_1 - \underline{r}_2)$ will have the same sign as that of $\sin \theta_2$.

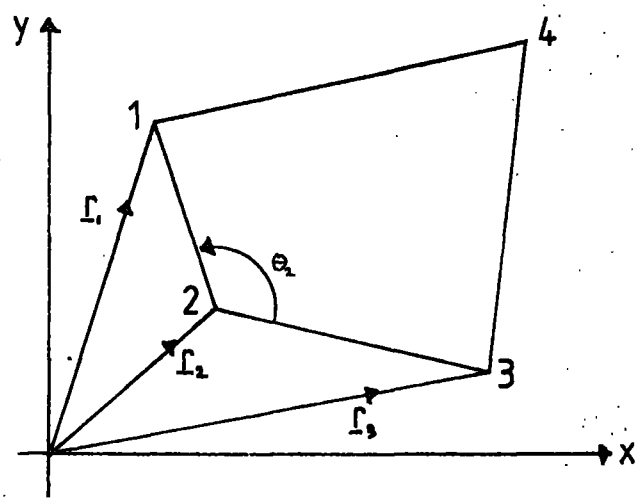

Fig. A.5

This component is, in terms of the co-ordinates of the nodes of the element, given by

$$f_2 = (x_1 y_2 + x_2 y_3 + x_3 y_1) - (x_2 y_1 + x_3 y_2 + x_1 y_3)$$

and so $0 < \theta_2 < \pi$ requires $f_2 > 0$ .This function is evaluated at each node of the quadrilateral. If the element is either numbered clockwise, is concave, or is crossed then at least one f_1, f_2, f_3, f_4 will be negative. This is illustrated in Fig. A.6.

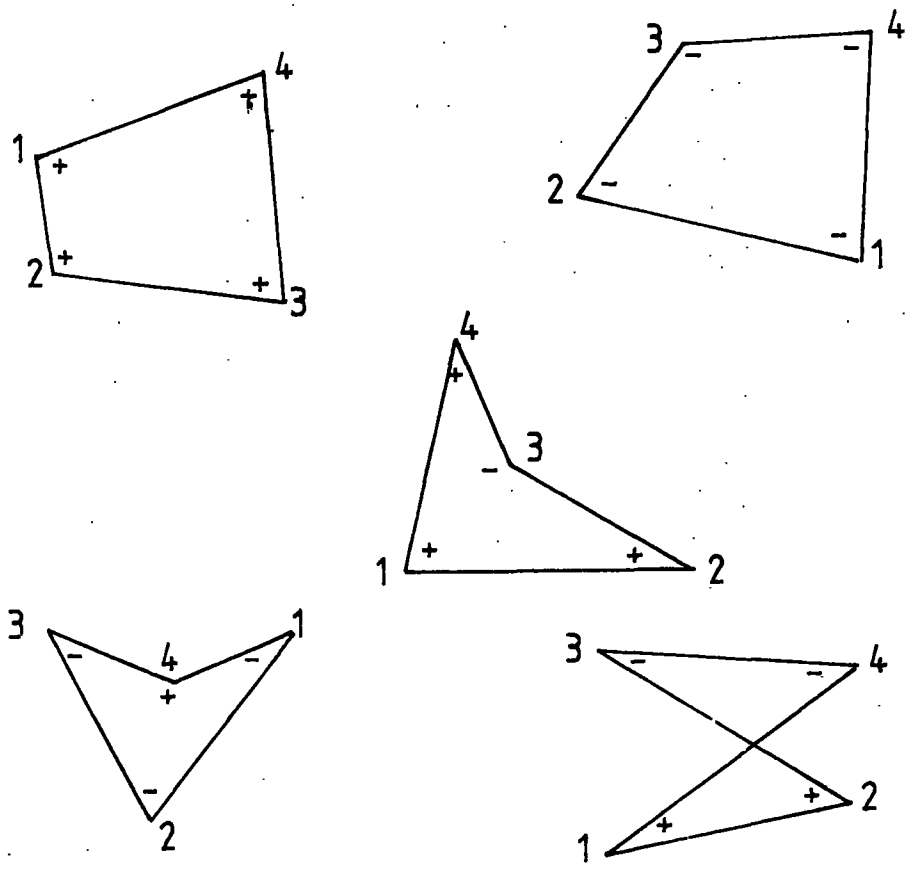

Fig. A.6. Sign of f at each node for different quadrilaterals.

Certain options are available in the program which are prompted when run at a terminal. In particular the program can either be used to find the static displacements due to

an initial loading (which may include body forces), or as the first stage in a time-stepping problem. For a grid with 2400 degrees of freedom this program uses around 15 c.p.u.

(b) TIMESTEP

Each time the routine TIMESTEP is called the displacements and velocities are advanced by 1 time-step. The Runge-Kutta algorithm is contained in RUNG and its subsidiary routines which perform various additions and multiplications of vectors and matrices. As it stands the program executes 15 time-steps, and has to be reloaded for more time-steps. For a grid of 2400 degrees of freedom 15 time-steps uses around 50 c.p.u. (the majority of which is used by the subroutine PROD).

(c) PLOTS

The output from ASSEMBLY and TIMESTEP, together with options that have been determined by the interactive program DISPLAY, from the input to this program. It produces a plotfile using the library* GHOST, which gives the graphical output. To produce the plots that are given for each example in Appendix B required around 60 c.p.u.

(d) REDUCE

The bandwidth b, of the stiffness matrix is related to the maximum nodal difference, d, of any element by

$$b = 4d + 3$$

if each node has two degrees of freedom (Desai and Abel (1972), p. 162). This program, using the algorithm of Grooms (1972), reduces the value of d for a grid. The program is interactive and to be used successfully requires a judicious choice of the input parameters. The output is in the form of a renumbering of the nodes, which is input into ASSEMBLY. It is not necessary for the user to know the renumbering.

4. Input files

Input files for the programs below must be prepared with the formats listed. In addition, for most programs, device 5 is attached to a terminal.

(a) ASSEMBLY

(i) File of grid data, attached to device 4. It is divided into sections. Below each named quantity is its program name and the format.

Section 1. Basic parameters.

No. of nodes	No. of elements	No. of materials	Scale option
NNP	NEL	NMAT	KM
I5	I5	I5	I5

Scale option = 1 if co-ordinates are in km.

= 0 if co-ordinates are in m.

Section 2. Material data.

Young's Modulus	Poisson's ratio	Density	Thickness
E(I)	PR(I)	RO(I)	TH(I)
E10.3	E10.3	E10.3	E10.3

1 line for each material type

Thickness is usually 1.0

Section 3. Nodal co-ordinates

Node number	x co-ord.	y co-ord.
M	X(M)	Y(M)
I5	E10.3	E10.3

1 line for each node, except when successive nodes are equally spaced along a straight line, in which case only the first and last need be entered.

Section 4. Element topology

Element no.	node 1	node 2	node 3	node 4
M	IE(M,1)	IE(M,2)	IE(M,3)	IE(M,4)
I5	I5	I5	I5	I5

For a triangular element set IE(M,4) = IE(M,3)

Axes are assumed with y vertically up. Nodes must be entered anti-clockwise.

1 line for each element, except when successive elements are such that numbers of corresponding nodes increase by 1 (i.e. IE(M+1,J) = IE(M,J) + 1), in which case only the first of such a chain has to be entered, but the last element must always be entered.

Section 5. Element materials

Element no.	Material no.
M	IE(M,5)
I5	I5

1 line for each element, except when successive elements have the same material, in which case only the first of such a chain has to be entered, but the last element must always be entered.

Section 6. Node type and initial loads and displacements

Node no.	Type code	Initial x-load/disp.	Initial y-load/disp.
M	KODE(M)	XLOAD(M)	YLOAD(M)
I5	I5	E10.3	E10.3

1 line for each node, except when successive nodes have same value for type code, x-load/disp. and y-load/disp; in which case only the first of such a chain has to be entered, but the last element must always be entered.

The type code indicates if the node has a prescribed load or displacement in the x and y directions. Free nodes have zero load. The code is given by the following table.

Type code	Nature of prescription	
	x-direction	y-direction
1	load	load
2	displacement	load
3	load	displacement
4	displacement	displacement

(ii) File of improved topology in unformatted form attached to device 3. This file is the output file to REDUCE.

(b) TIMESTEP

(i) Dumpfile of unformatted data, attached to device 3. This file is an output file to ASSEMBLY.

(ii) File of load changes at each time-step, attached to device 4.

Node no.		x-load/disp.		y-load/disp.
N		XLOAD(N)		YLOAD(N)
I5	3X	E10.4	3X	E10.4

Each time-step requires one line for each change in prescribed loads/displacements from previous time-step, but a line for last node must be entered for every time-step.

For plane wave excitation of the base nodes of a grid a file of this format is prepared by INPUT.

(c) PLOTS

(i) File of grid geometry in unformatted form attached to device 4. This file is an output file to ASSEMBLY.

(ii) File of displacements in unformatted form attached to device 3. This file is an output file from either ASSEMBLY (in the case of static displacemnets) TIMESTEP or FILESUM.

(iii) File of options in unformatted form attached to device 2 prepared by the interactive program DISPLAY.

(d) REDUCE

File of element topology attached to device 4, which is Section 4 of grid data file used by ASSEMBLY.

(e) INPUT

File of base nodes of the grid attached to device 3, in format 5I5.

(f) FILESUM

(i) File of static displacements in unformatted form attached to device 3. This is an output file of ASSEMBLY.

(ii) File of time-step displacements in unformatted form attached to device 4. This is an output file of TIMESTEP.

(g) DISPLAY

The input for this file is primarily in response to prompts at a terminal. However it is possible to attach to device 3

a list of the elements and nodes required in the displays. Also, if the stress plot for a static distribution is required, timestep 1 should be chosen.

5. Output files

As well as the output files listed below most programs are attached through device 6 to a terminal for messages and prompts.

(a) ASSEMBLY

(i) File of input data in tabular form (optional), attached to device 7.

(ii) Unformatted file of grid geometry, attached to device 8.

(iii) Unformatted file of static displacements attahced to device 10.

(iv) Unformatted file of data attached to device 9, used as input to TIMESTEP.

(b) TIMESTEP

(i) Unformatted file of data, attached to device 8, used as input for next time-steps.

(ii) Unformatted file of time-step displacements attached to device 10.

(c) PLOTS

(i) File of stresses in tabular form (optional), attached to device 7.

(ii) Plot file, attached to device 9.

(d) REDUCE

Unformatted file of improved topology, attached to device 8.

(e) INPUT

File of loadchanges, attached to device 7, in format required by TIMESTEP.

(f) FILESUM

Unformatted file of sum of two displacement files, attached to device 7.

(g) DISPLAY

Unformatted file of options attached to device 7.

```
C
C
C      PROGRAM ASSEMBLY
C      ================
C
C
C   PROGRAM READS IN DATA FOR GRID, ASSEMBLES STIFFNESS AND MASS
C   MATRICES, FORMS INITIAL LOAD VECTOR, MODIFIES MATRICES AS
C   APPROPRIATE TO TAKE INTO ACCOUNT THE BOUNDARY CONDITIONS.
C   THEN, EITHER, EVALUATES THE DISPLACEMENTS FOR THE STATIC FORCES,
C   OR, READS IN DAMPING COEFFICIENTS (IF ANY), AND DUMPS ALL
C   NECESSARY DATA IN UNFORMATTED FORM NEEDED FOR TIMESTEP
C   CALCULATIONS. FULL PRINT OUT OF INPUT DATA CAN BE REQUESTED.
C
C
      COMMON T, TMAX, NEL, NNP, NEQ, IMAX, ISTOP, ISTEP, ISBAND
      COMMON /ONE/ E(10), PR(10), RO(10), TH(10), IE(1200,5), X(1184),
     +       Y(1184), XCEN(1200), YCEN(1200), NMAT, NSTAT, MTYP
      COMMON /TWO/ BT(3,6), D(3,3), B(3,10), QK(10,10), Q(10),
     +             XQ(5), YQ(5)
      COMMON /THREE/ BK(2368,107), CA(2368), RMASS(2368), BODY(2368)
      COMMON /FOUR/ XLOAD(1184), YLOAD(1184), KODE(1184)
      COMMON /FIVE/ DISP(2368), VEL(2368), R(2368), R1(2368),
     +       R2(2368), R3(2368)
      COMMON /SIX/ NODE(1200), IFORM
C
C
      CALL DATAIN
      CALL TEST
      CALL CENT
      CALL INITIA
      CALL ASEMBL
      CALL LOAD1
      CALL RVEC
      IF (NSTAT .EQ. 0) GO TO 10
      CALL MODIF2
      CALL BANSOL
      STOP
   10 CONTINUE
C     CALL DAMP
      CALL MODIF1
      ISTEP = 0
      CALL DUMP
      STOP
      END
C
C
      SUBROUTINE DATAIN
C     =================
C
      COMMON T, TMAX, NEL, NNP, NEQ, IMAX, ISTOP, ISTEP, ISBAND
      COMMON /ONE/ E(10), PR(10), RO(10), TH(10), IE(1200,5), X(1184),
     +       Y(1184), XCEN(1200), YCEN(1200), NMAT, NSTAT, MTYP
      COMMON /SIX/ NODE(1200), IFORM
      DIMENSION TITLE(9), X1(1184), Y1(1184)
C
      DATA MAXEL, MAXNP, MAXMAT, MAXBW
     +     / 1200,  1184,      10,     54/
C
C  PROBLEM IDENTIFICATION AND DESCRIPTION.
```

```
C
      WRITE (6,190)
      READ (5,165) (TITLE(I),I=1,9)
      WRITE (7,195) (TITLE(I),I=1,9)
      WRITE (6,200)
      READ (5,180) NSTAT
      ISTOP = 0
      READ (4,170) NNP, NEL, NMAT, KM
      WRITE (7,205) NNP, NEL, NMAT
C
C   CHECKS TO BE SURE INPUT DATA DOES NOT EXCEED STORAGE CAPACITY.
C
      IF (NNP .LE. MAXNP) GO TO 10
      ISTOP = ISTOP + 1
      WRITE (6,210) MAXNP
   10 IF (NEL .LE. MAXEL) GO TO 15
      ISTOP = ISTOP + 1
      WRITE (6,215) MAXEL
   15 IF (NMAT .LE. MAXMAT) GO TO 20
      ISTOP = ISTOP + 1
      WRITE (6,220) MAXMAT
   20 IF (ISTOP .EQ. 0) GO TO 25
      WRITE (6,225) ISTOP
      STOP
   25 READ (4,175) (E(I),PR(I),RO(I),TH(I),I=1,NMAT)
      WRITE (7,230)
      WRITE (7,235) (I,E(I),PR(I),RO(I),TH(I),I=1,NMAT)
C
C   READ AND PRINT NODAL DATA.
C
      WRITE (7,240)
      WRITE (6,245)
      READ (5,180) K
      N = 1
   30 READ (4,185) M, X(M), Y(M)
      IF (M - N) 35, 50, 40
   35 WRITE (6,250) M
      ISTOP = ISTOP + 1
      GO TO 30
   40 DF = M + 1 - N
      RX = (X(M) - X(N - 1)) / DF
      RY = (Y(M) - Y(N - 1)) / DF
   45 X(N) = X(N - 1) + RX
      Y(N) = Y(N - 1) + RY
   50 IF (K .NE. 1) GO TO 55
      WRITE (7,255) N, X(N), Y(N)
   55 N = N + 1
      IF (M - N) 60, 50, 45
   60 IF (N .LE. NNP) GO TO 30
      IF (KM .NE. 1) GO TO 70
      DO 65 I = 1, NNP
        X(I) = X(I) * 1000.0
        Y(I) = Y(I) * 1000.0
   65 CONTINUE
   70 CONTINUE
C
C   READ NODAL NUMBERING OF ELEMENTS.
C
      WRITE (7,260)
   75 L = 0
```

```
   80 READ (4,170) M, (IE(M,I),I=1,4)
   85 L = L + 1
      IF (M - L) 90, 100, 95
   90 WRITE (6,265) M
      ISTOP = ISTOP + 1
      GO TO 80
   95 IE(L,1) = IE(L - 1,1) + 1
      IE(L,2) = IE(L - 1,2) + 1
      IE(L,3) = IE(L - 1,3) + 1
      IE(L,4) = IE(L - 1,4) + 1
      IE(L,5) = IE(L - 1,5)
      GO TO 85
  100 IF (NEL .GT. L) GO TO 80
C
C  READ ELEMENT MATERIAL TYPE.
C
      L = 0
  105 READ (4,170) M, IE(M,5)
  110 L = L + 1
      IF (M - L) 115, 125, 120
  115 WRITE (6,270) M
      ISTOP = ISTOP + 1
      GO TO 105
  120 IE(L,5) = IE(L - 1,5)
      GO TO 110
  125 IF (NEL .GT. L) GO TO 105
C
C  WRITE ELEMENT PROPERTIES.
C
      IF (K .NE. 1) GO TO 135
      DO 130 L = 1, NEL
        WRITE (7,275) L, (IE(L,I),I=1,5)
  130 CONTINUE
  135 IF (ISTOP .EQ. 0) GO TO 140
      WRITE (6,280) ISTOP
C
C  READS IN IMPROVED TOPOLOGY AND RENUMBERS NODE CO-ORDINATES.
C
  140 WRITE (6,285)
      READ (5,180) IFORM
      IF (IFORM .NE. 1) GO TO 155
      READ (3) ((IE(I,J),I=1,1200),J=1,4), NODE
      DO 145 M = 1, NNP
        X1(NODE(M)) = X(M)
        Y1(NODE(M)) = Y(M)
  145 CONTINUE
      DO 150 M = 1, NNP
        X(M) = X1(M)
        Y(M) = Y1(M)
  150 CONTINUE
C
C  COMPUTE MAXIMUM NODAL DIFFERENCE AND SEMI-BANDWIDTH.
C
  155 MAXDIF = 0
      IELEM = 1
      DO 160 I = 1, NEL
        DO 160 J = 1, 4
          DO 160 K = 1, 4
            LL = IABS(IE(I,J) - IE(I,K))
            IF (LL .LE. MAXDIF) GO TO 160
```

```
            MAXDIF = LL
            IELEM = I
  160 CONTINUE
      ISBAND = 2 * (MAXDIF + 1)
      NEQ = 2 * NNP
      WRITE (6,290) IELEM, ISBAND, MAXBW
      IF (ISBAND .LE. MAXBW) RETURN
      ISTOP = ISTOP + 1
      RETURN

  165 FORMAT (9A4)
  170 FORMAT (5I5)
  175 FORMAT (4E10.3)
  180 FORMAT (I5)
  185 FORMAT (I5, 2E10.3)
  190 FORMAT ('0ENTER TITLE')
  195 FORMAT ('1', 9A4/)
  200 FORMAT ('0IF YOU ARE FINDING STATIC DISPLACEMENTS DUE TO'/
     +        ' INITIAL LOADS AND BODY FORCES, TYPE ''1'';'/
     +        ' IF YOU ARE FINDING STATIC DISPLACEMENTS DUE TO'/
     +        ' INITIAL LOADS ONLY, TYPE ''2'';'/
     +        ' OTHERWISE PRESS ''RETURN''.'// ' -----')
  205 FORMAT ('0INPUT TABLE 1.. BASIC PARAMETERS'//,
     +        5X,' NUMBER OF NODAL POINTS. . . . . .', I5/
     +        5X, ' NUMBER OF ELEMENTS. . . . . .', I5/
     +        5X, ' NUMBER OF DIFFERENT MATERIALS . . . . .', I5/)
  210 FORMAT ('0TOO MANY NODAL POINTS, MAXIMUM =', I5)
  215 FORMAT ('0TOO MANY ELEMENTS, MAXIMUM =', I5)
  220 FORMAT ('0TOO MANY MATERIALS, MAXIMUM =', I5)
  225 FORMAT ('0EXECUTION HALTED BECAUSE OF', I5, ' FATAL ERRORS'/)
  230 FORMAT ('0INPUT TABLE 2.. MATERIAL PROPERTIES'//
     +        '  MATERIAL',5X, 'MODULUS OF', 6X, 'POISSON''S',
     +        7X, 'MATERIAL', 7X, 'MATERIAL'/
     +        4X, 'NUMBER', 5X, 'ELASTICITY', 8X, '  RATIO', 8X,
     +        'DENSITY', 6X, 'THICKNESS')
  235 FORMAT ((I10,4(1PE15.3)))
  240 FORMAT ('0INPUT TABLE 3.. NODAL POINT DATA'//
     +        5X, 'NODAL'/5X, 'POINT', 8X, 'X-COORD', 8X, 'Y-COORD')
  245 FORMAT ('0DO YOU WANT THE NODAL AND ELEMENT PROPERTIES LISTED?'/
     +        ' TYPE ''1'' FOR YES;  PRESS ''RETURN'' FOR NO.'/
     +        ' -----')
  250 FORMAT (5X, 'ERROR IN NODE NUMBERED', I5/)
  255 FORMAT (I10, 2(1PE15.3))
  260 FORMAT ('0INPUT TABLE 4.. ELEMENT DATA'//
     +        11X, 'GLOBAL INDICES OF ELEMENT NODES'/3X, 'ELEMENT',
     +        7X, '1', 7X, '2', 7X, '3', 7X, '4', 2X, 'MATERIAL')
  265 FORMAT (5X, 'ERROR IN NODAL NUMBERING OF ELEMENT', I5/)
  270 FORMAT (5X, 'ERROR IN MATERIAL NUMBER OF ELEMENT', I5/)
  275 FORMAT (I10, 4I8, I10)
  280 FORMAT ('0ASSEMBLY AND SOLUTION WILL NOT BE PERFORMED,',
     +        I5, 'FATAL ERRORS')
  285 FORMAT ('0IF USING NEW NODAL NUMBERING, TYPE ''1''''/' -----')
  290 FORMAT ('0SEMI-BANDWIDTH OF ELEMENT', I5, ' = ', I4/
     +        'MAXIMUM ALLOWED = ', I4/
     +        'THERE MAY BE OTHER ELEMENTS WITH THIS BANDWIDTH ALSO.')
      END
C
C
C
C
```

```
      SUBROUTINE TEST
C     ===============
C
      COMMON T, TMAX, NEL, NNP, NEQ, IMAX, ISTOP, ISTEP, ISBAND
      COMMON /ONE/ E(10), PR(10), RO(10), TH(10), IE(1200,5), X(1184),
     +       Y(1184), XCEN(1200), YCEN(1200), NMAT, NSTAT, MTYP
      DIMENSION F(4)
C
C  TESTS GRID FOR POSSIBLE INCORRECT NUMBERING OF ELEMENTS.
C  THIS TEST IDENTIFIES ANY ELEMENTS THAT ARE NOT CONCAVE, OR ARE
C  NUMBERED IN THE WRONG DIRECTION.
C
      DO 35 M = 1, NEL
        ICOUNT = 0
        DO 20 I = 1, 4
          J = I
          K = I + 1
          IF (IE(M,3) .EQ. IE(M,4)) GO TO 10
          J = MOD(J,4) + 1
          K = MOD(K,4) + 1
          GO TO 15
10        IF (I .EQ. 4) GO TO 20
          J = MOD(J,3) + 1
          K = MOD(K,3) + 1
15        F(I) = (X(IE(M,I))*Y(IE(M,J)) + X(IE(M,J))*Y(IE(M,K))
     +          + X(IE(M,K))*Y(IE(M,I))) - (X(IE(M,J))*Y(IE(M,I))
     +          + X(IE(M,K))*Y(IE(M,J)) + X(IE(M,I))*Y(IE(M,K)))
          IF (F(I) .GT. 0) ICOUNT = ICOUNT + 1
20      CONTINUE
        IF (ICOUNT .EQ. 0) GO TO 30
        IF (ICOUNT .EQ. 4) GO TO 35
        IF (ICOUNT .NE. 3) GO TO 25
        IF (IE(M,3) .EQ. IE(M,4)) GO TO 35
25      WRITE (6,40) M
        ISTOP = ISTOP + 1
        GO TO 35
30      WRITE (6,45) M
        ISTOP = ISTOP + 1
35    CONTINUE
      IF (ISTOP .EQ. 0) RETURN
      STOP
C
40    FORMAT ('ELEMENT', I5, ' IS NOT CONCAVE')
45    FORMAT ('0ELEMENT', I5, ' IS NUMBERED IN THE WRONG DIRECTON')
      END
C
C
      SUBROUTINE CENT
C     ===============
C
      COMMON T, TMAX, NEL, NNP, NEQ, IMAX, ISTOP, ISTEP, ISBAND
      COMMON /ONE/ E(10), PR(10), RO(10), TH(10), IE(1200,5), X(1184),
     +       Y(1184), XCEN(1200), YCEN(1200), NMAT, NSTAT, MTYP
      COMMON /TWO/ BT(3,6), D(3,3), B(3,10), QK(10,10), Q(10),
     +             XQ(5), YQ(5)
C
C  CALCULATES THE CENTROID OF EACH ELEMENT.
C
      DO 20 M = 1, NEL
        R3 = 0.0
```

```
      R4 = 0.0
      S3 = 0.0
      S4 = 0.0
      DO 10 N = 1, 4
        NN = IE(M,N)
        XQ(N) = X(NN)
        YQ(N) = Y(NN)
10    CONTINUE
      DO 15 I = 1, 4
        J = MOD(I,4) + 1
        K = MOD(J,4) + 1
        L = MOD(K,4) + 1
        R1 = YQ(I) * (XQ(J) - XQ(L))
        R2 = R1 * (XQ(L) + XQ(I) + XQ(J))
        R3 = R3 + R1
        R4 = R4 + R2
        S1 = XQ(I) * (YQ(J) - YQ(L))
        S2 = S1 * (YQ(L) + YQ(I) + YQ(J))
        S3 = S3 + S1
        S4 = S4 + S2
15    CONTINUE
      XCEN(M) = R4 / (R3*3.0)
      YCEN(M) = S4 / (S3*3.0)
20  CONTINUE
C
      RETURN
      END
C
C
      SUBROUTINE INITIA
C     =================
C
      COMMON T, TMAX, NEL, NNP, NEQ, IMAX, ISTOP, ISTEP, ISBAND
      COMMON /TWO/ BT(3,6), D(3,3), B(3,10), QK(10,10), Q(10),
     +             XQ(5), YQ(5)
      COMMON /THREE/ BK(2368,107), CA(2368), RMASS(2368), BODY(2368)
      COMMON /FIVE/ DISP(2368), VEL(2368), R(2368), R1(2368),
     +       R2(2368), R3(2368)
C
C   TO SET TO ZERO ARRAYS AS REQUIRED.
C
      DO 15 I = 1, 3
        DO 10 J = 1, 6
          BT(I,J) = 0.0
10    CONTINUE
      DO 15 J = 1, 3
        D(I,J) = 0.0
15  CONTINUE
      DO 20 I = 1, NEQ
        DISP(I) = 0.0
        VEL(I) = 0.0
        RMASS(I) = 0.0
        BODY(I) = 0.0
        R(I) = 0.0
        CA(I) = 0.0
        DO 20 J = 1, ISBAND
          BK(I,J) = 0.0
20  CONTINUE
      RETURN
      END
```

```
C
C
      SUBROUTINE ASEMBL
C     ==================
C
      COMMON T, TMAX, NEL, NNP, NEQ, IMAX, ISTOP, ISTEP, ISBAND
      COMMON /ONE/ E(10), PR(10), RO(10), TH(10), IE(1200,5), X(1184),
     +       Y(1184), XCEN(1200), YCEN(1200), NMAT, NSTAT, MTYP
      COMMON /TWO/ BT(3,6), D(3,3), B(3,10), QK(10,10), Q(10),
     +             XQ(5), YQ(5)
      COMMON /THREE/ BK(2368,107), CA(2368), RMASS(2368), BODY(2368)
      COMMON /SIX/ NODE(1200), IFORM
      DIMENSION LP(8), QST(2,8), DA(2,2)
C
C
C   STORE ELEMENT CO-ORDINATES AND NODAL NUMBERS FOR
C   STRESS/STRAIN CALCULATIONS.
C
      WRITE (8) X, Y, XCEN, YCEN, IE, NODE, IFORM, NEL, NNP, NSTAT
C
C   COMPUTE ELEMENT STIFFNESSES AND LOADS ONE BY ONE.
C
   10 DO 70 M = 1, NEL
        IF (IE(M,5) .GT. 0) GO TO 15
        ISTOP = ISTOP + 1
        GO TO 80
   15   CALL QUAD(M, AREA)
        IF (AREA .GT. 0.0) GO TO 20
        ISTOP = ISTOP + 1
        WRITE (6,90) M
C
C   FORM MATRIX NEEDED TO RECOVER INTERNAL DISPLACEMENT
C   IN STRESS/STRAIN CALCULATION.
C
   20   DO 25 I = 1, 2
          DO 25 J = 1, 8
            QST(I,J) = 0.0
   25   CONTINUE
        IF (IE(M,3) .EQ. IE(M,4)) GO TO 50
        DET = QK(10,9) * QK(9,10) - QK(9,9) * QK(10,10)
        DA(1,1) = QK(10,10) / DET
        DA(1,2) = -QK(9,10) / DET
        DA(2,1) = DA(1,2)
        DA(2,2) = QK(9,9) / DET
        DO 30 I = 1, 2
          DO 30 J = 1, 8
            DO 30 K = 1, 2
              KK = K + 8
              QST(I,J) = QST(I,J) + DA(I,K) * QK(KK,J)
   30   CONTINUE
C
C   CONDENSE ELEMENT STIFFNESS MATRIX FROM 10X10 TO 8X8,
C   AND ELEMENT LOADS FROM 10X1 TO 8X1.
C
        DO 45 J = 1, 2
          IJ = 10 - J
          IK = IJ + 1
          PIVOT = QK(IK,IK)
          DO 40 K = 1, IJ
            F = QK(IK,K) / PIVOT
```

```
            QK(IK,K) = F
            DO 35 I = K, IJ
              QK(I,K) = QK(I,K) - F * QK(I,IK)
              QK(K,I) = QK(I,K)
   35       CONTINUE
            Q(K) = Q(K) - QK(IK,K) * Q(IK)
   40     CONTINUE
          Q(IK) = Q(IK) / PIVOT
   45   CONTINUE
C
C  STORE ELEMENT PROPERTIES FOR STRESS/STRAIN CALCULATIONS.
C
   50   WRITE (8) QST, B, D
C
C  ASSEMBLE STIFFNESS MATRIX AND BODY FORCE VECTOR.
C
   55   LIM = 8
        IF (IE(M,3) .EQ. IE(M,4)) LIM = 6
        DO 60 I = 2, LIM, 2
          IJ = I / 2
          LP(I - 1) = 2 * IE(M,IJ) - 1
          LP(I) = 2 * IE(M,IJ)
   60   CONTINUE
        DO 65 LL = 1, LIM
          I = LP(LL)
          BODY(I) = BODY(I) + Q(LL)
          DO 65 MM = 1, LIM
            J = LP(MM) - I + 1
            IF (J .LE. 0) GO TO 65
            BK(I,J) = BK(I,J) + QK(LL,MM)
   65   CONTINUE
C
C  ASSEMBLE MASS MATRIX.
C
        LIM = LIM / 2
        AMASS = RO(MTYP) * TH(MTYP) * AREA / FLOAT(LIM)
        DO 70 J = 1, LIM
          K = 2 * IE(M,J)
          L = K - 1
          RMASS(K) = RMASS(K) + AMASS
          RMASS(L) = RMASS(K)
   70 CONTINUE
C
C  FORM THE RECIPROCAL MASS MATRIX.
C
      DO 75 I = 1, NEQ
        RMASS(I) = 1.0 / RMASS(I)
   75 CONTINUE
   80 IF (ISTOP .EQ. 0) GO TO 85
      WRITE (6,95) ISTOP
      STOP
   85 WRITE (6,100)
      RETURN
C
   90 FORMAT (5X, '0AREA OF ELEMENT', I5, '  IS NEGATIVE'/)
   95 FORMAT ('0SOLUTION WILL NOT BE PERFORMED BECAUSE OF',
     +         I5, '   DATA ERRORS'/)
  100 FORMAT ('0ASSEMBLY OF STIFFNESS AND MASS MATRICES COMPLETE')
      END
C
```

```
C
      SUBROUTINE QUAD(M, TOTALA)
C     ==========================
C
      COMMON /ONE/ E(10), PR(10), RO(10), TH(10), IE(1200,5), X(1184),
     +       Y(1184), XCEN(1200), YCEN(1200), NMAT, NSTAT, MTYP
      COMMON /TWO/ BT(3,6), D(3,3), B(3,10), QK(10,10), Q(10),
     +             XQ(5), YQ(5)
C
      MTYP = IE(M,5)
      TOTALA = 0.0
C
C  CONSTRUCT STRESS-STRAIN MATRIX OF ELASTIC CONSTANTS.
C
      IF (NMAT .EQ. 1 .AND. M .GT. 1) GO TO 10
      CF = E(MTYP) / ((1.0 + PR(MTYP))*(1.0 - 2.0*PR(MTYP)))
      D(1,1) = CF * (1.0 - PR(MTYP))
      D(1,2) = CF * PR(MTYP)
      D(2,1) = D(1,2)
      D(2,2) = D(1,1)
      D(3,3) = CF * (1.0 - 2.0*PR(MTYP)) / 2.0
C
C  CONSTRUCT VECTORS OF THE CO-ORDINATES OF AN ELEMENT.
C
   10 DO 15 N = 1, 4
        NN = IE(M,N)
        XQ(N) = X(NN)
        YQ(N) = Y(NN)
   15 CONTINUE
      XQ(5) = XCEN(M)
      YQ(5) = YCEN(M)
C
C  INITIALISE QUADRILATERAL STIFFNESS MATRIX, LOAD VECTOR,
C  AND STRAIN DISPLACEMENT MATRIX.
C
      DO 25 II = 1, 10
        Q(II) = 0.0
        DO 20 JJ = 1, 10
          QK(II,JJ) = 0.0
   20   CONTINUE
        DO 25 JJ = 1, 3
          B(JJ,II) = 0.0
   25 CONTINUE
C
C  FORM STIFFNESS MATRIX OF QUADRILATERAL ELEMENT.
C
      IF (IE(M,4) .NE. IE(M,3)) GO TO 30
      CALL CST(1, 2, 3, TOTALA)
      GO TO 35
   30 CALL CST(1, 2, 5, AREA)
      TOTALA = TOTALA + AREA
      CALL CST(2, 3, 5, AREA)
      TOTALA = TOTALA + AREA
      CALL CST(3, 4, 5, AREA)
      TOTALA = TOTALA + AREA
      CALL CST(4, 1, 5, AREA)
      TOTALA = TOTALA + AREA
   35 RETURN
      END
C
```

```
C
      SUBROUTINE CST(I, J, K, AREA)
C     ==============================
C
      COMMON /ONE/ E(10), PR(10), RO(10), TH(10), IE(1200,5), X(1184),
     +       Y(1184), XCEN(1200), YCEN(1200), NMAT, NSTAT, MTYP
      COMMON /TWO/ BT(3,6), D(3,3), B(3,10), QK(10,10), Q(10),
     +             XQ(5), YQ(5)
      DIMENSION CB(3,6), LC(6), LT(3), TK(6,6)
C
      LT(1) = I
      LT(2) = J
      LT(3) = K
C
C   COMPUTE STRAIN-DISPLACEMENT MATRIX FOR TRIANGLE.
C
      BT(1,1) = YQ(J) - YQ(K)
      BT(1,3) = YQ(K) - YQ(I)
      BT(1,5) = YQ(I) - YQ(J)
      BT(2,2) = XQ(K) - XQ(J)
      BT(2,4) = XQ(I) - XQ(K)
      BT(2,6) = XQ(J) - XQ(I)
      BT(3,1) = BT(2,2)
      BT(3,3) = BT(2,4)
      BT(3,5) = BT(2,6)
      BT(3,2) = BT(1,1)
      BT(3,4) = BT(1,3)
      BT(3,6) = BT(1,5)
      AREA = (BT(2,2)*BT(1,5) - BT(2,6)*BT(1,1)) / 2.0
      FK = 1.0 / (4.0*AREA)
C
C   COMPUTE D * B
C
      DO 10 II = 1, 3
        DO 10 JJ = 1, 6
          CB(II,JJ) = 0.0
          DO 10 KK = 1, 3
            CB(II,JJ) = CB(II,JJ) + D(II,KK) * BT(KK,JJ)
   10 CONTINUE
C
C   COMPUTE (B**T) * D * B
C
      DO 15 II = 1, 6
        DO 15 JJ = 1, 6
          TK(II,JJ) = 0.0
          DO 15 KK = 1, 3
            TK(II,JJ) = TK(II,JJ) + BT(KK,II) * CB(KK,JJ)
   15 CONTINUE
C
C   ADD TRIANGLE STIFFNESS TO QUADRILATERAL STIFFNESS.
C   ADD TRIANGLE STRAIN-DISPLACEMENT MATRIX TO QUADRILATERAL
C   STRAIN-DISPLACEMENT MATRIX.
C
      DO 20 II = 1, 3
        LC(2*II) = 2 * LT(II)
        LC(2*II - 1) = 2 * LT(II) - 1
   20 CONTINUE
      DO 30 II = 1, 6
        LL = LC(II)
        DO 25 JJ = 1, 6
```

```
          MM = LC(JJ)
          QK(LL,MM) = QK(LL,MM) + TK(II,JJ) * TH(MTYP) * FK
   25   CONTINUE
        DO 30 JJ = 1, 3
          B(JJ,LL) = B(JJ,LL) + BT(JJ,II) * FK * 2.0
   30 CONTINUE
C
C  DEVELOP BODY FORCE FOR ELEMENT.
C
      IF (NSTAT .NE. 1) RETURN
      BODYF = -AREA * RO(MTYP) * TH(MTYP) * 9.81 / 3.0
      DO 35 II = 1, 3
        JJ = 2 * LT(II)
        Q(JJ) = Q(JJ) + BODYF
   35 CONTINUE
      RETURN
      END
C
C
      SUBROUTINE LOAD1
C     ================
C
      COMMON T, TMAX, NEL, NNP, NEQ, IMAX, ISTOP, ISTEP, ISBAND
      COMMON /FOUR/ XLOAD(1184), YLOAD(1184), KODE(1184)
      COMMON /SIX/ NODE(1200), IFORM
      DIMENSION  XLOAD1(1184),YLOAD1(1184), KODE1(1184)
C
C  READS THE INITIAL VALUES OF THE APPLIED LOADS,
C  AND BOUNDARY CONSTRAINTS.
C
      WRITE (7,70)
      WRITE (6,75)
      READ (5,60) II
      N = 1
   10 READ (4,65) M, KODE(M), XLOAD(M), YLOAD(M)
      IF (KODE(M) .GE. 1 .AND. KODE(M) .LE. 4) GO TO 15
      WRITE (6,80) M
      ISTOP = 1
      GO TO 10
   15 K = 2 * N
      J = K - 1
      IF (M .EQ. N) GO TO 25
   20 KODE(N) = KODE(N - 1)
      XLOAD(N) = XLOAD(N - 1)
      YLOAD(N) = YLOAD(N - 1)
   25 IF (II .EQ. 0) GO TO 50
C
C  PRINTS TABLE OF INITIAL LOADS AND CONSTRAINTS.
C
      I = KODE(N)
      GO TO (30, 35, 40, 45), I
   30 WRITE (7,85) N, YLOAD(N), XLOAD(N)
      GO TO 50
   35 WRITE (7,90) N, XLOAD(N), YLOAD(N)
      GO TO 50
   40 WRITE (7,95) N, XLOAD(N), YLOAD(N)
      GO TO 50
   45 WRITE (7,100) N, XLOAD(N), YLOAD(N)
   50 N = N + 1
      IF (M - N) 55, 25, 20
```

```
   55 IF (N .LE. NNP) GO TO 10
C
C  RENUMBER LOADS ETC. IF USING IMPROVED NODAL NUMBERING.
C
      IF (IFORM .NE. 1) GO TO 58
      DO 56 M = 1,NNP
        XLOAD1(NODE(M)) = XLOAD(M)
        YLOAD1(NODE(M)) = YLOAD(M)
        KODE1(NODE(M)) = KODE(M)
   56 CONTINUE
      DO 57 M = 1,NNP
        XLOAD(M) = XLOAD1(M)
        YLOAD(M) = YLOAD1(M)
        KODE(M) = KODE1(M)
   57 CONTINUE
   58 IF (ISTOP .EQ. 0) RETURN
      STOP
C
   60 FORMAT (I5)
   65 FORMAT (2I5, 2E10.3)
   70 FORMAT ('0INPUT TABLE 6.. INITIAL LOADS AND DISPLACEMENTS'//
     +         5X,'NODAL'/5X, 'POINT', 9X, 'X-LOAD', 9X,
     +         'Y-LOAD', 8X, 'X-DISP.', 8X, 'Y-DISP.')
   75 FORMAT ('0DO YOU WANT TO OUTPUT ALL THE INITIAL LOADS?'/
     +         ' TYPE ''1'' FOR YES;  PRESS ''RETURN'' FOR NO'/
     +         ' ------')
   80 FORMAT ('0NODE', I5, ' HAS AN ILLEGAL VALUE FOR KODE')
   85 FORMAT (I10, 2(1PE15.3))
   90 FORMAT (I10, 15X, 2(1PE15.3))
   95 FORMAT (I10, 1PE15.3, 30X, 1PE15.3)
  100 FORMAT (I10, 30X, 2(1PE15.3))
      END
C
C
      SUBROUTINE RVEC
C     ===============
C
      COMMON T, TMAX, NEL, NNP, NEQ, IMAX, ISTOP, ISTEP, ISBAND
      COMMON /THREE/ BK(2368,107), CA(2368), RMASS(2368), BODY(2368)
      COMMON /FOUR/ XLOAD(1184), YLOAD(1184), KODE(1184)
      COMMON /FIVE/ DISP(2368), VEL(2368), R(2368), R1(2368),
     +        R2(2368), R3(2368)
C
C  FORMS THE INITIAL LOAD VECTOR R.
C
      DO 30 N = 1, NNP
        I = KODE(N)
        GO TO (10, 15, 10, 20), I
   10   R(2*N - 1) = BODY(2*N - 1) + XLOAD(N)
        IF (I .EQ. 3) GO TO 25
   15   R(2*N) = BODY(2*N) + YLOAD(N)
        IF (I .EQ. 1) GO TO 30
   20   R(2*N - 1) = XLOAD(N)
        IF (I .EQ. 2) GO TO 30
   25   R(2*N) = YLOAD(N)
   30 CONTINUE
      RETURN
      END
C
C
```

```
      SUBROUTINE MODIF2
C     =================
C
      COMMON T, TMAX, NEL, NNP, NEQ, IMAX, ISTOP, ISTEP, ISBAND
      COMMON /FOUR/ XLOAD(1184), YLOAD(1184), KODE(1184)
C
C  CALLS 'GEBC' FOR THOSE NODES WHICH HAVE PRESCRIBED DISPLACEMENTS.
C
      DO 15 M = 1, NNP
        IF (KODE(M) .EQ. 1) GO TO 15
        IF (KODE(M) .EQ. 3) GO TO 10
        CALL GEBC(XLOAD(M), 2*M - 1)
        IF (KODE(M) .EQ. 2) GO TO 15
   10   CALL GEBC(YLOAD(M), 2*M)
   15 CONTINUE
      RETURN
      END
C
C
      SUBROUTINE GEBC(U, N)
C     =====================
C
      COMMON T, TMAX, NEL, NNP, NEQ, IMAX, ISTOP, ISTEP, ISBAND
      COMMON /THREE/ BK(2368,107), CA(2368), RMASS(2368), BODY(2368)
      COMMON /FIVE/ DISP(2368), VEL(2368), R(2368), R1(2368),
     +        R2(2368), R3(2368)
C
C  MODIFIES STIFFNESS MATRIX, IN SEMIBANDED FORM, AND LOAD VECTOR
C  FOR PRESCRIBED DISPLACEMENT 'U' AT DEGREE OF FREEDOM 'N'.
C
      DO 15 M = 2, ISBAND
        K = N - M + 1
        IF (K .LE. 0) GO TO 10
        R(K) = R(K) - BK(K,M) * U
        BK(K,M) = 0.0
   10   K = N + M - 1
        IF (K .GT. NEQ) GO TO 15
        R(K) = R(K) - BK(N,M) * U
        BK(N,M) = 0.0
   15 CONTINUE
      BK(N,1) = 1.0
      R(N) = U
      RETURN
      END
C
C
      SUBROUTINE BANSOL
C     =================
C
      COMMON T, TMAX, NEL, NNP, NEQ, IMAX, ISTOP, ISTEP, ISBAND
      COMMON /THREE/ BK(2368,107), CA(2368), RMASS(2368), BODY(2368)
      COMMON /FIVE/ DISP(2368), VEL(2368), R(2368), R1(2368),
     +        R2(2368), R3(2368)
C
C  SYMMETRIC BAND MATRIX SOLVER.
C  COMPUTED DISPLACEMENTS ARE STORED IN R.
C
      NRS = NEQ - 1
      DO 15 N = 1, NRS
        M = N - 1
```

```
      MR = MINO(ISBAND,NEQ - M)
      PIVOT = BK(N,1)
      DO 15 L = 2, MR
        CP = BK(N,L) / PIVOT
        I = M + L
        J = 0
        DO 10 K = L, MR
          J = J + 1
          BK(I,J) = BK(I,J) - CP * BK(N,K)
10      CONTINUE
        BK(N,L) = CP
15    CONTINUE
      DO 20 N = 1, NRS
        M = N - 1
        MR = MINO(ISBAND,NEQ - M)
        CP = R(N)
        R(N) = CP / BK(N,1)
        DO 20 L = 2, MR
          I = M + L
          R(I) = R(I) - BK(N,L) * CP
          R(NEQ) = R(NEQ) / BK(NEQ,1)
20    CONTINUE
      DO 25 I = 1, NRS
        N = NEQ - I
        M = N - 1
        MR = MINO(ISBAND,NEQ - M)
        DO 25 K = 2, MR
          L = M + K
          R(N) = R(N) - BK(N,K) * R(L)
25    CONTINUE
C
C     STORE DISPLACEMENTS FOR STRESS/STRAIN DISPLAY.
C
      WRITE (10) R
      RETURN
      END
C
C
      SUBROUTINE DAMP
      ===============
C
C
      COMMON T, TMAX, NEL, NNP, NEQ, IMAX, ISTOP, ISTEP, ISBAND
      COMMON /THREE/ BK(2368,107), CA(2368), RMASS(2368), BODY(2368)
C
C     TO READ IN DAMPING COEFFICIENTS, AND ASSEMBLE THE DAMPING MATRIX.
C
      WRITE (7,20)
      WRITE (6,25) NNP
10    WRITE (6,30)
      READ (5,15) N, COEF
      IF (N .EQ. NNP .AND. COEF .EQ. 0.0) RETURN
      WRITE (7,35) N, COEF
      I = 2 * N - 1
      CA(I) = COEF
      CA(I + 1) = COEF
      IF (N .LT. NNP) GO TO 10
      RETURN
C
15    FORMAT (I5, E10.4)
20    FORMAT ('0INPUT TABLE 5.. DAMPING COEFFICIENTS.'//
```

```
     +         5X, 'NODAL', 8X, 'DAMPING'/
     +         5X, 'POINT', 4X, 'COEFFICIENT')
  25 FORMAT ('0ENTER NODE AND DAMPING COEFFICIENT',
     +         ' FOR ALL NODES WITH DAMPING.'/
     +         ' LIST MUST END WITH LAST NODE',
     +         ' EVEN IF IT IS UNDAMPED'/
     +         ' LAST NODE IS NUMBER',I5)
  30 FORMAT (' .....----------')
  35 FORMAT (I10, 1PE15.3)
     END
C
C
     SUBROUTINE MODIF1
C    =================
C
     COMMON T, TMAX, NEL, NNP, NEQ, IMAX, ISTOP, ISTEP, ISBAND
     COMMON /THREE/ BK(2368,107), CA(2368), RMASS(2368), BODY(2368)
     COMMON /FOUR/ XLOAD(1184), YLOAD(1184), KODE(1184)
     COMMON /FIVE/ DISP(2368), VEL(2368), R(2368), R1(2368),
    +       R2(2368), R3(2368)
C
C  ASSEMBLES THE INITIAL FORCE VECTOR AND MODIFIES THE STIFFNESS AND
C  DAMPING MATRICES TO ACCOUNT FOR THE GEOMETRIC BOUNDARY CONDITIONS.
C
C
C  CONVERT SEMI-BANDED MATRICES TO BANDED FORM.
C
     DO 10 I = 1, NEQ
       DO 10 J = 1, ISBAND
         BK(I,2*ISBAND - J) = BK(I,ISBAND + 1 - J)
  10 CONTINUE
     L = ISBAND - 1
     DO 15 J = 1, L
       M = NEQ - J
       DO 15 I = 1, M
         BK(I + J,ISBAND - J) = BK(I,ISBAND + J)
  15 CONTINUE
     DO 20 I = 1, L
       K = L + 1 - I
       DO 20 J = 1, K
         BK(I,J) = 0.0
  20 CONTINUE
C
C  MODIFY DAMPING AND STIFFNESS MATRICES, AND FORM INITIAL
C  DISPLACEMENT VECTOR.
C
     DO 40 N = 1, NNP
       I = KODE(N)
       GO TO (40, 25, 30, 35), I
  25   DISP(2*N - 1) = XLOAD(N)
       CALL GEOMBC(2*N - 1)
       GO TO 40
  30   DISP(2*N) = YLOAD(N)
       CALL GEOMBC(2*N)
       GO TO 40
  35   DISP(2*N - 1) = XLOAD(N)
       DISP(2*N) = YLOAD(N)
       CALL GEOMBC(2*N - 1)
       CALL GEOMBC(2*N)
  40 CONTINUE
```

```
      RETURN
      END
C
C
      SUBROUTINE GEOMBC(N)
C     ====================
C
      COMMON T, TMAX, NEL, NNP, NEQ, IMAX, ISTOP, ISTEP, ISBAND
      COMMON /THREE/ BK(2368,107), CA(2368), RMASS(2368), BODY(2368)
C
C  MODIFIES DAMPING AND STIFFNESS MATRICES FOR THE
C  PRESCRIBED DISPLACEMENT AT DEGREE OF FREEDOM N.
C
      IBAND = 2 * ISBAND - 1
      DO 10 M = 1, IBAND
        BK(N,M) = 0.0
   10 CONTINUE
      CA(N) = 0.0
      BK(N,ISBAND) = 1.0
      RETURN
      END
C
C
      SUBROUTINE DUMP
C     ===============
C
      COMMON T, TMAX, NEL, NNP, NEQ, IMAX, ISTOP, ISTEP, ISBAND
      COMMON /THREE/ BK(2368,107), CA(2368), RMASS(2368), BODY(2368)
      COMMON /FOUR/ XLOAD(1184), YLOAD(1184), KODE(1184)
      COMMON /FIVE/ DISP(2368), VEL(2368), R(2368), R1(2368),
     +       R2(2368), R3(2368)
      COMMON /SIX/ NODE(1200), IFORM
C
C  UNFORMATTED WRITE OF DATA ONTO DEVICE ATTATCHED TO 9.
C
      WRITE (9) T, TMAX, NEL, NNP, NEQ, IMAX, ISTOP, ISTEP,
     +          ISBAND, LNUM
      WRITE (9) BK, CA, RMASS, BODY
      WRITE (9) XLOAD, YLOAD, KODE
      WRITE (9) DISP, VEL, R, R1, R2, R3
      WRITE (9) NODE,IFORM
      RETURN
      END
```

```
C
C
C     PROGRAM TIMESTEP
C     ================
C
C
C  READS UNFORMATTED ASSEMBLY DATA AND TIMESTEP DATA,
C  THEN CALCULATES DISPLACEMENTS FOR FIFTEEN TIMESTEPS.
C
      COMMON T, TMAX, NEL, NNP, NEQ, IMAX, ISTOP, ISTEP,
     +       ISBAND, LNUM
      COMMON /ONE/ BK(2368,107), CA(2368), RMASS(2368), BODY(2368)
      COMMON /TWO/ XLOAD(1184), YLOAD(1184), KODE(1184)
      COMMON /THREE/ DISP(2368), VEL(2368), R(2368), R1(2368),
     +       R2(2368), R3(2368)
      COMMON /FOUR/ NODE(1200), IFORM
C
      CALL GET
      IF (ISTEP .GE. 1) GO TO 10
      CALL TIM
   10 DO 15 I = 1, 15
        CALL TMSTEP
        IF (ISTEP .GE. IMAX) GO TO 20
   15 CONTINUE
      CALL DUMP
   20 STOP
      END
C
C
      SUBROUTINE GET
C     ==============
C
      COMMON T, TMAX, NEL, NNP, NEQ, IMAX, ISTOP, ISTEP,
     +       ISBAND, LNUM
      COMMON /ONE/ BK(2368,107), CA(2368), RMASS(2368), BODY(2368)
      COMMON /TWO/ XLOAD(1184), YLOAD(1184), KODE(1184)
      COMMON /THREE/ DISP(2368), VEL(2368), R(2368), R1(2368),
     +       R2(2368), R3(2368)
      COMMON /FOUR/ NODE(1200), IFORM
C
C  UNFORMATTED READ OF DATA FROM DEVICE ATTATCHED TO 3.
C
      READ (3) T, TMAX, NEL, NNP, NEQ, IMAX, ISTOP, ISTEP,
     +         ISBAND, LNUM
      READ (3) BK, CA, RMASS, BODY
      READ (3) XLOAD, YLOAD, KODE
      READ (3) DISP, VEL, R, R1, R2, R3
      READ (3) NODE, IFORM
      RETURN
      END
C
C
      SUBROUTINE TIM
C     ==============
C
      COMMON T, TMAX, NEL, NNP, NEQ, IMAX, ISTOP, ISTEP,
     +       ISBAND, LNUM
      COMMON /THREE/ DISP(2368), VEL(2368), R(2368), R1(2368),
     +       R2(2368), R3(2368)
C
```

```
C   READS TIMESTEP, MAXIMUM TIME, AND INITIALISES R3.
C
      WRITE (6,20)
      READ (5,15) T, TMAX
      IMAX = IFIX(TMAX/T + 0.1)
      DO 10 I = 1, NEQ
        R3(I) = R(I)
   10 CONTINUE
C
C   STORE TIMESTEP VALUES FOR USE IN STRESS/STRAIN CALCULATIONS.
C
      WRITE (10) T, TMAX, IMAX
C
C   SET LINE COUNTER FOR FILE ATTATCHED TO 4 TO '1000'.
C
      LNUM = 1000
      RETURN
C
   15 FORMAT (2E10.4)
   20 FORMAT ('0ENTER TIME-STEP AND MAXIMUM TIME'/
     +        ' ----------**********')
      END
C
C
      SUBROUTINE TMSTEP
C     =================
C
      COMMON T, TMAX, NEL, NNP, NEQ, IMAX, ISTOP, ISTEP,
     +       ISBAND, LNUM
      COMMON /TWO/ XLOAD(1184), YLOAD(1184), KODE(1184)
      COMMON /THREE/ DISP(2368), VEL(2368), R(2368), R1(2368),
     +       R2(2368), R3(2368)
C
C   SETS UP THE VECTORS R1, R2, R3, VEL AND CALLS THE RUNGE-KUTTA ROUTINE
C
      ISTEP = ISTEP + 1
      DO 10 I = 1, NEQ
        R1(I) = R3(I)
   10 CONTINUE
      CALL LOAD2
      DO 15 I = 1, NEQ
        R3(I) = R(I)
        R2(I) = (R1(I) + R3(I)) / 2.0
   15 CONTINUE
      DO 35 N = 1, NNP
        M = KODE(N)
        GO TO (35, 20, 25, 20), M
   20   I = 2 * N - 1
        GO TO 30
   25   I = 2 * N
   30   VEL(I) = (R3(I) - R1(I)) / T
        M = M + 1
        IF (M .EQ. 5) GO TO 25
   35 CONTINUE
      CALL RUNG
C
C   STORE DISPLACEMENTS FOR STRESS/STRAIN CALCULATIONS.
C
      WRITE (10) DISP
      RETURN
```

```
      END
C
C
      SUBROUTINE LOAD2
C     ================
C
      COMMON T, TMAX, NEL, NNP, NEQ, IMAX, ISTOP, ISTEP,
     +       ISBAND, LNUM
      COMMON /ONE/ BK(2368,107), CA(2368), RMASS(2368), BODY(2368)
      COMMON /TWO/ XLOAD(1184), YLOAD(1184), KODE(1184)
      COMMON /THREE/ DISP(2368), VEL(2368), R(2368), R1(2368),
     +       R2(2368), R3(2368)
      COMMON /FOUR/ NODE(1200), IFORM
C
C     ALTERS THE LOAD VECTOR AT EACH TIME STEP.  READS ONE CARD FOR
C     EACH CHANGE.  MUST HAVE A CARD FOR THE LAST NODE POINT.
C
   10 READ (4'LNUM,55) M, X, Y
C
C     RENUMBERS NODE IF IMPROVED TOPOLOGY IN USE.
C
      IF (IFORM .NE. 1) GO TO 15
      N = NODE(M)
      GO TO 20
   15 N = M
C
C     FORMS NEW LOAD VECTOR.
C
   20 XLOAD(N) = X
      YLOAD(N) = Y
      LNUM = LNUM + 1000
      I = KODE(N)
      GO TO (25, 30, 25, 35), I
   25 R(2*N - 1) = BODY(2*N - 1) + XLOAD(N)
      IF (I .EQ. 3) GO TO 40
   30 R(2*N) = BODY(2*N) + YLOAD(N)
      IF (I .EQ. 1) GO TO 45
   35 R(2*N - 1) = XLOAD(N)
      IF (I .EQ. 2) GO TO 45
   40 R(2*N) = YLOAD(N)
   45 IF (M .LT. NNP) GO TO 10
      RETURN
C
   50 FORMAT (I5)
   55 FORMAT (I5, 2(3X,E10.4))
      END
C
C
      SUBROUTINE RUNG
C     ===============
C
      COMMON T, TMAX, NEL, NNP, NEQ, IMAX, ISTOP, ISTEP,
     +       ISBAND, LNUM
      COMMON /ONE/ BK(2368,107), CA(2368), RMASS(2368), BODY(2368)
      COMMON /THREE/ DISP(2368), VEL(2368), R(2368), R1(2368),
     +       R2(2368), R3(2368)
      DIMENSION ST01(2368), ST02(2368), DEL1(2368), DEL2(2368),
     +          DEL3(2368), DEL4(2368), GAM1(2368), GAM2(2368),
     +          GAM3(2368), GAM4(2368)
C
```

```
C   ADVANCES THE DISPLACEMENT AND VELOCITY VECTORS 'DISP' AND 'VEL'
C   BY ONE TIMESTEP 'T' USIING A FOURTH ORDER RUNGE-KUTTA ROUTINE.
C
      CALL PROD(BK, DISP, STO1, NEQ, ISBAND)
      CALL MULT2(CA, VEL, GAM1, NEQ)
      CALL ADSUB(GAM1, STO1, NEQ, 1)
      CALL ADSUB(GAM1, R1, NEQ,.0)
      CALL SCALE(GAM1, NEQ, -T)
      CALL MULT1(RMASS, GAM1, NEQ)
      DO 10 I = 1, NEQ
   10 DEL1(I) = VEL(I) * T
C
      DO 15 I = 1, NEQ
        STO1(I) = GAM1(I)
        STO2(I) = DEL1(I)
        DEL2(I) = VEL(I)
   15 CONTINUE
      CALL SCALE(STO2, NEQ, 0.5)
      CALL ADSUB(STO2, DISP, NEQ, 1)
      CALL PROD(BK, STO2, GAM2, NEQ, ISBAND)
      CALL SCALE(STO1, NEQ, 0.5)
      CALL ADSUB(DEL2, STO1, NEQ, 1)
      CALL SCALE(DEL2, NEQ, T)
      CALL ADSUB(STO1, VEL, NEQ, 1)
      CALL MULT2(CA, STO1, STO2, NEQ)
      CALL ADSUB(GAM2, STO2, NEQ, 1)
      CALL ADSUB(GAM2, R2, NEQ, 0)
      CALL SCALE(GAM2, NEQ, -T)
      CALL MULT1(RMASS, GAM2, NEQ)
C
      DO 20 I = 1, NEQ
        STO1(I) = GAM2(I)
        STO2(I) = DEL2(I)
        DEL3(I) = VEL(I)
   20 CONTINUE
      CALL SCALE(STO2, NEQ, 0.5)
      CALL ADSUB(STO2, DISP, NEQ, 1)
      CALL PROD(BK, STO2, GAM3, NEQ, ISBAND)
      CALL SCALE(STO1, NEQ, 0.5)
      CALL ADSUB(DEL3, STO1, NEQ, 1)
      CALL SCALE(DEL3, NEQ, T)
      CALL ADSUB(STO1, VEL, NEQ, 1)
      CALL MULT2(CA, STO1, STO2, NEQ)
      CALL ADSUB(GAM3, STO2, NEQ, 1)
      CALL ADSUB(GAM3, R2, NEQ, 0)
      CALL SCALE(GAM3, NEQ, -T)
      CALL MULT1(RMASS, GAM3, NEQ)
C
      DO 25 I = 1, NEQ
        STO1(I) = GAM3(I)
        STO2(I) = DEL3(I)
        DEL4(I) = VEL(I)
   25 CONTINUE
      CALL ADSUB(STO2, DISP, NEQ, 1)
      CALL PROD(BK, STO2, GAM4, NEQ, ISBAND)
      CALL ADSUB(DEL4, STO1, NEQ, 1)
      CALL SCALE(DEL4, NEQ, T)
      CALL ADSUB(STO1, VEL, NEQ, 1)
      CALL MULT2(CA, STO1, STO2, NEQ)
      CALL ADSUB(GAM4, STO2, NEQ, 1)
```

```
      CALL ADSUB(GAM4, R3, NEQ, 0)
      CALL SCALE(GAM4, NEQ, -T)
      CALL MULT1(RMASS, GAM4, NEQ)
C
      CALL ADSUB(DEL2, DEL3, NEQ, 1)
      CALL SCALE(DEL2, NEQ, 2.0)
      CALL ADSUB(DEL2, DEL1, NEQ, 1)
      CALL ADSUB(DEL2, DEL4, NEQ, 1)
      CALL SCALE(DEL2, NEQ, 1/6.0)
      CALL ADSUB(DISP, DEL2, NEQ, 1)
C
      CALL ADSUB(GAM2, GAM3, NEQ, 1)
      CALL SCALE(GAM2, NEQ, 2.0)
      CALL ADSUB(GAM2, GAM1, NEQ, 1)
      CALL ADSUB(GAM2, GAM4, NEQ, 1)
      CALL SCALE(GAM2, NEQ, 1/6.0)
      CALL ADSUB(VEL, GAM2, NEQ, 1)
      RETURN
      END
C
C
      SUBROUTINE SCALE(A, N, SCAL)
C     ============================
C
      DIMENSION A(2368)
C
C  TO MULTIPLY A VECTIOR 'A' BY A SCALAR 'SCAL' AND STORE IN 'A';
C  N = DIMENSION OF 'A'.
C
      DO 10 I = 1, N
        A(I) = SCAL * A(I)
   10 CONTINUE
      RETURN
      END
C
C
      SUBROUTINE ADSUB(A, B, N, L)
C     ============================
C
      DIMENSION A(2368), B(2368)
C
C  TO ADD OR SUBTRACT FROM A VECTOR 'A' A VECTOR 'B' AND
C  STORE IN 'A';  N = DIMENSION OF 'A' AND 'B'.
C  WHEN L=1  A + B IS FORMED.
C  WHEN L=0  A - B IS FORMED.
C
      IF (L .EQ. 0) GO TO 15
      DO 10 I = 1, N
        A(I) = A(I) + B(I)
   10 CONTINUE
      RETURN
   15 DO 20 I = 1, N
        A(I) = A(I) - B(I)
   20 CONTINUE
      RETURN
      END
C
C
C
C
```

```
C
C
      SUBROUTINE PROD(A, B, C, N, L)
C     ==============================
C
      DIMENSION A(2368,107), B(2368), C(2368)
C
C  TO FIND THE PRODUCT OF A BANDED MATRIX STORED IN CONDENSED
C  FORM 'A(I,J)' WITH A COLUMN VECTOR 'B(I)'.
C  THE RESULT IS STORED IN 'C(I)'.
C  N = DIMENSION OF 'B' AND 'C'.
C  L = SEMIBANDWIDTH OF'A'.  THUS 'A' IS N X (2*L - 1).
C
      LL = 2 * L - 1
      DO 10 I = 1, N
        C(I) = 0.0
   10 CONTINUE
      DO 15 J = 1, LL
        DO 15 I = 1, N
          M = I + J - L
          IF (M .LE. 0) GO TO 15
          IF (M .GT. N) GO TO 15
          C(I) = C(I) + A(I,J) * B(M)
   15 CONTINUE
      RETURN
      END
C
C
      SUBROUTINE MULT1(A, B, N)
C     =========================
C
      DIMENSION A(2368), B(2368)
C
C  TO FIND THE PRODUCT OF A DIAGONAL MATRIX 'A' STORED IN CONDENSED
C  FORM WITH A COLUMN VECTOR 'B', AND STORE IN 'B'.
C  N = DIMENSION OF 'B'.
C
      DO 10 I = 1, N
        B(I) = A(I) * B(I)
   10 CONTINUE
      RETURN
      END
C
C
      SUBROUTINE MULT2(A, B, C, N)
C     ============================
C
      DIMENSION A(2368), B(2368), C(2368)
C
C  TO FIND THE PRODUCT OF A DIAGONAL MATRIX 'A' STORED IN CONDENSED
C  FORM WITH A COLUMN VECTOR 'B', AND STORE IN 'C'.
C  N = DIMENSION OF 'B'.
C
      DO 10 I = 1, N
        C(I) = A(I) * B(I)
   10 CONTINUE
      RETURN
      END
C
C
```

```
      SUBROUTINE DUMP
C     ===============
C
C  UNFORMATTED WRITE OF COMMON BLOCKS ONTO DEVICE ATTATCHED TO 8.
C
      COMMON T,.TMAX, NEL, NNP, NEQ, IMAX, ISTOP, ISTEP,
     +       ISBAND, LNUM
      COMMON /ONE/ BK(2368,107), CA(2368), RMASS(2368), BODY(2368)
      COMMON /TWO/ XLOAD(1184), YLOAD(1184),.KODE(1184)
      COMMON /THREE/ DISP(2368), VEL(2368), R(2368), R1(2368),
     +       R2(2368), R3(2368)
      COMMON /FOUR/ NODE(1200), IFORM
C
      WRITE (8) T, TMAX, NEL, NNP, NEQ, IMAX, ISTOP, ISTEP,
     +          ISBAND, LNUM
      WRITE (8) BK, CA, RMASS, BODY
      WRITE (8) XLOAD, YLOAD, KODE
      WRITE (8) DISP, VEL, R, R1, R2, R3
      WRITE (8) NODE, IFORM
      RETURN
      END
```

```
C
C
C      PROGRAM PLOTS
C      =============
C
C
C
C   PROGRAM RECOVERS OPTION PARAMETERS, AND ACCORDINGLY PRODUCES
C   THE REQUIRED DISPLAY PLOTS.
C
      COMMON QST(600,2,8), B(600,3,10), C(600,3,3),
     +       DISP(2368), T, TMAX, NELEM(600), ITIM(10),
     +       IMAX, NNP, NEL, NELDIS, NFRMS, NSTAT
      COMMON /ONE/ X(1184), Y(1184), XCEN(1200), YCEN(1200), IE(1200,5)
      COMMON /TWO/ STRAIN(3), STRESS(6), PRINC(600,3)
      COMMON /THREE/ TITLE(8), XMAX, XMIN, YMAX, YMIN, XSP, YSP,
     +               XMAP1, XMAP2, YMAP1, YMAP2, STMAX
      COMMON /FOUR/ STHETA, CTHETA
      COMMON /FIVE/ IOUTLN(50), NNOD
      COMMON /SIX/ IGRID, ISECT, ISTRS, IDISPL, IFRM
      COMMON /SEVEN/ XDISP(300,10), YDISP(300,10), IX(10), IY(10),
     +               L1, L2, NODE(1200), IFORM
C
      CALL RECOVR
      CALL PAPER(1)
      IF (ISECT .NE. 0) GO TO 10
      IF (ISTRS .EQ. 0) GO TO 20
   10 CALL PLTPAR
      IF (ISECT .EQ. 0) GO TO 15
C
C   PLOT GRID SECTION.
C
      CALL DISGRD
      IFRM = IFRM - 1
      IF (IFRM .GE. 1) CALL FRAME
   15 IF (ISTRS .EQ. 0) GO TO 20
C
C   PLOT STRESS PLOTS.
C
      CALL DISPLS
      IFRM = IFRM - 1
      IF (IFRM .GE. 1) CALL FRAME
   20 IF (IGRID .EQ. 0) GO TO 25
C
C   PLOT WHOLE GRID.
C
      CALL PSCALE
      CALL GRDPLT
      IFRM = IFRM - 1
      IF (IFRM .GE. 1) CALL FRAME
   25 IF (IDISPL .NE. 1) GO TO 30
C
C   PLOT DISPLACEMENT/TIME GRAPHS.
C
      CALL DISPL
      CALL GHOS
   30 CALL GREND
      STOP
      END
C
C
```

```
      SUBROUTINE RECOVR
C     =================
C
      COMMON QST(600,2,8), B(600,3,10), C(600,3,3),
     +       DISP(2368), T, TMAX, NELEM(600), ITIM(10),
     +       IMAX, NNP, NEL, NELDIS, NFRMS, NSTAT
      COMMON /ONE/ X(1184), Y(1184), XCEN(1200), YCEN(1200), IE(1200,5)
      COMMON /THREE/ TITLE(8), XMAX, XMIN, YMAX, YMIN, XSP, YSP,
     +               XMAP1, XMAP2, YMAP1, YMAP2, STMAX
      COMMON /FIVE/ IOUTLN(50), NNOD
      COMMON /SIX/ IGRID, ISECT, ISTRS, IDISPL, IFRM
      COMMON /SEVEN/ XDISP(300,10), YDISP(300,10), IX(10), IY(10),
     +               L1, L2, NODE(1200), IFORM
      DIMENSION D1(2,8), D2(3,10), D3(3,3)
C
C  RECOVERS OPTION PARAMETERS AND GRID GEOMETRY.
C
C  RECOVER PARAMETERS.
C
      READ (2) STMAX, TITLE, NELEM, NELDIS, ITIM, IX, IY, IGRID, ISECT,
     +       ISTRS, IDISPL, IFRM, NFRMS, IOUTLN, NNOD, L1, L2
      READ (4) X, Y, XCEN, YCEN, IE, NODE, IFORM, NEL, NNP, NSTAT
C
C  RENUMBER OUTLINE AND DISPLAY NODES IF IMPROVED TOPOLOGY IN USE.
C
      IF (IFORM .NE. 1) GO TO 35
      IF (ISTRS .EQ. 0) GO TO 15
      DO 10 I = 1, NNOD
        N = IOUTLN(I)
        IOUTLN(I) = NODE(N)
   10 CONTINUE
   15 IF (IDISPL .EQ. 0) GO TO 35
      IF (L1 .EQ. 0) GO TO 25
      DO 20 I = 1, L1
        N = IX(I)
        IX(I) = NODE(N)
   20 CONTINUE
   25 IF (L2 .EQ. 0) GO TO 35
      DO 30 I = 1, L2
        N = IY(I)
        IY(I) = NODE(N)
   30 CONTINUE
   35 IF (ISTRS .EQ. 0) RETURN
C
C  FORM MATRICES FOR STRESS/STRAIN CALCULATIONS.
C
   40 K = 1
      DO 60 I = 1, NEL
        READ (4) D1, D2, D3
        IF (I .NE. NELEM(K)) GO TO 60
        DO 45 M = 1, 2
          DO 45 N = 1, 8
            QST(K,M,N) = D1(M,N)
   45   CONTINUE
        DO 50 M = 1, 3
          DO 50 N = 1, 10
            B(K,M,N) = D2(M,N)
   50   CONTINUE
        DO 55 M = 1, 3
          DO 55 N = 1, 3
```

```
            C(K,M,N) = D3(M,N)
   55    CONTINUE
         IF (K .EQ. NELDIS) RETURN
         K = K + 1
   60 CONTINUE
      WRITE (6,65) NELDIS, NEL
      STOP
C
   65 FORMAT ('0ERROR:-  NUMBER OF DISPLAY ELEMENTS (', I5,
     +        ') EXCEEDS GRID ELEMENTS (',I5,').')
      END
C
C
      SUBROUTINE PLTPAR
C     =================
C
      COMMON QST(600,2,8), B(600,3,10), C(600,3,3),
     +       DISP(2368), T, TMAX, NELEM(600), ITIM(10),
     +       IMAX, NNP, NEL, NELDIS, NFRMS, NSTAT
      COMMON /ONE/ X(1184), Y(1184), XCEN(1200), YCEN(1200), IE(1200,5)
      COMMON /THREE/ TITLE(8), XMAX, XMIN, YMAX, YMIN, XSF, YSF,
     +               XMAP1, XMAP2, YMAP1, YMAP2, STMAX
C
C  TO DETERMINE THE PLOT PARAMETERS OF THE SECTION OF GRID
C  CHOSEN FOR DISPLAY.
C
C  DETERMINE MAXIMUM AND MINIMUM VALUES OF X AND Y CO-ORDINATES.
C
      XMAX = -1.0E10
      YMAX = -1.0E10
      XMIN = 1.0E10
      YMIN = 1.0E10
      DO 10 I = 1, NELDIS
        K = NELEM(I)
        DO 10 J = 1, 4
          IF (X(IE(K,J)) .GT. XMAX) XMAX = X(IE(K,J))
          IF (X(IE(K,J)) .LT. XMIN) XMIN = X(IE(K,J))
          IF (Y(IE(K,J)) .GT. YMAX) YMAX = Y(IE(K,J))
          IF (Y(IE(K,J)) .LT. YMIN) YMIN = Y(IE(K,J))
   10 CONTINUE
C
C  CALCULATE PLOT SCALES.
C
      BORDER = (YMAX - YMIN) / 16.0
      YMAP1 = YMIN - BORDER
      YMAP2 = YMAX + BORDER
      XMAP1 = XMIN - BORDER
      XMAP2 = XMAX + BORDER
      YSF = 0.9
      XSF = YSF * (XMAP2 - XMAP1) / (YMAP2 - YMAP1)
      RETURN
      END
C
C
C
C
C
C
C
C
```

```
      SUBROUTINE DISGRD
C     =================
C
      COMMON QST(600,2,8), B(600,3,10), C(600,3,3),
     +       DISP(2368), T, TMAX, NELEM(600), ITIM(10),
     +       IMAX, NNP, NEL, NELDIS, NFRMS, NSTAT
      COMMON /ONE/ X(1184), Y(1184), XCEN(1200), YCEN(1200), IE(1200,5)
      COMMON /THREE/ TITLE(8), XMAX, XMIN, YMAX, YMIN, XSP, YSP,
     +               XMAP1, XMAP2, YMAP1, YMAP2, STMAX
      COMMON /SIX/ IGRID, ISECT, ISTRS, IDISPL, IFRM
C
C  PLOT THE GRID OF ELEMENTS FOR STRESS/STRAIN DISPLAY.
C
C  DRAW BORDER ROUND THE DISPLAY.
C
      CALL CSPACE(0.0, XSP, 0.0, 1.0)
      CALL PSPACE(0.0, XSP, 0.0, 1.0)
      CALL MAP(0.0, 1.0, 0.0, 1.0)
      CALL BORDER
      CALL PSPACE(0.0, XSP, 0.0, YSP)
      CALL MAP(XMAP1, XMAP2, YMAP1, YMAP2)
C
C  DRAW ELEMENTS.
C
      DO 20 I = 1, NELDIS
        K = NELEM(I)
        IF (I .EQ. 1) GO TO 10
        IF (IE(K,1) .EQ. IE(NELEM(I - 1),1)) GO TO 15
   10   CALL POSITN(X(IE(K,1)), Y(IE(K,1)))
   15   CALL JOIN(X(IE(K,2)), Y(IE(K,2)))
        CALL JOIN(X(IE(K,3)), Y(IE(K,3)))
        CALL JOIN(X(IE(K,4)), Y(IE(K,4)))
        CALL JOIN(X(IE(K,1)), Y(IE(K,1)))
   20 CONTINUE
C
C  WRITE ELEMENT NUMBERS.
C
      IF (ISECT .EQ. 2) GO TO 40
      CALL CTRMAG(5)
      IF (ISECT .EQ. 3) GO TO 30
      DO 25 I = 1, NELDIS
        K = NELEM(I)
        CALL PLOTNI(XCEN(K), YCEN(K), K)
   25 CONTINUE
      GO TO 40
   30 DO 35 I = 1, NELDIS
        K = NELEM(I)
        CALL PLOTNI(XCEN(K), YCEN(K), IE(K,5))
   35 CONTINUE
C
C  ANNOTATE PLOT.
C
   40 CALL CTRMAG(15)
      IPLACE = (XSP*77.0) - 20
      CALL PLACE(IPLACE, 4)
      CALL TYPECS('ELEMENT MESH', 12)
      IF (ISECT .EQ. 2) GO TO 50
      CALL LINEFD(2)
      CALL SPACE(-17)
      IF (ISECT .EQ. 3) GO TO 45
```

```
      CALL TYPECS('(WITH ELEMENT NUMBERS)', 22)
      GO TO 50
   45 CALL TYPECS('(WITH MATERIAL NUMBERS)', 23)
C
C  WRITE OUT TITLE.
C
   50 CALL CTRMAG(30)
      CALL PLACE(4, 2)
      CALL ITALIC(1)
      CALL TYPECS(TITLE, 32)
      CALL ITALIC(0)
C
      RETURN
C
      END
C
C
      SUBROUTINE DISPLS
      =================
C
C
      COMMON QST(600,2,8), B(600,3,10), C(600,3,3),
     +       DISP(2368), T, TMAX, NELEM(600), ITIM(10),
     +       IMAX, NNP, NEL, NELDIS, NFRMS, NSTAT
      COMMON /TWO/ STRAIN(3), STRESS(6), PRINC(600,3)
C
C  RECOVERS DISPLACEMENTS OF EACH ELEMENT.
C  CALLS STRSTR TO CALCULATE THE STRESSES AND STRAINS.
C  CALLS VECPLT TO PLOT PRINCIPAL STRESSES.
C
      REWIND 3
      IF (NSTAT .NE. 0) GO TO 10
      READ (3) T, TMAX, IMAX
   10 WRITE (7,35)
      J = 1
      DO 30 I = 1, IMAX
        READ (3) DISP
        IF (I .NE. ITIM(J)) GO TO 30
        TIM = FLOAT(I) * T
        IF (NSTAT .NE. 0) GO TO 15
        WRITE (7,45) I, TIM
   15   WRITE (7,40)
        DO 25 K = 1, NELDIS
          CALL STRSTR(K)
          DO 20 JJ = 1, 3
            PRINC(K,JJ) = STRESS(JJ + 3)
   20     CONTINUE
          M = NELEM(K)
C         WRITE (7,40) M, STRESS
   25   CONTINUE
        CALL OUTLIN
        CALL VECPLT(TIM)
        IF (J .EQ. NFRMS) RETURN
        J = J + 1
        CALL FRAME
   30 CONTINUE
      RETURN
   35 FORMAT ('1', 10X, 'STRESSES AT ELEMENT CENTROIDS')
   40 FORMAT ('0ELEMENT', 6X, 'X-STRESS', 7X, 'Y-STRESS', 8X,
     +        'TAU-XY', 11X,
     +        'PRINCIPAL STRESSES',8X,'ANGLE OF 1'/
```

```
     +        64X,'1',12X,'2',10X,'TO X-AXIS'/)
   45 FORMAT ('-TIMESTEP NUMBER', I5, 8X, 'TIME = ', 1PE15.4)
   50 FORMAT (2X, I5, 1X, 6(1PE15.4))
      END
C
C
      SUBROUTINE STRSTR(K)
C     ====================
C
      COMMON QST(600,2,8), B(600,3,10), C(600,3,3),
     +       DISP(2368), T, TMAX, NELEM(600), ITIM(10),
     +       IMAX, NNP, NEL, NELDIS, NFRMS, NSTAT
      COMMON /ONE/ X(1184), Y(1184), XCEN(1200), YCEN(1200), IE(1200,5)
      COMMON /TWO/ STRAIN(3), STRESS(6), PRINC(600,3)
      DIMENSION Q(10)
C
C  CALCULATES THE STRESS AND STRAIN IN EACH ELEMENT FOR GIVEN
C  DISPLACEMENTS OF THE NODES.
C
C  DETERMINE THE NODAL DISPLACEMENTS OF THE ELEMENT.
C
      M = NELEM(K)
      LIM = 4
      IF (IE(M,3) .EQ. IE(M,4)) LIM = 3
      DO 10 I = 1, LIM
        II = 2 * I
        JJ = 2 * IE(M,I)
        Q(II - 1) = DISP(JJ - 1)
        Q(II) = DISP(JJ)
   10 CONTINUE
      Q(9) = 0.0
      Q(10) = 0.0
C
C  CALCULATE THE DISPLACEMENT OF THE CONDENSED NODE.
C
      IF (LIM .EQ. 3) GO TO 20
      DO 15 I = 1, 2
        DO 15 J = 1, 8
          L = I + 8
          Q(L) = Q(L) + QST(K,I,J) * Q(J)
   15 CONTINUE
C
C  CALCULATE ELEMENT STRAINS.
C
      LIM = 10
      FAC = 0.25
      GO TO 25
   20 LIM = 6
      FAC = 1.0
   25 DO 30 I = 1, 3
        STRAIN(I) = 0.0
        DO 30 J = 1, LIM
          STRAIN(I) = STRAIN(I) + B(K,I,J) * Q(J) * FAC
   30 CONTINUE
C
C  CALCULATE X AND Y ELEMENT STRESSES.
C
      DO 35 I = 1, 3
        STRESS(I) = 0.0
        DO 35 J = 1, 3
```

```
          STRESS(I) = STRESS(I) + C(K,I,J) * STRAIN(J)
   35 CONTINUE
C
C  CALCULATE PRINCIPAL STRESSES AND ANGLE WITH X-AXIS.
C
      SP = (STRESS(1) + STRESS(2)) / 2.0
      SM = (STRESS(1) - STRESS(2)) / 2.0
      DS = SQRT(SM*SM + STRESS(3)*STRESS(3))
      STRESS(4) = SP + DS
      STRESS(5) = SP - DS
      IF (STRESS(3) .EQ. 0.0 .AND. SM .EQ. 0.0) GO TO 40
      STRESS(6) = 0.5 * ATAN2(STRESS(3),SM)
      RETURN
   40 STRESS(6) = 0.0
      RETURN
      END
C
C
      SUBROUTINE OUTLIN
C     =================
C
      COMMON /ONE/ X(1184), Y(1184), XCEN(1200), YCEN(1200), IE(1200,5)
      COMMON /THREE/ TITLE(8), XMAX, XMIN, YMAX, YMIN, XSP, YSP,
     +               XMAP1, XMAP2, YMAP1, YMAP2, STMAX
      COMMON /FIVE/ IOUTLN(50), NNOD
C
C  TO DRAW THE OUTLINE OF THE DISPLAY ELEMENTS.
C
C  SET UP FRAME.
C
   10 CALL CSPACE(0.0, XSP, 0.0, 1.0)
      CALL PSPACE(0.0, XSP, 0.0, 1.0)
      CALL MAP(0.0, 1.0, 0.0, 1.0)
      CALL BORDER
      CALL PSPACE(0.0, XSP, 0.0, YSP)
      CALL MAP(XMAP1, XMAP2, YMAP1, YMAP2)
C
C  DRAWS THE OUTLINE REQUIRED.
C
      CALL POSITN(X(IOUTLN(1)), Y(IOUTLN(1)))
      DO 15 I = 2, NNOD
        CALL JOIN(X(IOUTLN(I)), Y(IOUTLN(I)))
   15 CONTINUE
      RETURN
      END
C
C
      SUBROUTINE VECPLT(TIM)
C     ======================
C
      COMMON QST(600,2,8), B(600,3,10), C(600,3,3),
     +       DISP(2368), T, TMAX, NELEM(600), ITIM(10),
     +       IMAX, NNP, NEL, NELDIS, NFRMS, NSTAT
      COMMON /ONE/ X(1184), Y(1184), XCEN(1200), YCEN(1200), IE(1200,5)
      COMMON /TWO/ STRAIN(3), STRESS(6), PRINC(600,3)
      COMMON /THREE/ TITLE(8), XMAX, XMIN, YMAX, YMIN, XSP, YSP,
     +               XMAP1, XMAP2, YMAP1, YMAP2, STMAX
      COMMON /FOUR/ STHETA, CTHETA
      COMMON /SIX/ IGRID, ISECT, ISTRS, IDISPL, IFRM
C
```

```
C   PLOTS THE PRINCIPAL STRESSES AT THE CENTROIDS OF THE
C   DISPLAY ELEMENTS.
C
C   TO FIND MAXIMUM VALUE OF STRESSES TO BE PLOTTED.
C
      IF (STMAX .GT. 1.0E-7) GO TO 15
      STMAX = ABS(PRINC(1,1))
      IF (ABS(PRINC(1,2)) .GT. STMAX) STMAX = ABS(PRINC(1,2))
      DO 10 I = 2, NELDIS
        IF (ABS(PRINC(I,1)) .GT. STMAX) STMAX = ABS(PRINC(I,1))
        IF (ABS(PRINC(I,2)) .GT. STMAX) STMAX = ABS(PRINC(I,2))
   10 CONTINUE
C
C   FORM SCALE FACTOR.
C
   15 SCALE = (YMAP2 - YMAP1) / (10.0*STMAX)
C
C   START PLOT OF STRESSES.
C
      DO 25 I = 1, NELDIS
C
C   FIND SINE AND COSINE OF ANGLE WITH X=AXIS, WITH SCALE FACTOR.
C
        STHETA = SIN(PRINC(I,3)) * SCALE
        CTHETA = COS(PRINC(I,3)) * SCALE
C
C   PLOT STRESSES.
C
        K = NELEM(I)
        DO 25 J = 1, 2
          XPLT = XCEN(K) + FLOAT((-1)**(J + 1)) * PRINC(I,J)
     +               * TRIG(J + 1)
          YPLT = YCEN(K) + PRINC(I,J) * TRIG(J)
          IF (ISTRS .EQ. 1) GO TO 20
          IF (PRINC(I,J) .LE. 0.0) CALL POSITN(XPLT, YPLT)
          IF (PRINC(I,J) .GT. 0.0) CALL GPOINT(XPLT, YPLT)
          XPLT = 2.0 * XCEN(K) - XPLT
          YPLT = 2.0 * YCEN(K) - YPLT
          IF (PRINC(I,J) .LE. 0.0) CALL JOIN(XPLT, YPLT)
          IF (PRINC(I,J) .GT. 0.0) CALL GPOINT(XPLT, YPLT)
          GO TO 25
   20     CALL POSITN(XPLT, YPLT)
          XPLT = 2.0 * XCEN(K) - XPLT
          YPLT = 2.0 * YCEN(K) - YPLT
          IF (PRINC(I,J) .GT. 0.0) CALL BROKEN(5, 5, 5, 5)
          CALL JOIN(XPLT, YPLT)
          CALL FULL
   25 CONTINUE
C
C   ANNOTATE PLOT.
C
      CALL CTRMAG(18)
      IPLACE = (XSP*64.0) - 42
      CALL PLACE(IPLACE, 6)
      CALL TYPECS('(DOTTED LINES TENSIONAL)', 24)
      CALL LINEFD(-2)
      CALL SPACE(-28)
C
C   HEADINGS FOR STRESS VECTORS.
C
```

```
      IF (NSTAT .NE. 0) GO TO 30
      CALL TYPECS('STRESS VECTORS AFTER  ', 22)
      CALL TYPENF(TIM, 4)
      CALL CTRSET(2)
      CALL TYPECS(' S.', 3)
   30 CALL CTRSET(1)
C     CALL PLACE(7, 6)
C     CALL TYPECS('MAXIMUM STRESS = ', 17)
C     CALL TYPENE(STMAX, 2)
C     CALL TYPECS(' P', 2)
C     CALL CTRSET(2)
C     CALL TYPECS('A.', 2)
C     CALL CTRSET(1)
C
      XLABEL = XMAP1 + (YMAP2 - YMAP1) / 6.0
      YLABEL = YMAP2 - (YMAP2 - YMAP1) / 6.0
      CALL POSITN(XLABEL, YLABEL)
      N = INT(ALOG10(STMAX))
      E = 10.0 ** N
      XLABEL = XLABEL + 2.0 * E * SCALE
      CALL JOIN(XLABEL, YLABEL)
      CALL SPACE(2)
      CALL TYPENE(E, 1)
      CALL TYPECS(' P', 2)
      CALL CTRSET(2)
      CALL TYPECS('A.', 2)
      CALL CTRSET(1)
      RETURN
      END
C
C
      FUNCTION TRIG(J)
C     ================
C
      COMMON /FOUR/ STHETA, CTHETA
C
C  TRIG(J) EQUALS CTHETA OR STHETA ACCORDING AS J IS EVEN OR ODD.
C
      TRIG = ((CTHETA + STHETA) + FLOAT((-1)**J)
     +       *(CTHETA - STHETA)) / 2.0
      RETURN
      END
C
C
      SUBROUTINE PSCALE
C     =================
C
      COMMON QST(600,2,8), B(600,3,10), C(600,3,3),
     +       DISP(2368), T, TMAX, NELEM(600), ITIM(10),
     +       IMAX, NNP, NEL, NELDIS, NFRMS, NSTAT
      COMMON /ONE/ X(1184), Y(1184), XCEN(1200), YCEN(1200), IE(1200,5)
      COMMON /THREE/ TITLE(8), XMAX, XMIN, YMAX, YMIN, XSP, YSP,
     +               XMAP1, XMAP2, YMAP1, YMAP2, STMAX
C
C  TO CALCULATE PLOT SCALES AND PARAMETERS.
C
C  ASSIGN MAXIMUM AND MINIMUM VALUES OF X AND Y,
C  YMAX BEING THE GREATEST DEPTH (WHETHER +VE OR -VE).
C
      XMAX = RAMAX(X,NNP)
```

```
      YMAX = RAMAX(Y,NNP)
      XMIN = RAMIN(X,NNP)
      YMIN = RAMIN(Y,NNP)
C
C   CALCULATE PLOT SCALES.
C
      BORDER = (YMAX - YMIN) / 16.0
      YMAP1 = YMIN - BORDER
      YMAP2 = YMAX + BORDER
      XMAP1 = XMIN - BORDER
      XMAP2 = XMAX + BORDER
      YSP = 0.9
      XSP = YSP * (XMAP2 - XMAP1) / (YMAP2 - YMAP1)
      RETURN
      END
C
C
      SUBROUTINE GRDPLT
C     =================
C
      COMMON QST(600,2,8), B(600,3,10), C(600,3,3),
     +       DISP(2368), T, TMAX, NELEM(600), ITIM(10),
     +       IMAX, NNP, NEL, NELDIS, NFRMS, NSTAT
      COMMON /ONE/ X(1184), Y(1184), XCEN(1200), YCEN(1200), IE(1200,5)
      COMMON /THREE/ TITLE(8), XMAX, XMIN, YMAX, YMIN, XSP, YSP,
     +               XMAP1, XMAP2, YMAP1, YMAP2, STMAX
      COMMON /SIX/ IGRID, ISECT, ISTRS, IDISPL, IFRM
C
C   TO PLOT GRID FOR REFERENCE WITH ELEMENT NUMBERS.
C
C   DRAW A BORDER AND A BOX ROUND THE MODEL.
C
      CALL CSPACE(0.0, XSP, 0.0, 1.0)
      CALL PSPACE(0.0, XSP, 0.0, 1.0)
      CALL MAP(0.0, 1.0, 0.0, 1.0)
      CALL BORDER
      CALL PSPACE(0.0, XSP, 0.0, YSP)
      CALL MAP(XMAP1, XMAP2, YMAP1, YMAP2)
C
C   DRAW ELEMENTS.
C
      DO 20 I = 1, NEL
        IF (I .EQ. 1) GO TO 10
        IF (IE(I,1) .EQ. IE((I - 1),1)) GO TO 15
   10   CALL POSITN(X(IE(I,1)), Y(IE(I,1)))
   15   CALL JOIN(X(IE(I,2)), Y(IE(I,2)))
        CALL JOIN(X(IE(I,3)), Y(IE(I,3)))
        CALL JOIN(X(IE(I,4)), Y(IE(I,4)))
        CALL JOIN(X(IE(I,1)), Y(IE(I,1)))
   20 CONTINUE
C
C   WRITE ELEMENT NUMBERS
C
      IF (IGRID .EQ. 2) GO TO 40
      CALL CTRMAG(5)
      IF (IGRID .EQ. 3) GO TO 30
      DO 25 I = 1, NEL
        CALL PLOTNI(XCEN(I), YCEN(I), I)
   25 CONTINUE
      GO TO 40
```

```
   30 DO 35 I = 1, NEL
        CALL PLOTNI(XCEN(I), YCEN(I), IE(I,5))
   35 CONTINUE
C
C  ANNOTATE PLOT.
C
   40 CALL CTRMAG(15)
      IPLACE = (XSP*77.0) - 20
      CALL PLACE(IPLACE, 4)
      CALL TYPECS('ELEMENT MESH', 12)
      IF (IGRID .EQ. 2) GO TO 50
      CALL LINEFD(2)
      CALL SPACE(-17)
      IF (IGRID .EQ. 3) GO TO 45
      CALL TYPECS('(WITH ELEMENT NUMBERS)', 22)
      GO TO 50
   45 CALL TYPECS('(WITH MATERIAL NUMBERS)', 23)
C
C  WRITE OUT TITLE.
C
C     CALL CTRMAG(30)
C     CALL PLACE(4,2)
C     CALL ITALIC(1)
C     CALL TYPECS(TITLE,36)
C     CALL ITALIC(0)
C
   50 RETURN
      END
C
C
      FUNCTION RAMAX(X, N)
C     ====================
C
      DIMENSION X(N)
C
C  TO FIND THE MAXIMUM VALUE OF AN ARRAY.
C
      RAMAX = X(1)
      DO 10 IMAX = 2, N
        RAMAX = AMAX1(RAMAX,X(IMAX))
   10 CONTINUE
C
      RETURN
      END
C
C
      FUNCTION RAMIN(X, N)
C     ====================
C
      DIMENSION X(N)
C
C  TO FIND THE MINIMUM VALUE OF AN ARRAY.
C
      RAMIN = X(1)
      DO 10 IMIN = 2, N
        RAMIN = AMIN1(RAMIN,X(IMIN))
   10 CONTINUE
C
      RETURN
      END
```

```
C
C
      SUBROUTINE DISPL
C     ================
C
      COMMON QST(600,2,8), B(600,3,10), C(600,3,3),
     +       DISP(2368), T, TMAX, NELEM(600), ITIM(10),
     +       IMAX, NNP, NEL, NELDIS, NFRMS, NSTAT
      COMMON /SEVEN/ XDISP(300,10), YDISP(300,10), IX(10), IY(10),
     +               L1, L2, NODE(1200), IFORM
C
C  FORMS X AND Y ARRAYS OF DISPLACEMENTS OF THE DISPLAY NODES.
C
      REWIND 3
      READ (3) T, TMAX, IMAX
      DO 15 ISTEP = 1, IMAX
        READ (3) DISP
        DO 10 I = 1, L1
          J = IX(I)
          XDISP(ISTEP,I) = DISP(2*J - 1)
   10   CONTINUE
        DO 15 I = 1, L2
          J = IY(I)
          YDISP(ISTEP,I) = DISP(2*J)
   15 CONTINUE
      RETURN
      END
C
C
      SUBROUTINE GHOS
C     ===============
C
      COMMON QST(600,2,8), B(600,3,10), C(600,3,3),
     +       DISP(2368), T, TMAX, NELEM(600), ITIM(10),
     +       IMAX, NNP, NEL, NELDIS, NFRMS, NSTAT
      COMMON /SEVEN/ XDISP(300,10), YDISP(300,10), IX(10), IY(10),
     +               L1, L2, NODE(1200), IFORM
C
C TO CREATE THE PLOTFILE FOR GRAPHIC DISPLAY.
C
      DIMENSION Y(300), X(300), ANNOT(24)
C     WRITE (6,50)
C     READ (5,55) (ANNOT(I),I=1,24)
      DO 10 I = 1, 300
        X(I) = T * I
   10 CONTINUE
      IPAGE = 0
      L = L1 + L2
      DO 55 J = 1, L
        CALL PSPACE(0.0, 1.0, 0.0, 1.0)
        CALL MAP(0.0, 1.0, 0.0, 1.0)
        IF (IPAGE .GT. 0) GO TO 15
C       CALL BORDER
        CALL CSPACE(0.0, 1.0, 0.0, 1.0)
C       CALL CTRMAG(10)
C       CALL PLACE(20, 2)
C       CALL TYPECS(ANNOT, 80)
   15   CALL CTRMAG(8)
        CALL CTRORI(1.0)
        IF (J .GT. L1) GO TO 30
```

```
      N = IX(J)
      IF (IFORM .NE. 1) GO TO 20
      CALL RENUM(N)
   20 DO 25 I = 1, IMAX
        Y(I) = XDISP(I,J)
   25 CONTINUE
      CALL PLOTCS(0.01, 0.85 - 0.2*IPAGE, 'X-DISP. NODE', 12)
      GO TO 45
   30 K = J - L1
      N = IY(K)
      IF (IFORM .NE. 1) GO TO 35
      CALL RENUM(N)
   35 DO 40 I = 1, IMAX
        Y(I) = YDISP(I,K)
   40 CONTINUE
      CALL PLOTCS(0.01, 0.85 - 0.2*IPAGE, 'Y-DISP. NODE', 12)
   45 CALL SPACE(1)
      CALL TYPENI(N)
      CALL CTRORI(0.0)
      YMAX = ABS(Y(1))
      DO 50 I = 2, IMAX
        IF (ABS(Y(I)) .LE. YMAX) GO TO 50
        YMAX = ABS(Y(I))
   50 CONTINUE
      IF (YMAX .EQ. 0) YMAX = 1.0
      YMAX = YMAX * 1.01
      CALL PSPACE(0.1, 0.97, 0.82 - 0.2*IPAGE, 0.98 - 0.2*IPAGE)
      CALL MAP(0.0, TMAX, -YMAX, YMAX)
      CALL AXES
      CALL NSCURV(X, Y, 1, IMAX)
      IPAGE = IPAGE + 1
      IF (IPAGE .LT. 5) GO TO 55
      IF (J .EQ. L) GO TO 55
      CALL FRAME
      IPAGE = 0
   55 CONTINUE
      RETURN
C
   60 FORMAT (17HOWRITE ANNOTATION)
   65 FORMAT (24A4)
      END
C
C
      SUBROUTINE RENUM(N)
C     ===================
C
      COMMON QST(600,2,8), B(600,3,10), C(600,3,3),
     +       DISP(2368), T, TMAX, NELEM(600), ITIM(10),
     +       IMAX, NNP, NEL, NELDIS, NFRMS, NSTAT
      COMMON /SEVEN/ XDISP(300,10), YDISP(300,10), IX(10), IY(10),
     +               L1, L2, NODE(1200), IFORM
C
C  RENUMBERS DISPLAY NODES IF IMPROVED TOPOLOGY IN USE.
C
      DO 10 I = 1, NNP
        IF (NODE(I) .EQ. N) GO TO 15
   10 CONTINUE
   15 N = I
      RETURN
      END
```

```
C
C
C       PROGRAM REDUCE
C       ==============
C
C
C
C
C   REDUCES THE NODAL DIFFERENCE OF A GRID.
C
      DIMENSION IE(1200,4), NODE(1200)
C
C   READ IN PROBLEM PARAMETERS.
C
      WRITE (6,80)
      READ (5,85) C
      WRITE (6,90)
      READ (5,100) ITNUM
      WRITE (6,95)
      READ (5,100) NEL
      WRITE (6,105)
      READ (6,100) NNP
      WRITE (6,110)
      READ (5,100) NODIF
      WRITE (6,115)
      READ (6,100) IREC
      WRITE (6,120)
      READ (5,100) MAXIT
      WRITE (6,125)
      READ (5,100) IFORM
      IF (IFORM .EQ. 1) GO TO 15
C
C   READ ELEMENT TOPOLOGY.
C
      READ (4,130) (I,(IE(I,J),J=1,4),I=1,NEL)
C
C   INITIALISE NODE VECTOR.
C
      DO 10 I = 1, NNP
        NODE(I) = I
   10 CONTINUE
      GO TO 20
C
C   READ ELEMENT TOPOLOGY AND NODE NUMBERING IN FREE FORMAT.
C
   15 READ (4) IE, NODE
C
C   START ITERATION.
C
   20 WRITE (6,135)
      ITER = 0
      INC = 0
   25 ITER = ITER + 1
C
C   COMPUTE MAXIMUM NODAL DIFFERENCE.
C
      MAXDIF = 0
      DO 30 I = 1, NEL
        DO 30 J = 1, 3
          JJ = J + 1
          DO 30 K = JJ, 4
```

```
            LL = IABS(IE(I,J) - IE(I,K))
            IF (LL .LE. MAXDIF) GO TO 30
            MAXDIF = LL
            IELEM = I
            M = MINO(IE(I,J),IE(I,K))
            N = MAXO(IE(I,J),IE(I,K))
   30 CONTINUE
C
      WRITE (6,140) ITER, IELEM, MAXDIF
C
C  STORE BEST RESULT SO-FAR.
C
      IF (ITER .EQ. 1) MINDIF = MAXDIF
      IF (MAXDIF .GE. MINDIF) GO TO 35
      MINDIF = MAXDIF
      IF (MINDIF .GT. IREC) GO TO 35
      REWIND 8
      WRITE (8) IE, NODE, NEL, NNP, ITER, IELEM, MAXDIF
   35 CONTINUE
      IF (MAXDIF .LE. NODIF) STOP
      IF (ITER .EQ. MAXIT) STOP
      IF (MOD(ITER,ITNUM) .EQ. 0) INC = INC + 1
C
C  COMPUTE SHIFT.
C
      IS = IFIX((MAXDIF/C) + 0.5) - INC
      IIS = 2 * IS
      IF (IIS .EQ. MAXDIF) IS = IS - 1
      IF (IS .LT. 1) IS = 1
      MS = M + IS
      NS = N - IS
C
C  RE-LABEL NODES.
C
      DO 55 I = 1, NEL
        DO 55 J = 1, 4
          IF (IE(I,J) .LT. M) GO TO 55
          IF (IE(I,J) .GT. M) GO TO 40
          IE(I,J) = MS
          GO TO 55
   40     IF (IE(I,J) .GT. MS) GO TO 45
          IE(I,J) = IE(I,J) - 1
          GO TO 55
   45     IF (IE(I,J) .LT. NS) GO TO 55
          IF (IE(I,J) .GE. N) GO TO 50
          IE(I,J) = IE(I,J) + 1
          GO TO 55
   50     IF (IE(I,J) .EQ. N) IE(I,J) = NS
   55 CONTINUE
C
C  RESET NODE VECTOR.
C
      DO 75 I = 1, NEL
        IF (NODE(I) .LT. M) GO TO 75
        IF (NODE(I) .GT. M) GO TO 60
        NODE(I) = MS
        GO TO 75
   60   IF (NODE(I) .GT. MS) GO TO 65
        NODE(I) = NODE(I) - 1
        GO TO 75
```

```
   65    IF (NODE(I) .LT. NS) GO TO 75
         IF (NODE(I) .GE. N) GO TO 70
         NODE(I) = NODE(I) + 1
         GO TO 75
   70    IF (NODE(I) .EQ. N) NODE(I) = NS
   75 CONTINUE
      GO TO 25
      STOP
C
   80 FORMAT ('0**********  SHIFT FACTOR (USUALLY = 2.2)')
   85 FORMAT (E10.4)
   90 FORMAT ('0------  NO. OF ITERATIONS BEFORE SHIFT REFINED')
   95 FORMAT ('0------  NO. OF ELEMENTS')
  100 FORMAT (I5)
  105 FORMAT ('0------  NO. OF NODES')
  110 FORMAT ('0------  ACCEPTABLE NODAL DIFFERENCE')
  115 FORMAT ('0------  MAX. NODAL DIFF. FOR RESULTS STORED')
  120 FORMAT ('0------  MAX. NO. OF ITERATIONS')
  125 FORMAT ('0IF GRID CO-ORDS. AND NODE VALUES IN FREE FORMAT ',
     +        'TYPE ''1'','/' OTHERWISE PRESS RETURN'/' ------')
  130 FORMAT (4I5)
  135 FORMAT ('1', 3X, 'ITERATION', 7X, 'ELEMENT', 6X, 'DIFFERENCE'//)
  140 FORMAT (5X, I5, 2(10X,I5))
      END
```

```
C
C
C       PROGRAM INPUT
C       =============
C
C
C   TO PREPARE INPUT FILE OF LOAD CHANGES AT EACH TIMESTEP.
C   EVALUATES DISPLACEMENTS ALONG BASE NODES OF A PLANE
C   WAVE AT VARIOUS ANGLES.
C
      DIMENSION NODE(100), START(100), FIN(100)
C
C   READS IN PARAMETERS.
C
      WRITE (6,75)
      WRITE (6,80)
      READ (5,85) NNOD
      READ (3,90) (NODE(I),I=1,NNOD)
      WRITE (6,65)
      READ (5,100) SPACE
      WRITE (6,95)
      READ (5,100) E
      WRITE (6,105)
      READ (5,100) PR
      WRITE (6,110)
      READ (5,100) RHO
      WRITE (6,115)
      READ (5,100) PER
      WRITE (6,120)
      READ (5,100) STEP
      WRITE (6,125)
      READ (5,100) AMP
      WRITE (6,130)
      READ (5,100) ANG
      WRITE (6,70)
      READ (5,85) ITYPE
C
C   CALCULATES PLANE WAVE VELOCITY, AND PULSE START AND FINISH
C   TIMES AT EACH NODE.
C
      PI = 4.0 * ATAN(1.0)
      IF (ITYPE .EQ. 2) GO TO 10
      VEL = SQRT(E*(1.0 - PR)/((1.0 + PR)*(1.0 - 2.0*PR)*RHO))
      GO TO 15
   10 VEL = SQRT(E/(2.0*(1.0 + PR)*RHO))
   15 ANG = ANG * PI / 180.0
      DO 20 I = 1, NNOD
        START(I) = (I - 1) * SPACE * SIN(ANG) / VEL
        FIN(I) = START(I) + PER
   20 CONTINUE
C
C   CALCULATES NODAL DISPLACEMENTS, AND WRITES IN REQUIRED FORMAT.
C
      TIM = STEP + 1.0E-6
   25 DO 50 I = 1, NNOD
        IF (TIM .LE. START(I)) GO TO 40
        IF (TIM .GE. FIN(I)) GO TO 40
        T = TIM - START(I)
        DISP = AMP * (1.0 - COS(2.0*PI*T/PER))
        IF (ITYPE .EQ. 2) GO TO 30
```

```
      DISPX = DISP * SIN(ANG)
      DISPY = DISP * COS(ANG)
      GO TO 35
30    DISPX = DISP * COS(ANG)
      DISPY = DISP * SIN(ANG)
35    WRITE (7,135) NODE(I), DISPX, DISPY
      GO TO 50
40    IF (I .NE. NNOD) GO TO 45
      WRITE (7,85) NODE(I)
      GO TO 50
45    IF (TIM .LE. START(I)) GO TO 50
      IF (TIM .LT. FIN(I) + STEP) WRITE (7,85) NODE(I)
50  CONTINUE
    IF (TIM .GE. FIN(NNOD)) GO TO 55
    TIM = TIM + STEP
    GO TO 25
55  DO 60 I = 1, 200
      WRITE (7,85) NODE(NNOD)
60  CONTINUE
    STOP
C
65  FORMAT ('0**********  NODE SPACING')
70  FORMAT ('0FOR P-WAVES TYPE ''1''; FOR S-WAVES TYPE ''2''.'/
   +        ' -----')
75  FORMAT ('0ENTER DATA')
80  FORMAT ('0-----  NUMBER OF NODES')
85  FORMAT (I5)
90  FORMAT (5I5)
95  FORMAT ('0**********  YOUNG''S MODULUS')
100 FORMAT (E10.4)
105 FORMAT ('0**********  POISSON''S RATIO')
110 FORMAT ('0**********  DENSITY')
115 FORMAT ('0**********  PERIOD')
120 FORMAT ('0**********  TIMESTEP')
125 FORMAT ('0**********  AMPLITUDE')
130 FORMAT ('0**********  ANGLE (IN DEG.)')
135 FORMAT (I5, 2(3X,E10.4))
    END
```

```
C
C
C      PROGRAM FILESUM
C      ===============
C
C
C   ADDS THE STATIC DISPLACEMENTS TO THE DISPLACEMENTS
C   AT EACH TIME STEP.
C   STATIC DISPLACEMENTS ARE IN FILE ATTATCHED TO DEVICE 3.
C   TIME STEP DISPLACEMENTS ARE IN FILE ATTATCHED TO DEVICE 4.
C   SUM OF DISPLACEMENTS ARE WRITTEN ON FILE ATTATCHED TO DEVICE 7.
C
      DIMENSION DISP1(2368), DISP2(2368)
      READ (3) DISP1
      READ (4) T, TMAX, IMAX
      WRITE (7) T, TMAX, IMAX
      DO 15 I = 1, IMAX
        READ (4) DISP2
        DO 10 J = 1, 2368
          DISP2(J) = DISP2(J) + DISP1(J)
   10   CONTINUE
        WRITE (7) DISP2
   15 CONTINUE
      RETURN
      END
```

```
C
C
C     PROGRAM DISPLAY
C     ===============
C
C
C
C
C  PROGRAM TO DETERMINE WHICH DISPLAY OPTIONS ARE REQUIRED.
C
      DIMENSION NELEM(600), ITIM(10), IX(10), IY(10), IOUTLN(50),
     +          TITLE(8)
C
C  DETERMINES IF PLOT OF WHOLE GRID IS REQUIRED.
C
   10 ISTRS = 0
      WRITE (6,145)
      READ (5,120) IGRID
C
C  IF GRID SECTION IS REQUIRED READS IN SECTION ELEMENTS, AND
C  DETERMINES IF PLOT SECTION AND/OR STRESS PLOTS ARE REQUIRED.
C
      WRITE (6,150)
      READ (5,120) ISECT
      IF (ISECT .NE. 1) GO TO 85
C
C  READS IN SECTION ELEMENTS.
C
      WRITE (6,155)
      READ (5,120) J
      K = 1
      IF (J .EQ. 3) GO TO 15
      WRITE (6,160)
   15 IF (J .EQ. 3) GO TO 20
      WRITE (6,175)
      READ (5,125) NEL1, NEL2
      GO TO 25
   20 READ (3,125) NEL1, NEL2
   25 IF (NEL1 .EQ. 0) GO TO 40
      IF (NEL2 .EQ. 0) GO TO 35
      IDIFF = NEL2 - NEL1 + 1
      DO 30 N = 1, IDIFF
        NELEM(K) = NEL1 + N - 1
        K = K + 1
   30 CONTINUE
      GO TO 15
   35 NELEM(K) = NEL1
      K = K + 1
      GO TO 15
   40 NELDIS = K - 1
      WRITE (6,165)
      READ (5,120) ISECT
      IF (ISECT .NE. 1) GO TO 45
      WRITE (6,170)
      READ (5,130) (TITLE(I),I=1,8)
   45 WRITE (6,180)
      READ (5,120) ISTRS
      IF (ISTRS .EQ. 0) GO TO 85
C
C  READS IN THE OUTLINE NODES.
C
```

```
      WRITE (6,185)
      READ (5,120) J
      K = 1
      IF (J .EQ. 3) GO TO 50
      WRITE (6,190)
   50 IF (J .EQ. 3) GO TO 55
      WRITE (6,175)
      READ (5,125) NODE1, NODE2
      GO TO 60
   55 READ (3,125) NODE1, NODE2
   60 IF (NODE1 .EQ. 0) GO TO 75
      IF (NODE2 .EQ. 0) GO TO 70
      IDIFF = NODE2 - NODE1 + 1
      DO 65 N = 1, IDIFF
        IOUTLN(K) = NODE1 + N - 1
        K = K + 1
   65 CONTINUE
      GO TO 50
   70 IOUTLN(K) = NODE1
      K = K + 1
      GO TO 50
   75 NNOD = K - 1
C
C  READ THE TIMESTEP NUMBERS AT WHICH DISPLAY IS REQUIRED.
C
      WRITE (6,195)
      READ (5,135) (ITIM(I),I=1,5)
      WRITE (6,200)
      READ (5,135) (ITIM(I),I=6,10)
      NFRMS = 0
      DO 80 I = 1, 10
        IF (ITIM(I) .NE. 0) NFRMS = NFRMS + 1
   80 CONTINUE
C
C  READ IN VALUE OF MAXIMUM STRESS.
C
      WRITE (6,205)
      READ (5,140) STMAX
C
   85 CONTINUE
      WRITE (6,210)
      READ (5,120) IDISPL
      IF (IDISPL .NE. 1) GO TO 110
C
C  READ IN DISPLAY NODES.
C
      DO 90 I = 1, 10
        IX(I) = 0
        IY(I) = 0
   90 CONTINUE
      L1 = 0
      L2 = 0
      WRITE (6,215)
      DO 95 I = 1, 10
        WRITE (6,220)
        READ (5,120) K
        IF (K .EQ. 0) GO TO 100
        IX(I) = K
        L1 = L1 + 1
   95 CONTINUE
```

```
  100 WRITE (6,225)
      DO 105 I = 1, 10
        WRITE (6,220)
        READ (5,120) K
        IF (K .EQ. 0) GO TO 110
        IY(I) = K
        L2 = L2 + 1
  105 CONTINUE
  110 CONTINUE
      IS = 0
      IG = 0
      IT = 0
      IF (ISTRS .NE. 0) IT = 1
      IF (IGRID .NE. 0) IG = 1
      IF (ISECT .NE. 0) IS = 1
      IFRM = IS + IT + IG + IDISPL
      IF (IFRM .NE. 0) GO TO 115
      WRITE (6,230)
      GO TO 10
C
C  DUMP OPTION PARAMETERS.
C
  115 WRITE (7) STMAX, TITLE, NELEM, NELDIS, ITIM, IX, IY, IGRID, ISEC
     +       ISTRS, IDISPL, IFRM, NFRMS, IOUTLN, NNOD, L1, L2
      STOP
C
  120 FORMAT (I5)
  125 FORMAT (2I5)
  130 FORMAT (8A4)
  135 FORMAT (5I5)
  140 FORMAT (E10.4)
  145 FORMAT ('0DO YOU WANT A PLOT OF THE WHOLE GRID?'/
     +         ' FOR GRID WITH ELEMENT NUMBERS TYPE ''1'','/
     +         ' FOR GRID WITHOUT ELEMENT NUMBERS TYPE ''2'','/
     +         ' FOR GRID WITH MATERIAL TYPE OF EACH ELEMENT TYPE',
     +         ' ''3'','/' OTHERWISE PRESS ''RETURN''.'/' -----')
  150 FORMAT ('0DO YOU WANT A SECTION OF THE GRID?'/
     +         ' IF YES, TYPE ''1''; OTHERWISE PRESS ''RETURN''.'/
     +         ' -----')
  155 FORMAT ('0IF SECTION ELEMENTS ARE TO BE READ FROM THE',
     +         'FILE ATTATCHED TO 3'' THEN TYPE ''3'';',
     +         ' OTHERWISE PRESS ''RETURN''.'/' -----')
  160 FORMAT ('0ENTER SECTION ELEMENTS'/
     +         ' FIRST AND LAST ELEMENTS OF A CONSECUTIVE STRING,'/
     +         ' OR INDIVIDUAL ELEMENTS MAY BE ENTERED.'/
     +         ' PRESS RETURN AT END OF LIST.')
  165 FORMAT ('0DO YOU WANT A PLOT OF THE SECTION OF THE GRID?'/
     +         ' FOR SECTION WITH ELEMENT NUMBERS TYPE ''1'','/
     +         ' FOR SECTION WITHOUT ELEMENT NUMBERS TYPE ''2'','/
     +         ' FOR SECTION WITH MATERIAL TYPE OF EACH ELEMENT TYPE',
     +         ' ''3'','/' OTHERWISE PRESS ''RETURN''.'/' -----')
  170 FORMAT ('0WRITE TITLE FOR GRID SECTION.')
  175 FORMAT (11H .....-----)
  180 FORMAT ('0DO YOU WANT STRESS PLOTS OF SECTION AT',
     +         ' SPECIFIED TIMESTEPS?'/
     +         ' FOR PLOTS WITH TENSIONS REPRESENTED',
     +         ' BY BROKEN LINES TYPE ''1'','/
     +         ' FOR PLOTS WITH TENSIONS REPRESENTED',
     +         ' BY TWO DOTS TYPE ''2'','/
     +         ' OTHERWISE PRESS ''RETURN''.'/' -----')
```

```
185 FORMAT ('0IF OUTLINE NODES ARE TO BE READ FROM THE FILE ',
   +        'ATTATCHED TO 3, THEN TYPE ''3'';'/
   +        ' OTHERWISE PRESS ''RETURN''.'/' -----')
190 FORMAT ('0ENTER OUTLINE NODES'/
   +        ' FIRST AND LAST NODES OF A CONSECUTIVE STRING,'/
   +        ' OR INDIVIDUAL NODES MAY BE ENTERED.'/
   +        ' PRESS ''RETURN'' AT END OF LIST.')
195 FORMAT ('0ENTER TIMESTEP NUMBERS FOR WHICH DISPLAY IS REQUIRED'/
   +        ' ENTER 5 NUMBERS PER LINE'/' 10 ENTRIES MAXIMUM'/
   +        ' .....*****.....*****.....')
200 FORMAT (' .....*****.....*****.....')
205 FORMAT ('0ENTER VALUE OF MAXIMUM STRESS EXPECTED',
   +        ' FOR A SERIES OF PLOTS.'/' IF CALCULATION OF MAXIMUM',
   +        'STRESS FOR EACH PLOT, IS PREFERRED, PRESS ''RETURN''.'/
   +        ' **********')
210 FORMAT ('0DO YOU WANT DISPLACEMENT/TIME GRAPHS',
   +        ' OF SPECIFIED NODES?'/
   +        ' IF YES, TYPE ''1''; OTHERWISE PRESS ''RETURN''.'/
   +        ' -----')
215 FORMAT ('0ENTER X DISPLAY NODES, ENDING LIST WITH 0')
220 FORMAT (' .....')
225 FORMAT ('0ENTER Y DISPLAY NODES, ENDING LIST WITH 0')
230 FORMAT ('0WHAT THE HELL DO YOU WANT?'/' LET''S TRY AGAIN')
    END
```